FLEXURAL BEHAVIOUR OF FERROCEMENT

by

Abdul Salam A. Alwash, B.Sc. M.Sc.

Thesis submitted

to the

University of Sheffield

for the

degree of Doctor of Philosophy

in the

Faculty of Engineering

Department of Civil and Structural Engineering

February, 1982.

SUMMARY

Ferrocement is often believed to be a form of reinforced concrete. However, in spite of the similarities between the two materials there are still major differences, indicating that ferrocement requires a separate study to establish its structural performances. On the other hand, although a large amount of research has been carried out on ferrocement, its flexural behaviour is still not fully understood.

The aim of this investigation is to study the structural behaviour of ferrocement plates under flexural loading and the influence of the different variables on the strength and deformation characteristics. The variables studied were the mesh number, strength, opening and distribution, presence of steel bars, and the thickness of the section and the mortar cover.

The experimental programme included 49 plates, 1000x300 mm in dimensions, reinforced with woven type steel wire mesh and tested under two lines load. Deformation measurements were taken from first application of the load up till failure and about 10000 crack measurements (crack width and spacing) were recorded.

The crack width data were dealt with statistically. The effect of the variables on the crack width was studied, quantitatively, by comparing the rate of growth of crack width of the plates. It was found that ferrocement cracking behaviour is characterized by almost a full development of the cracks at relatively early stages of the load (about 30-50% of the ultimate load) and the crack width is smaller and more uniformly distributed than in reinforced concrete. The mesh number and yield strength influenced significantly the crack width and spacing. There was a limit for the mesh number after which the enhancement in the cracking performance of the plates slowed down noticeably. Crack width prediction equations were derived from these tests

showed good correlation, whereas the published crack width formulae largely overestimated or underestimated the measured crack width.

The strength and deformation were influenced mainly by the yield strength and fraction volume of reinforcement in the loading direction. The deflection is most likely to exceed the serviceability criteria before the crack width. For a span-deflection ratio of 180, the mean crack width was mostly below 20 microns, and the load was about 15-30% of the ultimate load.

A procedure is proposed to analyse ferrocement sections under flexural loading. While application of reinforced concrete theory to predict the ultimate moment largely underestimated the experimental results, the proposed procedure predicted closely the experimental moment and deflection at first cracking, yielding and failure of the tested plates.

ACKNOWLEDGEMENTS

The author wishes to express his appreciation and gratitude to Dr. R.N. Swamy for his supervision, invaluable advice and encouragement. He also conveys his thanks to Professor T.H. Hanna and Professor D. Bond for their concern and for providing the facilities for this research to be carried out.

The author appreciates his family's help, patience and encouragement during the course of the work.

The author wishes to acknowledge the assistance of the technical and secretarial staff of the department of Civil and Structural Engineering, in particular Mr. R.N. Newman, Mr. G. Wallace, Mrs. D. Hutson and Miss W. Atkinson. He also wishes to thank Mrs. J. Czerny, for her patience in typing the thesis.

CONTENTS

LIST OF FIGURES

LIST OF TABLES

LIST OF PLATES

NOTATION

A_s	Cross-sectional area of mesh in loading direction.
A_{st}	Cross-sectional area of steel bars in loading direction.
b	Width of the plate.
C	Compressive force in the section.
c	Mortar cover (clear)
D	Section depth.
E_c	Modulus of elasticity of the composite.
E_f	Modulus of elasticity of fibres (mesh).
E_m	Modulus of elasticity of the matrix (mortar).
E_t	Modulus of elasticity of the composite in tension.
E_{cr}	Assumed modulus of elasticity of the composite during the linear range of the cracked stage.
f_{cu}	Cube compressive strength.
I	Second moment of area.
k	Ratio of neutral axis depth from the extreme compressive fibre to the depth of the section.
L	Plate span.
M	Moment on a plate or plate resisting moment.
M_{cr}	Moment at first cracking.
M_y	Moment at first yielding.
M_u	Ultimate moment.
n	Modular ratio (E_s/E_m).
R	Ratio of distances to neutral axis from extreme tensile fibre and from outermost mesh in tension.
r, r_2	Ratios M_{cr}/M, M_y/M respectively.
S	Crack spacing.
S_R	Specific surface of reinforcement (ratio of reinforcement surface area to the volume of the composite).

S_{RL}	Specific surface of reinforcement in loading direction.
T	Total tensile force of the section.
T_{st}	Tensile force carried by the steel bars.
V_R	Fraction volume of reinforcement (percentage of the volume of reinforcement to the total volume of the composite).
V_{RL}	Fraction volume of reinforcement in loading direction.
V_m	Fraction volume of the matrix (mortar).
W_m	Mean crack width.
W_m/ε_t	Rate of growth of crack width.
ε_c	Composite compressive strain.
ε_{cy}	Composite yielding compressive strain.
ε_{cu}	Composite ultimate compressive strain.
ε_f	Strain at a mesh level.
ε_t	Composite tensile strain.
ε_{tcr}	Composite tensile strain which define the strain limit at which the matrix cracks (equals plain mortar ultimate tensile strain).
ε_{ty}	Composite yielding tensile strain.
ε_{tu}	Composite ultimate tensile strain.
σ	Standard deviation.
σ_c	Composite compressive stress.
σ_{cy},σ_{cu}	Composite yielding compressive stress and composite ultimate compressive strength, respectively, in flexure ($\sigma_{cy} = \sigma_{cu} = 0.67\ f_{cu}$).
σ_f	Stress in a mesh.
σ_{fy}	Mesh yield strength (at 0.005 strain).
σ_{mu}	Mortar strength in tension.
σ_t	Composite tensile stress.
σ_{tcr}	Composite tensile stress at first cracking.

σ_{ty}	Composite first yielding tensile stress.
$\sigma_{t\ extra}$	Extra tensile stress carried by the composite after first yielding.
σ_{tu}	Composite ultimate tensile strength.
ω	Ratio of distance of two line load from support to span length.
Δ, Δ_c	Deflection and central deflection, respectively.
ϕ	Curvature of composite section.
$\phi_{cr}, \phi_y, \phi_u$	Curvature of composite section at first cracking, first yielding, and failure, respectively.

CHAPTER 1.

INTRODUCTION AND BACKGROUND

1.1 Introduction.

Plain concrete has low tensile strength, limited ductility, and little resistance to crack propagation. Flaws or microcracks exist in the material even before any load is applied, because of its inherent microstructure and volumetric changes during manufacturing. These flaws lead to a brittle failure of the material in tension at about one tenth of its compression strength.

In reinforced concrete, although the failure of the composite is ductile due to the ductile nature of reinforcement, the concrete suffers an extensive amount of cracking. In the past, working stresses were relatively low. Consequently, the cracks in the reinforced concrete members were small, and therefore insignificant. However, the present trends towards more economical designs, pressed for higher working stresses. This resulted in excessive crack widths and deflections which impair the appearance of the structure, weakening the members due to corrosion of steel, and damaging non-structural members. Thus, the serviceability criteria become more critical than the strength consideration. The concrete technologist is, therefore, faced with the problem of improving the inherent weak properties of concrete in order to cater for the designer's requirements. This, in turn, encouraged the search for new materials to partially replace reinforced concrete.

It is under such circumstances that ferrocement, among other materials, has emerged. The reinforcement of ferrocement consists of several layers of relatively fine wire mesh packed together with or without steel bars in the middle. Cement mortar is used to fill the gaps between the meshes and provide the cover for the reinforcement.

The major use of ferrocement has been in the developing countries where excellent properties of the material and successful field application with

relatively little theoretical basis, were observed. As ferrocement technology developed, so did the interest of engineers who began to view this material as a potentially significant material of construction.

The reinforcing mechanism in ferrocement not only improves many of the engineering properties of the brittle mortar, such as fracture, tensile and flexural strength, ductility, and impact resistance,but also provides advantages in terms of fabrication of products and components. For example, ferrocement may require less formwork than reinforced concrete. The section thickness of its members could be as little as 10 mm and due to the flexibility of the reinforcing mesh it has a high adaptability to complicated shapes and thus,is very attractive for precast units.

At the same time, the reinforcement in ferrocement is uniformly distributed in the section and has a high surface area. This results in improved mechanical properties compared to those of reinforced concrete. Within certain loading limits, it behaves as a homogeneous elastic material and these limits are wider than for normal concrete. In addition, because of the subdivision and distribution of the reinforcement, ferrocement exhibits better crack arrest mechanism and therefore enhances cracking behaviour.

After this, it is not surprising that ferrocement is receiving extensive attention both in the field of applications and the study of its properties.

1.2 Aim of the Investigation.

The investigation was carried out to study experimentally and analytically the flexural behaviour of ferrocement plates. This included the cracking, deformation, and strength and the influence of the important parameters on them.

The parameters studied were the number of meshes, the tensile strength of the mesh, presence of steel bars, mesh opening and distribution, thickness of the section and the mortar cover.

The aims of the study, in particular, are:

1. To study the cracking behaviour of ferrocement from a large number of crack width and spacing measurements, and repeating specimens of the same variables twice or three times.
2. To establish, quantitatively, the influence of the different parameters on the crack width and spacing.
3. To develop crack width prediction equation.
4. To investigate the deformation characteristics from first application of load up till failure and to study the relationship between crack width and deflection for the serviceability criteria.
5. To develop a method for predicting the strength of ferrocement plate.
6. To use fly ash, as a cheap material, to partially substitute the cement in the relatively rich mix used in ferrocement and to enhance its cohesiveness and workability.

1.3 Layout of the Thesis.

The thesis consists of seven chapters. Chapter 1 includes presentation of the problem, and the background and development of ferrocement.

In Chapter 2, the properties of the materials used and the development of an economical and suitable mortar mix is reported. The properties of the hardened mix are also given.

In Chapter 3, the details of the experimental programme, manufacturing technique, testing equipment, and testing procedure are discussed. The experimental programme consisted of seven series comprising 49 specimens. Special manufacturing technique was developed to ensure the required distribution of reinforcement. Also, a special equipment was designed to load the test specimens.

Chapter 4 is devoted to the study of the cracking behaviour. The cracking performance of the different specimens, in terms of the rate of growth

of crack width, is compared. The influence of the variables on the crack width and spacings were studied and crack width prediction equations are proposed.

In Chapter 5 the deformation characteristics of the specimens are reported. The relationship between crack width and deflection was identified and the behaviour of the plates from first application of load up till failure is traced. The effect of the variables on the load-deflection and load strain curves, ductility and stiffness is discussed.

Finally Chapter 6 is devoted to strength characteristics and analysis of the plates. A method is proposed to analyse the ferrocement section and to predict its moment capacity and deflection at any level of the load.

1.4 Review of Literature.

1.4.1 Historical Background.

Although other forms of ferrocement may have existed earlier, credit for using it should go to Joseph Louis Lambot in France, who constructed a rowing boat from a net of wires and thin bars, and filled with cement mortar. This type of reinforcement was the one which was first used in reinforced concrete. However, it never gained much popularity in spite of that early start, and subsequent reinforced concrete design tended towards the use of heavier bars. In the First World War, large scale use of ferrocement was in ship building, using a combination of lightweight reinforced concrete and ferrocement.

In the early 1940's, P.L. Nervi in Italy "rediscovered" this technique. His reason for it was:

"The fundamental idea behind the new reinforced concrete material ferro-cemento is the well known and elementary fact that concrete can stand large strains in the neighbourhood of the reinforcement and that the magnitude of the strains depends on the distribution and subdivision of the reinforcement through the mass of the concrete (1).

In addition to the use of ferrocement in boat building, Nervi demonstrated successfully its use in roofs of buildings and warehouses.

In the 1960's ferrocement began to be used in many countries, not only in boat building but also in civil engineering structures. Countries like the Soviet Union, Czechoslovakia and some developing countries used ferrocement successfully in precast roofs and low cost housing. Because of the universal availability of the basic component materials of ferrocement and the low skill needed for the construction of the structural forms, developing countries took more interest in the material to be used as a general purpose structural material. The report (2) of the National Academy of Sciences on the uses of ferrocement in developing countries explored the potentials of ferrocement and opened many fields of application.

In 1976 an International Ferrocement Information Centre (IFIC) was established at the Asian Institute of Technology in Bankok, Thailand. The Journal of Ferrocement which is published by the Centre indicated the amount of attention drawn worldwide to ferrocement.

In early 1977, the American Concrete Institute (ACI) had set up Committee 549 on ferrocement to review the present state-of-the-art and possibly to formulate a code of practice for this material. Later, in April, 1978, a symposium on Ferrocement - Materials & Application was held at the Annual Convention of the American Concrete Institute in Toronto, Canada, and resulted in the publication SP-61 by the American Concrete Institute.

It is now clear that ferrocement, a versatile construction material, has bright prospects and will definitely find better utilization in the near future.

1.4.2 Definition of Ferrocement.

Although ferrocement has been in use since the 1940's, still, its definition is not yet established. The reasons for this may be several.

Firstly, the material has been considered as a form of reinforced concrete and therefore, there was no real need for its definition. Secondly, the lack of investigation on the material which meant that its potentials and superior properties are not known. Thirdly, the very many different types of reinforcement used in this material led to uncertainty of the established properties. Until more data is established about the material, ferrocement will have no exact definition. Ramouldi (3) stated "Among the more pressing problems relating to the development of ferrocement is the question of its very definition". In what follows, some of the available definitions of ferrocement are reviewed.

Bigg (4) reported that ferrocement definition according to the American Bureau of Shipping is "A thin, highly reinforced shell of concrete in which the steel reinforcement is distributed widely throughout the concrete, so that the material under stress, acts approximately as homogeneous material. The strength properties of the material are to be determined by testing a significant number of samples ...".

It has been argued that the words thin, highly reinforced, and homogeneous may suggest different meanings to different people.

The Russians (5) definition, which was also adopted by Bigg (4), emphasized on the subdivision of the reinforcement. The definition was: "True Ferrocement is considered to be a mesh reinforced mortar with a compressive strength of at least 39.3 N/mm^2 and a specific surface K (ratio of surface area of steel wire to the volume of the composite) between 2.0 cm^2/cm^2 and 3.0 cm^2/cm^3."

This definition seems to lack the description of the material itself. Moreover, the restriction in the specific surface of reinforcement requires more experimental verification.

Shah (6) defined ferrocement as a composite material which consists of wire mesh as reinforcement and mortar as matrix. The basic characteristics of this reinforcement is the higher bond due to small diameter wire mesh and higher surface area.

The definition by ACI Committee 549 (7) was: "Ferrocement is a type of thin wall reinforced concrete construction, where usually a hydraulic cement is reinforced with layers of continuous and relatively small diameter mesh. Mesh may be made of metallic materials or other suitable materials". In this definition, ferrocement is not confined to only steel wire mesh but other types of meshes as well. However, the definition ignores an important type of reinforcement currently in use in ferrocement, i.e. the combination of steel rods and wire mesh. In addition, it does not emphasize the properties of the mesh reinforcement. These properties, as will be seen later, are important factors in producing sections of superior properties to reinforced concrete.

It can be seen from the above discussion that research is needed before reaching a truly representative definition for ferrocement.

1.4.3 Ferrocement constituents.

1.4.3.1 Matrix.

The matrix of ferrocement is usually cement mortar, consisting of cement, sand, water and perhaps some additive. The matrix should have some or all of the following requirements, depending on the use of the structure. High compressive strength, impermeability, hardness, resistance to chemical attack, low shrinkage, and workability.

Most of the available specifications concerning the properties of the mortar used in ferrocement depend on observation and practical consideration of the ferrocement uses, with some aid from the knowledge on concrete technology. From a concrete technology point of view, the main factors which affect the properties of the mortar are:

1. Water:cement ratio.
2. Sand:cement ratio.
3. Gradation, shape, maximum size, and purity of sand.
4. Quality, age, and type of cement.
5. Additives.
6. Curing condition.
7. Mixing, placing and compaction.

The limits of the above factors are affected by the requirements of the mortar which in turn depend on the use of ferrocement. In marine structures more restrictions are generally required (5,6) than in civil engineering structures.

In most applications, high strength and low shrinkage are required and therefore low water:cement ratio, between 0.35 to 0.55 (7), should be used. Workability should be high and therefore a suitable compromise should be arrived at to increase the water content to take account of the decrease in strength. Rich cement mortar is required to give compressive strength between 35 to 50 N/mm^2. Additives have been used to reduce the water content. Proper gradation (9) of sand could help provide workable mixes. On the other hand gradation of ordinary sand, light weight sand, expanded shale, or vermiculite have no effect on the tensile strength of ferrocement (10).

Portland cement type I, II, III and V are all suitable (11), and the choice depends on the type of structure. The maximum size of sand depends on the type of reinforcement. Generally passing sieve No. 8 (size 2.4 mm) is adequate. Compaction and curing should be carefully controlled. All other factors to give good quality mortar should be considered.

The national Academy of Science (2) reported some of the properties of mortar required for the use of ferrocement in developing countries. Water: cement ratio w/c = 0.4 and sand:cement ratio s/c = 2 were recommended. Gradation is not important other than to produce better workability. Sand should not have excess of fine particles. Silt and organic materials should be removed.

1.4.3.2 Reinforcement.

Ferrocement reinforcement is characterized by high surface area as compared to those used in reinforced concrete. It usually consists of layers of continuous mesh. These generally result from the assembly of continuous filaments. Different types of meshes are available almost in every country in the world. The principal types of wire mesh currently being used are given below:

1. Hexagonal wire mesh.
2. Welded wire mesh.
3. Woven wire mesh.
4. Expanded metal mesh.
5. Three dimensional mesh (i.e. Watson mesh).

1. Hexagonal or chicken wire mesh: This mesh is readily available in most countries and it is known to be the cheapest and easiest to handle. The mesh is fabricated from cold drawn wire which is generally woven into hexagonal patterns. Special patterns may include hexagonal mesh with longitudinal wires.

2. Welded wire mesh: In this mesh a grid pattern is formed by welding or cementing the perpendicular intersecting wires at their intersection. Although this mesh may have the advantage of easy moulding into the required shape, it has the disadvantage of the possibility of weak spots at the intersection of wires resulting from inadequate welding during the manufacture of the mesh (11).

3. Woven Wire mesh: In this mesh, the wires are interwoven to form the required grid and the intersections are not welded. The wires in this type of mesh are not straight. They are bent in the shape of zig-zag lines and large angle of bending might cause cracks along the mesh (12). However, the moulding performance of this mesh is as good as the hexagonal and the welded wire mesh (11).

4. Expanded Metal Mesh: This mesh is formed by cutting a thin sheet of expanded metal to produce diamond shape openings. This type of mesh is not as popular as the previous three types and weight for weight comparison, it is not as strong as woven mesh, but on cost to strength ratio, expanded metal has the advantage (11).

5. Watson Mesh: A specially designed three dimensional space frame mesh. It consists of straight high tensile wires and a transverse crimped wire which holds the high tensile wire together. The high tensile wires are placed in two parallel planes and are separated by mild steel wires transverse to the high tensile wires. Most of the mesh wires are straight, without twists, crimps or welds. The result is a very strong mesh, and completely flexible to conform to any shape.

The above mentioned types of meshes are mainly metallic materials. Vegetable fibre and glass fibre meshes are also available. At the same time, there is a wide variation in the properties of each type of mesh. This includes different mesh size, strength, ductility, manufacture and treatment. Research shows that the properties of the resulting ferrocement product is affected by the properties of the mesh.

Steel rods have been used together with wire mesh in the reinforcement of ferrocement. The rods could be used for making the frame-work of the structure upon which layers of mesh are laid. Longitudinal and transverse rods usually vary in diameter between 4 to 9 mm and they are mainly of mild steel. Steel rods are sometimes used as main reinforcing component. Bezukladov et al. (5) reported that the middle third of the mesh in ferrocement members can be replaced by steel rods without affecting the structural performance of the member.

Finally, steel fibres have been used (13,14) with wire mesh reinforcement to enhance some of the properties of ferrocement.

1.4.4 Mechanical Properties.

1.4.4.1 General.

Ferrocement is often thought of as a variation of conventional reinforced concrete. However, Nervi's (1) description of ferrocement in which he identifies the material by the high subdivision and distribution of the reinforcement may be the basic difference between ferrocement and reinforced concrete. No theoretical support was provided by Nervi, but later on, the importance of the subdivision of reinforcement was confirmed by experimental and theoretical studies (15,16) on closely spaced wire reinforcement. In addition to the subdivision, the amount of the reinforcement was believed, from the early experiments on ferrocement, to be very important. Oberti (1) found that steel content of 120 to 240 kg./m^3 of mortar will not practically enhance the elongation of the mortar. But increasing it to a range of 480 to 640 kg./m^3 increased the elongation to 5 times that of the mortar.

Recently, the subdivision and amount of reinforcement have been described using the terms specific surface which is defined as the ratio of the surface area of reinforcement to the volume of the composite, and the fraction volume which is defined as the percentage of the volume of the reinforcement to the volume of the composite.

These two terms have been found (5,17,18) to give good correlation to the load response of ferrocement. Bezukladov (5) found that ferrocement superior behaviour compared to reinforced concrete can be achieved when the specific surface of reinforcement exceeds 2.0 cm^2/cm^3. However, in most previous practical uses of ferrocement, the reinforcement had less specific surface. This, in addition to the many available types of meshes may result in a confusing picture about the properties of ferrocement.

1.4.4.2 Behaviour under Tension.

1. Elasticity and Stress-Strain Behaviour.

The stress-strain curve is characterized (5,17,19) by three stages, see Fig.1.1, namely, the elastic stage, the cracked stage, and the yielding stage. In the elastic stage, both reinforcement and mortar behave elastically and there is no evidence of crack formation. This stage is followed by a transitory stage or the quasi-elastic stage (19) which is between the elastic and the cracked stages. In this stage the cracks propagate and multiply producing a curvilinear stage, leading to the start of a second linear stage. The range of quasi-elastic stage in ferrocement is longer than in reinforced concrete (19). The term first crack, used by many investigators, usually lies in this stage. In the cracked stage or elasto-plastic stage, the matrix suffers some plastic strain and cracks increase in number rather than width. However, the stress in reinforcement is still in the elastic limit. The yielding stage is characterized by yielding of reinforcement which results in increasing of the crack width, while the number of cracks has almost reached its maximum.

A more detailed definition of these three stages, in connection with the crack width and the tensile strain in the extreme fibre was given by Walkus (19). Fig.1.1 and Table 1.1 give details of these stages and the associated crack width and tensile strain values. These values require more experimental verification, bearing in mind that they are assumed to be the same for any ferrocement section. Such assumption may not be valid because of the expected differences in performance of ferrocement sections, depending on the characteristics of the reinforcement.

The modulus of elasticity, both in the elastic and elasto-plastic stages has been predicted (17) using the following equations which are based on the law of composite.

Table 1.1 Working Phases, Stresses and Strains of Ferrocement under tensile loading (4).

No. of phase	Strength Phase	Techno-logical Phase	Max.width of Cracks 10^{-3} mm	Stress KN/m^2	Unit Elongation micro-strain
I	Linearly Elastic	tight	-	-	-
Ia	Quasi Elastic		20	3230	200
Ib	Non-Linearly Elastic	non corrosive	50	3530	290
II	Elastic-plastic		100	4220	645
III	Plastic	corrosive	>100	-	-

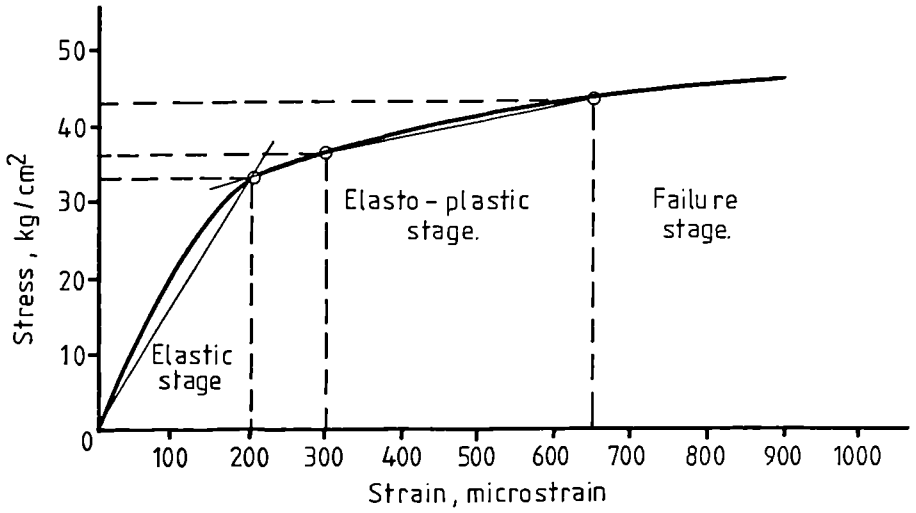

Fig. 1·1. Stress - strain curve for ferrocement under axial tension.(20)

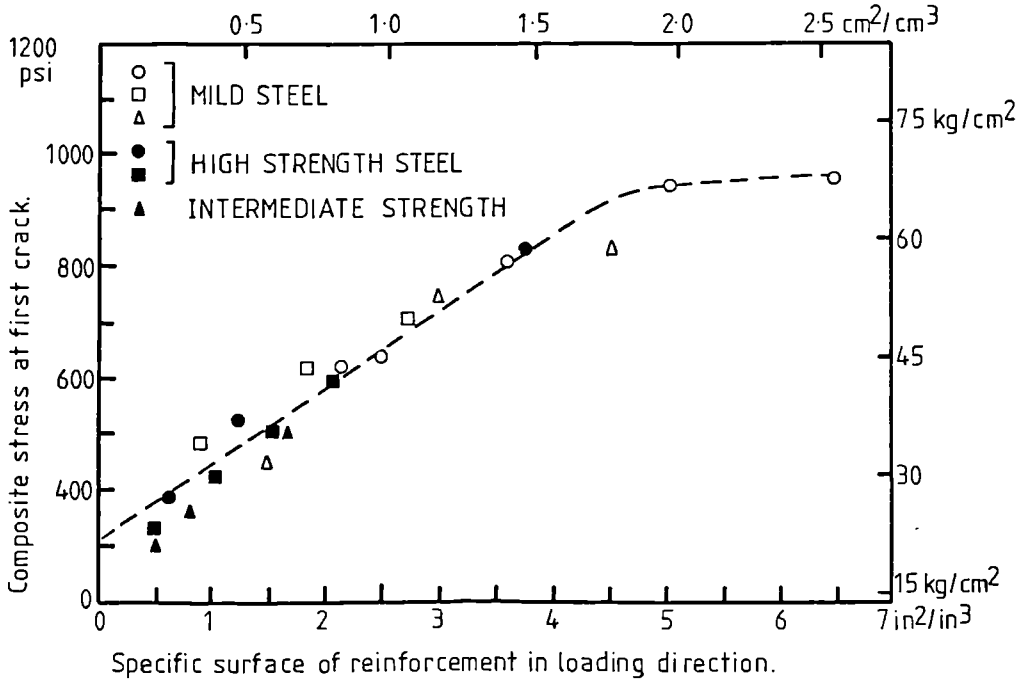

Fig. 1·2. Stress at first crack vs. specific surface of reinforcement. (17)

$$E_C = E_M V_M + E_{RL} \cdot V_{RL} \quad \text{(elastic stage)} \qquad (1.1)$$

$$E_C = E_{RL} \cdot V_{RL} \quad \text{(elasto-plastic)} \qquad (1.2)$$

where

E_C = Elastic modulus of the composite.

E_M = Modulus of elasticity of mortar.

E_{RL} = Elastic modulus of mesh.

V_{RL} = Volume fraction of longitudinal reinforcement in loading direction.

V_M = Volume fraction of mortar.

These equations, which take into account only the longitudinal reinforcement underestimate (17) the modulus of elasticity. A detailed analysis taking into account the orientation of the oblique reinforcing elements seems more appropriate for reinforcement like hexagonal mesh (11).

The characteristics of the stress-strain relationship are affected mainly by the characteristics of reinforcement, while rich mortar has no significant influence on it (5). Increasing the fraction volume of reinforcement (5,17) increases the modulus of elasticity. Increasing the specific surface increases (5) the stresses and elongation during crack formation. According to Bezukladov et al. (5), ferrocement should have specific surface of reinforcement between 2 and 3 cm^2/cm^3.

The stiffness of ferrocement is largely dependent on the geometry and ductility of reinforcement and independent of its strength. Cold worked reinforcement appears to give a stiffer composite than ductile mesh (21).

2. Cracking.

One of the best advantages of ferrocement is its cracking performance. Higher number of cracks with spacing as little as 5 mm result in smaller crack width and reflect the superior ferrocement performance compared to reinforced concrete.

The cracking behaviour was found (5,10,17) to be affected mainly by the properties of reinforcement including the reinforcement amount, type, ductility, proof stress, and spacing of transverse wires of the mesh. The specific surface, as a measure of the bond area, is an important factor. Increasing it results in smaller crack width and smaller crack spacing after failure (5,10,17,19,22,23). However,Nathan and Paramasivan (23) suggested that the cracking behaviour is influenced by the total bond stress between steel and mortar rather than just the bond area. This means that in addition to the specific surface, the proof stress of the reinforcement has also an influence on the cracking behaviour. In addition to the total bond stress, the ductility of reinforcement and the spacing of the transverse wires of the mesh affect the cracking behaviour. Increasing the ductility increases the crack width (10) and higher transverse wires spacing result in less number of cracks (24). Different types of meshes result in different cracking performances. For example, expanded metal mesh exhibits superior cracking performance compared to that of welded mesh.

The cracking behaviour is characterized by two stages. In the first stage, which follows after first cracking, the cracks increase in number with increase of load until they reach the ultimate or saturation limit. The second stage will begin then and is characterized by increase of the crack width more rapidly.

Based on the above description of cracking behaviour, Naaman (24) suggested equations to predict the crack width. The end of the above first stage was called the crack stabilization and the steel stress at the crack stabilization was calculated using the following equation:

$$f_{sta} = 20\ S_{RL} \leq 60\ KSi \quad \ldots\ldots \quad (1.3)$$

where

f_{sta} = The steel stress at crack stabilization, KSi .

S_{RL} = Specific surface of reinforcement, in^2/in^3.

The crack width prediction equations are as follows:-

For $S_{RL} \leq 3\ in^{-1}$

a) For any steel stress less than f_{sta}

$$W_{max} = \frac{1}{S_{RL}} \cdot \frac{f_{sta}}{E_R} = \frac{20}{E_R} \quad \ldots\ldots \quad (1.4)$$

Where E_R is the modulus of reinforcing system.

b) For steel stress larger than f_{sta} but less than yield strength

$$W_{max} = [6.9 + (f_s - f_{sta})] \frac{29000}{E_R} \times 10^{-4} \quad \ldots\ldots \quad (1.5)$$

For $S_{RL} > 3\ in^{-1}$ and, for any stress less than the yield strength or about 60 KSi

$$W_{max} = (15.5-3\ S_{RL})\ 10^{-4} \geq 0.0004 \text{ in.} \quad \ldots\ldots \quad (1.6)$$

3. Strength.

The investigations tend to define two strength values in the life of ferrocement specimen, namely, strength at first crack and strength at failure. From the previous discussion about the stress-strain relationship in tension, the first crack takes place in the transitory state which is a later stage beyond the elastic range. Therefore, the strength in the elasto-plastic stage has not been considered.

Bezakladov (5) found that the load at first crack increases with the specific surface of reinforcement up to a total specific surface of S_R = 3.0 to 3.5 cm^2/cm^3 after which reduction in the load takes place. Naaman & Shah (17), defining the first crack as the first deviation of linearity of the load-extension curve found that irrespective of the type and

size of the mesh the load at the first crack increases linearly with the specific surface of reinforcement, see Fig.1.2. From the figure it can be seen that the saturation limit of the specific surface takes place at S_L between 1.5 and 2.0 cm^2/cm^3, which is about the same range as that from Bezukladov. Increasing mortar strength was found (10) to have little effect on the strength at first crack. Attempts were made (25) to predict the strength at first crack based basically on the theory of reinforced concrete.

The ultimate strength is found to be dependent on the fraction volume of reinforcement and is not affected by the degree of dispersion. A one to one relationship has been reported by many authors (10,17,20,21,22,26) between the ultimate strength of the mesh and the ferrocement section. The ultimate strength does not depend on the thickness of the specimen or the strength of the mortar (21). It seems that it is basically a function of the properties of the reinforcing mesh and its orientation.

1.4.4.3 Behaviour under Compression.

Ferrocement behaviour in compression is reported (5,26,27,28) to be mainly affected by the mortar characteristics. Although the modulus of elasticity increases (28) with increase in the fraction volume of reinforcement, the ultimate strength is mainly determined by the compressive strength of the mortar.

Bezukladov et al. (5) reported that the specific surface and the fraction volume of reinforcement do not exert appreciable influence upon the compressive strength of ferrocement. Varying steel content from 0.7% to 2.8% increases compressive strength by 15% and this strength is determined chiefly by the prismatic strength of the mortar. Rao and Gowder (28) showed that the increase in the compressive strength with increase in percentage area of reinforcement is not significant and in any case steel area of more than 2-2.5% was not economical as it results in reduction in strength. Pama and

Lee (26) concluded, from tests, that the ultimate compressive strength of ferrocement depends on the fraction volume of mortar and is lower than that of equivalent pure mortar.

However, Johnston and Martar (21) showed recently that significant compressive strength gains can be realized by using mesh reinforcement in closed box or cylindrical arrangement which restrains the matrix. The transverse wires of the mesh contribute relatively more to the overall strength than the longitudinal wires, which is probably why the welded mesh showed better performance than expanded metal mesh.

Therefore, it seems that in addition to the mortar characteristics, the compressive strength is influenced by the type, orientation and mode of arrangement of meshes.

Both the modulus of elasticity and the compressive strength of ferrocement can be predicted using the composite theory (11).

1.4.4.4 Behaviour under Flexure.

1. Load-deflection and Stress-strain relationships.

The load-deflection and the stress-strain relationship for sections under bending are, as the case for section under tension, characterized by three stages (5,14,29,30,31), namely, the elastic, the elasto-plastic,and plastic stages. The end of the steeper linear portion of the load deflection curve corresponds to the first cracking of the mortar. No cracking was optically observed before this point, while the cracking was always observed soon after this load. The second part of the curve represents the elasto-plastic stage in which the multiple cracking takes place and the steel strain is less than the yield strain. The range and the slope at this stage increases with increase in steel content (22,31,32). The end of this stage is at the yielding of the steel which marks the beginning of the plastic stage.

The load-deflection curve can be idealized (26,29) to a trilinear curve with each of the above three stages considered as a straight line. Near ultimate load, the deflection can be approximated by an elastic-perfectly plastic bilinear analysis. Walkus (20) had divided the behaviour of ferrocement section under bending, as he did for section under tension, according to the serviceability and in connection with the crack width, see Table 1.2 and Fig. 1.1.

Table 1.2-Properties of ferrocement section under bending/ tensile zone (20).

Measured values	Technological State			
	Tight	Anti-corrosive I	Anti-corrosive II	Corrosive
Permissible width of micro-cracks (microns)	0-20	20-50	50-100	> 100
Stress, σ kg/cm^2	43	49.5	56	-
Unit elongation ε. 10^{-6}	130	325	650	-
Coefficient of deformability 10^{-3} . E, kg/cm^2	330	33	20	-

2. Cracking.

The cracking behaviour of ferrocement was studied mainly by observing the crack number at first cracking and at failure and the factors which influenced them. The more appropriate and systematic approach of measuring the crack width and separating the influences of the different factors on it, was neglected. Consequently, there are no experimental data to initiate or verify crack width prediction equations.

Recently, tests were carried out (24,31) to measure the crack width and present prediction equations for the crack width in connection with the factors considered. However, the amount of data in this field is far from

enough. In fact, from the above mentioned tests it was concluded (24) that extensive amount of work is required to decide the effect of the different factors on the cracking of ferrocement.

In general, it was believed that the cracking behaviour in bending is similar to that in tension (5,18,30). The subdivision, amount, type and ductility of reinforcement are the most important factors that affect the cracking behaviour. Increasing the specific surface decreases the crack width and spacing (30). Logan & Shah (18) presented a formula to predict the crack spacing depending mainly on the specific surface.

However, Naaman (24) from later tests, concluded that the specific surface did not seem to have as strong an influence on the cracking behaviour in flexure as in tension. This less pronounced effect found by Naaman could be explained by noticing that additional layers of meshes are placed away from the extreme fibre where the highest tensile stress takes place. Therefore they contribute less to the crack arresting mechanism which will be mainly provided by the outermost meshes. A more pronounced effect of the specific surface may be found by considering samples of different specific surface of the outermost layers.

According to Balaguru, Naaman and Shah (31), the crack width is mainly influenced by the strain level in the outermost layer of mesh and the spacing of the transverse wires as they are favourable positions for cracks.
A design equation based on the above mentioned two factors was suggested.

A more detailed review of literature about cracking behaviour can be found in Chapter 4.

3. Strength.

As in tension, the strength in flexure for a ferrocement member was considered at two stages of its life. They are the strength at first crack and the ultimate strength. Several methods were used to predict these

strengths and they all fall into one of the three theoretical models mentioned in sec. 1.4.5. A more detailed review of these methods can be found in Chapter 6. In any case, none of these methods is fully accepted as rationalized design method and more work is needed in this context.

The factors which influence the strength at first cracking and at failure are discussed separately as follows:

a. Strength at first cracking;-

There are several definitions of the first cracking load. Depending on the definition adopted, first cracking represents a certain point in the elasto-plastic stage of the life of the section. It is this non-uniqueness of the first cracking definition which has led to the uncertainty of the factors affecting it.

Some researchers(12,33) have found that the strength at first cracking increases with increase in steel content. Logan and Shah (18) concluded that the strength at first cracking increases with increase in the specific surface of reinforcement. However, Balaguru, Naaman, & Shah (31) could not find a clear relationship between the first cracking load and the specific surface.

It appears that the term first cracking itself is not suitable unless all are agreed on its definition. If it is defined as the instance of first movement of the existing flaws, then there is a doubt whether there is a factor, other than the ultimate tensile strength of the mortar, which will enhance it. But if it is defined as the instance in which a crack of a certain width appears, then the factors affecting the cracking behaviour will be expected to influence it.

It, therefore, follows that the term first cracking whenever used should be associated closely with its definition.

b. Ultimate Strength:-

The ultimate strength in bending is expected to reflect the combined influences of factors governing the tensile and compressive strength. Therefore, and as far as reinforcement is concerned, the amount, type, orientation and inherent geometry of the reinforcing meshes, in addition to their position relative to the neutral axis and to each other, are factors influencing the ultimate strength. As for the mortar,its strength was found to be of relatively little importance (34) on the ultimate bending moment . Thus, a mortar of medium compressive strength of 35 to 50 N/mm^2 is adequate (5,34). The thickness of the section has little influence on the ultimate strength, aside from the influence of depth as expected from analytical principles (34).

It follows, therefore, that the reinforcement characteristics have the greatest influence on the ultimate bending strength. Increasing the reinforcement content increases the ultimate strength (5,12,32,33,35), but the specific surface has no effect on it (5). The type of mesh also affects the ultimate strength. For example, members reinforced with expanded metal or welded wire mesh of a given cross-sectional area and used in their normal orientation, perform better than those reinforced with woven wire mesh or standard bars of the same cross-sectional area.

Orientation and geometry of the mesh have a significant effect on the ultimate strength. ACI Committee 549 (7), reported that different meshes exhibit weaknesses in different directions and therefore orientation becomes particularly important when strength under biaxial loading is considered. Expanded metal mesh imparts a considerable weakness in the secondary direction (34). Welded wire mesh, while having equal strength in both longitudinal and transverse directions, has weakness along planes at 45^{o} to the directions of the wires. Large weaving angles in woven wire mesh result in cracks along the mesh (12). This could result in premature failure.

In ferrocement, unlike in reinforced concrete, uniform distribution of the mesh along the section gives better ultimate strength than concentrating them near the fibres (34).

The steel strength was reported (34) to have relatively minor importance in the ultimate strength and it is controlled by the degree of cold working employed in the manufacturing process of the mesh. This result seems to be illogical especially for specimens reinforced with small numbers of meshes where flexural failure takes place due to fracture of the mesh (12).

1.4.4.5 Behaviour under Shear and Torsion.

Very little information is available about the shear strength of ferrocement, perhaps because ferrocement is generally used in thin panels where the span-depth ratio in flexure is large enough so that shear does not govern failure. In any case, the parallel and longitudinal alignment of the reinforcing layers in ferrocement precludes the inclusion of shear reinforcement equivalent to the bent up bars or stirrups used in reinforced concrete, so ferrocement is not suited to resisting shear.

Collen & Kirwan (35) reported that the ultimate shear strength increases with increase in steel content. For the woven wire mesh used, the maximum shear strength obtained was at steel content of 513 kg/m^3 and it was equal to 8.5 N/mm^2. Bezukladov et al. (5), from tests on ferrocement plates with in-plane shearing forces, obtained stress-strain curves which were characterized by two straight line stages. They found that the shearing modulus in the first stage was influenced by the specific surface of reinforcement, while in the second stage it was almost the same for the different series.

Pama et al. (26) suggested analytical expressions, based on the theory of law of mixture, to calculate the shearing and torsional rigidities. The experimental results from bending and anticlastic slabs and torsion on tubes tests were used to support the analytical expressions developed and

to show the success of the approach. They concluded that the elastic constants in the uncracked range for ferrocement are not much different from those of the mortar.

1.4.4.6 Behaviour under Fatigue and Impact.

1. Fatigue.

The fatigue behaviour of ferrocement is very important. Most of the structural members will be subjected to a certain type of repeated loading. Picard and Lachance reported (36) that the load which causes failure on a ferrocement member after $1x10^6$ cycles was only 27% of the ultimate load. Also, residual deflection during the unloading of the first cycle was noticed and this deflection increases with increase in the amplitude of the loading cycle. It is, therefore, essential to establish enough data on fatigue behaviour of ferrocement before setting its serviceability criteria.

Preliminary flexural fatigue tests by Wind Boats Limited (37) showed the following results:

Sample	Nominal stress level kg/cm^2	Cycles	Remarks
A	+ 44 to - 38.3	$2x10^6$	Cracked
B	+ 49.3 to - 42.3	$2x10^6$	No fracture
C	+ 77.5 to - 77.5	$1x10^5$	Cracked
D	+ 83.5 to - 83.5	$1x10^5$	Cracked

It was reported (11) that Karasudhi, Mathew, and Himityongskul (in their fatigue tests) showed that the fatigue strength of ferrocement is dependent on the fatigue properties of the reinforcement including both the wire mesh and the skeletal steel. The load-cycle curves for ferrocement specimens reinforced with three different meshes were given in the following form:

$$\text{Log}_{10} N = 12.27 - 0.128S \text{ (Welded wire mesh)} \quad \ldots\ldots\ldots \quad (1.7)$$

$$\text{Log}_{10} N = 7.417 - 0.031S \text{ (Expanded metal mesh)} \quad \ldots\ldots \quad (1.8)$$

$$\text{Log}_{10} N = 9.750 - 0.073S \text{ (Hexagonal wire mesh)} \quad \ldots\ldots\ldots \quad (1.9)$$

where N and S denote the number of cycles to failure and the maximum repeated load expressed as percentage of the ultimate static load.

Using equation 1.7 (for welded mesh) on data from Picard & Lachance (36) gave S = 49% while the experimental value was 27%. This indicates that there are other factors apart from the type of mesh which affect the load-cycle curves.

McKinnon and Simpson (38) reported that ferrocement specimens reinforced with ungalvanized welded mesh, and water cured showed better flexural fatigue results than those reinforced with galvanized welded mesh and steam cured. The deterioration in the fatigue properties due to galvanization of the mesh was confirmed by Bannet et al. (39).

Balaguru, Naaman and Shah (40) suggested an analytical model to predict the fatigue properties of ferrocement from the fatigue properties of its constituents, i.e., mortar and reinforcement. Expressions for the increase in the crack width and deflections, and the deterioration of the flexural rigidity due to repeated loads, were given. These expressions desparately require more experimental verification.

Singh (41), recently, from the comparison of his and other investigators' results, found that performance of ferrocement under repated loading is a function of such factors as:

1. Amount, type and disposition of reinforcement.
2. Mode and method of testing as well as criterion of failure.
3. Specimen form and size.
4. Type of cement and method of curing.

2. Impact.

Because of the importance of the impact resistance in the application of the material in marine structures,impact tests were some of the very early experiments carried out on ferrocement. Impact tests (37) on ferrocement

slabs demonstrated the high impact resistance of the material and showed that failure did not consist of the development of an actual hole in the slab, but rather a weakening of the wire mesh and a relatively dispersed breaking away of the mortar. This property is one of the advantages which encouraged the use of ferrocement in boat building. Impact tests to compare the performance of ferrocement with reinforced concrete were carried out by Bezukladov et al. (5). They found that a 25 mm thick ferrocement plate could give the same impact strength as 50 mm thick reinforced concrete plate.

Shah and Key (10) carried out impact tests to investigate the effect of the specific surface and tensile strength of the mesh.The rate of flow of water through the sample was used to measure the damage in the specimen due to impact loading. They found that the higher the specific surface or the tensile strength of the mesh, the lower the damage induced by impact loadings. Nathan & Paramasivam (23) carried out tests and showed that increasing the fraction volume of reinforcement increases the absorbed energy required to cause impact failure. It was reported (13,42,43) that inclusion of short steel fibres with wire mesh reinforcement in ferrocement greatly enhanced the impact strength.

1.4.5 Theoretical Models.

The theory governing the ferrocement has not been established yet. The state of knowledge and the experimental data available about the material are still in the stage of exploring its different properties. However, several theoretical models were used in predicting some of the mechanical properties of ferrocement. Most of these models fall into one of the following three main categories:

1. Using the theory of composite materials, mainly developed by Pama (11,26). This approach was used in predicting several mechanical properties of ferrocement. It considers ferrocement as composite material

consisting of mesh as reinforcement and mortar as a matrix. The skeletal bars are usually neglected.

2. Using reinforced concrete analysis. In this approach, the theory of reinforced concrete is used in analysing the section and mostly to predict the flexural strength.

3. Models based entirely on experimental results. A typical example of the use of this approach is that of Walkus (30,44). Section behaviour is divided into several stages and the mechanical properties found experimentally were fixed at these stages. This approach has the disadvantage of limitation inflicted by the limitation of the experimental programme.

None of the above approaches has proved to be fully adequate for the analysis of ferrocement and many theoretical models developed for the material still require further experimental confirmation. Therefore, ferrocement requires much more work before the development of its theory can be arrived at.

1.4.6 Practical Applications.

During the past ten years, ferrocement application has been extended widely. This was specially helped by publishing a report on the uses of the material in developing countries by the National Academy of Sciences (2) of the United States of America. The report explored the many advantages of the material like ease of fabrication, low skill and adaptability of the material for complicated shapes. On the other hand research progress helped developed countries to find many new potential uses of the material.

In marine applications, it includes a wide range of boat building varying in size between 10 to 30 m. It also includes (11), docks, buoys, floating breakwaters, submarine structures, floating and submerged oil reservoirs, offshore tanker terminals, floating bridges and others.

The in-land applications of the material, both in developing and developed countries, vary widely. The developing countries, making use of

the low skill required and the availability of the constituents, used the material in low cost housing, roofing, grain storage bins, agricultural buildings and similar applications (11,45). In developed countries applications include shell structures, water tanks, tunnel lining, permanent formwork, etc.

A good amount of literature is available (46,47,48) on both the possible applications of ferrocement and its manufacturing techniques. Moreover, it would be expected that the material will find even a greater range of application when its characteristics and theoretical prediction are fully established.

CHAPTER 2.

PROPERTIES OF MATERIALS AND MIX DESIGN.

2.1 Introduction.

Ferrocement is a composite material with cement mortar as the matrix and steel mesh as the reinforcement. The properties of any composite material are determined by the properties of the reinforcement and the matrix. Therefore, in order to understand the behaviour of the composite material, it is essential to establish the properties of its constituents.

In ferrocement, although the properties of the reinforcement have a more dominating effect on the behaviour of the composite, the properties of the mortar, such as compressive strength, shrinkage, durability, and permeability also control important properties of the resulting ferrocement. In addition, the nature of the reinforcement requires the mortar mix to be very workable in order to penetrate through the several layers of wire meshes and produce well compacted elements. On the other hand, the water content should be limited to reduce shrinkage. Therefore, the mortar mix should be designed carefully. Although the concrete technology provides extensive knowledge about mortars, its use in ferrocement requires a flexible approach in the use of that knowledge. At the same time, research on mortar for ferrocement is essential to obtain the best product.

In this Chapter, the properties of the materials used in this study were established. Several trial mixes were studied to reach the most suitable and economic mix to be used in the main experimental programme. The properties of the hardened mortar were then determined from that mix.

2.2 Properties of Reinforcement.

It has been established, in the review of literature, Chapter 1, that the reinforcement characteristics in ferrocement represent one of the most

influencing factors on the behaviour of the composite material. These characteristics may include the type, geometry, orientation, and mechanical properties of the mesh and bar reinforcement. The mechanical properties of the bar reinforcement can be established from standard tests used in reinforced concrete. Unfortunately, there are no such standard tests for the mesh reinforcement and different investigators used different tests. In this study, galvanized steel woven wire mesh and steel bars were used as reinforcement. The properties of the two types of reinforcement are discussed separately.

2.2.1 Steel Bars.

Mild steel bars 6 mm. in diameter were used. The mechanical properties were obtained from three tensile specimens tested in an Amsler machine. Fig. 2.2 shows a typical stress-strain curve for the bar. The strain was measured over a gauge length of 50 mm. using an extensometer placed at the central portion of the tested bar. Table 2.1 shows the average values for the properties of the three bar specimens tested.

2.2.2 Wire Mesh.

Three different types of woven steel wire mesh were used. All were galvanized with wire diameter equal to 0.914 mm. Two of them were of mild steel with mesh opening of 5.45 and 6.34 mm. respectively. The third type was of high tensile steel with mesh opening of 5.45 mm.

It was felt that the mechanical properties of the mesh should be obtained from tensile tests on a piece of mesh rather than a single wire taken from the mesh. Tests on single wires ignore the effect of the transverse wires in the mesh. Preliminary tensile tests showed that a single wire straightened itself completely near failure, while in the mesh test, the wires in the mesh were still zig-zag shaped, indicating that even at failure transverse wires prevented complete straightening of the longitudinal wires

and therefore should have an effect on the stress-strain curve.

Three specimens for each type of mesh were cut with the longitudinal direction along the longitudinal direction of the mesh in the ferrocement specimen. Hounsfield Tensometer machine (Plate 2.1) was used to perform the test. The mesh specimen was 300 mm. long and 50 mm. and 100 mm. wide at the strain measurement portion and at the grips respectively, Fig.2.1.A. Specially designed grips were used. Each grip consisted of two steel plates and the mesh specimen was sandwiched between these two plates. Plastic padding was used to bond the mesh to the grips and ensure uniform loading on it. The grips were attached to the testing machine with specially made attachment to ensure axial load on the specimen. Fig.2.1.C and Plate 2.2 show the gripping details.

To fix the mesh specimen to the grips, a mould (Fig.2.1.B), with the same dimension as the specimen, was used to ensure axial alignment of the mesh. One plate of each grip was first placed in position in the mould. A layer of plastic padding was then applied on each plate. The mesh was then put in position and the second plate of each grip, covered with a layer of plastic padding, was tightly pushed on top of its twin plate. A pin was pushed through the two holes of the twin plates to ensure perfect alignment. The specimen was left then for a few hours for the plastic padding to set and be ready for testing.

The strain measurements were taken using a 100 mm. mechanical demec gauge, with the demec points fixed on the grips as shown in plate 2.2. The gauge length of the mesh was 95 mm. and, therefore, the strain measurements from the demec gauges were adjusted by multiplying them by the ratio of the demec gauge length to the mesh gauge length. Plate 2.1 shows the tensile specimen mounted on the testing machine. In addition to the load and strain measurement, the load-extension graph for each test was obtained from the testing machine.

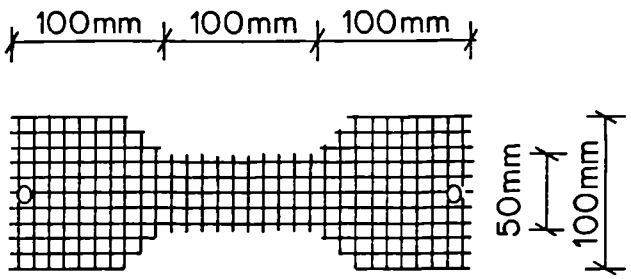

a) Shape of mesh test specimen

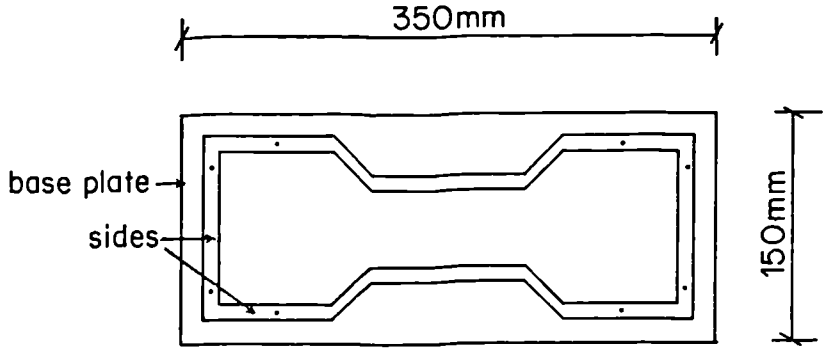

b) Perspex mould for fixing grips

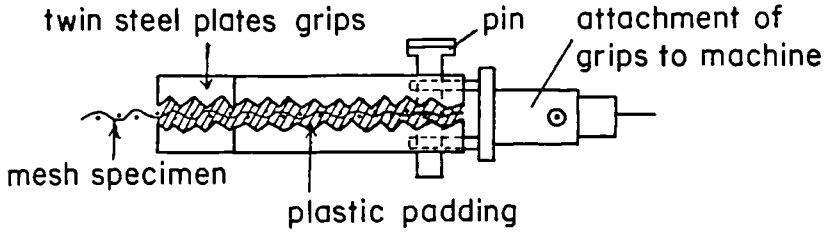

c) Details of gripping of mesh specimens

Fig2.1 Details of mesh tensile specimen

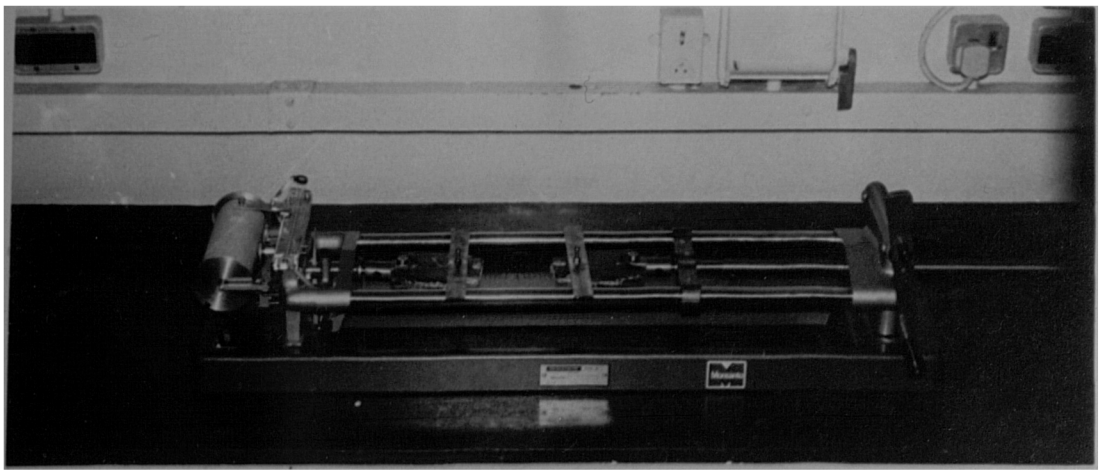

Plate. 2·1. Hounsfield Tensometer machine.

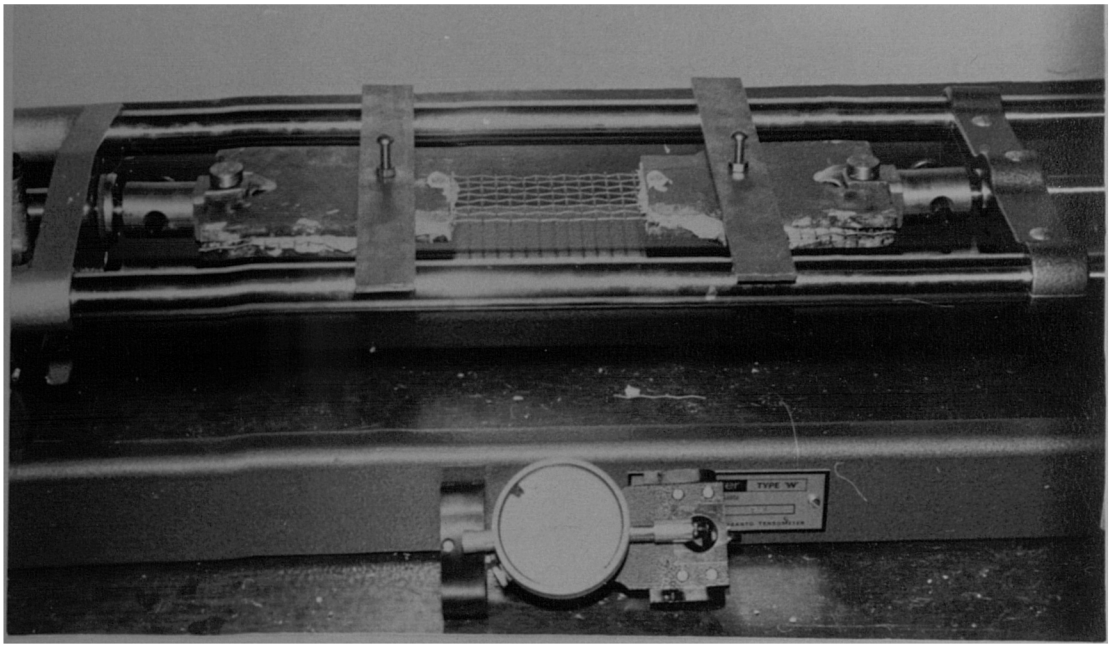

Plate. 2·2. Mesh tensile test.

Plate. 2·3. Steel plate tensile test to check grippings.

To check the efficiency of the plastic padding in preventing slippage in the grips of the mesh during testing, a tensile specimen was made by replacing the mesh with a steel plate. The steel plate was 5 mm thick and the other dimensions were the same as those of mesh specimen. The steel plate specimen was tested in the same machine and under the same range of loads. At different levels of loadings, the strain was measured on the steel plate and between the grips using mechanical demec gauges, Plate 2.3. There was no appreciable difference between the two strain readings. Therefore it was concluded that plastic padding was successful in preventing mesh slippage from the grips.

It was noticed that in the tensile mesh test, not all the wires of the mesh were cut simultaneously at failure. Therefore, single wires taken from each type of mesh were tested for their ultimate loads. The ultimate strength from the single wire tests was 2 to 4% higher than that obtained from the mesh tests. Hence the ultimate strength from the two tests could be considered practically the same.

The average values of some of the mechanical properties for the three types of meshes are given in Table 2.1. Figs. 2.2 and 2.3 show the stress-strain curves for these meshes. It is to be noticed that the modulus of elasticity for the mesh was less than the usual value for steel. This could be attributed to the nature of the woven mesh, where a certain amount of the extension under load is due to the straightening of the zig-zag shaped wires. Naaman (24) reported that the modulus of elasticity of woven wire mesh varies considerably and the term apparent modulus of elasticity was used instead.

2.3 Properties of Mortar Matrix.

2.3.1 Cement.

Ordinary Portland cement was used throughout the investigation. The cement was considered to comply with B.S.12 (49).

Table 2.1 Results of reinforcement tensile tests.

Type of Reinforcement	Ultimate Strength N/mm^2		Modulus of Elasticity N/mm^2		Yield Strength N/mm^2					
					0.2% offset		0.0035 strain		0.005 strain	
	Average	Range	Average	Range	Average	Range	Average	Range	Average	Range
Mild steel wire mesh mesh opening 5.45 mm wire dia. 0.914 mm	348.6	350.7 to 348.	91.4×10^3	89.57 to 94.5×10^3	209.5	205.7 to 213.4	197	191.5 to 201.2	218.4	213.6 to 220.5
Mild steel wire mesh mesh opening 6.34 mm wire dia. 0.914 mm.	331.3	326.6 to 337.5	110.3×10^3	108.1×10^3 to 112.5×10^3	225.9	219.9 to 235.2	219.1	212.2 to 228.7	246	241.2 to 252.9
High Tensile Steel wire mesh opening 5.45 mm wire dia. 0.914 mm.	1197	1190 to 1204	92.1×10^3	91×10^3 to 93.2×10^3	553	543 to 564	287.7	268.7 to 303.	394	379 to 406.5
Mild Steel Bar. Dia.=6 mm	469.6	469.2 to 469.9	207.4×10^3	201.2×10^3 to 213.6×10^3	302.9		303.1 to 303.2			

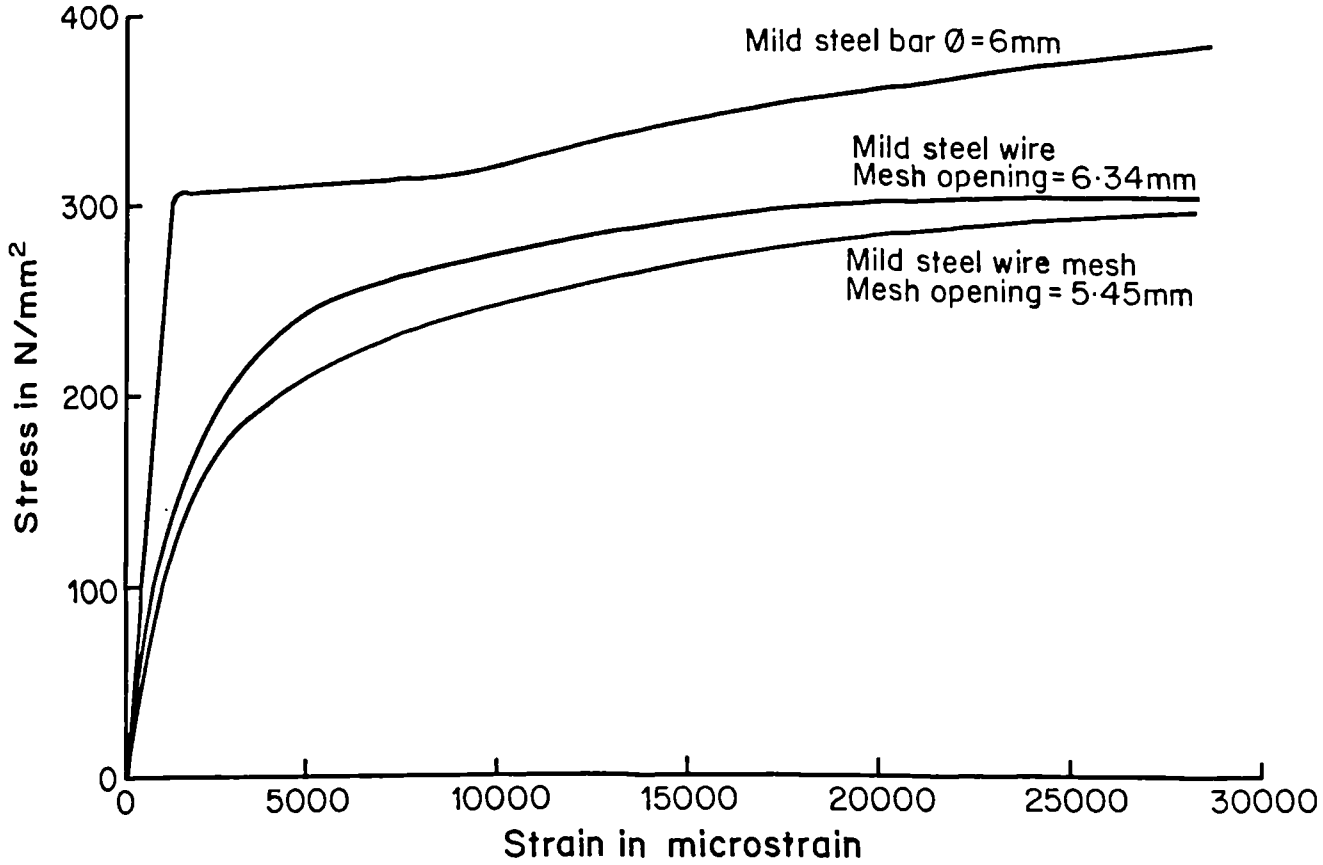

Fig2.2 Stress - strain relationships of the steel bars and mild steel meshes

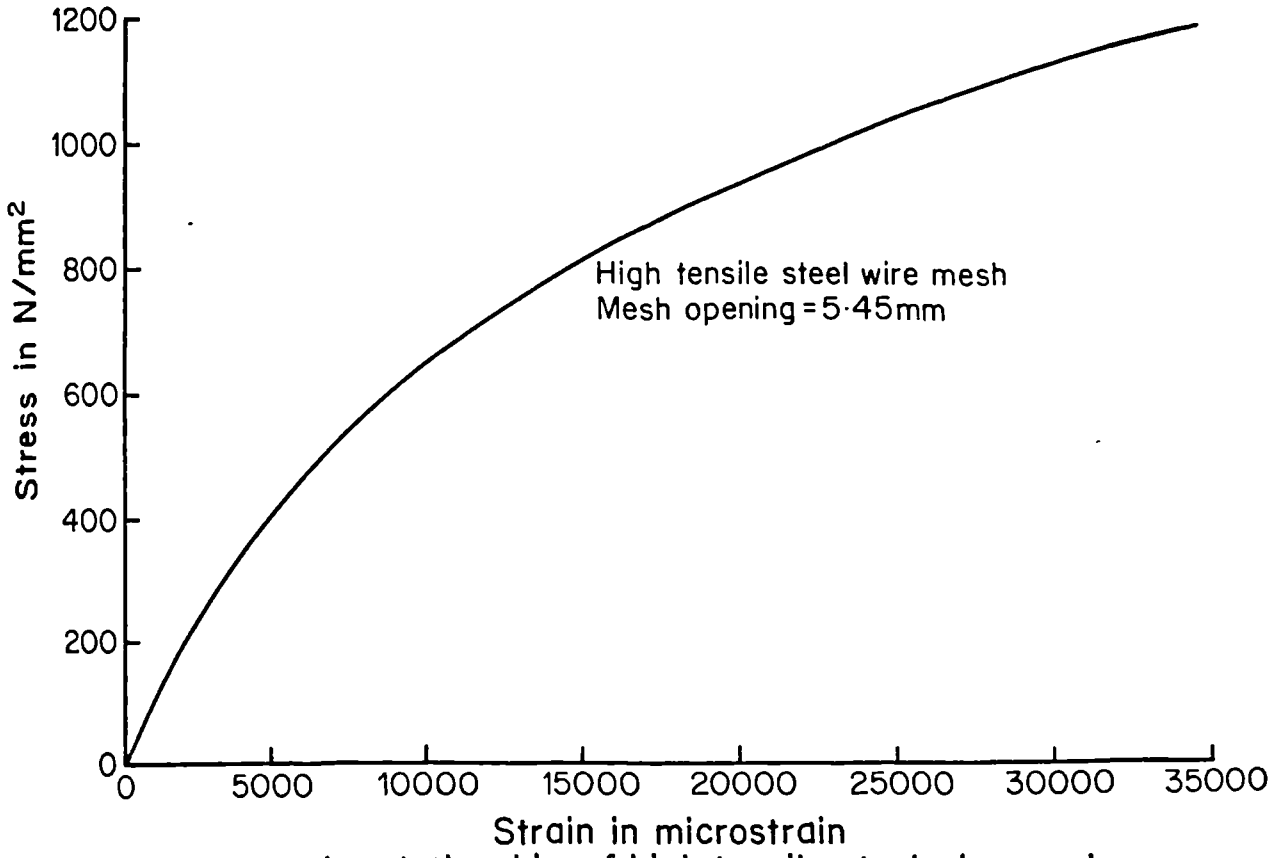

Fig 2.3 Stress - strain relationship of high tensile steel wire mesh

2.3.2 Fly Ash.

The fly ash used was obtained from the Ferry Bridge Power Station. The chemical composition as given by the supplier is shown in Table 2.2. The figures shown complied with B.S. 3892: 1965 (50) limits.

The fly ash was used in this investigation to replace a certain percentage of the cement and sand as will be shown in the section on mix design.

Table 2.2 Chemical composition of fly ash.

Compound	Symbol	% by weight	B.S.3892 limits
Silica	SiO_2	56.2	-
Alumina	Al_2O_3	26.2	-
Iron	Fe_2O_3	7.3	-
Titanium	TiO_2	1.0	-
Phosphate	P_2O_5	0.3	-
Calcium	CaO	1.6	-
Magnesium	MgO	0.7	4% Max.
Potassium	K_2O	2.5	-
Sodium	Na_2O	1.3	-
Sulphate	SO_3	0.7	2.5% Max.
Loss on ignition	-	2.2	7% Max.

2.3.3 Sand.

Washed natural river sand, of the same delivery batch was used throughout the investigation. The sand was sieved through sieve No. 14. Table 2.3 gives the sieve analysis results of the sand. All sand was dried thoroughly in a rotating furnace before use.

Table 2.3 Sieve analysis results for the sand.

B.S. Sieve size	Sieve opening	Percentage passing
14	1.2 mm	100
25	600 μm	86.5
52	300 μm	25.4
100	150 μm	2.9
200	75 μm	1.2

2.4 Mix Design.

Two main requirements are essential for mortars used in ferrocement. First, low shrinkage and relatively high strength are desirable which requires low water:cement (w/c) ratio and relatively high cement content. Second, high workability is required for the mortar to penetrate through several layers of wire mesh during casting. High workability can be achieved by increasing water:cement ratio which defies the first requirement. Alternatively, additives can be used to enhance the workability of the mix.

In concrete, Fly Ash has been used as an economical material to substitute a certain percentage of the cement. Swamy and Stavrides (51) have shown that fly ash increases the workability and cohesiveness of the mix.

Since ferrocement mortars require a relatively high cement content, fly ash could be suitable as an economical material to substitute partially the cement in the mix and at the same time to increase its workability. An experimental programme was set out to investigate the effect of fly ash on the mortar mixes and to obtain a mix with a cube strength between 35 and 48 N/mm^2 and workable enough to penetrate through up to ten mesh layers without excessive vibration and produce a well compacted product.

2.4.1 Experimental Programme.

The experimental programme consisted of 11 trial mixes. These were divided into 3 main groups. In the first group, the mixes consisted of water, cement and sand only. The proportions of the mixes were varied to study the effect on the workability and the compressive strength of the mix. In the second group, fly ash was used to replace partially the cement or the cement and sand content in the mixes. The variables were the mix proportions and the amount of replaced cement and sand, including the method of calculating that amount. The cement is usually partially replaced by equal weight of fly ash. However, the sand could either be replaced by equal

volume or by equal weight. The third group included mixes of approximately equal w/c and s/c ratios, but with different additives. One had no additives, the other had fly ash and the third had Febflow as water reducing agent. Febflow is a brown liquid (S.G. about 1.2), non toxic, containing no chlorides or nitrates. The manufacturer recommended a dosage of 3.26-6.7 gm/ Kg of fines (cement or cement + pfa). The amount used in this study was equal to 3.4 gm/1 Kg of cement. Details of all trial mixes are given in Table 2.4.

All the mixes were batched in a horizontal pan type mixer. Mixing procedure was according to ASTM (C305-65) (52) of mixing mortar. Details of this mixing procedure are given in sec. 3.5.3.

For each mix six 50 mm cubes were cast. The workability of the mix was observed visually and described according to its suitability for casting ferrocement specimens. Experience on the required workability was gained from the casting of the preliminary ferrocement specimens. The cubes were kept in a fog room until the date of testing. They then were tested in compression at a stress rate of 15 N/mm^2 according to B.S.1881 part 4 (53). Three of the six cubes were tested at the age of 7 days while the other at the age of 28 days.

2.4.2 Discussion of Results.

The cube strength results together with observed workability are shown in Table 2.4.

From the results of trial mixes TM1-4, the following observations can be made:

1. For mixes with no additive (only cement and sand), better workability was achieved, without increasing w/c, by increasing the amount of cement in the mix (see results of mixes TM1 and TM2). However, this resulted in undesirable increase in the compressive strength.

Table 2.4 Properties of trial mixes.

Trial Mix No.	Mix proportions before replacement by pfa		Amount and method of replacement by pfa		Mix proportion after replacement by pfa			Cube Strength N/mm^2		Workability
	w/c	Cement/ Sand	Cement %	Sand	w/c	$\frac{w}{c+pfa}$	pfa : C : S	7 days	28 days	
TM1	0.46	1:2.3	-	-	0.46	0.46	0:1:2.3	44.2	57.6	Very low
TM2	0.46	1:1.75	-	-	0.46	0.46	0:1:1.75	54.9	72.7	Good
TM3	0.4	1:1.5	15% by weight	-	0.54	0.46	0.18:1;1.75	44.9	61.5	high water content
TM4	0.48	1:2	20% by weight	10% by weight	0.60	0.4	0.50:1:2.25	43.7	58.0	very good
TM5	0.54	1:1.75	30% by weight	20% by weight	0.77	0.4	0.94:1:2	31.7	46.0	good water can be reduced
TM6	0.46	1:2.5	20% by weight	10% by volume	0.575	0.4	0.44:1:2.8	42.9	54.3	low
TM7	0.52	1:2.5	20% by weight	20% by volume	0.65	0.4	0.63:1:2.5	47.6	63.4	very good
TM8	0.45	1:2.5	-	-	0.45	0.45	0:1:2.5	46.4	62.0	low
TM9	0.45	1:2.5	- Feb Flow added	-	0.45	0.45	0:1:2.5	44.1	58.8	low to good
TM10	0.61	1:3	20% by weight	20% by volume	0.765	0.45	0.7:1:3	32.5	49.8	very good (water can be reduced)
TM11	0.54	1:3	20% by weight	20% by volume	0.71	0.42	0.7:1:3	34.2	50.8	very good

2. Introducing pfa to the mixes (mixes TM3 and TM4) enhanced the workability. Comparison between TM1 and TM4 shows that, at least, no loss of strength was suffered through addition of pfa.

Therefore the results from the first four mixes demonstrate the advantage of pfa. However, different investigators (51,54,55) have recommended different percentages of the cement or the cement and sand of concrete mixes to be replaced by pfa. In mixes TM3 to 7, the percentages of the replaced cement or cement and sand were varied. Also, two methods to calculate the weight of the replacing pfa were used. The first method was by replacing a percentage of the cement or cement and sand by weight. The second method was by replacing a percentage of the cement by weight and a percentage of the sand by volume. The second method was suggested by Jackson and Goodridge (54). They recommended a conversion factor equal to 0.6 which if multiplied by the weight of sand to be replaced will give the weight of the replacing pfa.

From the results of mixes TM3 to 7 the following observations can be made.

1. Mix TM5, which has pfa to cement ratio of 0.94 gave relatively low early strength. However, the high early strength was regained in mixes with pfa to cement ratio of 0.5 and 0.63 (mixes TM4 and TM7).

2. Replacement of 20% by weight of cement and 20% by volume of sand, by pfa, mix TM7, gave the best results.

3. Comparing the results of mixes TM1 and TM7 it can be seen that using pfa did not only enhance considerably the workability but also increased the compressive strength.

From the results of mixes TM7, TM8, and TM9 it can be seen that addition of pfa (TM7) gave better results than addition of Febflow (TM9) in both strength and workability. Also, addition of pfa resulted in an increase

in the strength of the mix compared to that with only cement and sand (TM8).

Mixes TM10 and TM11 were tried to reach the mix which fullfils the requirements for this investigation. The required mix was TM11 with pfa:c:s proportion equal to 0.7:1:3 and $w/(c+pfa) = 0.42$.

2.5 Properties of the Hardened Mortar.

The mix chosen in the previous section was used throughout the experimental programme of this study. Therefore it was essential to find some of the properties of the hardened mortar of the mix. These properties included compressive strength, flexural strength and static modulus of elasticity.

2.5.1 Compressive strength.

The compressive strength at different ages of the mortar was determined from 50 mm cubes. Mixing was carried out according to ASTM C305-65 (52). Casting was carried out on a vibrating table. A fog room was used for curing of the cubes. Compression test was carried out at stress rate of 15 N/mm^2 according to B.S.1881 part 4 (53). At each age, 3 cubes were tested. The test results are shown in Fig.2.4. From the figure it can be seen that most of the strength will be gained in the first year and the ratio of strength at 700 days to that at 28 is about 1.7. The strength at 7 days is about 0.66 of that at 28 days.

2.5.2 Flexural strength.

Six specimens size 500x100x25 mm were cast. Mixing and casting procedure were the same as that of specimens for compression test. At the age of 28 days flexural test was carried out under third point loading with a span equal to 450 mm. The stress rate was equal to 1.6 N/mm^2 per min according to B.S.1881 part 4 (53). The average value of the modulus of rupture for these specimens was equal to 4.3 N/mm^2 and S.D.= 0.53 N/mm^2. To

determine the other flexural properties of the mortar, specimens size 1000x300x25 mm were cast and tested at the age of 28 days under third point loading. These tests are included in the main test programme and their details and results will be discussed in the following chapters.

2.5.3 Static Modulus of Elasticity.

Three prisms size 50x50x150 mm were cast by the same procedure as specimens for the compression test. At 28 days the prisms were tested according to B.S.1881, part 4 (53). The average value of the static modulus of elasticity for the three specimens was equal to 25.1 kN/mm^2.

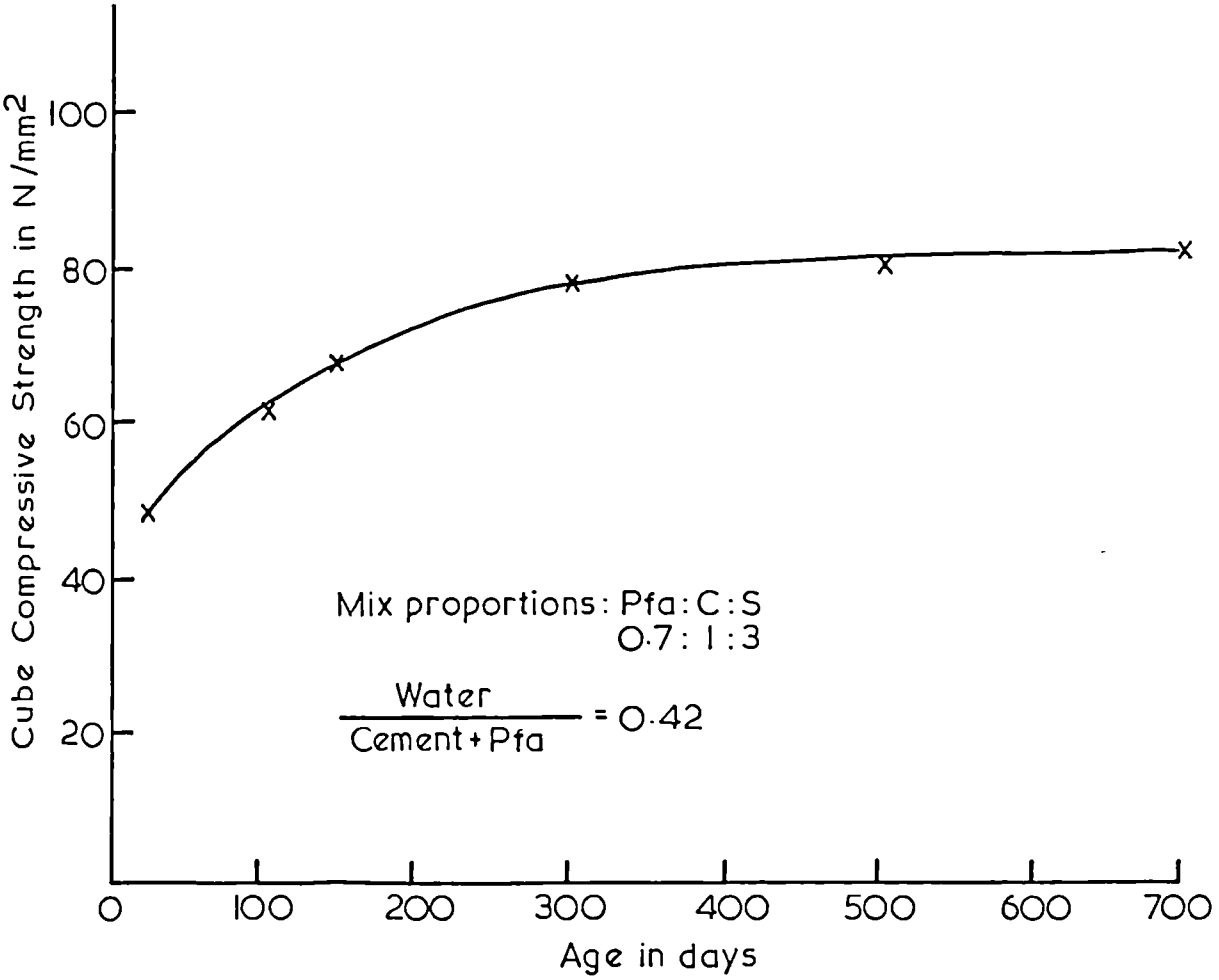

Fig. 2·4. Relationship between Cube Compressive Strength and Age of Mortar.

CHAPTER 3.

EXPERIMENTAL PROGRAMME.

3.1 Introduction.

In spite of the extensive amount of work carried out on ferrocement, its flexural behaviour is far from being clear. The literature review shows that the work on the flexural behaviour lacks two main aspects - firstly, the study of its basic features, namely the cracking, deformation and strength in relation to each other, and secondly, identifying quantitatively the factors which affect this behaviour. Research in this direction will not only help the settling of the design theory for ferrocement, but also assist in finding the optimum form of the material.

As the structural behaviour of the ferrocement section differs according to the type of the reinforcing mesh, it is essential to study the flexural behaviour of ferrocement reinforced with each type of mesh separately. In this study, only woven steel wire mesh was considered.

3.2 Variables Studied.

The objective of the experimental programme is to study the cracking, deformation, and strength characteristics in flexure of ferrocement section reinforced with woven type wire mesh. These characteristics included first cracking, crack width and spacing, deflection, compressive and tensile strains, and the strength at the elasto-plastic and ultimate stages.

The variables considered were:

1. Number of meshes in the section.
2. Strength of the mesh.
3. Presence of steel bars.
4. Mesh size and mesh distribution in the section.
5. Thickness of mortar cover.
6. Thickness of the section.

All these variables were included in the study of all of the above mentioned flexural characteristics. Although some of the variables were specifically selected for one of the characteristics, it was felt that including them in the study of the others will still provide important information. This therefore resulted in using one testing procedure throughout the testing programme. All other properties were kept constant.

3.3 Type of Test, Size of Test Specimen and Control Specimens.

The test chosen to fulfill the requirement of the study was the four lines loading flexural test. This type of loading arrangement has the advantages of constant moment zone and zero transverse shear which is not only essential in the study of cracking, but also provides a larger zone for the failure unlike the one point loading arrangement.

It was felt that the specimen size should be large enough to avoid the effect of scaling down the prototype. Therefore, the specimen chosen was a plate type 1000 mm in length and 300 mm in width. The supported length was 900 mm and the constant moment zone was 300 mm long.

To help carry out the crack width measurements, the test was arranged upside down, i.e. tensile face upward.

The control specimens, cast with each specimen, were six cubes, size 50 mm, for compression test and three plates 500x100x25 mm in dimension for flexural test.

3.4 Details of Experimental Programme.

The experimental programme included casting and testing seven series, each containing several sets of specimens. The specimens in each set have identical properties. A total of 49 specimens were cast and tested. The description of each series is given below, while the details are given in Table 3.1.

Table 3.1 Details of test programme.

Series designation	Number of Specimens	Specimen thickness mm	Mortar cover mm	Reinforcement Properties		
				Type of reinforcement	Mesh opening mm	Mesh ult. strength N/mm^2
S1	18	25	2	Wire mesh only	5.45	348.6
S2	8	25	2	" " "	5.45	119.7
S3	6	25	2	" " "	6.34	331.3
S4	4	25	2	Wire mesh and steel bars	5.45	348.6
S5	6	17 & 34	2	Wire mesh only	5.45	348.6
S6	4	25	4 & 6	" " "	5.45	348.6
S7	3	25	2	" " "	5.45	348.6

Series S1: In this series, the number of mild steel wire meshes was varied from none to the maximum possible number. The purpose of this series was to study the effect of steel content.

Series S2: This series is similar to S1 but using high strength steel mesh instead of mild steel mesh. The purpose was to study the effect of reinforcement strength.

Series S3: This series was again similar to S1, but the size of the mesh was different. The sets of specimens in this series have equal number of meshes with some of the sets in S1 but the percentage of steel content was different. In addition to the study of the effect of mesh size, the purpose of this series was to fill the gaps between steel percentages used in S1.

The meshes in specimens of series S1, S2, and S3 were uniformly distributed across the section with mortar cover equal to 2 mm.

Series S4: In this series, the reinforcements consisted of mild steel wire mesh and steel bars. The variable was the number of meshes used with the steel bars.

Series S5: The variable in this series was the thickness of the specimen. The percentage of steel content was kept constant. It was equal to the optimum value found from series S1 and S3. The reinforcement consisted of mild steel wire meshes uniformly distributed across the section.

Series S6: This series was the same as S5 but the variable here was the mortar cover.

Series S7: This series was a continuation of Series S4. The steel bars were removed but the distribution of the meshes was the same as in S4, i.e. concentrated near the outer faces.

The specimen designations used in this study were as follows:

1. Each series was given a serial number which follows the letter S, (S for abbreviation of series). Hence S3 refers to series number three.

2. Each set of specimens was given a letter which follows the series number. The letter indicates the number of meshes in the specimens of that set. The letters used were A, B, C, D, E, and F which stand for number of

meshes equal to 0, 2, 4, 6, 8 and 10, respectively. For example, S1D refers to a set of specimens in series one with number of meshes equal to 6.

3. The serial number of the specimen in the set was given after the letter which identify the set. The specimens in each set had the same properties. Therefore S2 B1 refers to specimen number one, of the set B (two meshes) of the second series.

4. In series S6 a figure was used between the series number and the set letter. This figure indicates the value of mortar cover thickness of the specimens. Whenever this figure is not mentioned then the value of the cover is equal to 2 mm. For example S6 4D1 refers to specimen number one of the set D (6 meshes) of the series number 6, with mortar cover equal to 4 mm.

Details of the sets of specimens in each series and the properties of the section of each set are given in Tables 3.2 to 3.5. It is to be noticed that the number of specimens in each set of series S1 was three. However, this number was decreased in the subsequent series. The reasons for having a large number of specimens were firstly to establish the repeatability of the test results and secondly because of the importance of the results from series S1 to define the optimum amount of reinforcement which was used in later tests. Thirdly, the tests gave an idea about the amount of scatter in the results, especially in the study of cracking. It showed that the scatter could be very small and the number of repeated specimens in the subsequent series was reduced depending on the importance of the series itself.

3.5 Specimen Manufacture.

Different investigators have used different techniques in manufacturing ferrocement specimens. However, the difficulty arises when the mesh distribution is considered important and a specified mortar cover is required. For

Table 3.2 Details of Series S1, S2, and S3.

Series No.	Set Designation	No.of specimens in set	No.of meshes in specimen	Specific Surface S_R cm^2/cm^3	Fraction Volume V_R %	Notes
S1	S1A	3	0	0	0	1. Mild Steel wire mesh 2. Mesh opening 5.45 mm 3. Specimen thickness 25 mm 4. Mortar cover 2 mm
	S1B	3	2	0.7	1.61	
	S1C	3	4	1.41	3.22	
	S1D	3	6	2.11	4.83	
	S1E	3	8	2.82	6.44	
	S1F	3	10	3.52	8.05	
S2	S2B	2	2	0.7	1.61	Same as S1 except high tensile steel wire mesh.
	S2C	2	4	1.41	3.22	
	S2D	2	6	2.11	4.83	
	S2E	2	8	2.82	6.44	
S3	S3C	2	4	1.29	2.94	Same as S1 except mesh opening equal to 6.34 mm
	S3D	2	6	1.93	4.41	
	S3E	2	8	2.57	5.88	

Mesh distribution for the sets of Series S1, S2 and S3

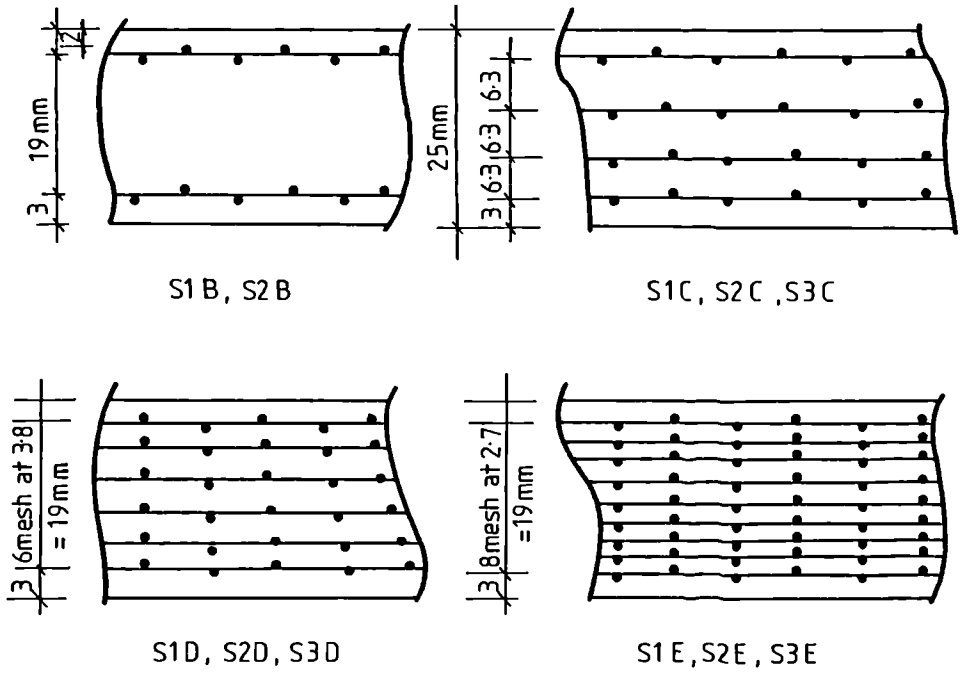

S1F 10 meshes packed together with no spacers between them.

Note : all meshes are woven wire mesh with wire diameter equal to .914 mm.

Table 3.3 Details of Series S4 and S7.

Series	Set Design	No.of specimens inset	No.of meshes in each specimen	S_R cm^2/cm^3	V_R %	Notes	Reinforcement Distribution
S4	S4A	1	0	0.1	1.51	1. All specimens are reinforced with 6 mm mild steel bars longitudinally at 100 mm and transversely at 300 mm. 2. Specimen thickness = 25 mm 3. Mortar cover = 2 mm 4. Mild steel wire mesh with 5.45 mm mesh opening.	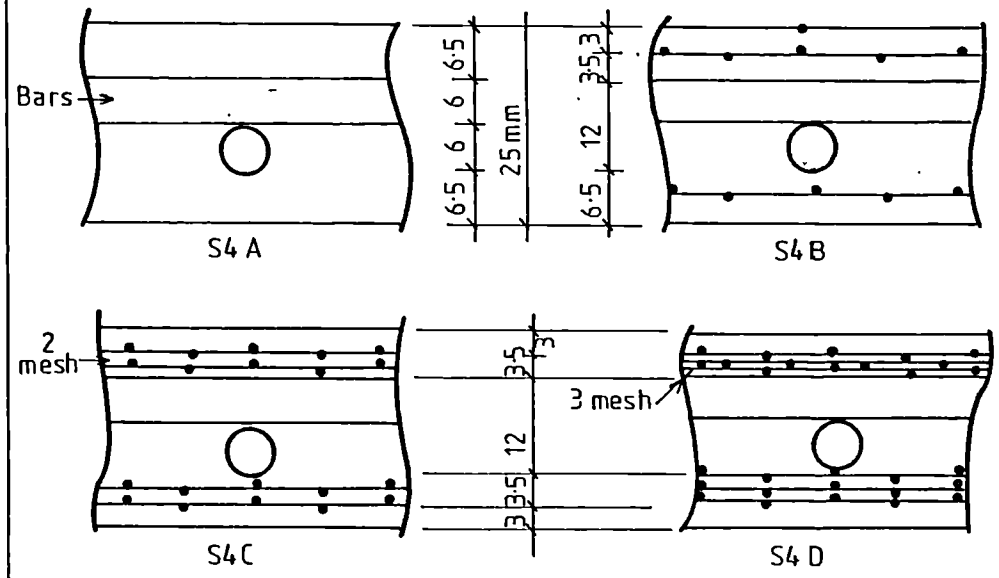
	S4B	1	2	0.8	3.12		
	S4C	1	4	1.51	4.73		
	S4D	1	6	2.22	6.34		
S7	S7A	2	0	0	0	Same as S4 but with no steel bars	S7C same as S4C but with no steel bars.
	S7C	1	4	1.41	3.22		

Table 3.4 Details of Series S5.

Set Designation	No.of Specimens in set	No.of meshes	Specimen thickness mm	S_R cm^2/cm^3	V_R %	Notes	Reinforcement distribution
S5C	3	4	17	2.11	4.83	1. Mild Steel wire mesh only 2. Mesh opening 5.45 mm 3. Mortar cover 2 mm	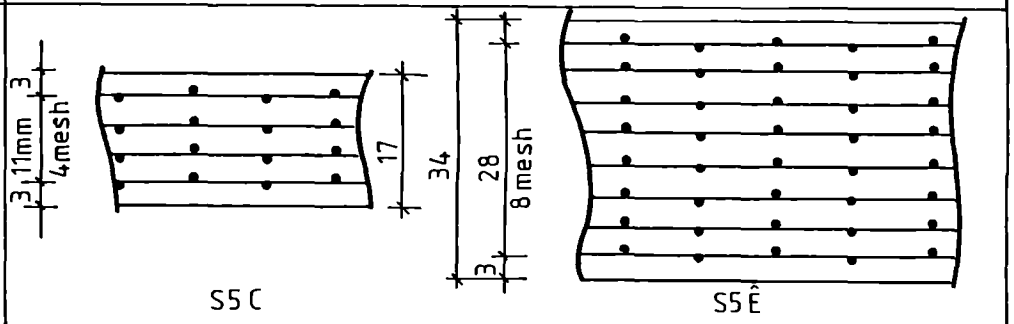
S3E	3	8	34	2.11	4.83		

Table 3.5 Details of Series S6.

Set Designation	No.of Specimens in set	No.of meshes	Mortar Cover mm	S_R cm^2/cm^3	V_R %	Notes	Reinforcement distribution
S64D	2	6	4	2.11	4.83	1. Mild Steel wire mesh only 2. Mesh opening 5.45 mm 3. Section thickness = 25 mm	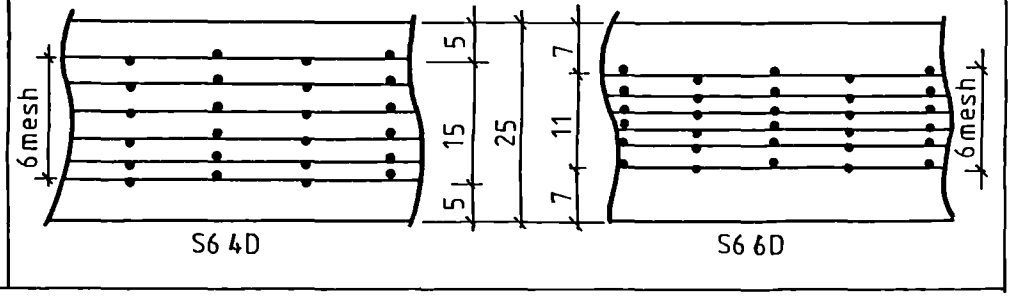
S66D	2	6	6	2.11	4.83		

example, a section 25 mm thick, reinforced with eight uniformly distributed layers of mesh and a mortar cover of 2 mm, would involve the vertical spacing of meshes at about 2.7 mm. A 1 mm movement in the position of the mesh would lead to about 40% error. It is obvious, therefore, that a high degree of accuracy in placing the meshes is essential. Moreover, meshes should be held in position during casting.

A specially developed technique was used in this study to manufacture the test specimens. It is based on packing the meshes in a specially developed mould. The meshes were kept in position using fine steel wires running across the mould and using mortar spacers between the meshes. The mortar was then poured in with as little disturbance as possible. Several preliminary specimens were cast and cut to check the success of the technique. Throughout the experimental programme, specimens of different series were also cut to check the distribution of reinforcement. Plate 3.1 shows cut sections of specimens from Series S1.

It should be mentioned here that the upper layer of mesh (on the compressive side) tends to settle due to the weight of mortar poured on top during casting. However, this settlement was accepted as it was on the compression side which is of less significance than the tensile side.

In the following sections details of the mould and the casting technique are given.

3.5.1 Casting Mould.

The casting mould consisted of four aluminium angles as sides and a perspex plate as base. These two materials were chosen for their durability and to provide smooth surfaces. The sides were fixed to the base by screws. The long sides had five sets of holes each, and they were opposite to each other. A pair of holes, one at each side, defined the position of a layer of mesh. Fine steel wires were threaded through the holes on one side,

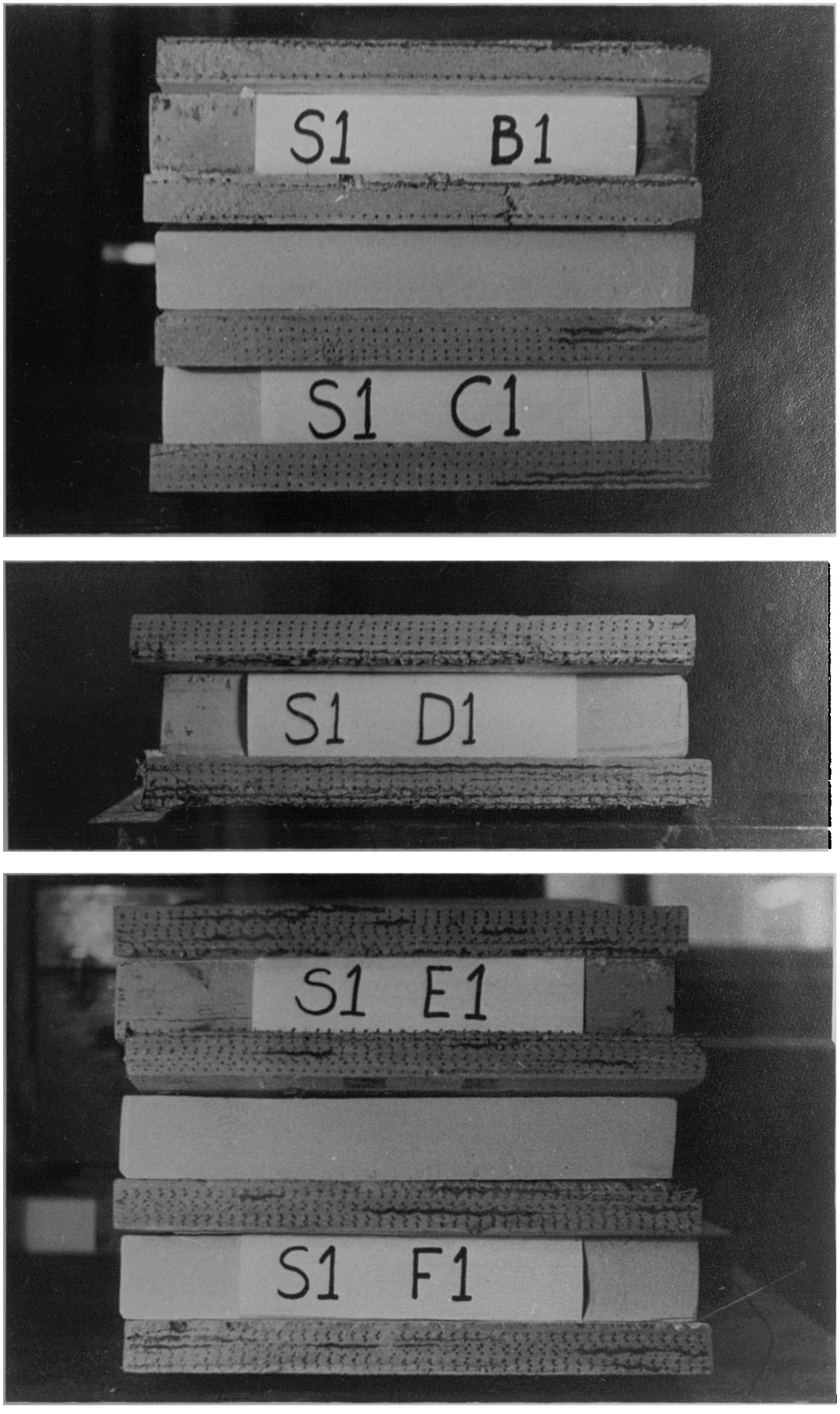

Plate.3·1. Cut sections of specimens from series S1.

running across the mould and threaded again through the corresponding holes on the other side. The ends of the wires were fastened to bolts fixed on the base plate outside the casting area. These wires provided support for the layer of mesh. Each layer was then supported by five wires. Mortar spacers, made from the same mortar as that of the specimens, and of a specified thickness were used to provide the required spacing in areas between the supporting wires. Fig.3.1 shows a schematic diagram for the details of the mould.

3.5.2 Reinforcement and Preparation for Casting.

A woven type galvanized steel wire mesh was used in this study. It was supplied in flat sheets of 1200x1000 mm in dimensions with the least dimension along the rolling direction (warp). Each sheet was cut into four mesh layers using shears. The longitudinal direction of the mesh layer was along the least dimension of the sheet (i.e. warp direction).

The meshes were cleaned using carbon tetrachloride to remove any oil on them. They were then straightened to get rid of any warping suffered through handling of the mesh. This process was essential to ensure a uniform spacing of the mesh along the test specimen. In specimens which had more than two meshes, each of the two meshes, separated by mortar spacers, were tied together using fine steel wire. This was to ensure that the spacing of the two meshes relative to each other will remain the same and thus cause less error in the spacing of the meshes.

In the case of specimens with steel bars, the bars were tied to form a mesh with the required spacing. The placing of the bar mesh in the mould was carried out in the same way as the wire meshes.

To prepare the mould for casting, it was first oiled. The first set of wires was threaded through the holes to support the first layer of wire mesh and provide the required cover. Mortar spacers (one in the middle of the

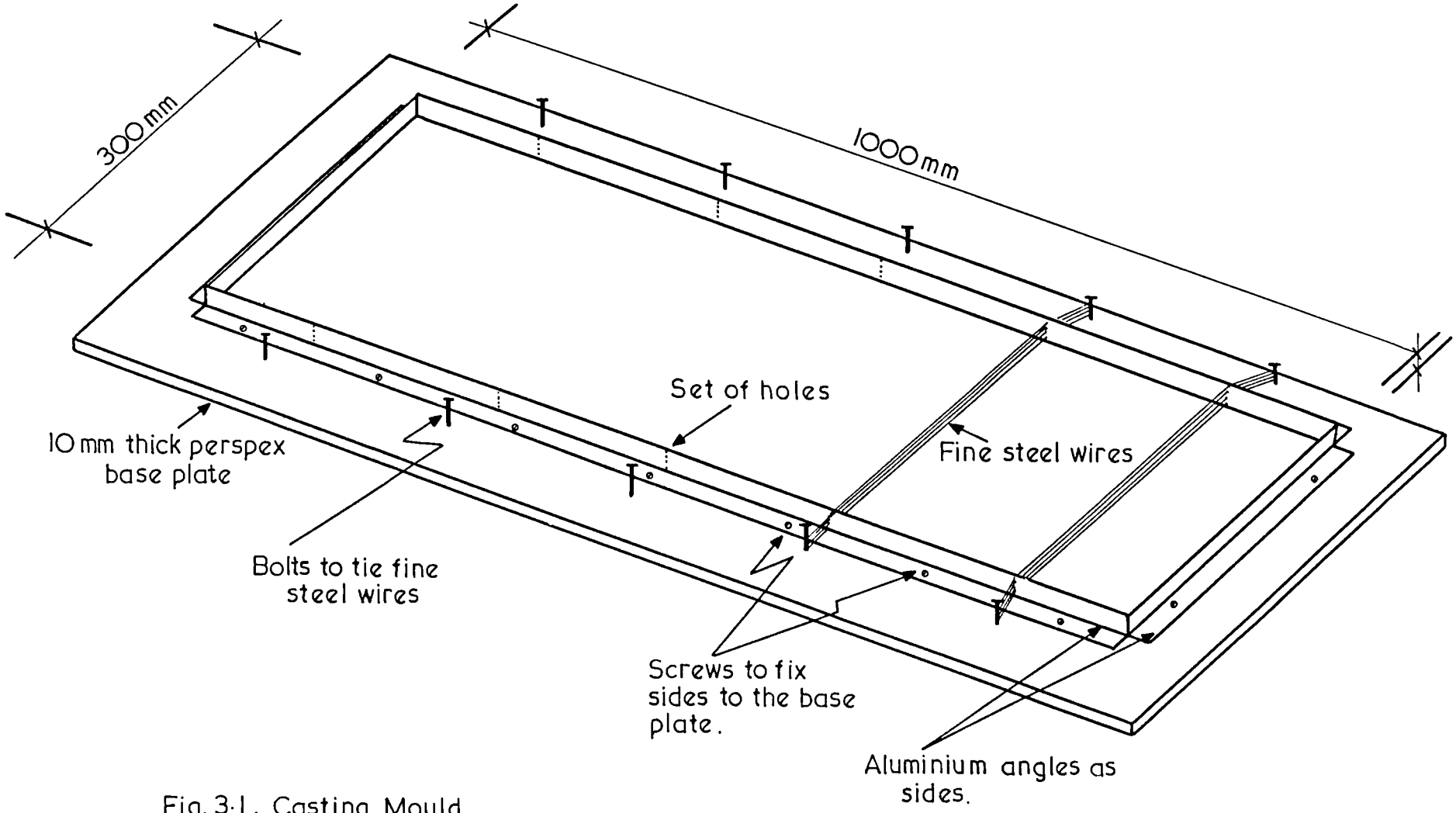

Fig. 3·1. Casting Mould.

span of each wire) were used to support these wires. The first layer of mesh was then placed and another set of wires was threaded to hold it in position. The next set of wires were fixed to support the next layer of mesh and mortar spacers were used in the areas between these wires. Equal number of spacers were used for each layer of mesh and for all the specimens. The next layer of mesh was then placed. This procedure was continued until the last set of wires were fixed to hold the last layer of mesh in position. Plate 3.2 shows the reinforcement packed in the mould, ready for casting.

3.5.3 Mixing, Casting, and Curing.

The mixing was carried out in a horizontal pan type mixer. The mixing procedure was according to ASTM specification (C305-65) (52) of mixing mortars. The fly ash, cement, and water were first mixed for 30 seconds. Then, sand was added while mixing continued for another 30 seconds. Mixing was continued for a further 30 seconds, after which the mixer was stopped for 90 seconds for the mixture to settle. During that time, any lumps on the blades were quickly removed. The mixing was resumed for a further 60 seconds, after which the mortar was ready for casting.

Casting was carried out on a vibrating table. One specimen was cast at a time. The specimen mould, with the reinforcement packed in, was placed, together with moulds for the control specimens, on the vibrating table, see Plate 3.3. The control specimens consisted of 6 cubes of 50 mm, for compression tests and 3 plates of 500x100x25 mm in dimension for flexural tests. Casting was carried out while the vibrating table was in operation. The mortar was applied in thin layers to reduce the disturbance of the mesh spacing caused by the weight of mortar. Control specimens were cast at the same time as the test specimen and these were cast in two layers. All specimens and control specimens were subjected to the same vibration time, equal to six minutes. Then, the specimens,after being trowelled, were

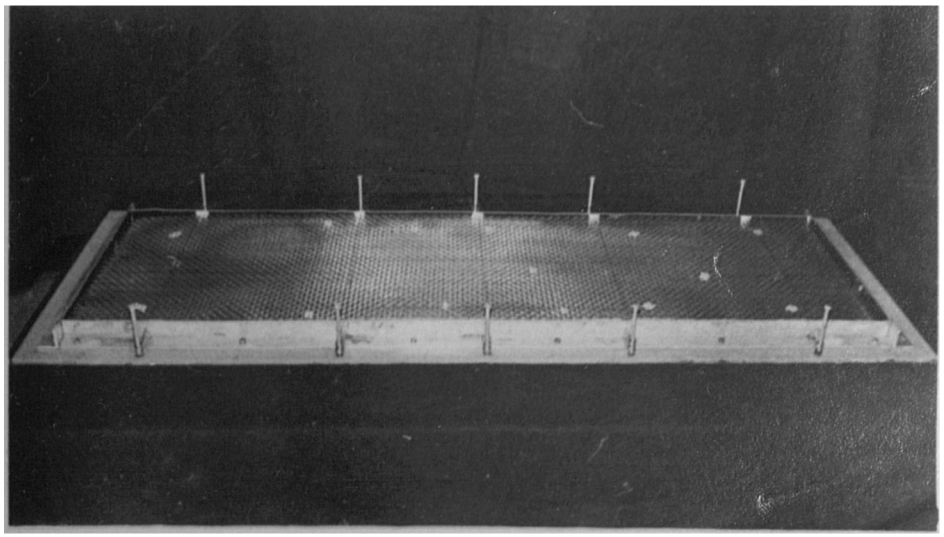

Plate. 3·2. Reinforcement packed in the mould ready for casting.

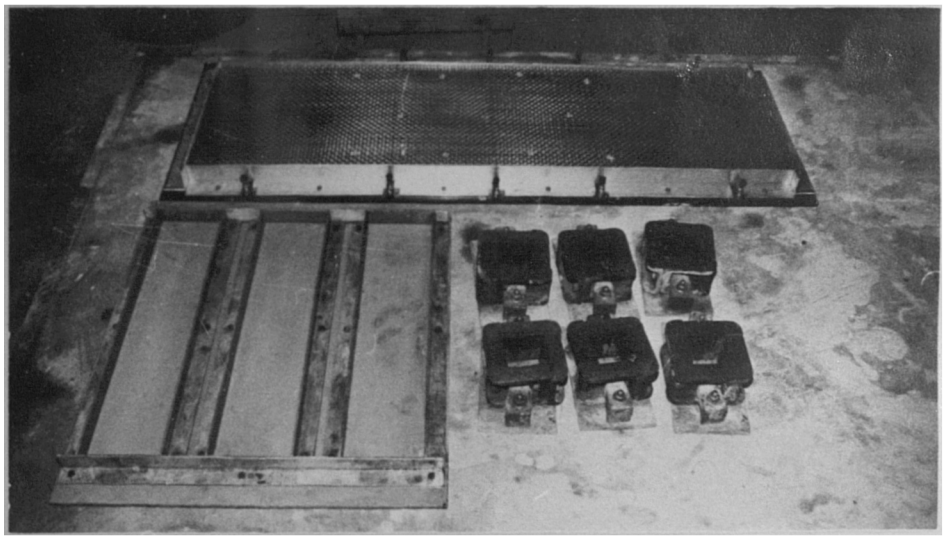

Plate. 3·3. Casting arrangement.

covered with polythene sheets and left on the vibrating table for 24 hours. All the specimens were then stripped, marked and transferred to the fog room. The specimens were kept in a fog room where the temperature was 21° C and the humidity was 98%. At the age of 27 days they were transferred to the laboratory for instrumentation and to be tested the following day.

3.6 Test Equipment.

3.6.1 Testing Rig.

A testing rig was specially designed to carry out the tests in this investigation. The rig design was based on the following requirements:

1. Four line loading flexural test.
2. Crack width measurements and therefore tensile face of the specimen upward, with access to it.
3. Large deflection is expected.
4. Free supports to eliminate end restraints.
5. Crack width measuring device is to be mounted on the rig.

The testing rig consisted of a screw jack to supply the load, a proving ring to measure the load, loading frame to apply the load equally on the two lines of loading, and supporting frame with roller supports to hold the specimen, see Fig.3.2. The load is transferred from the proving ring to the loading frame through a steel bar with a steel ball at each end. The steel bar passes through a sleeve to direct the load vertically, see Plate 3.4.

Two parallel steel tubes are fixed to the rig to act as rails supporting the crack width measuring device. They ran parallel to the longitudinal direction of the specimen.

Preliminary tests were carried out in the rig before starting the programme of tests for the investigation. The rig was checked under the required range of loads against movements and stability.

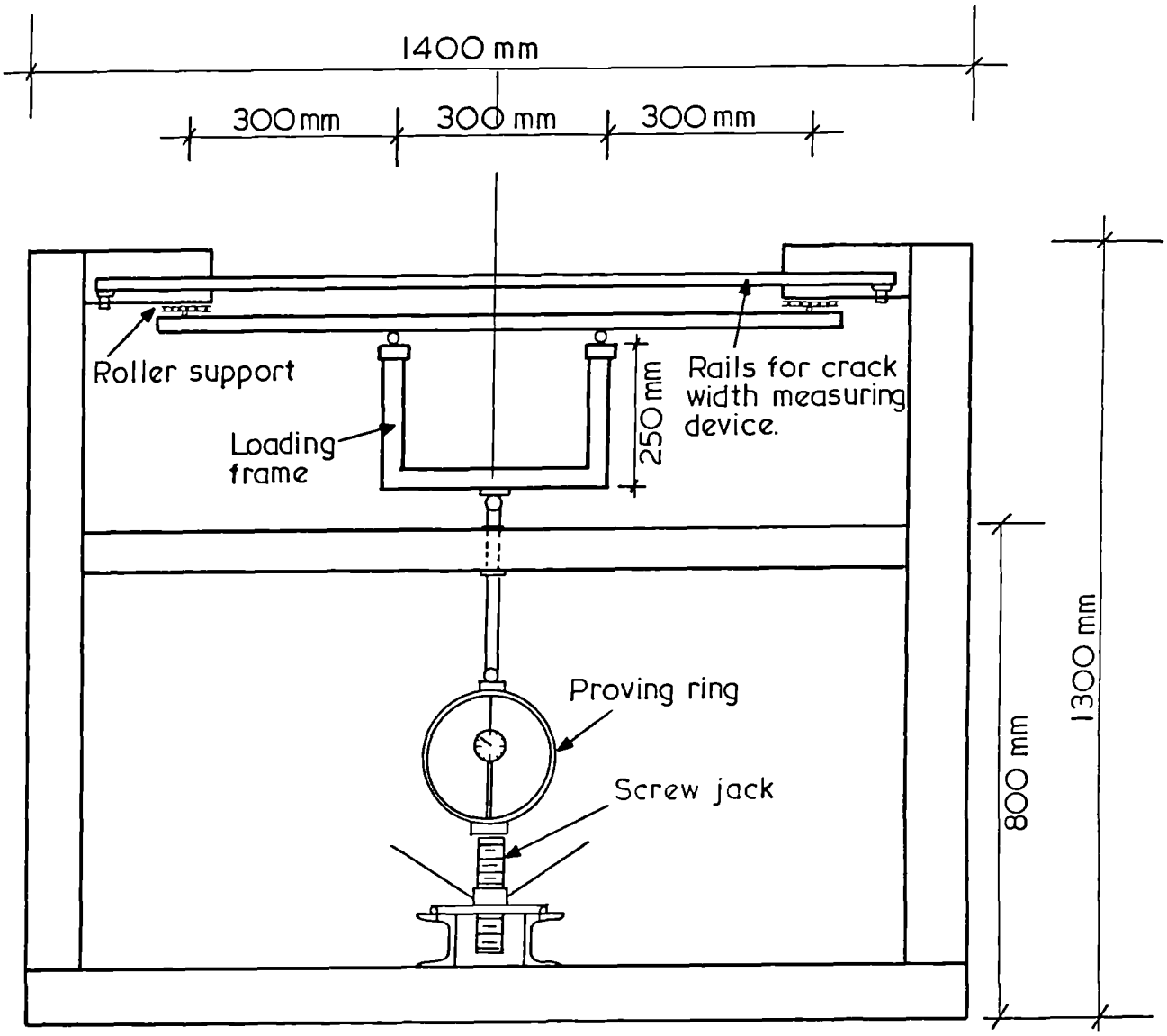

Testing Rig.

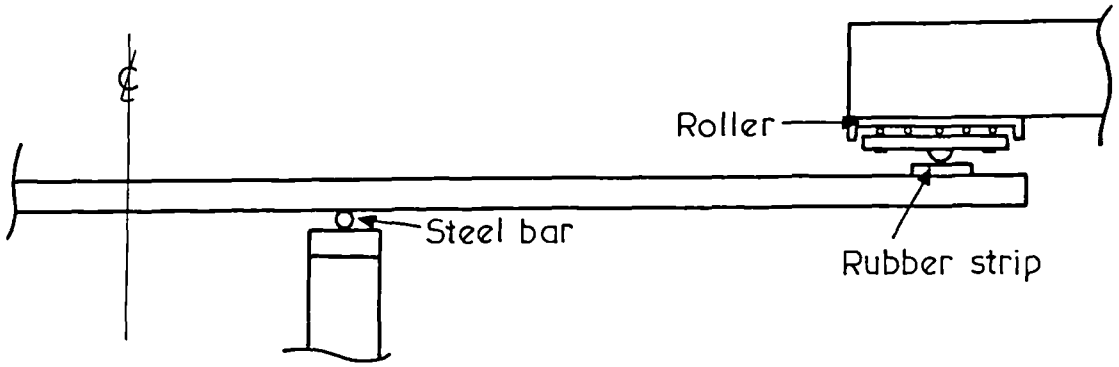

Details of supports and loading frame.

Fig. 3.2. Schematic diagram for the testing rig.

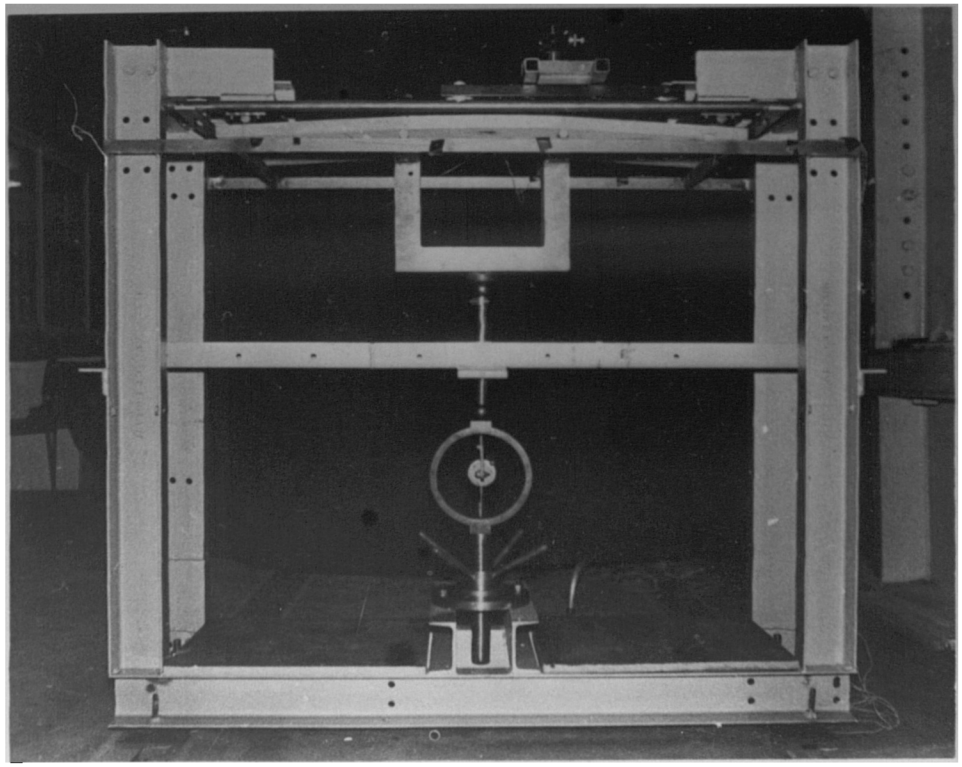

a) Front view.

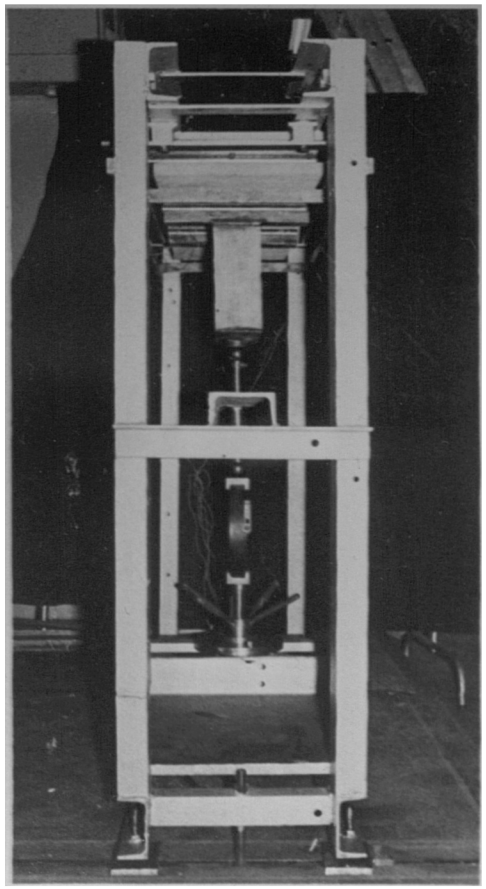

b) Side view

Plate. 3·4. Testing rig.

3.6.2 Crack width Measuring Device.

The crack width measuring device consisted of a micrometer microscope, a trolley to carry the microscope, and a source of illumination. The micrometer microscope had a magnification power of 80 and a least division on the micrometer of 0.89×10^{-3} mm. The trolley was specially designed to be mounted on the rig, see Plate 3.5. It is capable of travelling along two steel tubes, as rails, in the longitudinal direction of the specimen and parallel to its tensile face. The microscope itself was fixed to a steel base which sits on two box section steel bars running perpendicular to the longitudinal direction of the specimen. The microscope can be moved along the steel bars while the trolley is stationary. Therefore, the microscope can be moved to any point on the face of the specimen by combination of the trolley movement and the sliding of the microscope in a plane parallel to the face of the specimen.

The trolley weighed very little and when not required for crack width measurements, could be pushed to the side of the constant moment zone or lifted up from the rig. During crack width measurement, a light source was attached to the trolley to supply the illumination.

3.7 Test Measurements and Instrumentation.

The measurements required were the loads, strains, and deflection from first application of the load until failure. In addition, the load at first cracking and the crack width and spacing at different levels of loading were also obtained.

The load was measured using a proving ring placed between the screw jack and the specimen. Two different proving rings were used throughout the test programme with maximum capacities of 1000 and 2000 kg. respectively. The 1000 kg proving ring was used for specimens with low ultimate load. The use of two proving rings was to ensure that the measured loads fall within a

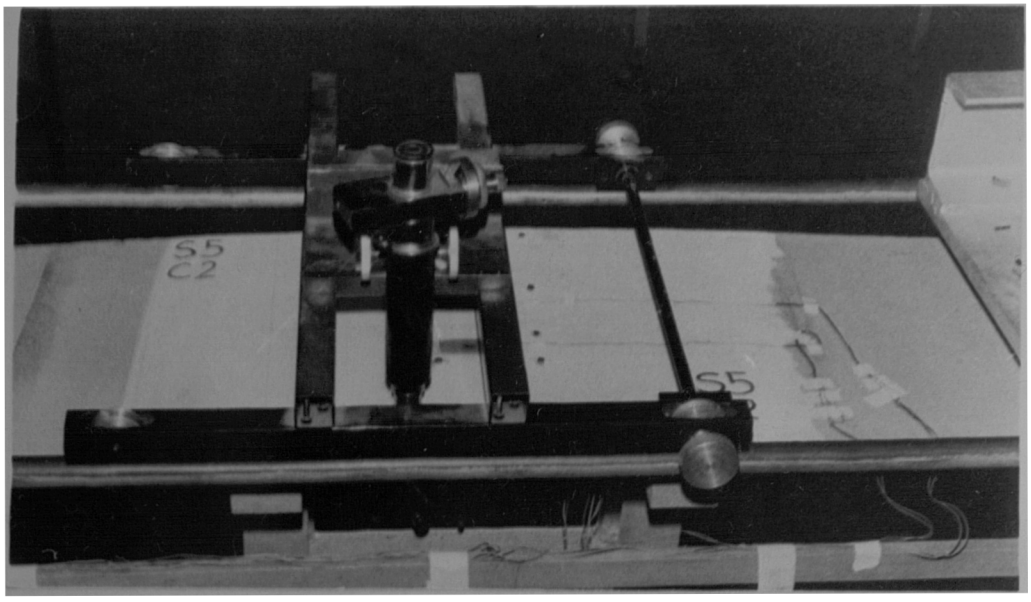

Plate. 3·5. The microscope and the trolley mounted on the rig.

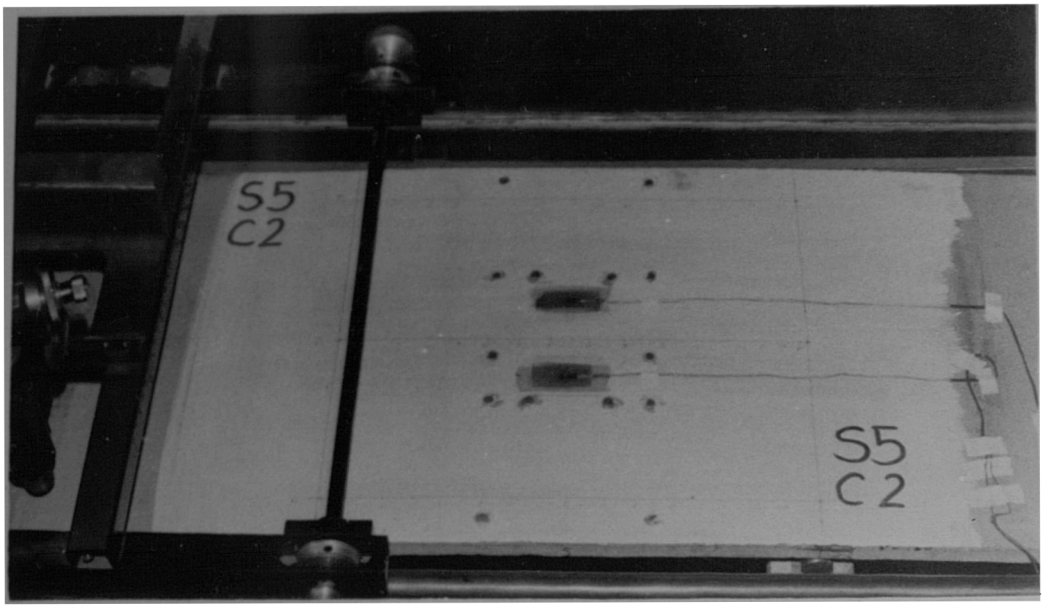

Plate. 3·6. Instrumentation on the tensile face of the specimen.

reasonable range of the proving ring capacity. Both proving rings were calibrated using the same machine several times during the period of the experimental programme.

The strain measurements included strains on the compression and tensile faces and on the side of the specimen. Strains along the lines of crack width measurements were also obtained. The strain measurements were taken using Demec gauges and electric resistance strain gauges. Fig.3.3 shows the type and positions of strain measurements on the two faces of the specimen. Demec gauges were used to measure the strain on the tensile face (see Plate 3.6). A 100 mm gauge length was used for measuring strains along the lines of crack width measurement, while for the general tensile strain on the face, two of 100 mm and two of 50 mm gauge lengths were used. The use of 50 mm gauge length here is to reduce the error resulting from high curvature near ultimate load.

All Demec points were stuck to the specimen by first rubbing its place with emery paper. Then, the place was cleaned using carbon tetrachloride. Plastic Padding was used to stick the Demec points in position.

Electric resistance foil type strain gauges were used to measure the strains on the compressive and tensile faces and on the side of the specimen, see Fig.3.3. On the tensile face, two strain gauges of 5 mm gauge length, and 2.10 gauge factor, were used for strain measurement mainly within the elastic limit of the mortar i.e. before cracking. The sensitivity of electrical resistance strain gauge, is higher than that of the Demec gauge. So, it was hoped that more accurate readings could be obtained by using them. In fact the strain reading from the electrical strain gauges were used to sense the occurrence of first cracking. The small gauge length was chosen because of greater possibility of the cracks not crossing the gauges.

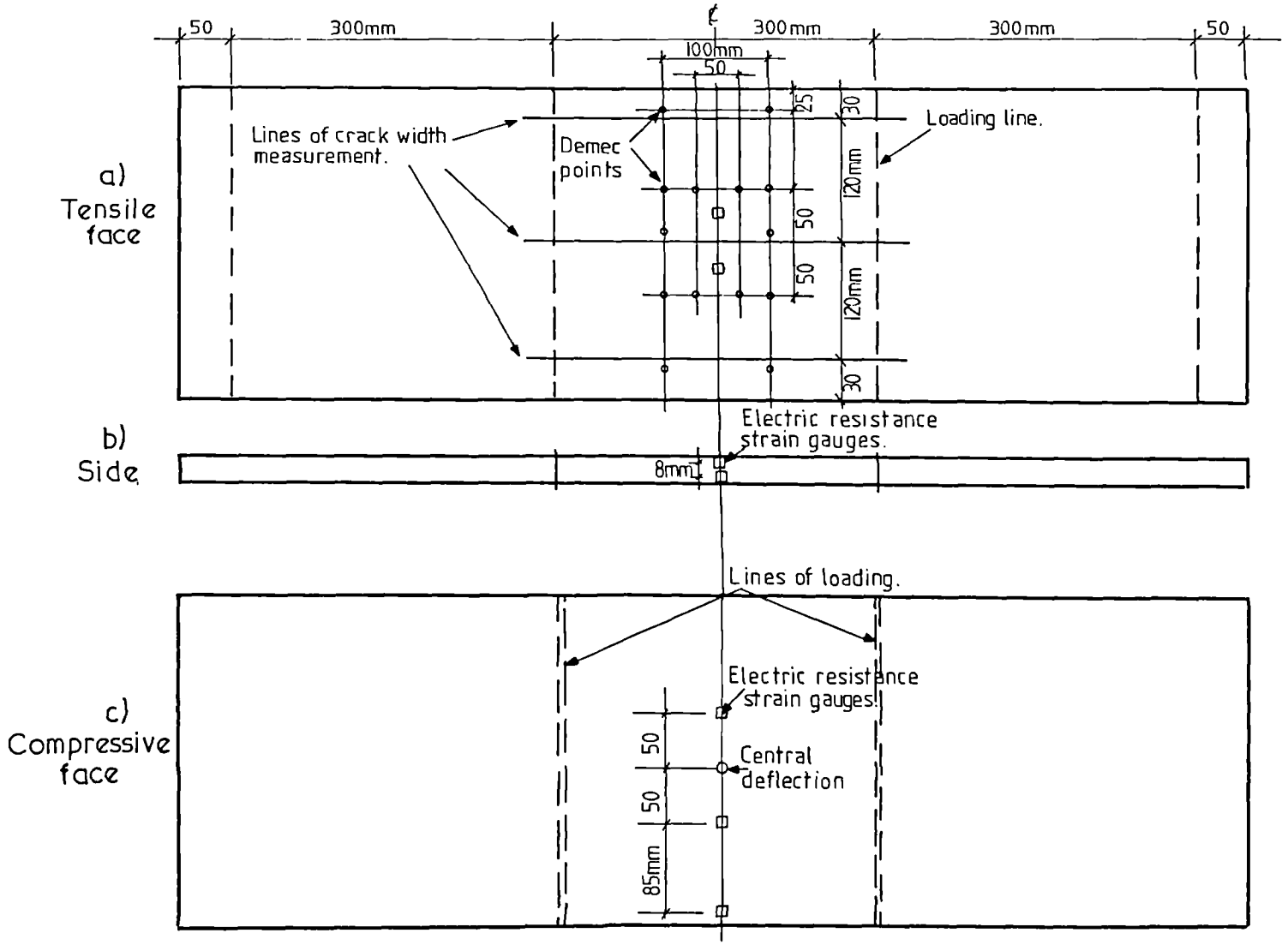

Fig.3·3. Position of strain, deflection and crack width measurement.

Therefore,the gauges might give an idea about the strains between cracks. The electrical resistance strain gauges on the side of the specimen were similar to those on the tensile face. They were used to give an indication of the strain distribution along the section of the specimen.

On the compressive face three strain gauges of 20 mm gauge length and 2.10 gauge factor, were used. Higher gauge length was chosen here, since the higher the gauge length, the better the average strain reading obtained.

From experience of previous work (12) it was found that electrical resistance strain gauges could give reliable reading of the strains on the mortar if attention was paid in their attaching process. In this study, the process of sticking the gauges was by first rubbing well their place on the mortar with emery paper. This was to remove the relatively soft mortar on the surface. The surface was then washed with carbon tetrachloride to remove any loose particles. An adhesive, type P2 was used to seal the mortar surface. It was applied in a very thin layer and left for at least two hours to harden. Then, the gauge was stuck on top of it. The adhesive used this time was an instantaneous adhesive. For curing, this adhesive requires very light pressure and human body temperature. Therefore, after removing any excess of adhesive and ensuring that the thin layer of adhesive under the gauge was free from air bubbles, finger pressure was applied on the full gauge for 30 seconds. After finishing sticking of all the gauges, wires were soldered to the gauges to connect them to the strain reading devices during testing.

It should be mentioned that early in the test programme electrical resistance crack propagation gauges were used to measure the depth of the cracks on the side of the specimen. These gauges were abandoned later due to their unreliable results.

Deflection at mid span was measured using a dial gauge with a least division equal to 0.025 mm.

3.8 Testing Procedure.

The testing of the specimen was carried out at the age of 28 days. Load was applied incrementally. For the range from first application of load until first cracking, the load increments were small, mainly to get more representative recorded reading of the load at first cracking. The magnitude of the load increments was increased after that and near failure, the load was increased continuously until failure. Each test took from twelve to twenty five load increments. Load, deflection and strains were taken at each increment of loading. Near failure where the load was applied continuously, load, deflection and compressive strain were recorded instananeously at selected stages and at failure.

The load at first cracking was recorded for all specimens. The first crack was detected using a magnifying glass and with the aid of light source. The occurrence of the first crack was detected from observing the increments of deflection and the tensile strain from the electric resistance strain gauges. Soon after their readings deviate from linearity the first crack appeared. The width of the first crack was measured for selected specimens.

Crack width and spacing measurements were taken at selected increments (at least four increments) during the period from first cracking until shortly after yielding of the specimen. At each of these load increments, all cracks within the constant moment area and crossed by one of the three grid lines (see Fig.3.3), were marked and their width and distance from the loading line were measured.

After failure, the number of cracks, spacing and the maximum crack width were taken. The specimen was then photographed at the cracked area.

Each test took between four to seven hours a large part of that time was spent on crack width measurements.

CHAPTER 4.

CRACKING BEHAVIOUR

4.1 Introduction.

Cement mortar in ferrocement, like concrete in reinforced concrete, has a tensile strength of the order of one tenth of its compressive strength. The tensile strain at which it cracks is about one hundred microstrain and this figure is only a fraction of that at ultimate load in the steel which it surrounds. It is for this reason, and the tendency towards more economical design that in reinforced concrete, cracking and crack width become very important as it hinders increasing the allowable stresses. Extensive studies have been carried out on the cracking behaviour of reinforced concrete. The factors which affect cracking have been investigated, and equations to predict the mean and the maximum crack width at any level of load are now established.

Ferrocement is considered as a form of reinforced concrete. However, it shows better cracking performance than reinforced concrete. The material exhibits larger number of cracks and hence smaller crack width. For the same steel stress, reinforced concrete crack width equations predict substantially smaller crack width in ferrocement than in reinforced concrete (18). Therefore, crack width equations developed for reinforced concrete cannot be used for ferrocement. In addition, the factors found to affect the cracking behaviour in reinforced concrete are not necessarily the same in ferrocement. This is due to the different reinforcing mechanism of the two materials. At the same time, the criteria for the crack width for reinforced concrete might not be applicable to ferrocement.

It is clear, therefore, that cracking of ferrocement requires a separate and extensive study. The studies should include the cracking behaviour, the factors affecting it, and the development of equations to predict the crack

width. Such studies will not only enable a better understanding of ferrocement but also put the designer in a better position to decide the level of allowable stresses and servicability of the material.

4.2 Review of Literature.

Most of the work carried out on the cracking behaviour of ferrocement sections in flexure have been limited to the general observation of the cracking and crack number, and the properties of the section at first cracking. Instead of studying the crack width and crack spacing throughout the elasto-plastic and plastic stages, investigators were more concerned with the first crack which represents only a single moment in the life of the section. There were also attempts to define the optimum reinforcement amount which produces ferrocement section, by comparing the load at the first crack of the section. However, different definitions for the first crack were adopted by different investigators, such as those that relate it to the onset of the non-linearity of the load-deflection curve, to the occurrence of certain crack widths, or to the establishment of a certain tensile strain in the mortar. These definitions, depending on the technique of the experimental measurements, may not represent the same single stage in the life of the section, and therefore the term first crack in itself does not have much meaning.

Bezukladov et al. (5) compared the cracking behaviour of ferrocement sections at the first visible crack which corresponds to 0.05 mm in width. They found that the stresses and relative elongations during crack formation increased with an increase in the specific surface (S_R) of the reinforcement to a specific limit equalling 3.0 to 3.5 cm^2/cm^3 and an increase in S_R above that will lead to a decrease in the stresses at crack formation. They also observed that the enhancement in the behaviour of the section as compared to reinforced concrete starts when S_R is more than 2.0 cm^2/cm^3.

Naaman & Shah (17), from tensile tests on ferrocement, found that increasing the specific surface of reinforcement in the longitudinal direction (S_L) increased the stress at the first crack and the number of cracks at failure. No increase in the stress was observed when S_L exceeded about 2.0 cm^2/cm^3.

Shah & Key (10) reported that leakage tests performed on specimens under tension showed that there was no leakage of water through the specimen up to a crack width of 0.05 mm. It was observed that the number of cracks at fracture and the width of cracks were significantly influenced by the specific surface. The average number of cracks at failure varied linearly with increase in the specific surface of reinforcement.

Walkus (19,20,30) defined ferrocement as a material with a minimum specific surface, S_L, of 1.0 cm^2/cm^3 and an upper limit of 1.5 cm^2/cm^3 due to practical considerations of placing steel in a given section. Considering the cracking behaviour of ferrocement in flexure similar to that in tension, Walkus divided the behaviour of the section into 4 stages according to the crack width and the servicability. Table 1.2 shows the properties of the section at each stage. It can be seen that crack width over 0.1 mm are unacceptable.

To Walkus, microcracks are inherent in ferrocement even under no loading. At the initial stages of loading they are of the order of a few microns, but when their width enlarges and becomes tens of microns they become practically significant. This may be why the cracking moment is only a relative term.

One of the first attempts to measure the crack width of ferrocement beams under flexure was made by Logan & Shah (18). It was found that increasing the specific surface of mesh reinforcement increases the number of cracks at failure and decreases the crack width for a given steel stress. The following equation was given for prediction of the average crack spacing at failure. It is, essentially the same as that derived for reinforced concrete.

$$S = \frac{\theta}{\eta} \times \frac{1}{S_{LT}} \quad \ldots\ldots \quad (4.1)$$

where S = Spacing in cm.

θ = Ratio of average crack spacing to minimum crack spacing.

η = Ratio of bond strength between the mesh and the mortar to the tensile strength of the mortar.

S_{LT} = Specific surface, surface area of reinforcement in the longitudinal direction in the tensile zone divided by the initial mortar volume in the tensile zone.

Combining the maximum stresses in the extreme tensile layer of mesh which was calculated using cracked elastic analysis, with the maximum crack width for different series of specimen, the following equation was developed for prediction of maximum crack width:

$$W_b = \frac{3.5 \times 10^{-9} \times f_s^{1/3}}{S_{LT}^{1/3}} \quad \ldots\ldots \quad (4.2)$$

where W_b = maximum crack width, in.

f_s = stress in the extreme tensile layer of mesh, psi.

It was also shown that for the same steel stress,crack width in ferrocement is much smaller than that in reinforced concrete.

Rajagoplan and Parameswaran (56) have suggested, from theoretical analysis, that the optimum amount of reinforcement after which the increase in the cracking moment is not appreciable, is equal to $S_R = 3.15\ cm^2/cm^3$. They have also suggested an equation to predict the crack spacing. The equation is similar to eq. (4.1) by Logan & Shah (18) but includes the fraction volume of the matrix. The equation is as follows:

$$S = \frac{1.5}{\eta} \frac{V_m}{S_{LT}} \quad \ldots\ldots \quad (4.3)$$

where S = Average spacing of cracks.

V_m = The matrix volume ratio.

Rajagoplan and Parameswaran have also suggested an expression to predict the maximum crack width. It is based on the assumption that the average crack spacing multiplied by the steel strain equals the average crack width. The crack width is then modified to account for the strain gradient in the beam. The maximum crack width is assumed to be equal to 1.5 times the average crack width. The expression obtained is given below:

$$W = \frac{2.25\ V_m\ (\sigma_{fm}-420)\ (D-a)}{\eta\ S_{LT}\ E_f\ (D'-a)} \quad \ldots\ldots \quad (4.4)$$

where:-

W = Maximum crack width in cm.

σ_{fm} = Stress in the extreme mesh layer, kg./cm^2.

a = Depth of neutral axis from extreme compression edge, cm.

D = Total depth of the ferrocement beam, cm.

D' = Depth from the extreme compression edge to the last layer of mesh, cm.

E_f = Modulus of elasticity of the mesh, kg/cm^2.

Paul and Pama (11) derived the following theoretical equation to predict crack width for ferrocement members under tension. They have suggested that the equation can also be used for members under flexure.

$$W = \frac{\pi}{S_L}\ \frac{\sigma_{mu}}{E_f\ C_b\ \tau_u}\ \left[\sigma_f^* - \frac{\sigma_{mu}}{2}\ (R+m)\right] \quad \ldots\ldots \quad (4.5)$$

where:-

S_L = Specific surface of reinforcement in loading direction.

σ_{mu} = Ultimate tensile strength of the mortar.

C_b = Bond correction factor of equivalent aligned fibre.

τ_u = Ultimate bond stress,

σ_f^* = Fibre stress at the crack.

R = Ratio of area of matrix in the assumed aligned fibre model to the cross-sectional area of fibre, A_{mm}/A_f.

m = Modular ratio, E_f/E_m.

It can be seen that equation (4.5) is rather complicated and needs verification by experimental data.

The first systematic work to measure the crack width of beams under flexural loading was made by Balaguru, Naaman and Shah (31). They tested beams reinforced with different numbers of meshes and measured the crack width at different levels of loads. The meshes used were $^1/_4$ in. woven mesh and $^1/_2$ in. woven and welded mesh. They concluded that the influence of S_R on the cracking performance of ferrocement in flexure is not as strong as in tension. However, they found that everything else being equal, specimens reinforced with $^1/_4$ in. mesh gave a better cracking performance than those reinforced with $^1/_2$ in. mesh. A linear regression analysis carried out on the crack width measurements and the tensile strain in the extreme layer of mesh, found from a mathematical model, yielded the following equations:

For $^1/_2$ in. welded mesh reinforcement

$$W_{av} = 0.206 + 0.335\ \varepsilon_s \quad \ldots\ldots \quad (4.6)$$

For $^1/_2$ in. woven mesh reinforcement

$$W_{av} = 0.353 + 0.42\ \varepsilon_s \quad \ldots\ldots \quad (4.7)$$

For $^1/_4$ in. woven mesh reinforcement

$$W_{av} = 0.254 + 0.186\ \varepsilon_s \quad \ldots\ldots \quad (4.8)$$

where:-

W_{av} = The average crack width, 10^{-3} in.

ε_s = Steel strain, 10^{-3} in/in.

To study the influence of other variables found important in reinforced concrete, the regression analysis was repeated with combinations of these variables and the steel strain. The three other variables considered were: the cover measured from the cut surfaces, the area of tension zone divided by

number of wires in tension, and the ratio of distance to neutral axis from extreme tension fibre and from centroid of steel. From the regression analysis, they found that the standard error was not improved by addition of any of these three terms. Hence, it was concluded that the maximum crack width would seem to be primarily dependent on the tensile strain in the extreme layer of mesh. However, the cover was varied only between 0.4 and 1.7 mm which is a small range and there were no tests carried out specially to determine the effect of the cover.

A design equation was suggested by Balaguru et al. (31) based on the assumption that mortar between cracks is completely free and the number of cracks equals the number of transverse wires. The equation was in the following form:

$$W = \varepsilon_s S R \quad \ldots\ldots \quad (4.9)$$

where:

W = Average crack width.

ε_s = Tensile steel strain in the extreme layer of steel.

S = Spacing of transverse wires.

R = Ratio of distances to neutral axis from extreme tension fibre and from the outermost layer of mesh.

The equation was found to give upper bound limit for the crack width. This equation was used (40,57) in crack width prediction for section under static flexural load which in turn was used in the analysis of crack width for sections under fatigue load.

Naaman (24) reporting on the experimental work mentioned in Ref. (31), gave general equations for the average and maximum crack width in terms of the tensile stress in steel rather than the tensile strain. These equations are given below:

$$W_{av.} = (0.271\ f_s - 3.73)\ 10^{-4} \quad \ldots\ldots \quad (4.10)$$

$$W_{max} = (0.324\ f_s - 4.36)\ 10^{-4} \quad \ldots\ldots \quad (4.11)$$

and to include the modulus of elasticity of the mesh

$$W_{av.} = \frac{23000}{E_R}\ (0.271\ f_s - 3.73)\ 10^{-4} \quad \ldots\ldots \quad (4.12)$$

where

$W_{av.}, W_{max}$ = Average and maximum crack width respectively, in.

f_s = Steel stress, Ksi.

E_R = Modulus of reinforcing system, Ksi.

Naaman reported that the number of cracks reached a steady value soon after occurrence of first crack and the spacing independent of the number of meshes used is equal to the spacing of transverse wires. He also reported that the overall average ratio between maximum crack width and the average crack width was equal to 1.21 with a standard deviation of 0.14. Naaman, however, concluded that the exhaustive experimental work combined with scrupulous analysis are still necessary in ferrocement to better ascertain the influence of the major parameters and separate their effects.

Recently, Balaguru (58), presented theoretical equations to predict the crack spacing. The equation is basically the same as that suggested by Logan and Shah (18) (eq. 4.1), to predict the ultimate crack spacing, but he included the curvature of the beam as the important factor which controls the cracking. The equation is:

$$S = \sqrt{\frac{\psi_u}{\psi}}\ \frac{\theta}{\eta}\ \frac{1}{S_{LT}} \quad \ldots\ldots \quad (4.13)$$

where ψ and ψ_u are the curvature of the beam at the given load and at failure respectively.

Assuming that the curvature of the beam at ultimate equals the curvature at yielding and that the average crack width equals the average tensile strain

in the tension face multiplied by the crack spacing, Balaguru gave the following equation:

$$W_{av.} = \sqrt{\psi \, \psi_y} \; \frac{\theta \, (h-c)}{\eta \, S_{LT}} \qquad \ldots\ldots \qquad (4.14)$$

where $W_{av.}$ = Average crack width.

ψ_y = Curvature of the beam at yielding.

h = Total depth of the section.

c = Depth of neutral axis from compression face.

Balaguru also suggested that the properties of the section required in eq. 4.14 could be found using linear elastic analysis, the same as that used in reinforced concrete. This method of analysis may not give accurate results for the depth of the neutral axis and the curvature of ferrocement beams. Also, in Balaguru's theoretical model, the assumption $\psi_y = \psi_u$ could be invalid as ψ_u is substantially higher than ψ_y (11). In any case, the derived equations need verification by experimental results.

From the literature review, it can be seen that the cracking behaviour in flexure and the factors affecting this behaviour are an area which needs more study, not only for the prediction of the crack width but, perhaps, for reaching a better understanding of the potential of ferrocement.

4.3 Scope and Experimental Programme.

The following aspects were studied:

(1) Comparison of the cracking performance of specimens reinforced with mild steel wire mesh, high tensile steel wire mesh, and combination of mild steel wire mesh and steel bars.

(2) Effect of the number of the steel wire mesh on the crack width and spacing for specimens reinforced as in (1) above.

(3) Effect of the mesh distribution and the presence of steel bars in the section on the cracking performance and crack width.

(4) For the same amount of reinforcement, the effect of mortar cover and thickness of the section on the cracking performance and crack width.

(5) Derivation of crack width prediction equation.

The experimental programme consisted of seven series, comprising 44 specimens. Since cracking is essentially a random phenomenon, specimens with the same variables were repeated twice or three times. In addition, a large number of crack width and crack spacing measurements, at each of the selected stages of loading and for each specimen, were taken. The reason for that was to establish the repeatability of the tests and to obtain more reliable results.

Full details of the test programme, instrumentation, and test procedure are given in Chapter 3.

4.4 Treatment of the Results.

For each specimen, the results included the crack width and spacing, together with the corresponding tensile strain on the face of the specimen, recorded for at least four different load stages between the first crack and soon after yielding. All the cracks in the constant moment zone and crossing any of the three grid lines, shown in Fig.3.3, were considered. The number of crack width measurements at each stage varied between 20 and 90, depending on the type of specimen and level of load. A total number of crack width measurements of about 10,000 were taken.

A statistical approach was adopted to deal with that large number of crack width readings. The statistical approach does not only make the comparison of the data easier, but also gives more reliable results as it deals with the total population of the cracks rather than single cracks. A statistical computer programme was used to calculate the following values for each specimen and at each stage of crack width measurements:-

1. The mean, the maximum measured, the standard deviation and the coefficient of variation of the total population of the crack width readings.
2. The maximum crack width. Assuming normal distribution, the crack width with 2.28% chance of being exceeded was calculated.
3. Coefficient of skewness and coefficent kurtosis. These two values measure the skewness of the distribution from normality.
4. The average of the tensile strain measured (gauge length 100 mm) along the three lines of crack width measurement.

Tables 4.1 to 4.6 give details of the cracking characteristics at each stage of crack width measurement and for all specimens.

For each specimen, the mean crack width and the standard deviation were plotted against the corresponding average tensile strain on the face of the specimen. A linear regression was carried out and the slope of the best fit line together with the intercept and the correlation coefficient were found for all the specimens. Figs. 4.1 to 4.6 show the graphs of the mean crack width against the average tensile strain relationship and Table 4.7 gives the characteristics of the equations found from the linear regression for these relationships.

The slope of the linear relationship between the mean crack width and the average tensile strain on the face of the specimen, W_m/ε_t, will be referred to as the rate of growth of crack width, because it represents the rate of increase in the mean crack width with respect to the tensile strain. It should be noticed that W_m/ε_t equals the crack spacing, if the mortar between cracks is assumed to carry no tensile stress.

Relating the mean crack width to the tensile strain at the level of the crack is a beneficial approach in studying the effect of the different variables on the crack width. The tensile strain is a primary factor which affects the crack width. Moreover, this factor will repeat itself in every

Table 4.1 Cracking Characteristics of Specimens of Series S1.

Specimen	Load kN	No. of cracks*	Mean of crack width (microns)	Standard deviation σ (microns)	Coeff.of variation %	Max. crack width (measured) microns	Average tensile strain on the face ε_{av} micro-strain
S1 B1	1.176	22	33.9	13.3	39.2	56.3	1323
	1.312	23	46.9	14.5	30.8	71.4	1715
	1.450	23	182.5	78.7	43.2	313.4	6810
S1 B2**	0.9	10	39.3	9.1	23.1	51.8	802
	1.16	24	40.6	18.3	45.1	74.1	1315
	1.29	26	64.2	38.5	60	134.8	1608
	1.37	27	181.3	95.1	52.5	321.5	4960
S1 B3	0.848	28	11.2	4.5	40.7	25	436
	1.018	30	23.2	8.7	37.6	42	858
	1.169	31	30.7	10.9	35.6	53.6	1168
	1.305	33	38.2	15.7	41	74.1	1543
S1 C1	1.230	28	19.6	5.3	26.9	30.4	740
	1.504	29	29.7	7.5	25.2	44.7	1076
	1.777	31	38.3	10.5	27.3	56.3	1425
	2.188	34	54.2	19.0	35.0	84.8	2130
	2.461	36	73.6	29.9	40.6	125	2924
	2.735	37	104.1	45	43.3	195.6	4249
S1 C2	0.957	29	13.2	4.0	30.2	21.4	768
	1.552	38	24.8	7.7	31.2	40.2	1574
	2.078	38	39.4	11.7	29.6	68.8	2419
	2.557	38	83.8	26.5	31.6	142.9	4895
S1 C3	1.271	33	15.2	4.5	29.4	23.2	847
	1.668	40	23.2	7.5	32.6	34.8	1338
	2.085	42	32.7	11.6	35.5	50.9	1909
	2.461	43	52.7	19.4	36.8	88.4	2951
	2.741	44	100	40.7	40.8	174.1	5560
S1 D1	1.121	18	8.3	2.3	28.1	13.4	446
	1.586	37	14.3	4.1	28.5	23.2	984
	2.085	40	23.2	6.6	28.5	37.5	1540
	2.680	44	28.9	10.4	35.8	48.2	2178
	3.172	46	42.7	13.8	32.3	72.3	3182
	3.637	46	78.7	24.9	31.6	120.5	5430
S1 D2	1.278	36	13.4	4.8	36.2	21.4	884
	1.832	44	19.8	8.3	41.8	40.2	1475
	2.365	48	27.7	12.2	43.9	52.7	2055
	3.097	49	49.5	22.1	44.6	90.2	3512
	3.384	49	68.8	29.5	42.9	119.7	4971
S1 D3	1.258	48	8.7	3.0	34.6	13.4	703
	1.818	59	14.1	5.2	37.3	25	1210
	2.598	63	22.1	8.1	36.8	39.3	1982
	3.377	65	38.0	17	44.7	86.6	3356
	3.884	69	66.8	32.4	48.5	144.7	6225

*Total number of cracks crossing the three grid lines.

**Neglected in the analysis due to inconsistency of results.

Table 4.1 Cracking Characteristics of Specimens of Series S1.

Specimen	Load kN	No. of cracks*	Mean of crack width (microns)	Standard deviation σ (microns)	Coeff. of variation %	Max. crack width (measured) microns	Average tensile strain on the face ε_{av} microstrain
S1 E1	1.271	33	13.4	3.7	28.0	21.4	684
	2.338	41	25.2	6.2	24.6	35.7	1571
	2.912	42	32.4	8.6	26.5	51.8	2055
	3.418	44	40.4	10.9	27.0	67.0	2740
	3.938	45	54.7	17.7	32.3	93.8	3704
S1 E2	2.092	44	13.7	4.5	32.7	23.2	1174
	2.639	53	18.3	5.0	27.1	27.7	1574
	3.193	54	23.6	6.9	29.1	37.5	1988
	3.685	58	28.5	9.9	34.7	47.3	2475
	4.417	60	44.4	15.5	34.9	83.1	3799
S1 E3	1.572	50	11.5	3.6	31.0	21.4	805
	2.618	55	20.3	6.4	31.4	36.6	1568
	3.671	57	31.9	10.1	31.7	58.0	2490
	4.663	58	63.5	19.6	30.9	109.0	4884
	5.155	58	103.6	31.6	30.5	175.0	7936
S1 F1	1.805	31	10.0	2.6	25.5	15.2	729
	2.393	47	12.8	4.0	31.3	23.2	1055
	2.953	50	15.5	4.9	31.9	24.1	1360
	3.720	52	20.5	6.9	33.6	33	1822
	5.046	56	33.4	10.0	30.1	56.3	2952
S1 F2	1.805	44	9.8	3.1	31.4	17.9	811
	2.625	55	14.8	5.1	34.5	31.3	1301
	3.460	56	21.1	6.7	31.5	41.1	1748
	4.198	64	26.2	9.9	37.8	58.9	2340
	4.923	66	37.1	14.4	38.9	78.6	3368
S1 F3	1.545	37	8.7	2.3	25.7	14.3	670
	2.625	54	16.1	4.3	27.0	25.9	1405
	3.692	57	24.2	6.6	27.4	36.6	2188
	4.704	58	36.6	10.4	28.5	60.7	3318
	5.689	59	69.6	22.3	32.1	118.8	6410

*Total number of cracks crossing the three grid lines.

Table 4.2 Cracking Characteristics of Specimens of Series S2.

Specimen	Load kN	No. of cracks*	Mean of crack width microns	Standard deviation σ microns	Coeff. of variation %	Measured max. crack width W_{max} microns	Average tensile strain on the face ε_t microstrain
S2 B1	0.882	20	15.8	6.8	43.2	28.6	526
	1.073	29	25.8	8.0	30.8	36.6	1255
	1.244	31	35.5	9.7	27.4	49.1	1732
	1.552	32	47.3	11.8	24.9	65.2	2284
	1.942	33	64	14.3	22.3	87.5	3042
S2 B2	1.217	41	23.9	9.8	40.8	53.6	1532
	1.504	42	35.1	12.7	36.1	70.6	2165
	1.805	42	44.1	14.7	33.3	84.8	2813
	2.321	44	62.3	20.6	33.1	108.1	4036
S2 C1	1.463	47	16.4	4.1	24.9	26.8	1075
	2.290	50	30.7	7.6	24.7	48.2	2146
	3.104	52	44	10.4	23.7	65.2	3109
	3.665	53	53.9	12.5	23.2	77.7	3790
	4.184	58	60.1	18.5	30.8	90.2	4525
S2 C2	1.482	53	12.0	4.0	33.7	20.5	1253
	2.167	63	20.5	7.1	34.4	37.5	2160
	3.083	70	30.2	11.2	37.1	56.3	3424**
	4.010	80	37.8	14.9	39.5	69.7	4782
S2 D1	1.600	40	12.6	3.2	25.7	17.9	1058
	2.74	60	22.9	7.8	34.3	36.6	2178
	3.898	66	33.0	10.3	31.4	57.2	3431
	5.037	73	42.6	14.0	32.9	72.3	4652
	6.130	80	53.4	18.2	34.2	95.6	6083
S2 D2	1.653	46	12.7	4.0	31.0	19.7	1090
	2.704	57	26.2	7.5	28.5	40.2	2160
	3.915	67	37.0	13.5	36.5	61.6	3335
	5.055	71	47.6	16.5	34.6	77.7	4692
S2 E1	1.618	45	8.8	2.9	32.5	14.3	766
	2.775	62	17.4	5.7	32.6	31.3	1627
	3.898	70	23.6	8.2	34.7	45.5	2481
	5.587	76	34.0	10.8	31.8	69.6	3842
S2 E2	1.907	50	10.7	3.1	28.9	18.8	1088
	3.024	65	18.8	5.4	28.7	32.2	2009
	4.683	82	28.0	9.9	35.4	48.2	3502
	6.154	86	37.4	12	32.0	64.3	4879

*Total number of cracks crossing the three grid lines.

**Neglected in the analysis due to inconsistency of the results.

Table 4.3 Cracking Characteristics of Specimens of Series S3.

Specimen	Load kN	No.of* cracks	Mean of crack width microns	Standard deviation σ microns	Coefficient of variation %	Measured max.crack width W_{max} microns	Average tensile strain on the face ε_t microstrain
S3 C1	0.977	32	13.4	4.1	30.4	20.5	648
	1.264	35	22.0	6.6	29.8	31.3	1215
	1.764	38	37.4	12.3	32.8	53.6	2092
	2.250	40	87.5	31.0	35.4	134.8	4260
S3 C2	0.847	28	13.5	5.1	37.7	31.3	504
	1.285	36	24.4	7.7	31.5	42.9	1166
	1.688	38	35.7	11.4	32.0	56.3	1790
	2.092	39	55.4	19.1	34.5	92.9	2697
	2.311	39	91.8	36.4	39.7	171.5	4263
S3 D1	1.230	33	15.8	4.1	26.1	23.2	895
	1.805	34	28.2	5.2	18.6	39.3	1495
	2.352	36	40.6	8.2	20.2	58.0	2147
	2.858	36	59.4	11.2	18.8	86.6	3098
	3.336	36	98.0	19.7	20.1	141.9	5022
S3 D2	1.278	31	12.1	4.5	37.2	21.4	716
	1.811	40	20.8	8.1	39.2	38.4	1328
	2.352	44	29.4	11.8	40.1	58.0	1984
	2.871	45	46.4	19.0	41	100.0	3094
	3.350	46	88.2	38.8	44	205.4	6102
S3 E1**	1.230	33	10.6	2.9	27.1	18.8	696
	2.092	41	23.9	7.0	29.5	36.6	1504
	2.899	42	39.4	10.1	25.7	63.4	2311
	3.658	42	71.2	18.1	25.4	116.1	4039
S3 E2	1.504	39	9.6	3.4	35.1	17.0	759
	2.064	51	14.5	5.2	35.7	25.9	1220
	2.865	55	24.0	7.9	33.0	39.3	1910
	3.644	56	40.0	12.4	31.0	71.4	2989
	4.116	56	63.6	19.7	31.0	116.1	4763

*Total number of cracks crossing the three grid lines.

**Neglected due to low ultimate strength.

Table 4.4 Cracking Characteristics of Specimens of Series S4 and S7.

Specimen	Load kN	No.of* cracks	Mean of crack width microns	Standard deviation σ microns	Coefficient of variation %	Measured max.crack width W_{max} microns	Average tensile strain on the face ε_t microstrain
S4 A	1.265	18	16.9	6.2	37.0	33	300
	2.120	32	25.6	10.2	40.0	47.3	864
	3.364	33	44.0	13.9	31.6	68.8	1682
S4 B	0.797	17	9.4	3.3	35.1	17.0	337
	1.057	32	15.1	5.5	36.5	32.2	661
	1.453	38	20.3	7.9	38.8	45.5	996
	2.023	46	27.3	10.8	39.7	50.9	1514
	2.699	51	39.5	18.9	48.0	80.4	2325
S4 C	1.323	28	10.4	2.8	26.6	15.2	640
	1.677	37	12.9	4.5	35.0	19.7	902
	2.220	42	18.9	6.3	33.2	32.2	1307
	3.10	47	27.50	9.7	35.2	45.5	2014
	4.063	53	42.0	16.3	38.8	75.0	3262
S4 D	1.866	37	9.4	2.7	28.8	14.3	785
	3.023	61	15.9	5.8	36.4	28.6	1522
	4.14	65	26.1	10.1	38.6	47.3	2449
	5.12	66	51.1	22.1	43.3	90.2	4714
S7 C	1.169	36	15.2	4.4	28.7	22.3	788
	1.665	38	26.6	7.0	26.1	36.6	1347
	2.120	38	40.8	9.9	24.3	56.3	1973**
	2.462	38	99.3	29.3	29.5	156.3	4025**

*Total number of cracks crossing the three grid lines.

**Neglected due to the inconsistency of the results.

Table 4.5 Cracking Characteristics of Specimens of Series S5.

Specimen	Load kN	No.of* cracks	Mean of crack width microns	Standard deviation σ microns	Coefficient of variation %	Measured max.crack width W_{max} microns	Average tensile strain on the face ε_t microstrain
S5 C1	1.162	35	12.0	s.6	21.4	17.9	732
	1.654	43	19.8	4.4	22.3	27.7	1258
	2.256	51	27.2	8.2	30.1	47.3	2009
	3.035	55	46.1	15.5	33.6	90.2	3270
	3.487	55	81.4	28.2	34.6	178.6	5411
S5 C2	1.176	35	13.2	4.4	33.4	20.5	880
	2.023	48	25.3	8.8	34.7	45.5	1755
	2.830	50	42.8	12.6	29.4	67.9	3086
	3.295	52	69.8	21.8	31.2	114.3	5041
S5 C3	1.203	33	15.1	3.9	25.8	26.8	880
	1.777	46	22.9	6.8	28.5	41.1	1539
	2.557	48	39.9	11.9	29.9	69.7	2565
S5 E1	2.191	29	15.2	3.9	25.6	21.4	670
	3.915	35	34.4	9.3	26.9	53.6	1523
	5.049	36	55.2	14.9	27.0	87.5	2417
	6.071	36	101.3	27.3	26.9	167.0	4271
S5 E2	2.188	29	12.1	3.2	26.1	18.8	629
	3.336	39	22.9	7.2	31.5	34.8	1331
	4.459	41	35.4	10.4	29.4	56.3	2036
	5.539	41	59.2	17.1	28.9	109.8	3286
S5 E3	2.433	32	14.2	4.6	32.6	20.5	662
	3.496	37	26.1	7.8	29.9	39.3	1237
	4.530	39	39.8	12.0	30.1	67.0	1887
	5.126	39	60.0	16.3	27.2	105.4	2714

*Total number of cracks crossing the three grid lines.

Table 4.6 Cracking Characteristics of Specimens of Series S6.

Specimen	Load kN	No.of* cracks	Mean of crack width microns	Standard deviation σ microns	Coefficient of variation %	Measured max. crack width W_{max} microns	Average tensile strain on the face ε_t microstrain
S6 4D1	0.984	35	11.1	3.6	32.2	20.5	670
	1.545	39	20.9	5.5	26.1	35.7	1345
	2.065	42	30.7	10.3	33.6	57.2	2014
	2.625	46	40.2	15.0	37.4	71.4	2734
	3.138	46	60.0	20.8	34.7	108.1	3957
S6 4D2	1.011	36	9.9	2.5	24.8	17.9	543
	1.517	40	18.5	3.6	19.3	23.2	1087
	2.065	43	27.9	6.8	24.4	37.5	1760
	2.858	46	44.0	12.5	28.5	66.1	2466
	3.377	46	65.2	18.3	28.1	110.7	4050
S6 6D1	0.765	28	12.7	3.1	24.6	17.0	574
	1.224	35	22.8	6.3	27.7	38.4	1191
	1.764	38	35.5	10.8	30.3	51.8	2058
	2.338	38	52.7	14.9	28.2	75.0	2912
	3.090	40	80.4	26.7	33.2	118.8	4679
S6 6D2	0.807	26	13.3	2.9	22.1	19.7	512
	1.244	38	19.9	5.6	28.4	29.5	909
	1.805	39	32.7	8.6	26.4	44.7	1535
	2.564	39	54.5	15.3	28.1	85.7	2639
	3.336	39	94.6	28.2	29.9	163.4	4759

*Total number of cracks crossing the three grid lines.

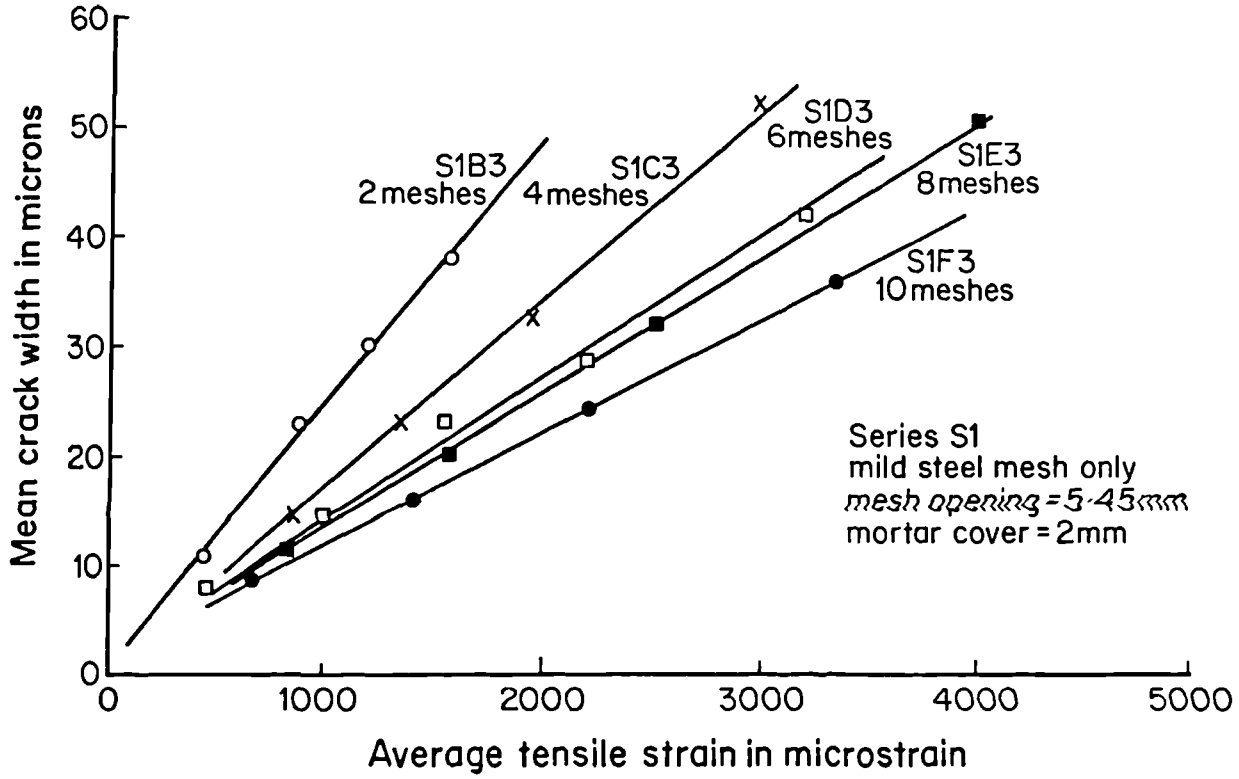

Fig.4.1. Mean crack width against average tensile strain on the face of the specimen, series S1.

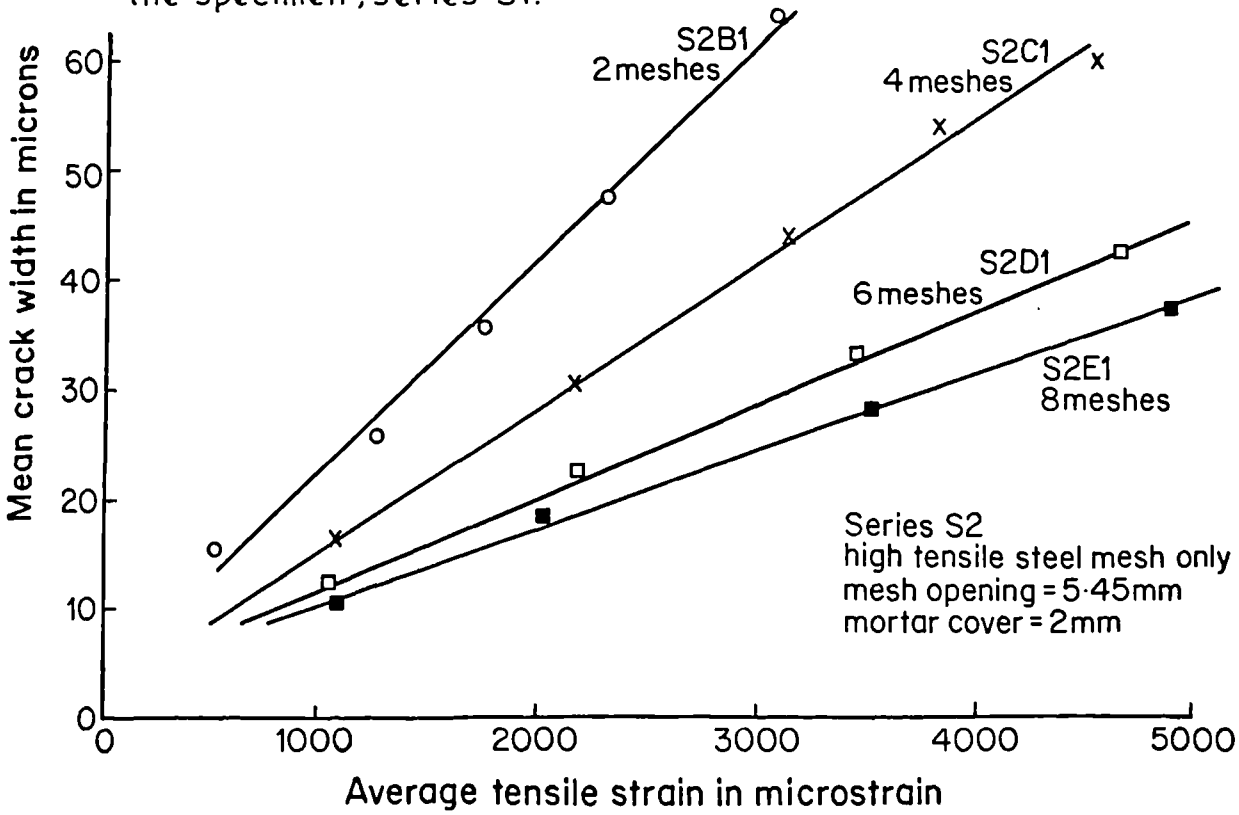

Fig.4.2. Mean crack width against average tensile stain on the face of the specimen, series S2.

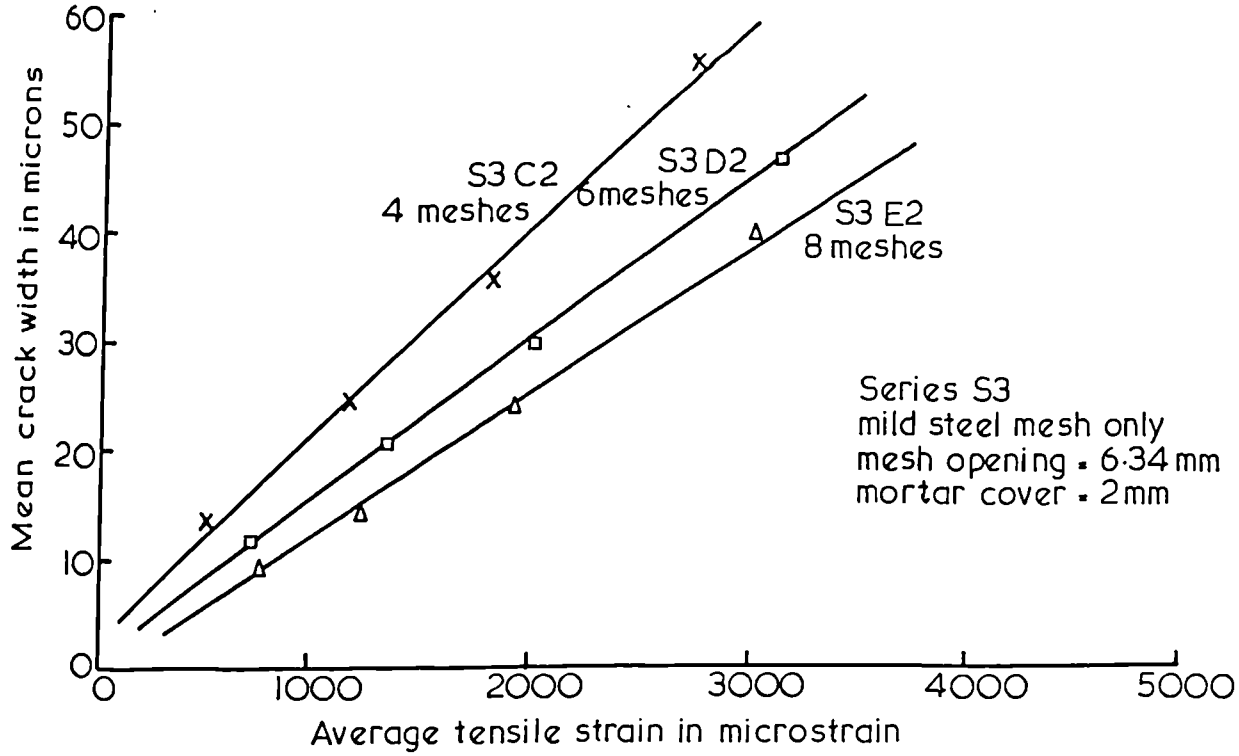

Fig.4·3. Mean crack width against the average tensile strain on the face of the specimen, series S3.

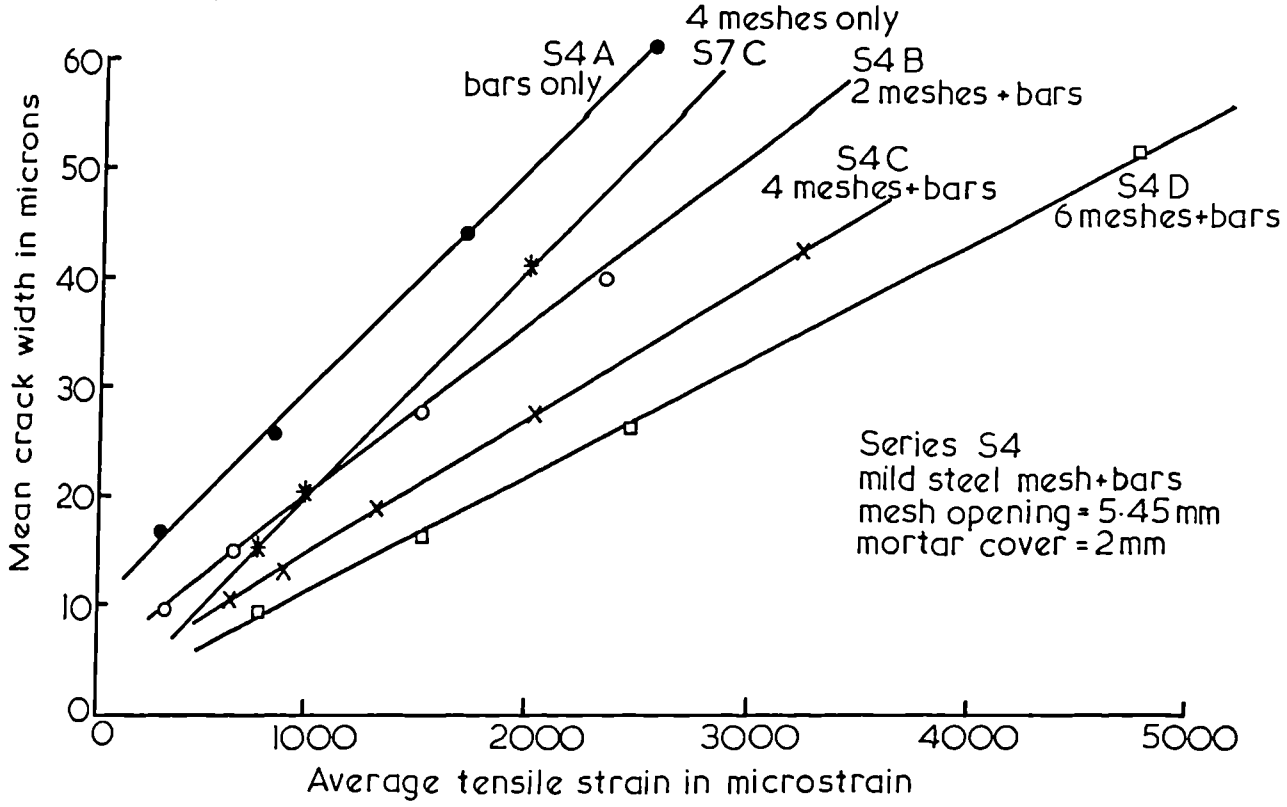

Fig.4·4. Mean crack width against average tensile strain on the face of the specimen series S4 and S7.

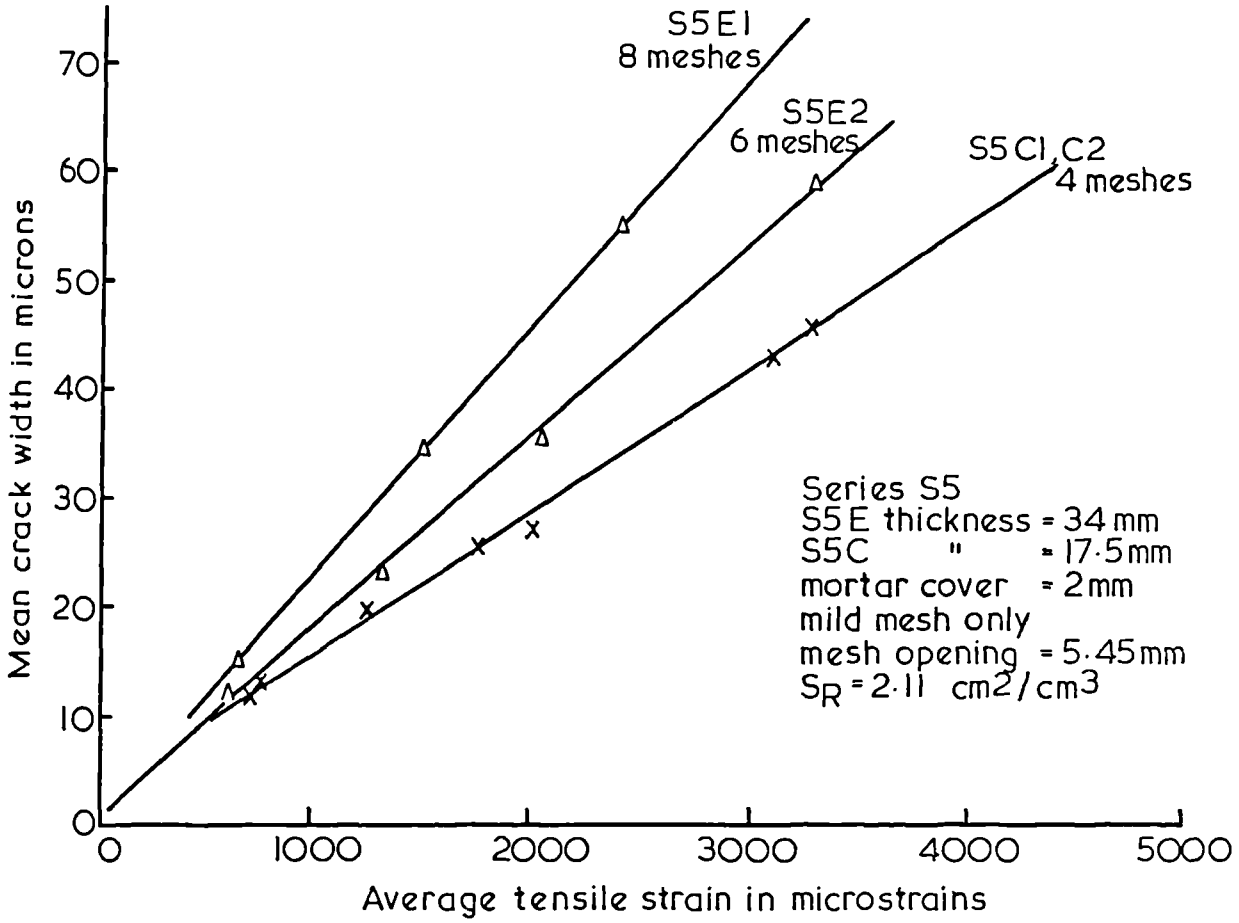

Fig. 4·5. Mean crack width against average tensile strain on the face of the specimen, series S5.

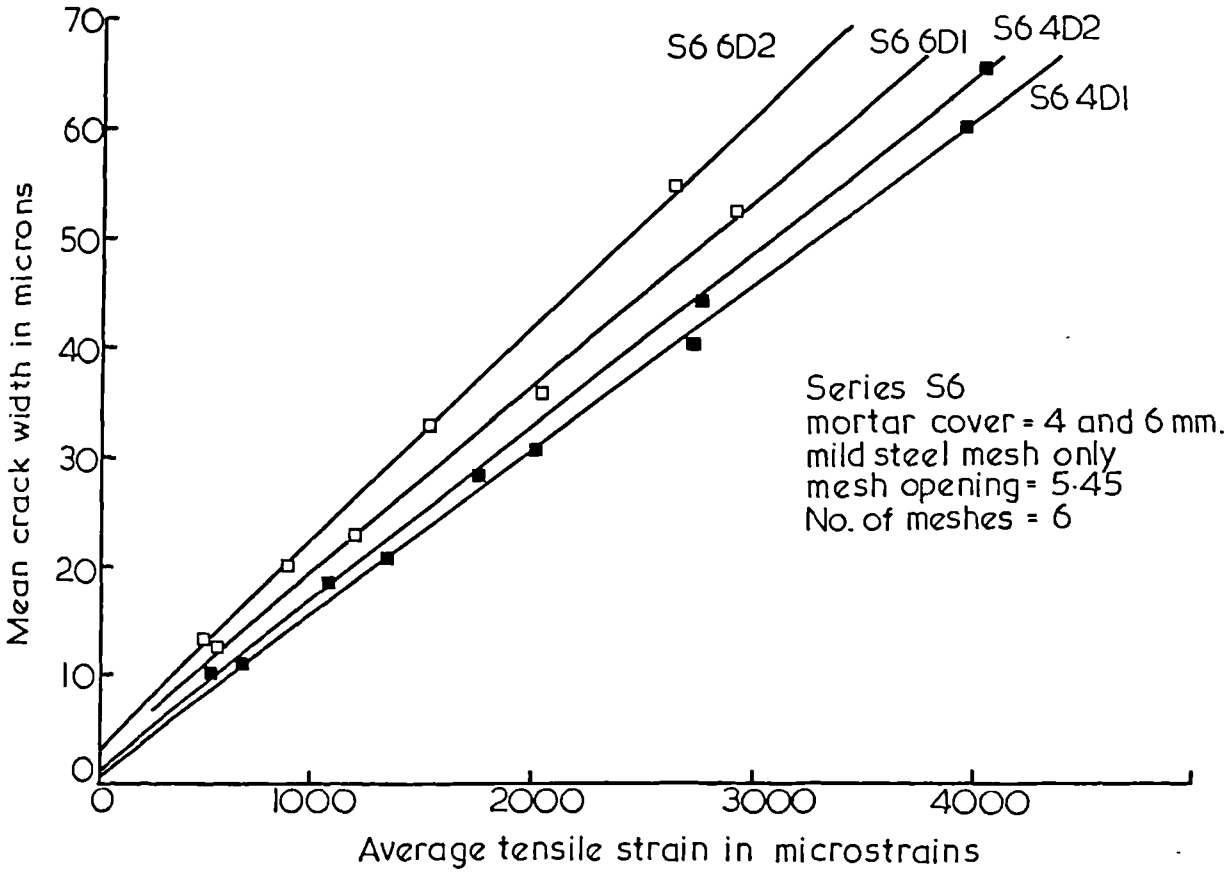

Fig. 4·6. Mean crack width against average tensile strain on the face of the specimen, series S6.

Table 4.7 Results of the linear regression on mean crack width and average tensile strain.

No.	Specimen Designation	W_m/ε_t mm	Intercept microns	Correlation coeff.	Mean of slope
1	S1 B1*	26.88	-0.44	0.9999	
2	S1 B2	35.6	4.08	0.994	25.68
3	S1 B3	24.47	1.33	0.996	
4	S1 C1	23.82	3.46	0.9996	
5	S1 C2	17.3	-1.46	0.9992	19.75
6	S1 C3	18.13	-0.98	0.9998	
7	S1 D1	14.1	0.37	0.997	
8	S1 D2	13.84	0.125	0.9993	12.86
9	S1 D3	10.65	1.48	0.9997	
10	S1 E1	13.57	3.95	0.9994	
11	S1 E2	11.65	0.045	0.9998	12.74
12	S1 E3	13.0	0.21	0.9999	
13	S1 F1	10.65	1.55	0.998	
14	S1 F2	10.65	1.42	0.998	10.65
15	S1 F3	10.65	1.25	0.999	
16	S2 B1	19.45	3.29	0.995	17.3
17	S2 B2	15.14	1.44	0.9991	
18	S2 C1	13.0	2.95	0.997	10.66
19	S2 C2	8.32	1.92	0.9983	
20	S2 D1	8.07	4.79	0.9993	8.83
21	S2 D2	9.58	3.87	0.994	
22	S2 E1	8.08	3.36	0.997	7.49
23	S2 E2	6.9	3.9	0.998	
24	S3 C1	20.82	-2.69	0.9967	20.93
25	S3 C2	21.03	0.32	0.9976	
26	S3 D1	19.85	-1.86	0.9999	17.01
27	S3 D2	14.16	1.91	0.9999	
28	S3 E1*	18.26	-2.76	0.9997	13.7
29	S3 E2	13.7	-1.57	0.9995	
30	S4 A	19.8	10	0.9957	19.8
31	S4 B	14.9	4.92	0.9993	14.9
32	S4 C	12.18	2.58	0.9994	12.2
33	S4 D	10.73	0.21	0.9994	10.7
34	S7 C	21.6	-2.05	0.9996	21.6
35	S5 C1	13.22	2.25	0.9970	
36	S5 C2	13.56	1.28	0.9999	13.9
37	S5 C3	14.9	1.21	0.9965	
38	S5 E1	22.86	-0.18	0.9999	
39	S5 E2	17.83	-0.08	0.999	21
40	S5 E3	22.28	-1.2	0.9991	
41	S6 4D1	14.78	0.87	0.9993	15.3
42	S6 4D2	15.73	1	0.996	
43	S6 6D1	16.62	2.86	0.9992	17.9
44	S6 6D2	19.27	3.1	0.9999	

*Neglected in calculating the average due to inconsistency of the results.

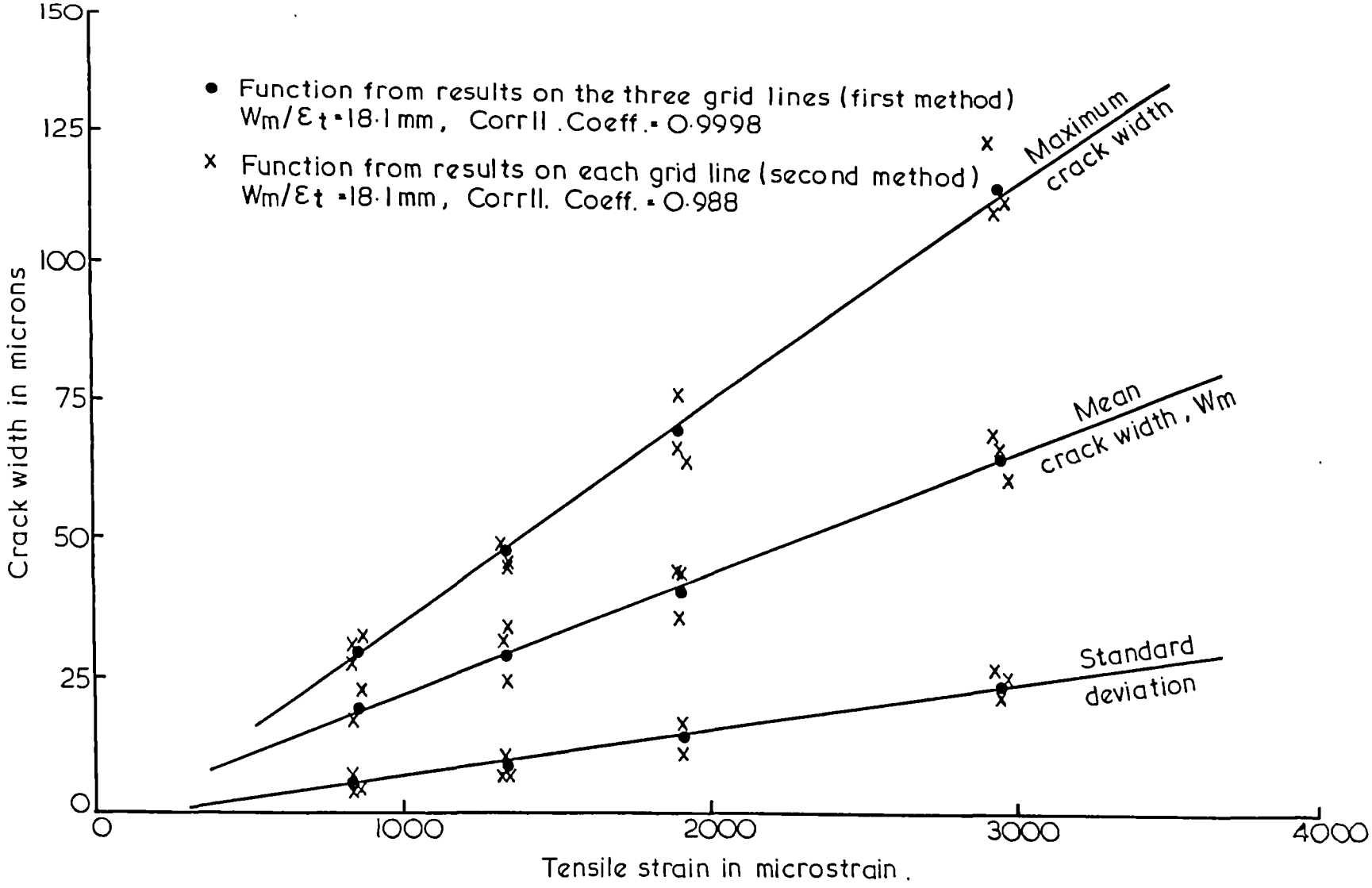

Fig. 4·7. Results of the two methods of analysis of the crack width data for specimen S1C3.

specimen and therefore cannot be eliminated for the sake of the study of the effect of the other factors on the crack width. Consequently, replacing the crack width by the rate of growth of crack width, W_m/ε_t, eliminates the repeated variable and simplifies the analysis of the effect of the other factors as they are mainly independent variables.

This approach has been used satisfactorily in dealing with the cracking in reinforced concrete (59,60,61). It could be even more appropriate for ferrocement as it has been suggested that for such material (31,70) the steel strain is the most important factor affecting the crack width. Although in this study, the tensile strain on the face of the specimen was considered instead of the steel tensile strain, the strain on the face could be assumed to be in direct proportion to the steel strain.

It is to be mentioned that an alternative method for finding the rate of growth of crack width W_m/ε_t was considered. Instead of calculating the average tensile strain along the three lines of crack width measurement and relating it to the total population of the crack width, the mean crack width of the cracks on each line was plotted against the corresponding tensile strain. Although the values of W_m/ε_t using this method were practically the same as those from the first method, the correlation coefficient of the relationship using the first method was found to be higher. Since in the first method the considered crack population is larger, and the larger the population the nearer the distribution to normal (62), therefore the first method was adopted. Fig.4.7 shows typical results for a specimen calculated by the two methods.

4.5 The Relationship Between the Maximum and the Average Crack Width.

The relationship between the maximum and the average crack width was found by two methods. The first method was by calculating the average ratio of the measured maximum crack width to the mean. The second method was by

using a statistical approach. It depends on the relationship between the mean and the standard deviation of the population of the crack width readings. The principles of the second method are as follows:

1. The slopes of the linear relationships between the mean crack width and the average tensile strain (W_m/ε_t) for the different specimens were plotted against the corresponding slopes of the linear relationships between the standard deviation and the average tensile strain (σ/ε_t), see Fig.4.8. The best fit line forced through the origin was found. The equation of this line is

$$\sigma/\varepsilon_t = b\ W_m/\varepsilon_t$$

where the slope (b) can be calculated using the following relation (62):

$$b = \Sigma[(\sigma/\varepsilon_t)\ (W_m/\varepsilon_t)]/\Sigma(W_m/\varepsilon_t)^2$$

Thus, the standard deviation is defined in terms of the mean crack width.

2. Assuming a normal distribution, the maximum crack width with 2.28% chance of being exceeded, is:

$$W_{max} = W_m + 2\sigma$$

Substituting σ in the above equation by its value in terms of W_m, found in step 1, gives the probabilistic relationship between W_m and W_{max}.

It is relevant to notice that the slope of the best fit line (b) is equal to the coefficient of variation divided by 100. The value of this slope found from analysing the results of all the tested specimens was equal to 0.354 which gives an overall coefficient of variation equal to 35.4%. The average value of the coefficient of variation of crack width found at each loading stage (Tables 4.1 to 4.6) was equal to 32% which is in good agreement with above one.

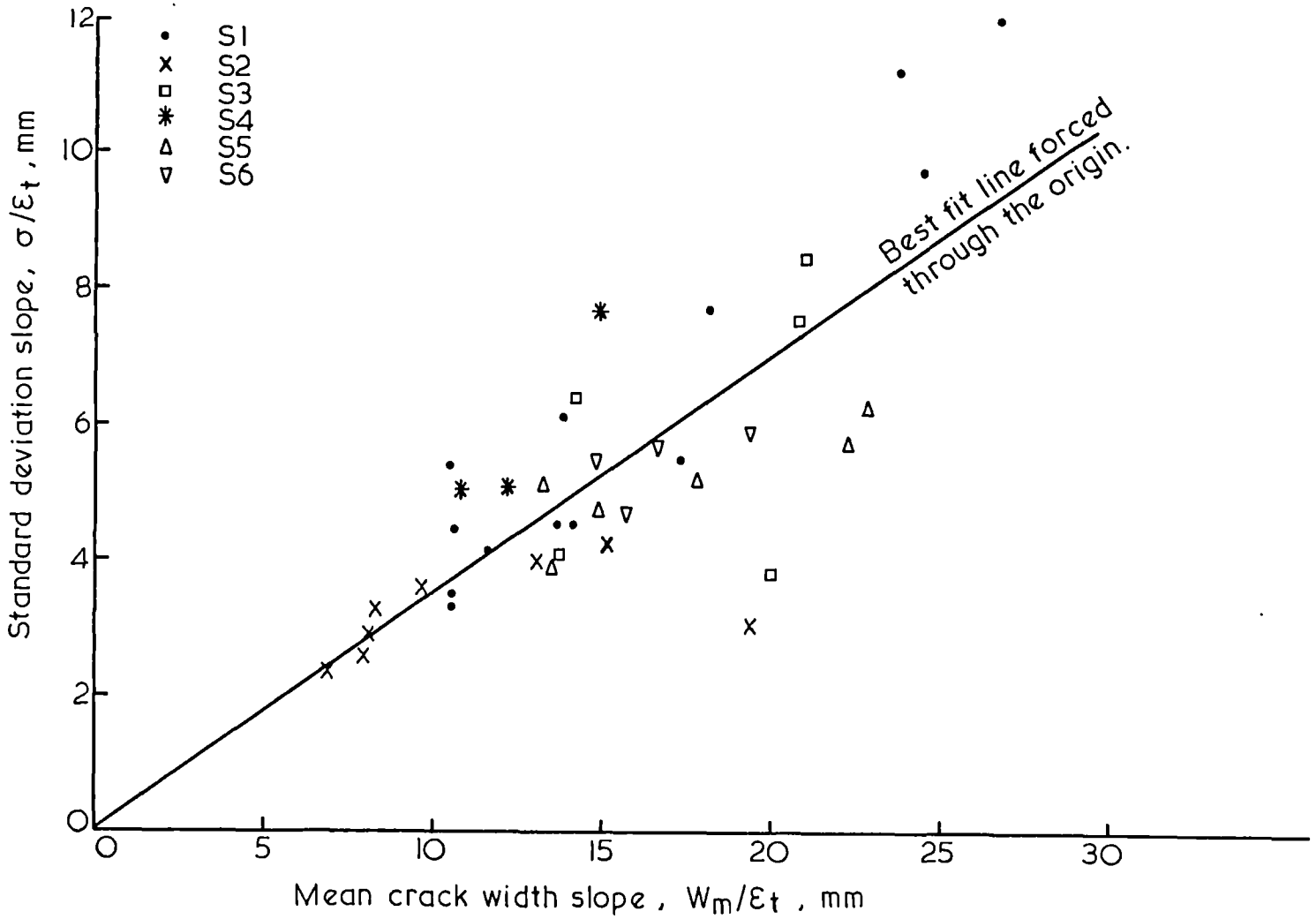

Fig. 4.8. Standard deviation slope vs. mean crack width slope.

The values of W_{max}/W_m for specimens of each series as well as the overall value for all specimens were calculated using the two described methods and are given in Table 4.8. The overall value of W_{max}/W_m found using the first method was 1.69 with a standard deviation equal to 0.21, while that found using the second method was 1.71. The two methods, therefore, gave comparable results.

To the best of the writer's knowledge, the only other W_{max}/W_m value for ferrocement found experimentally was reported by Naaman (24). It was equal to 1.21 with standard deviation equal to 0.14. The procedure used is similar to that of the first method described above, while the reported value, as can be seen, is less than the one obtained from this study. It may be worth noticing, however, that in Naaman's specimens the zone over which the cracks were measured was only 125 mm, while in this study the zone was 300 mm. Thus, higher number of crack width measurements at each loading stage were taken in this study and hence a more accurate value of the mean crack width (62) would be expected.

In table 4.9, values of W_{max}/W_m found for reinforced concrete members are given. It can be seen that these values are relatively higher than those for ferrocement, indicating that ferrocement shows a more uniform cracking performance than reinforced concrete.

Table 4.8 Values of W_{max}/W_m for the different series.

	W_{max}/W_m	S1	S2	S3	S4	S5	S6	Overall
First method	Average	1.72	1.69	1.72	1.79	1.64	1.58	1.69
	Range	(2.28-1.42)	(1.38-2.24)	(1.42-2.33)	(1.46-2.24)	(1.41-1.96)	(1.26-1.86)	(1.26-2.33)
Second method (probabilistic)	-	1.82	1.53	1.68	1.95	1.58	1.66	1.71

Table 4.9 Values of W_{max}/W_m for ferrocement and reinforced concrete.

	Reinforced Concrete				Fibrous Concrete	Ferrocement	
	Broms (63)	Base et al. (60)	Borges (64)	Illston et al. (65)	Al-Taan (61)	Naaman (24)	Present Investigation
Average	2	2*	1.72 or 1.66*	2	2.03 or 2.24*	1.21	1.69 or 1.71*
Range	-	-	-	1.5 - 2.88	1.29 - 2.88	-	1.26 - 2.23

*probabilistic.

4.6 Cracking Behaviour of Ferrocement.

4.6.1 First Cracking.

Some investigators have used the characteristics of the section at first cracking as a measure of its superior performance. There were attempts to define the amount of reinforcement which produces the optimum ferrocement section, by comparing the load at the first crack. The results were contradictory.

In this investigation the load at the first crack was recorded for each specimen. The first crack was defined as that which can first be seen using a magnifying glass. The crack width at the first crack was measured for several specimens and found to be of the order of a few microns. Strain and deflection measurements helped anticipating its occurrence. In Fig.4.9 the load at the first crack is plotted against the specific surface of reinforcement, S_R, for specimens with the same section thickness and mortar cover. The figure shows no optimum amount of reinforcement, in terms of S_R. In fact the results are scattered and there seems to be no clear relationship between the load at first crack and the specific surface.

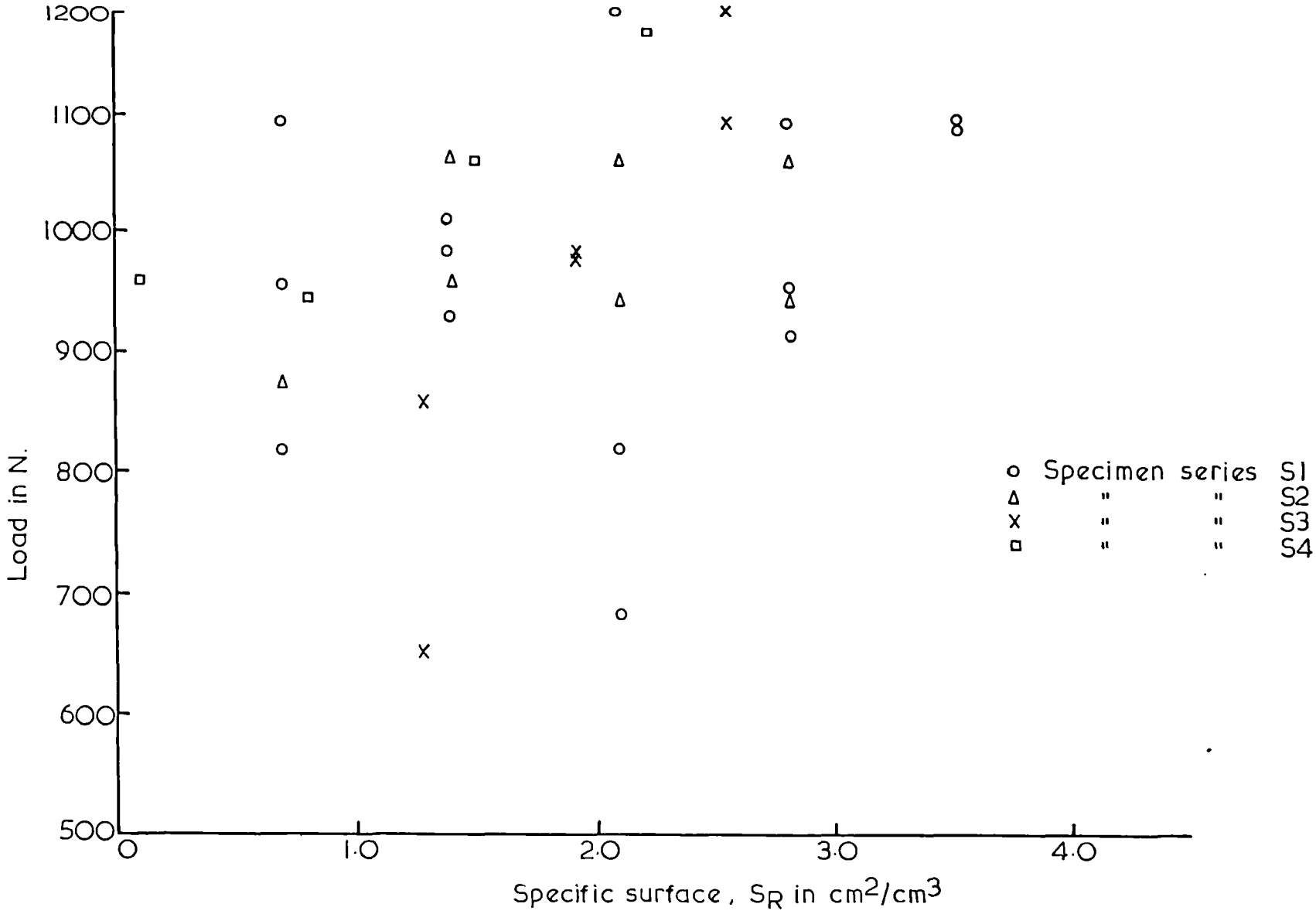

Fig.4.9. Load at first crack vs. specific surface of reinforcement.

4.6.2 Behaviour from First Cracking Till Failure.

The development of crack spacing and crack width with load is shown in Fig.4.10 for specimens reinforced with mild steel mesh (Series S1), and in Fig.4.11 for specimens reinforced with high tensile steel mesh (Series S2). The two figures show that the crack width increases linearly with the load. However, for specimens with mild steel mesh, and at a certain stage of the load, the crack width starts to increase at a faster rate. This stage of loading corresponds to the beginning of yielding of the specimen. The faster increase in the crack width was not observed in specimens with high tensile steel mesh for the range of crack width measurements taken in this study.

In terms of the crack number and spacing, the cracking behaviour is characterized by two stages. The first stage occurs immediately after the first cracking in which the cracks increase in number rapidly, followed by a second stage when crack spacing decreases at a much slower rate. The number of cracks appear to reach almost a saturation limit at a certain stage of loading. Most of the cracks found after failure are actually formed at about 30-50% of the ultimate load. The early development of the crack number represents a major difference in the cracking behaviour of ferrocement and other similar materials. Al-Taan (61) reported, from tests on conventionally reinforced concrete beams with steel fibres, that the number of cracks visible at the service load, (35-45% of the ultimate load) was about half the number near failure. The full development of the number of cracks in ferrocement at the early stages of loading utilizes the advantage of higher crack number and hence less crack width at the critical stage of loading, i.e. the service load.

Fig.4.12 shows the frequency distribution of the crack width measurements at different loading stages for four specimens, reinforced with six meshes each, two specimens with mild steel and the other two with high tensile steel.

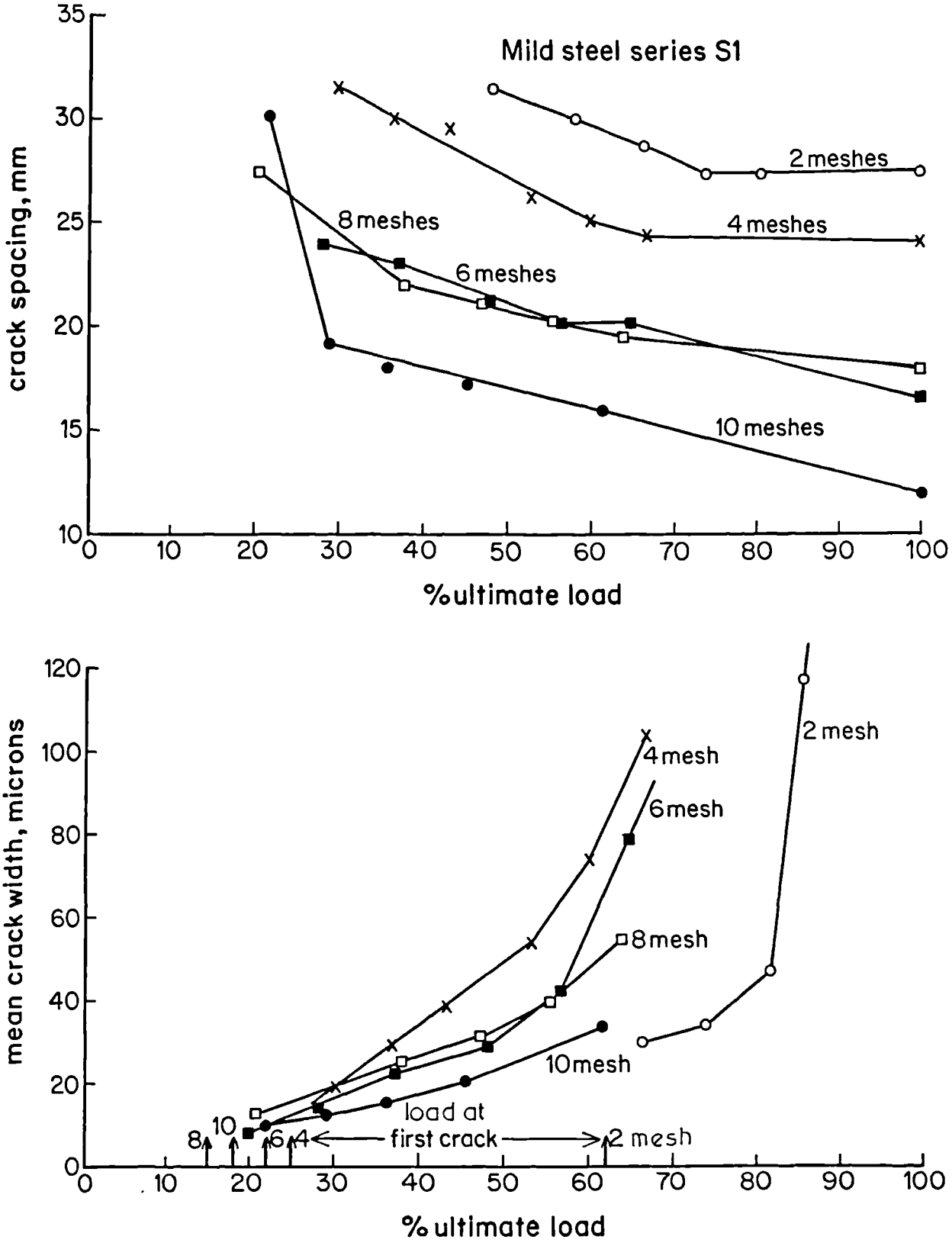

Fig. 4.10 Crack width and spacing against percentage of the ultimate load for specimens from series S1

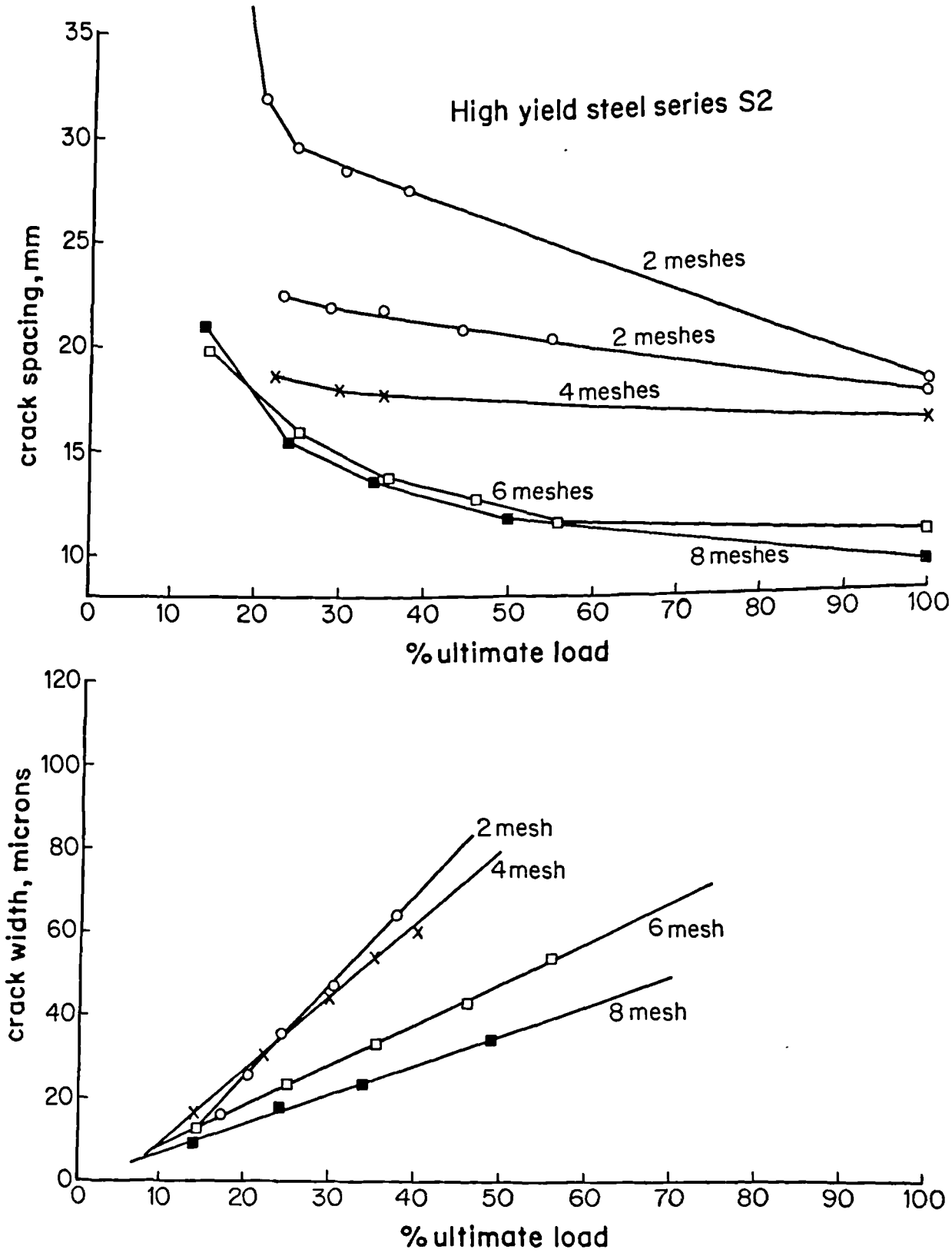

Fig. 4.11 Crack width and spacing against percentage of ultimate load for specimens from series S2

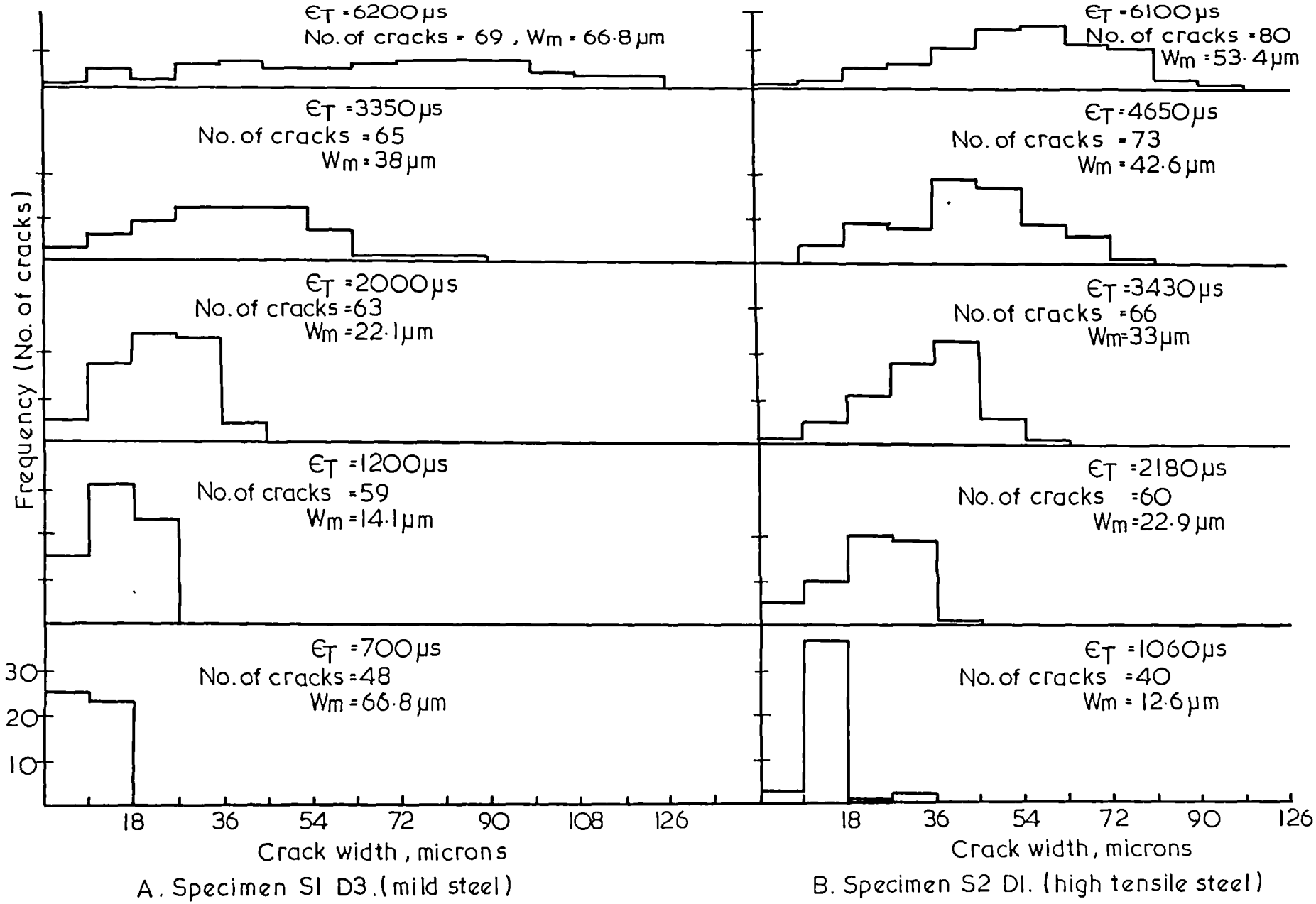

Fig. 4·12. A & B. Crack width distribution for specimens reinforced with six meshes from series S1 and S2.

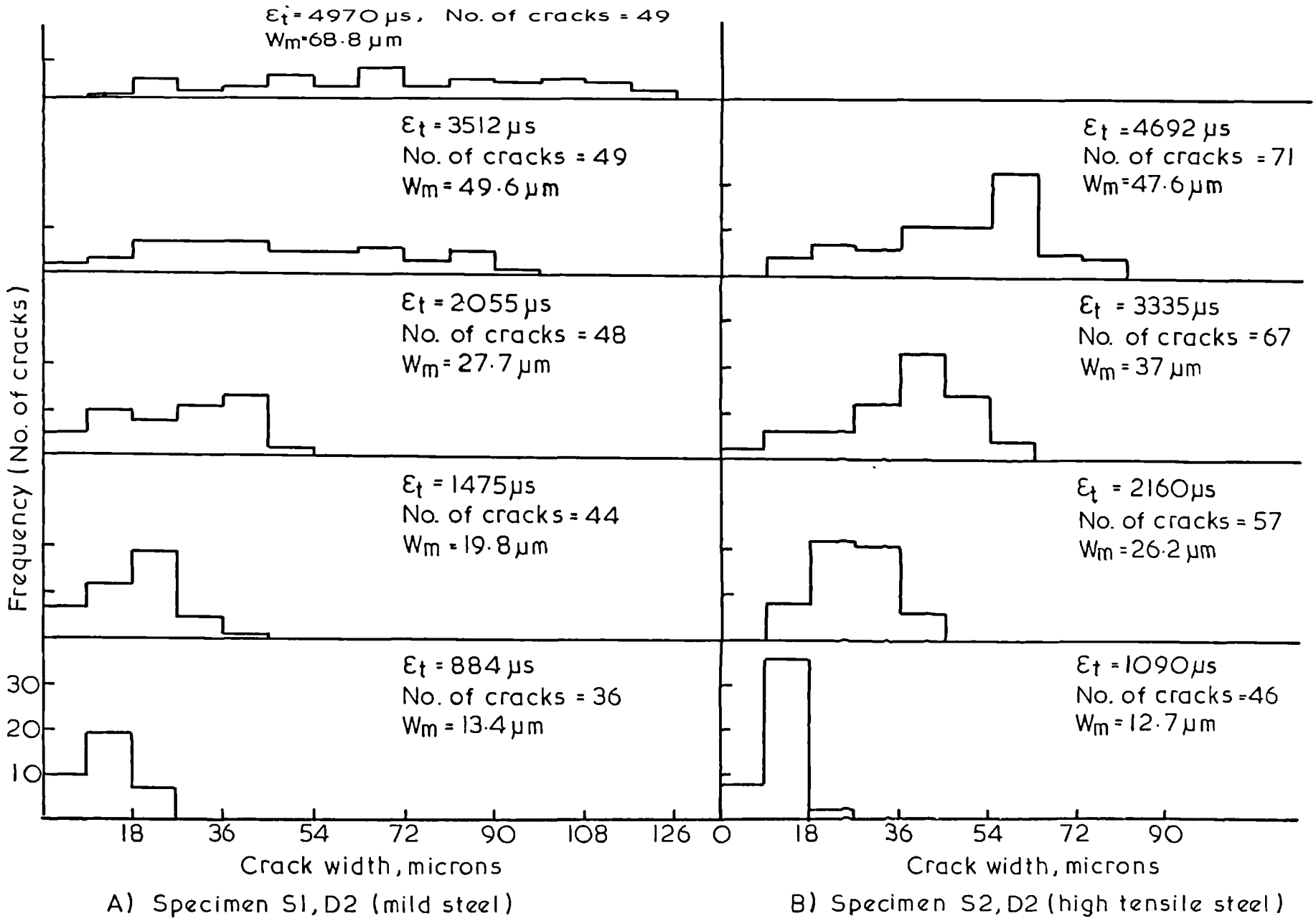

A) Specimen S1, D2 (mild steel)

B) Specimen S2, D2 (high tensile steel)

Fig. 4·12. C and D. Crack width distribution for specimens reinforced with six mesh from series S1 and S2.

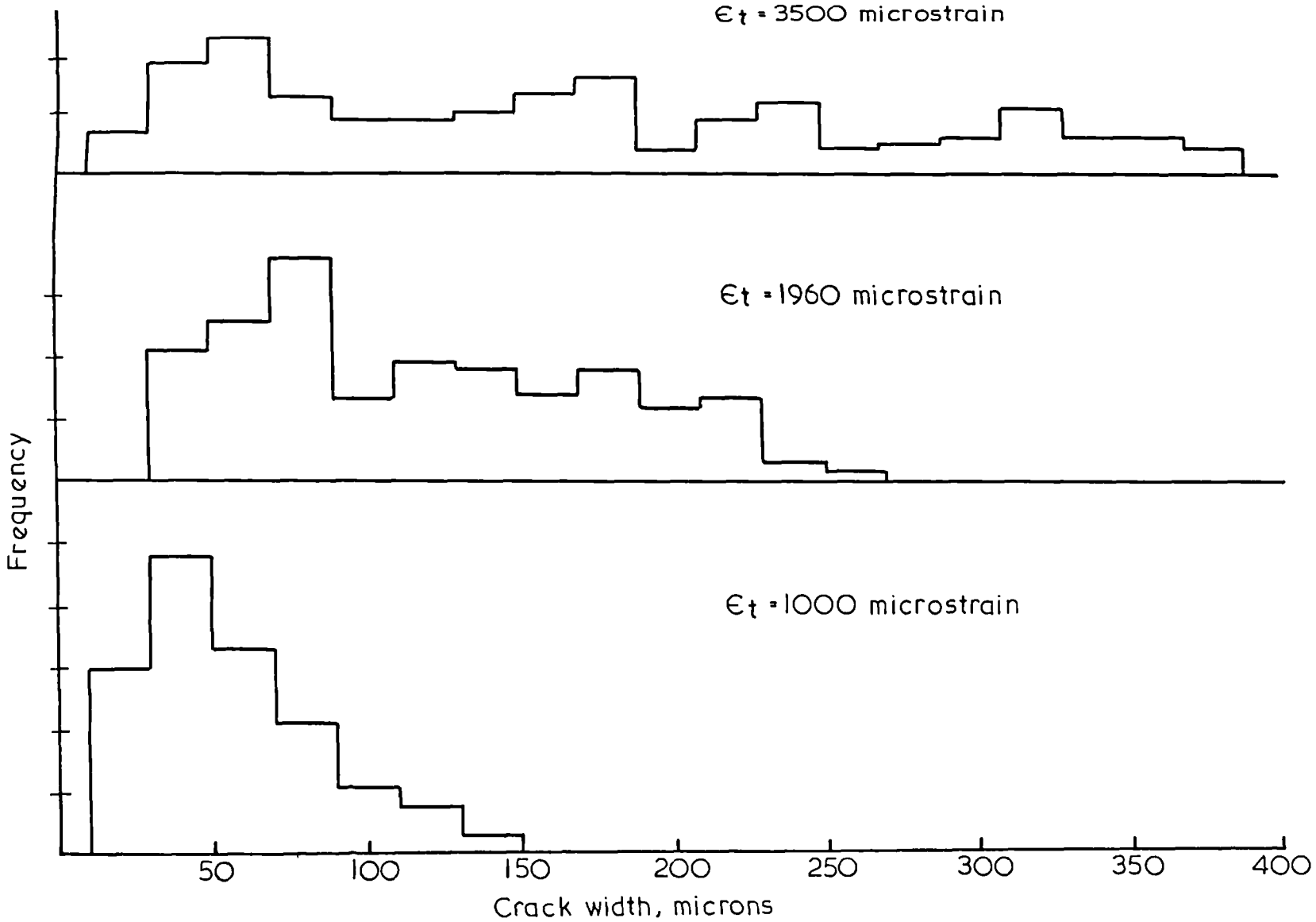

Fig. 4-13. Crack width distribution in reinforced concrete one way slab (59).

Fig.4.13 shows the frequency distribution of the crack width in a reinforced concrete slab spanning one way (59). Comparison of the two figures shows that with the increase in load, the crack width distribution in ferrocement becomes single peaked, symmetrical, and reasonably uniform, being thus near to normal distribution. In reinforced concrete as the load increases, more peaks develop and the distribution deviates more from normality. Also, in reinforced concrete the highest peak is at the range of smaller crack widths which indicates that more cracks are developing with the load and this does not seem to slow the widening of the maximum crack. In ferrocement, as mentioned earlier, full development of the number of cracks takes place at early stages of the load thus keeping the maximum crack width relatively small. After that, the cracks increase in width proportionally and uniformly. This may be the reason why, from Figs. 4.12 and 4.13, for the same tensile strain on the face of the specimens, the maximum crack width in reinforced concrete is 4-5 times higher than in ferrocement.

Fig.4.12 shows also the random nature of cracking. For the same tensile strain, specimens with the same variables have exhibited different numbers of cracks, Fig.4.12, A and C. This clearly demonstrates the necessity for repeating the specimens for the same variables and favours the use of statistical approach in dealing with cracking.

4.6.3 Crack Spacing After Failure.

As mentioned in the previous section, the crack spacing reaches almost a saturation limit at about 30-50% of the ultimate load and does not decrease considerably at failure. For this reason, the crack spacing after failure becomes important as it gives an indication of the crack spacing at stages well before failure.

In Fig.4.14, the crack spacing after failure (ultimate crack spacing), is plotted against the specific surface of reinforcement, S_R, for the specimens of

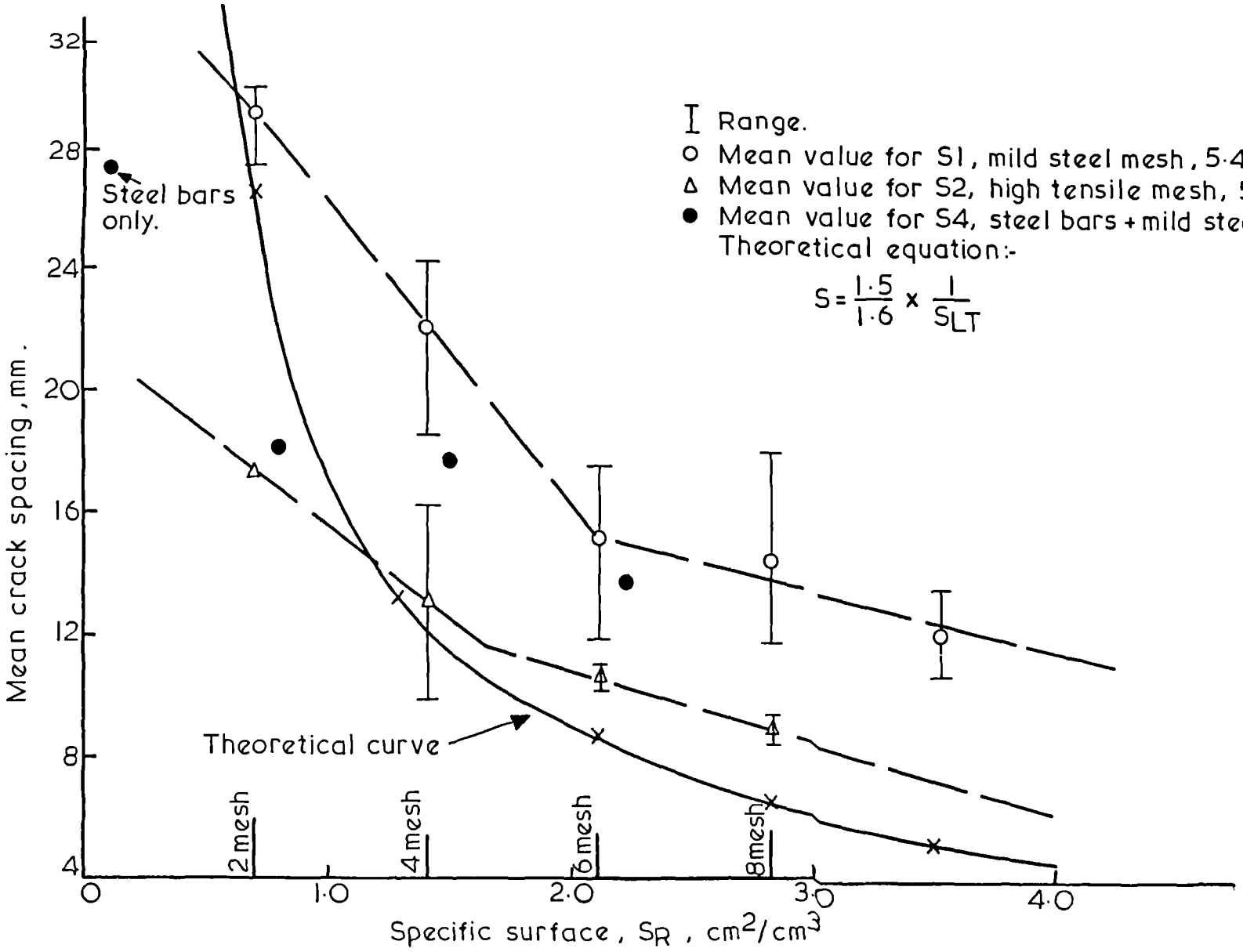

Fig. 4·14. Crack spacing after failure vs. specific surface.

Series S1, S2, and S4. The specimens of these series represent three different types of reinforcement although the size of mesh is the same. These three types are mild steel mesh only (Series S1), high tensile steel mesh only, (Series S2), and longitudinal and transverse steel bars spaced at 100 and 300 mm respectively plus varying numbers of meshes (0,2,4,6) placed near the extreme tensile and compressive fibres (Series S4). The figure shows that, for any number of meshes, the ultimate spacing for high tensile steel specimens is less than that for mild steel ones, while those of steel bars and mesh are in between. The figure also shows that addition of two meshes to the reinforcements of the specimen with steel bars only (in Series S4) resulted in a large decrease in the ultimate spacing (from 27 mm to 18 mm). This result clearly demonstrates the advantage of the mesh reinforcement over the conventional steel bars. However, careful combination of the two reinforcements could be as effective as the mesh reinforcement alone, see results of Series S4.

A clear feature in Fig.4.14 is that, irrespective of the type of reinforcement, increasing the specific surface decreases the ultimate spacing of cracks. This is also clear in Plates 4.1 to 4.4, where the tensile faces of typical specimens from Series S1 to S4, after failure, are shown. However, the decrease in the ultimate spacing appears to slow down after a certain amount of reinforcement, suggesting that increasing the steel content beyond that amount does not result in appreciable decrease in the ultimate spacing of cracks.

Naaman (24) reported that, in his tests, the ultimate spacing of cracks was equal to the spacing of transverse wires of the mesh. In this study, the smallest ultimate spacing was about two times the spacing of the transverse wires. Therefore, the basic assumption in Balaguru, Naaman, and Shah crack width equation (eq. 4.9) could not be verified in this study. Nevertheless, the transverse wires were still found to be a favourable location for cracks.

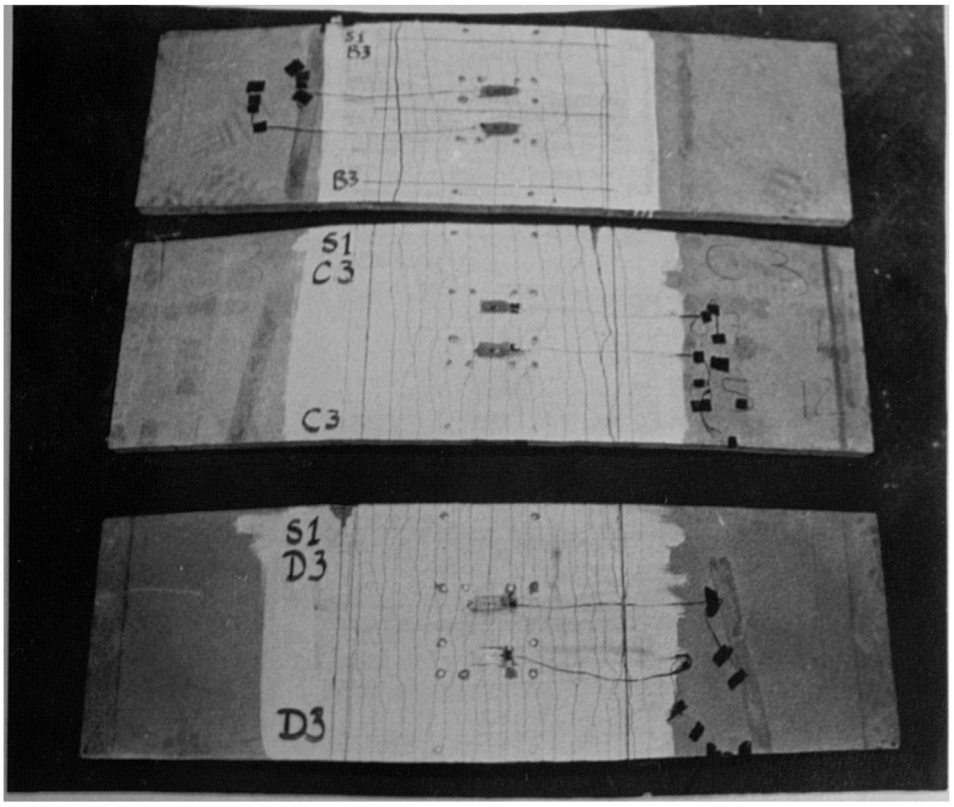

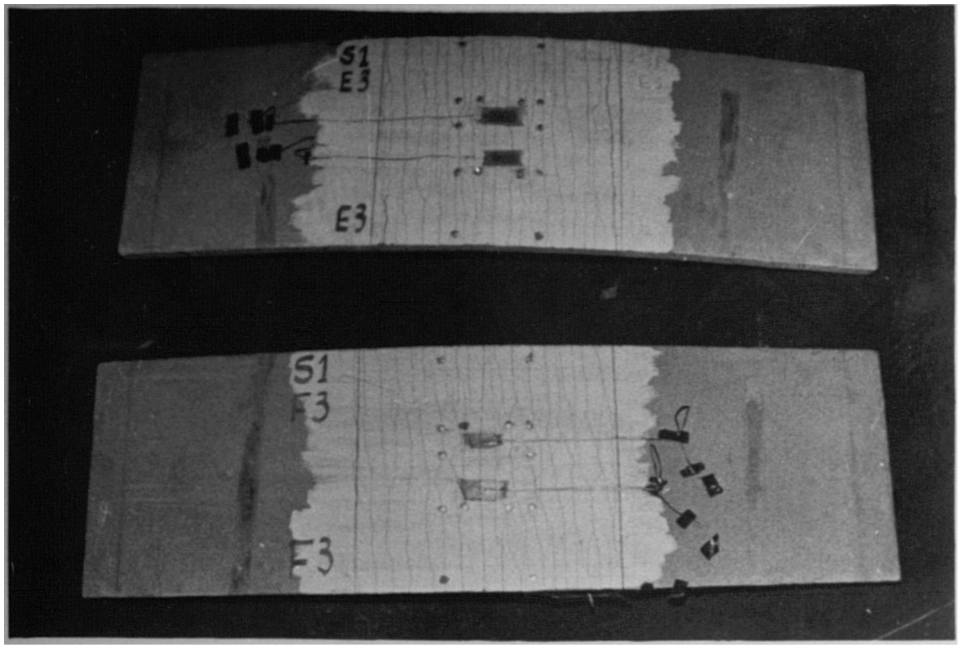

Plate 4.1. Cracking intensity at failure of typical specimens from series S1.

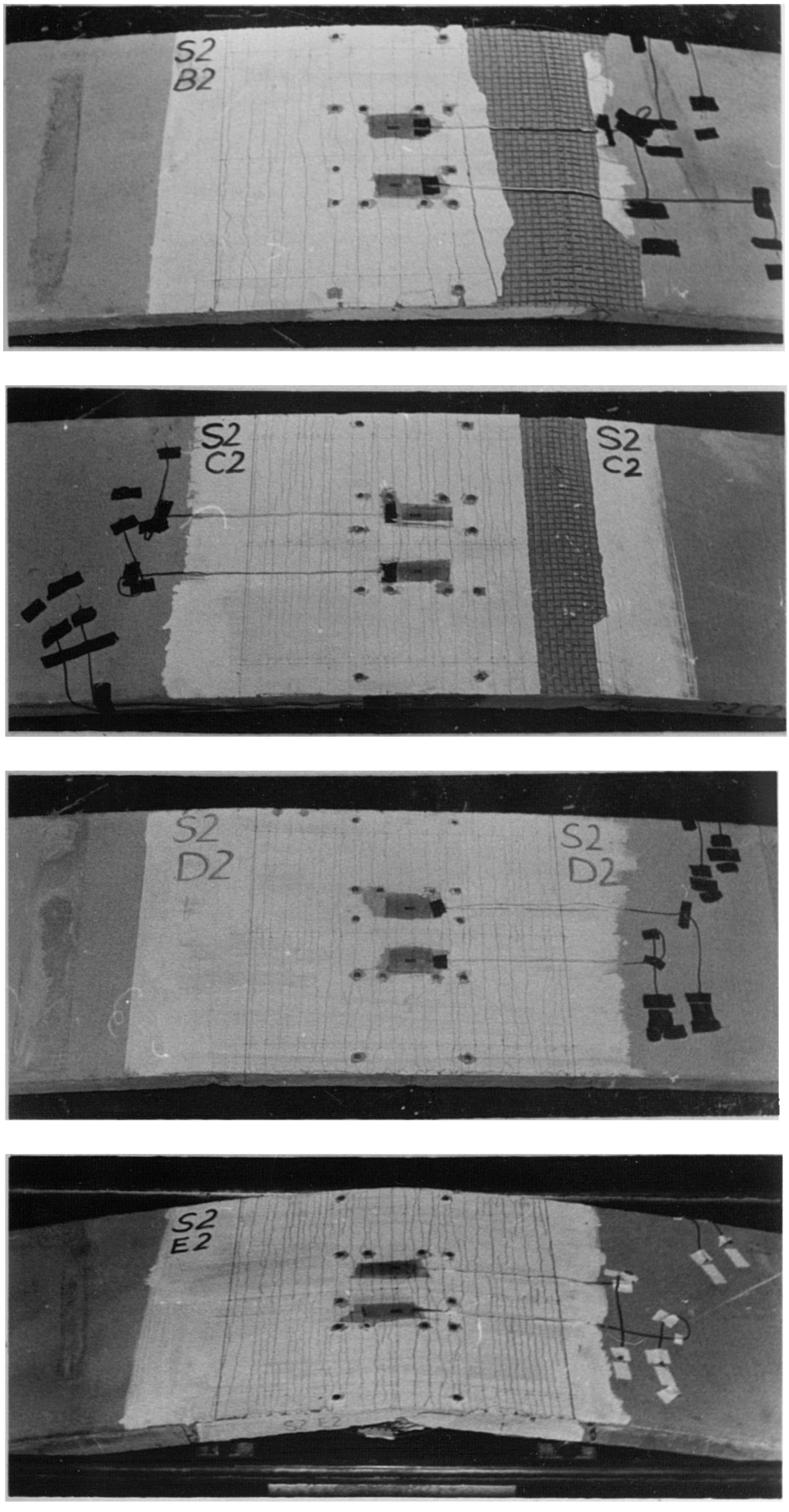

Plate. 4·2. Cracking intensity at failure of typical specimens from series S2.

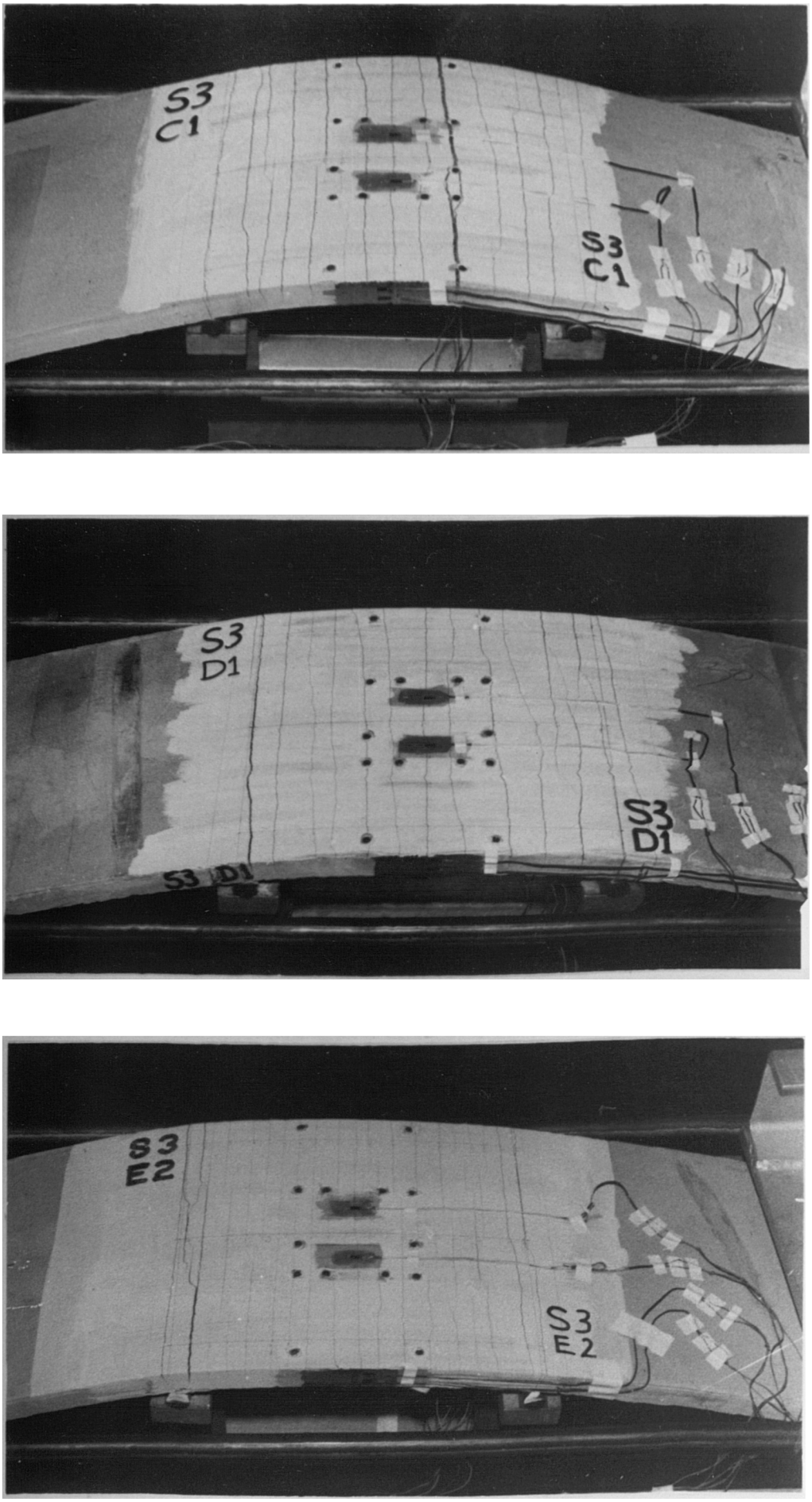

Plate 4·3. Cracking intensity at failure of typical specimens from series S3.

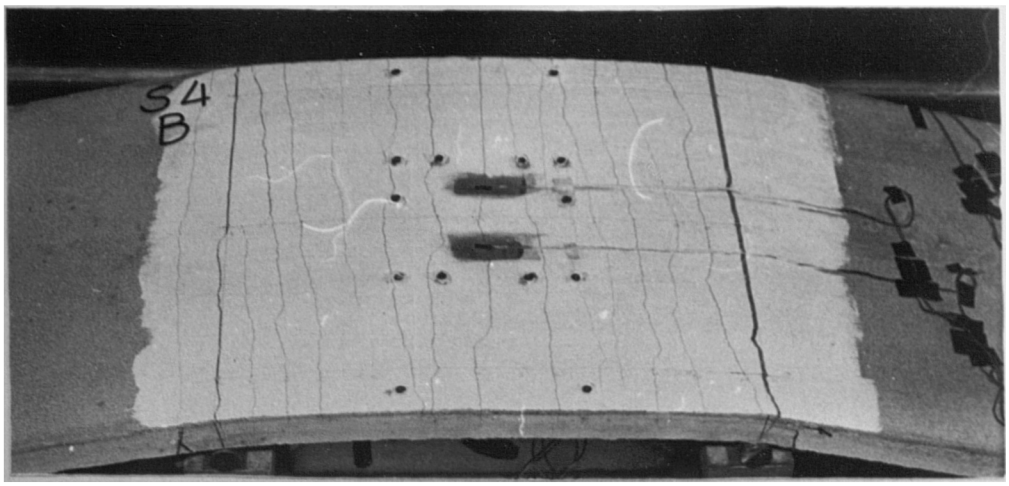

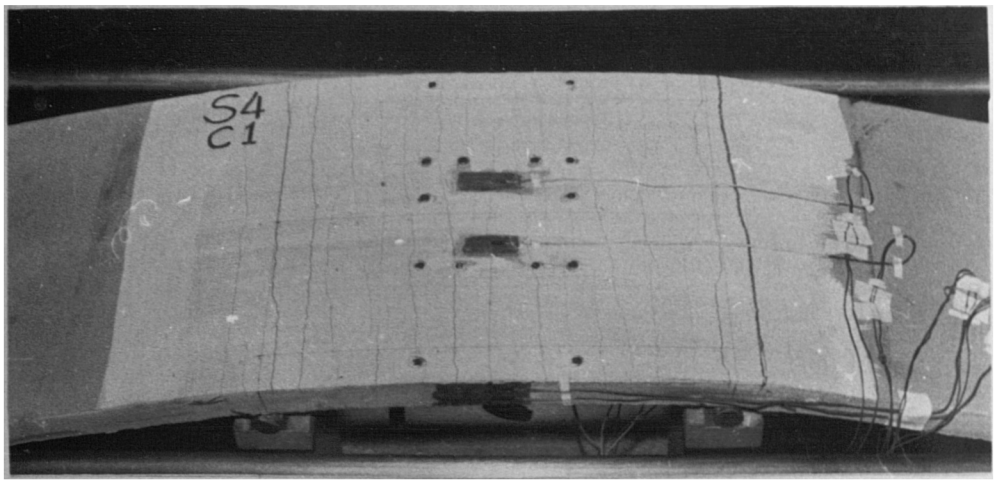

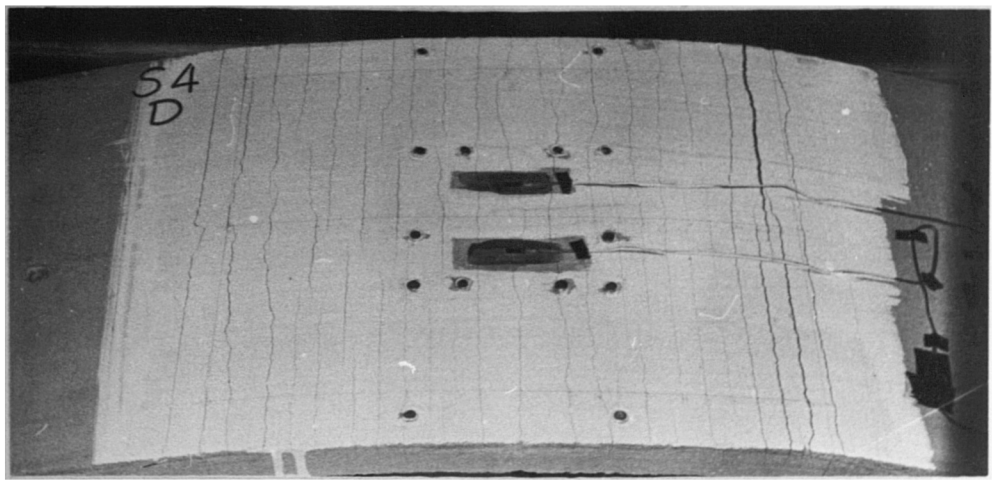

Plate. 4·4. Cracking intensity at failure of typical specimens from series S4.

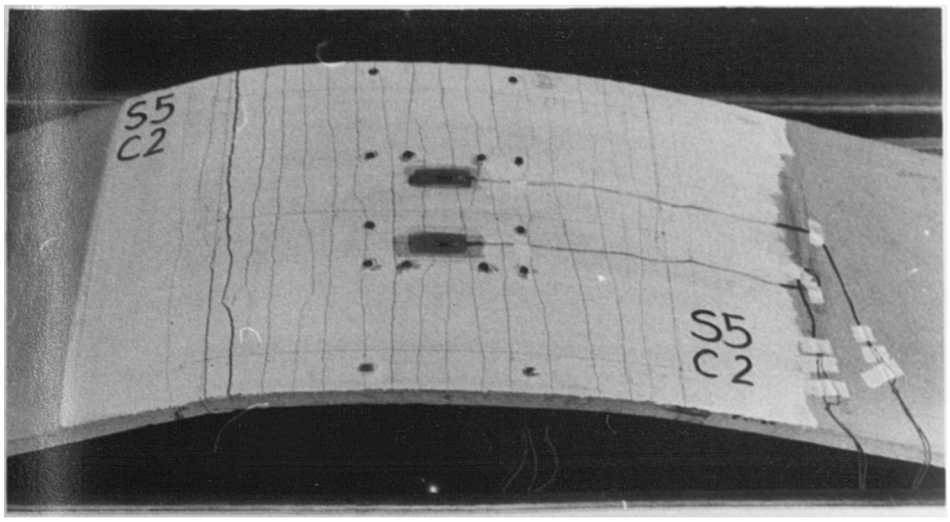

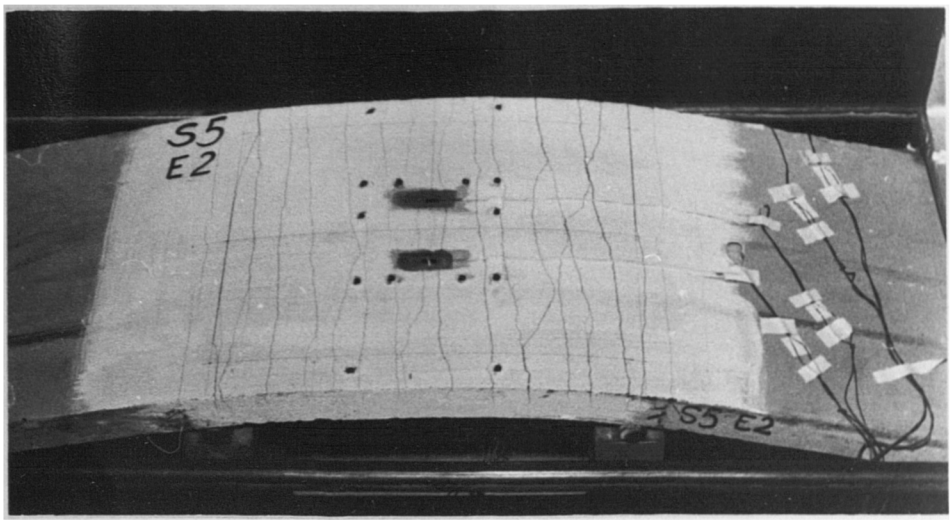

Plate. 4·5. Cracking intensity at failure of typical specimens from series S5.

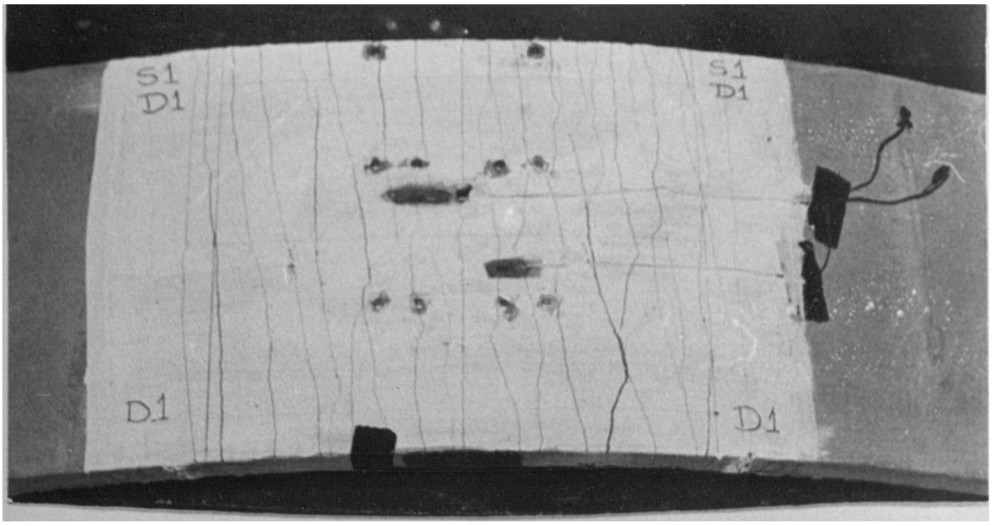

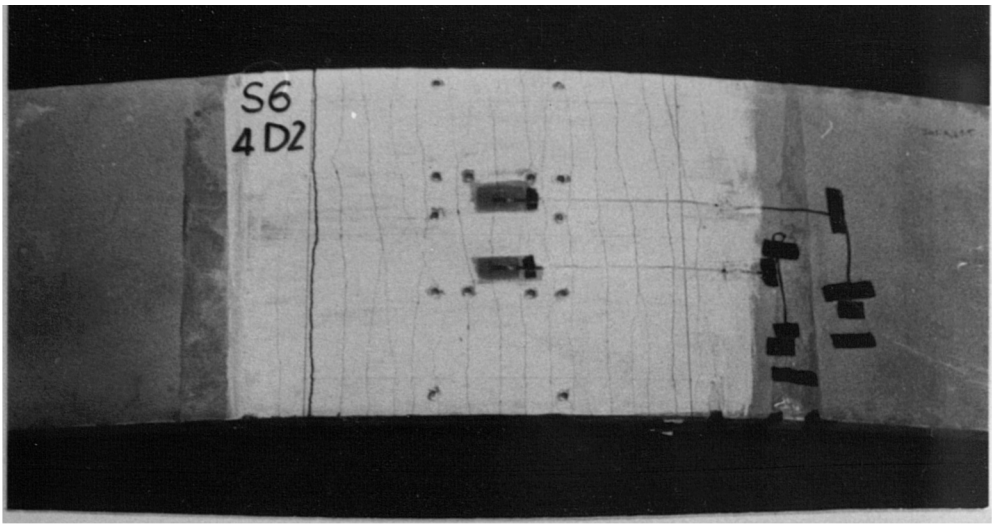

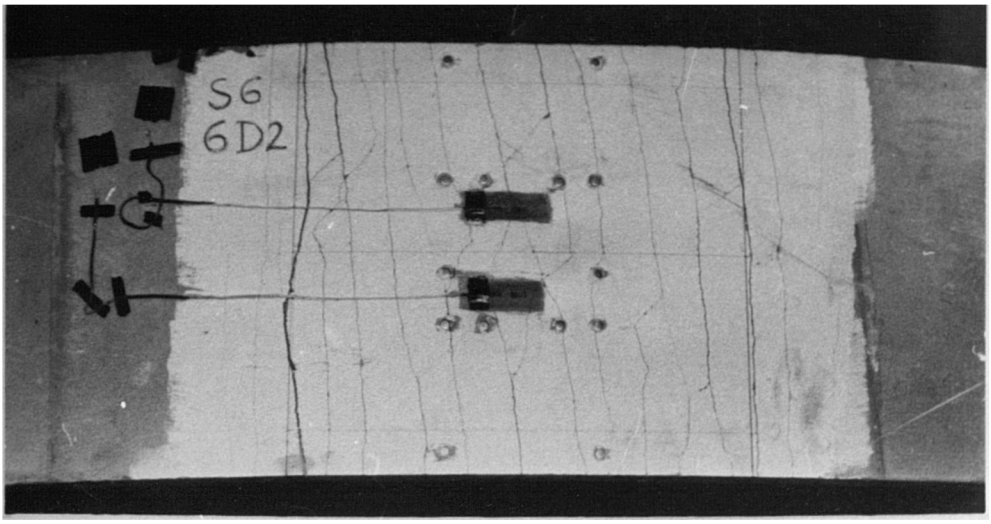

Plate.4-6. Cracking intensity at failure of typical specimens from series S6 and set S1 D.

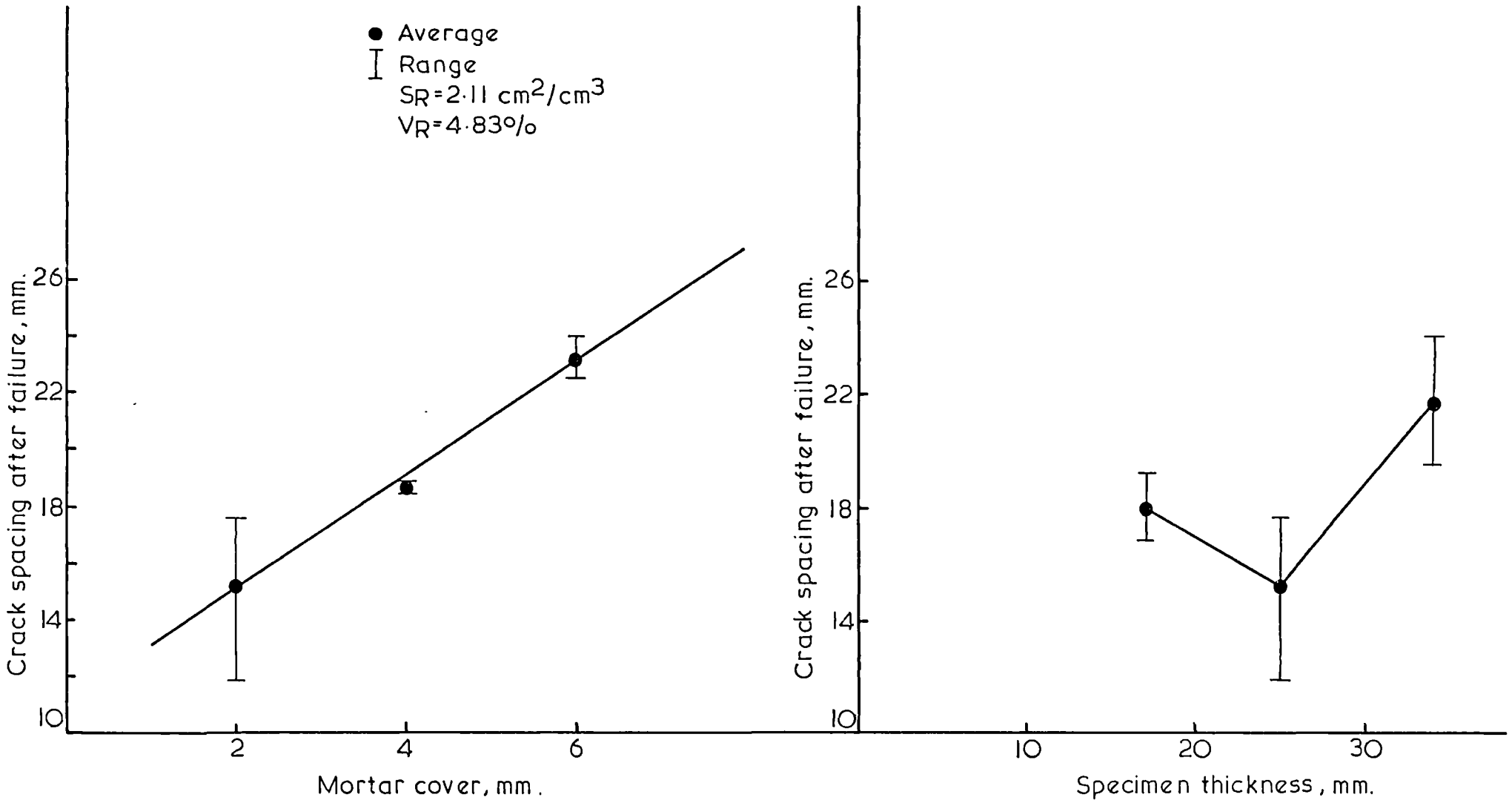

Fig. 4·15. Effect of mortar cover and specimen thickness on the crack spacing after failure.

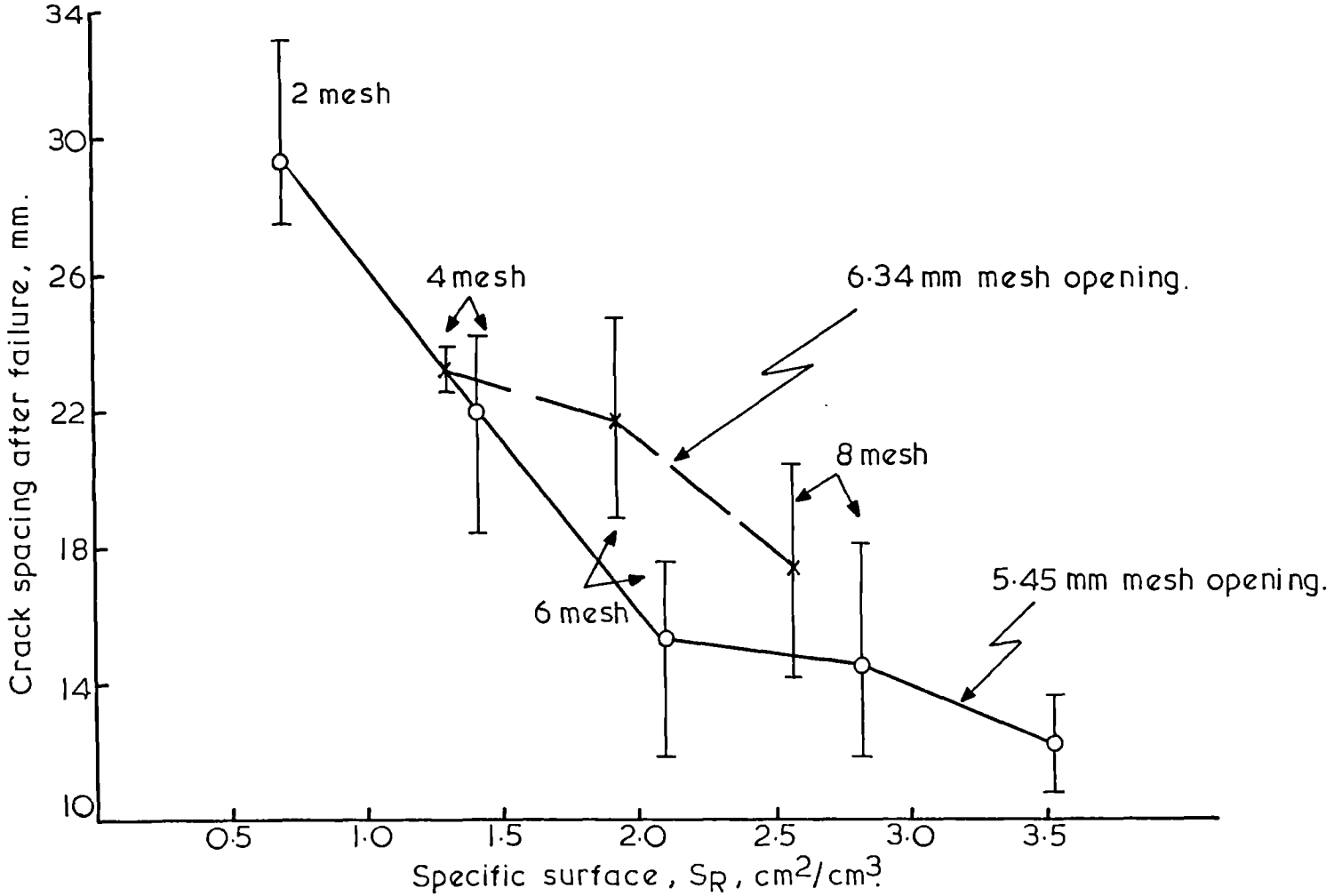

Fig. 4·16. Effect of mesh opening on the crack spacing after failure.

The crack spacing equation 4.1, which was recommended by many investigators (18,56,58) was used to find the ultimate spacing for the range of specific surface used in this study. The results are plotted in Fig.4.14. It can be seen that the predicted values mainly underestimate the experimental results, and that the equation does not include variables, other than the specific surface, found important in this study. On the other hand, the predicted results, although different, show similar trend with respect to change in the specific surface as those found in this study.

In Fig.4.15, the crack spacing after failure is plotted against the mortar cover and thickness of the section, for specimens with the same specific surface and fraction volume of reinforcement. The figure shows that increasing the mortar cover decreases the final spacing, see Plate 4.5, and the relation appears to be linear. An increase in the mortar cover from 2 mm to 6 mm increased the average crack spacing by about 1.5 times.

From Fig.4.15, the section thickness showed no regular effect on the crack spacing. The crack spacing results for sections 17.5 and 25 mm thick, are comparable, while those for 34 mm thick were relatively higher. This might suggest that for the type and amount of reinforcement used in these tests, the 25 mm thick section gives optimum results.

The effect of the mesh opening on the crack spacing after failure is shown in Fig.4.16. For the same number of meshes and wire diameter, specimens with 6.34 mesh opening gave relatively higher crack spacing. These results suggest that the finer the mesh the more the number of cracks that develop.

4.6.4 Cracking Mechanism.

The cracking process in ferrocement could be explained by considering the tensile stresses in the steel and mortar during cracking of the section. First cracking takes place when the tensile strain in the extreme fibre of the section reaches the ultimate tensile strain of the mortar. When this happens,

the tensile force in the mortar at the position of the crack will be transferred to the steel wire mesh resulting in a stress concentration in the wires. However, the mesh will load the mortar between cracks through bond stresses. The stress distribution in the steel wire mesh and mortar are shown in the schematic diagram in Fig.4.17.

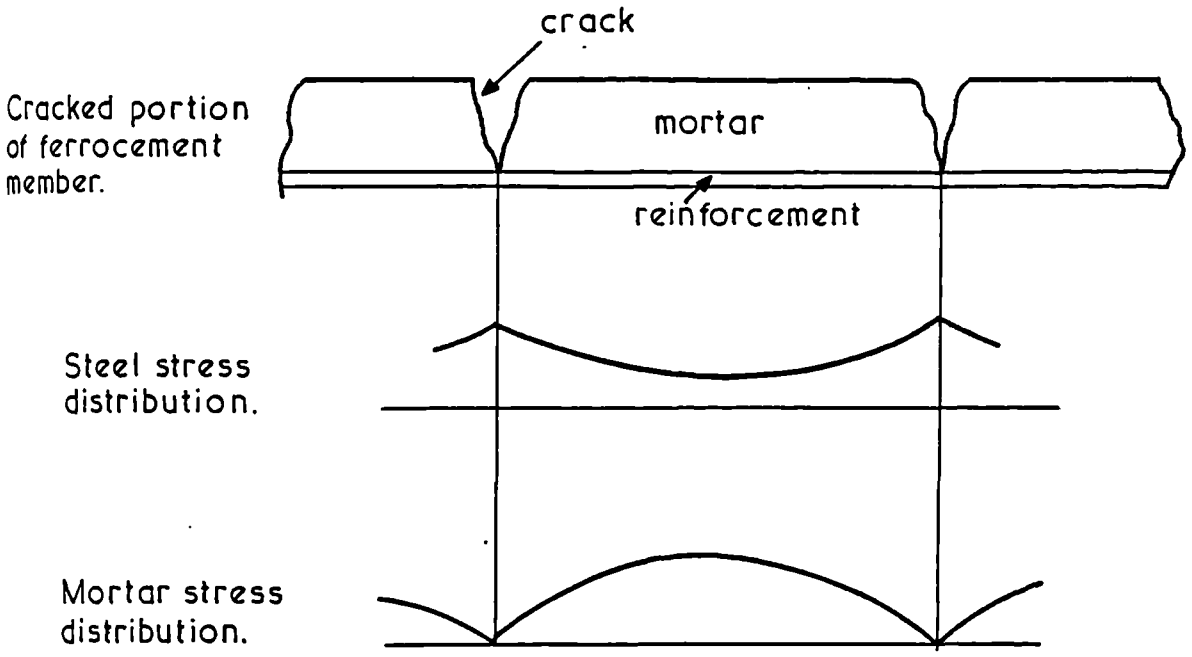

Fig.4.17 Stress distribution in the cracked portion in a ferrocement member.

Upon increasing the load, the stresses in the steel and mortar will increase until the tensile strain of mortar between two cracks reaches its ultimate tensile strain where another crack will develop. This process will continue as long as the stress in the steel has not reached its yield strength. Accordingly, the number of cracks that develop in the section depends on the capability of steel to load the mortar. The higher the number of meshes and the more the subdivision of reinforcement in the mesh, the more efficient becomes the loading process of the mortar. However, the further

the meshes are from the extreme tensile fibre the less their contribution to the loading process and it would be expected that after a certain number of meshes, addition of more meshes will not result in a significant increase in the crack number. This probably explains the slowing down of the decrease in the spacing shown in Fig.4.14.

4.7 Effect of Variables on the Crack Width.

The effect of the different variables on the cracking behaviour was investigated by studying, quantitatively, the effect of these variables on the crack width. This was achieved by comparing the rate of growth of crack width, W_m/ε_t, for the sets of specimens of the different series. For a certain tensile strain, a higher value of W_m/ε_t means a higher crack width. One should notice that in establishing the values of W_m/ε_t, the mean crack width, W_m, was calculated from the total population of the readings recorded at each stage of loading. Thus, the value of W_m/ε_t defines, statistically, the trend of the total population of cracks, rather than a single crack.

The variables included the properties of reinforcement (series S1 to S4 and series S7), section depth (series S5), and thickness of the mortar cover (series S6). The influences of these variables on the cracking behaviour are discussed separately in the following sections.

4.7.1 Effect of Properties of the Reinforcement.

4.7.1.1 Steel Content.

Most investigators express the steel content in terms of the specific surface and the fraction volume of reinforcement (S_R and V_R, respectively). The same expressions were used in this study. The average rate of growth of crack width (W_m/ε_t) of the specimens in each of the sets of series S1 to S4 is plotted against the specific surface in Fig.4.18 and against the reinforcement fraction volume in Fig.4.19. These figures show that, in general, increasing S_R and V_R decreases the rate of growth of crack width, hence, reduces the crack width for a given tensile strain, see Figs. 4.1 to 4.4.

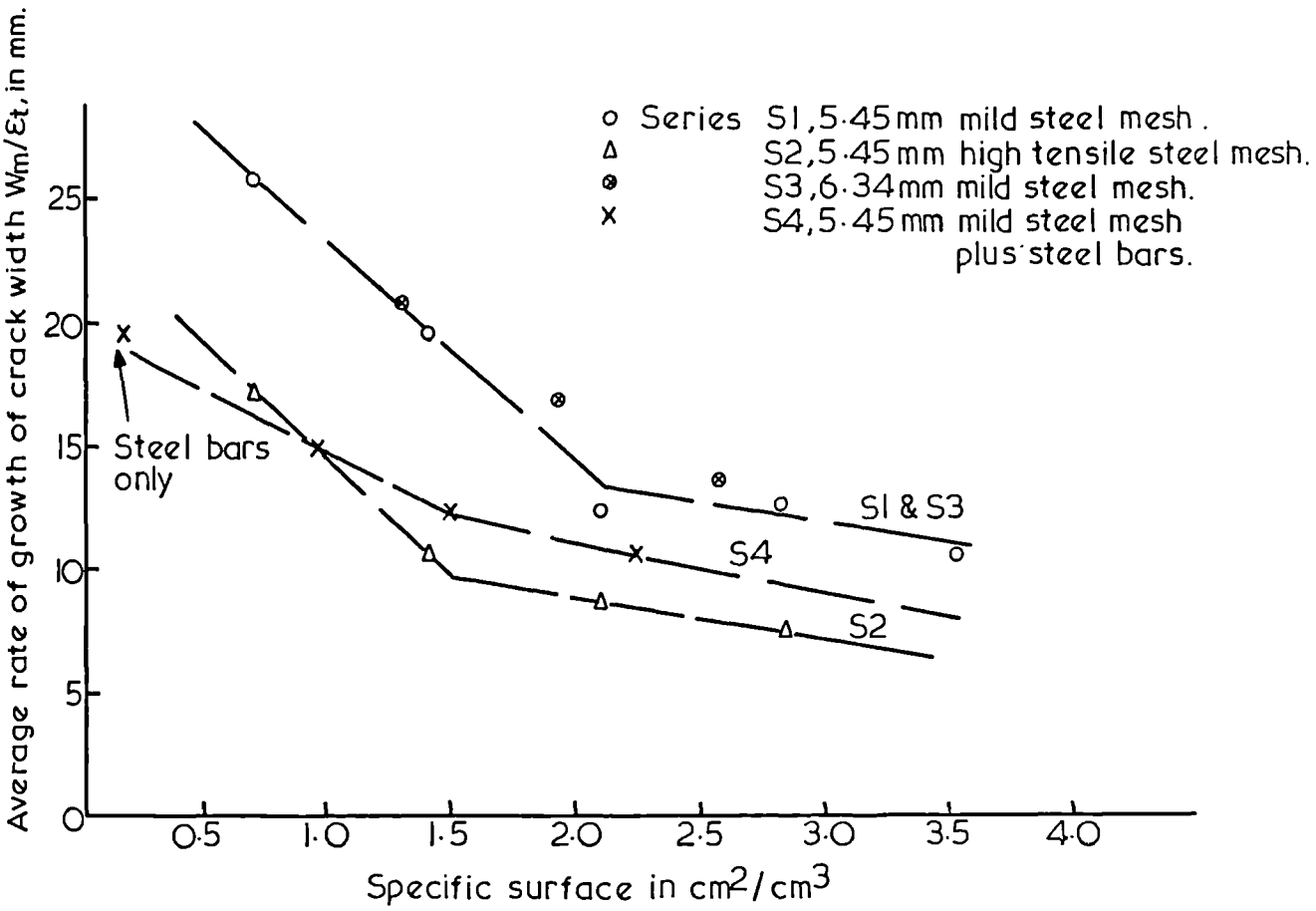

Fig. 4·18. Rate of growth of crack width vs. specific surface of reinforcement.

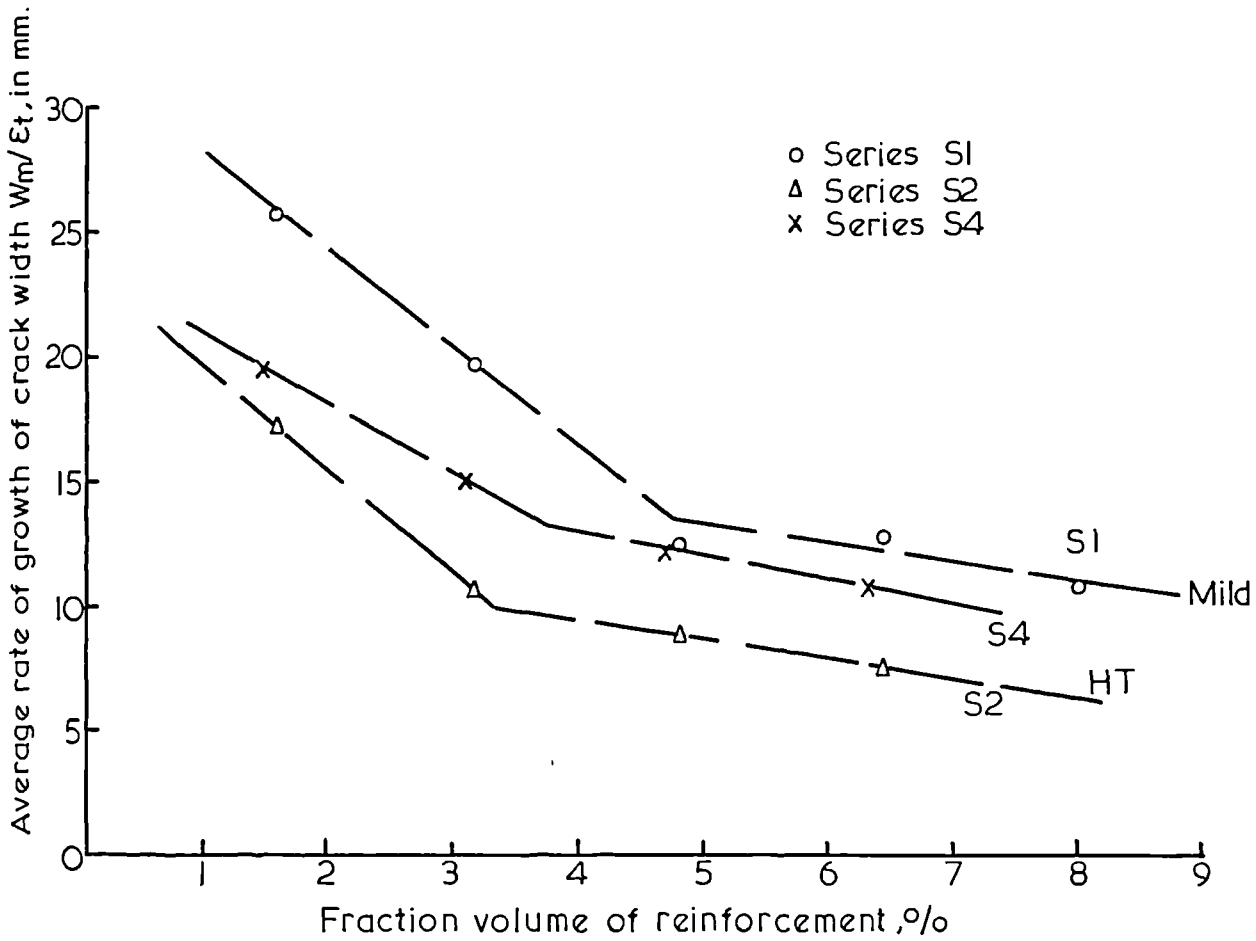

Fig. 4·19. Rate of growth of crack width vs. fraction volume of reinforcement, series S1, S2 and S4.

This was the result irrespective of the type of reinforcement. The same conclusion could be reached, indirectly, by noticing that in Fig.4.14 the final crack spacing decreases with an increase in S_R. The decrease in the rate of growth of crack width in Figs. 4.18 and 4.19 appears to slow down after a certain amount of reinforcement. This amount of reinforcement could be considered as a saturation limit for the reinforcement at which increasing the amount of reinforcement does not result in a considerable reduction in the crack width.

Limits for the amount of reinforcement in ferrocement sections had been suggested by many investigators (5,18,30,56) and the principles from which these limits were established differ from one investigator to another. Most of these limits were established from comparing the enhancement in the loads or the deformation at first cracking with increase in the specific surface of reinforcement. The fact that the first cracking represents a certain moment in the life of the specimen and the difficulty to define it resulted in unrepeatable results, see Table 4.10. However, in this study the saturation limit of reinforcement has been established by considering the history of the total population of cracks, rather than considering a single crack or a single moment in the life of the specimen. Table 4.10 gives the amount of reinforcement limits found in this study and those suggested by other investigators.

Table 4.10 Reinforcement limits for ferrocement section.

Author	Rajagoplain theoretical (56)	Bezukladov et al. (5)	Walkus (30)	Logan and Shah (18)	Balagura Naaman and Shah (31)	Present investigator		
						Mild steel mesh only	High tensile mesh only	Mild mesh & steel bars
Specific surface of reinforcement S_R cm^2/cm^3	3.15	2.0	2.0-3.0	Load at first cracking increases linearly with increase in specific surface	No increase in load at first cracking with increase in S_R	2.1	1.5	1.5

The enhanced cracking behaviour with the increase of steel content was explained in sec. 4.6.3. It was shown that the greater the steel content, the more are the forces available to load the mortar and therefore creating more cracks rather than increasing the width of the already established cracks. It should be noticed that the regression lines in Fig.4.18, specially those after the steel saturation limit for series S1, S2, and S4 are parallel. This indicates that the effect of increasing the specific surface has the same trend in spite of the different type of reinforcement. In this study, however, the specific surface was increased through increasing the number of meshes rather than increasing the specific surface of the mesh itself. Using a mesh with a higher specific surface and then varying the number of meshes would be expected to produce a curve lower than those in Fig. 4.18 but parallel to them. It may be appropriate, therefore, in studies which involve the size of mesh as a variable, to define the subdivision of the reinforcement in the single mesh as well as the subdivision of the total reinforcement, i.e. S_R. In contrast, the ratio S_R/V_R seems to define uniquely the reinforcement subdivision of the single mesh. On the other hand, such definition may not be necessary when the section is subjected to direct loading.

4.7.1.2 Steel yield strength.

In series S1 and S2, the steel mesh used was the same except that of S2 was high tensile steel with ultimate strength of (1197 N/mm^2) and yield strength, at 0.005 strain of (394 N/mm^2). While those in S1 are mild steel mesh with ultimate strength (348.6 N/mm^2) and yield strength (218.4 N/mm^2). The modulus of elasticity for both meshes are nearly the same, see Table 2.1. The rates of growth of crack width for specimens of these two series are shown in Fig.4.18, their final crack spacings in Fig.4.14 and the tension face of typical specimens from the two series are shown in Plates 4.1 and 4.2. It can be seen that the high tensile steel specimens (S2) showed a better cracking performance than the mild steel ones in terms of both the crack width

and spacing. Also, the saturation limit of reinforcement in series S2 is smaller than that in series S1. It is, therefore, clear that the yield strength of the mesh has a major influence on the cracking behaviour of ferrocement.

The curves in Fig.4.18 for both series S1 and S2 could be considered to consist of two segments each. The equations for the four segments of these two curves were found using linear regression and they are as follows:

1. For mild steel mesh

   a - segment (1)

$$W_m/\varepsilon_t = 32.45 - 9.2\ S_R \quad \ldots\ldots \quad (4.15)$$

   b - segment (2)

$$W_m/\varepsilon_t = 16.5 - 1.57\ S_R \quad \ldots\ldots \quad (4.16)$$

2. For high tensile steel mesh

   a - segment (1)

$$W_m/\varepsilon_t = 23.9 - 9.4\ S_R \quad \ldots\ldots \quad (4.17)$$

   b - segment (2)

$$W_m/\varepsilon_t = 12.79 - 1.88\ S_R \quad \ldots\ldots \quad (4.18)$$

where

W_m = Mean crack width, microns.

ε_t = Average tensile strain on the face, 1×10^{-3} mm/mm.

S_R = Total specific surface, cm^2/cm^3.

The above four equations represent the relationship between the mean crack width, tensile strain, and the specific surface for specimens reinforced with the mild and high tensile steel woven wire mesh used in this study. From these equations it can be seen that the slopes of the line before and after saturation limit for these two curves are similar and the two curves could be assumed parallel with the pivot axis being the straight line connecting the saturation limit points, see Fig.4.20. The equation for

the pivot axis line was obtained by first solving the above four equations to find the coordinates of the saturation limit points of the two curves. The coordinates of these points, together with the corresponding mesh yield strength are:

For σ_y = 218.4 N/mm^2, then S_R = 2.09 cm^2/cm^3 and W_m/ε_t = 13.22 mm

For σ_y = 394 N/mm^2, then S_R = 1.48 cm^2/cm^3 and W_m/ε_t = 10.01 mm.

From the above coordinates, the pivot axis can be defined by either of the following two equations:

$$S_R = 2.85 - 3.5\text{x}10^{-3}\ \sigma_y \quad \ldots\ldots \quad (4.19)$$

$$W_m/\varepsilon_t = 17.2 - 18.3\text{x}10^{-3}\ \sigma_y \quad \ldots\ldots \quad (4.20)$$

where

σ_y = yield strength of the mesh at 0.005 strain, N/mm^2.

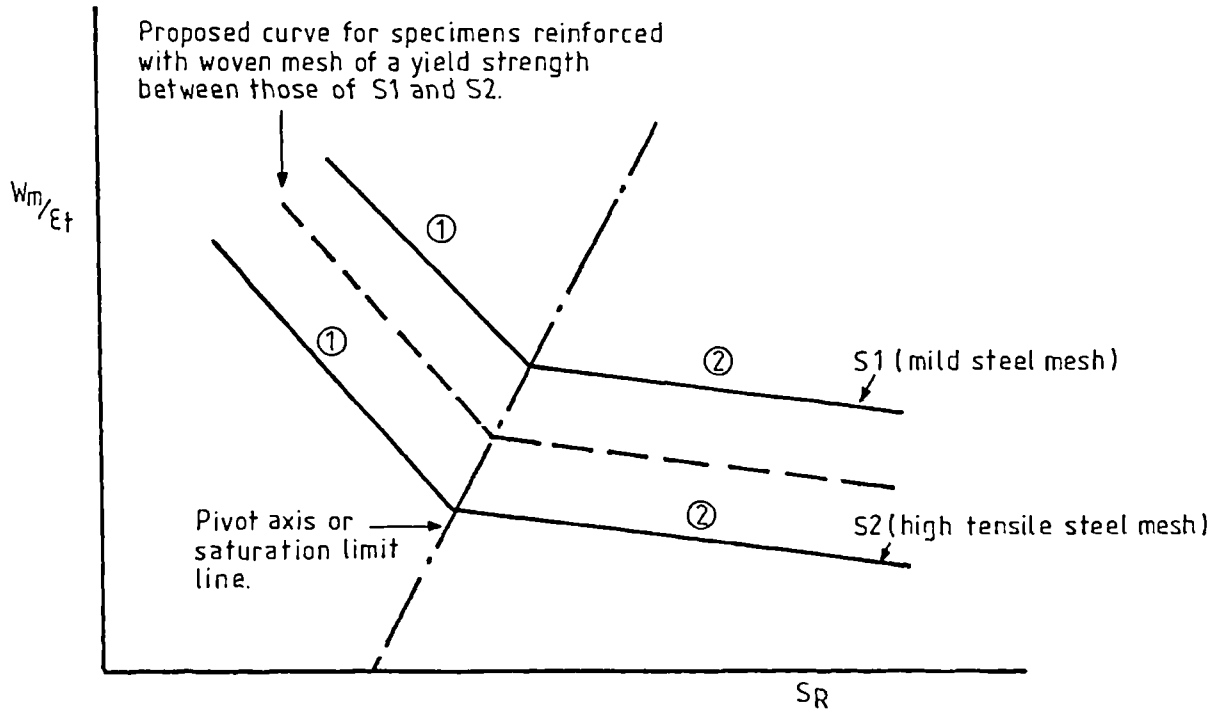

Fig.4.20 Trend of the curves expressing the relationship between W_m/ε_t and S_R for different mesh yield strength.

The better cracking performance of specimens reinforced with high tensile steel wire mesh compared to specimens reinforced with mild steel wire mesh can be explained by noticing that, although the initial modulus of elasticity for both type of meshes are almost equal, the yielding point is higher for high tensile mesh. Therefore, the range of the stress between the first cracking and yielding of the mesh is higher for the specimens with high tensile steel. This, eventually, will allow more cracks to develop rather than widening of the already existing cracks. This can be seen from comparing Figs. 4.10 and 4.11 in which rapid widening of the cracks took place in mild steel mesh specimen after about 50% of the ultimate load while those of high tensile specimen in spite of the fact that their maximum load is higher, were still increasing in width linearly. The same conclusion can be reached by comparing the frequency distribution of the crack width for typical specimens from series S1 and S2, shown in Fig.4.12. Up to a tensile strain on the face equal to 2000 microstrain the two specimens showed fairly similar number of cracks and crack width. However, as the load increases, additional cracks continue to form more substantially in the specimen with the high tensile mesh. At a tensile strain equal to about 6000 microstrain the specimen with the mild steel mesh had 69 cracks with mean crack width, W_m = 66.8 microns, while that with high tensile mesh had 80 cracks with a mean crack width of 53.4 microns.

4.7.1.3 Presence of Reinforcing Bars and Mesh Distribution.

Series S4 was designed to study the effect of reinforcing the specimen with reinforcing bars of 6 mm diameter in addition to steel wire mesh. The longitudinal bars were spaced at 100 mm, while the transverse bars were spaced at 300 mm. The steel wire mesh used was the mild steel mesh used in series S1. The number of meshes was varied from none to maximum possible of six meshes equally distributed on both sides of the bars. In specimen S7 C the bars were removed with the meshes remaining in the same position: this is to find the effect of reinforcing bars on the behaviour of the section.

Figs. 4.18 and 4.19, show that for the same specific surface, S_R, or the same fraction volume of reinforcement, V_R, the rate of growth of crack width, W_m/ε_t, for the specimens of series S4 are somewhere between those for the specimens reinforced with high tensile mesh (S2) and those for the specimens reinforced with mild steel mesh (S1). This indicates that replacing some of the mild steel meshes in the specimens of series S1, by reinforcing bars, changed the cracking performance. The presence of the reinforcing bars is appreciated in Fig.4.19 more than in Fig.4.18, because the bars have, relatively, low S_R but high V_R.

In Fig.4.21, the values of W_m/ε_t for series S4 and S7 are plotted against V_R. The following points can be noticed from Figs. 4.18, 4.19 and 4.21:

1. Superior cracking performance of ferrocement compared to that of reinforced concrete (S4 A) starts in specimens with more than four meshes in case of mild steel while those with high tensile steel mesh showed better performance even with two meshes.

2. Enhancement in the cracking behaviour in ferrocement with bars was not appreciable when the number of meshes increased to more than two at each side of the bars. The vertical spacing of the meshes in this specimen is the same as that in specimen S1 D, i.e. 2 mm (S1 D gave the steel saturation limit of series S1).

3. The curve of S4 in Fig.4.19 is nearly parallel, specially after the saturation limit, to the curves of S1 and S2, indicating the similar effect of increasing the number of meshes on the cracking behaviour in these series. The saturation limit was smaller than that of S1 both in terms of V_R and S_R. This may be due to the fact that the yield strength and the modulus of elasticity of the reinforcing bars were higher than those of mild steel mesh.

4. Removal of the reinforcing bars (as in S7 C and S1 B) resulted in considerable deterioration in the cracking behaviour. Also, from comparing S7 C and S1 C, concentration of the meshes near the fibres did not, at least, enhance the cracking behaviour.

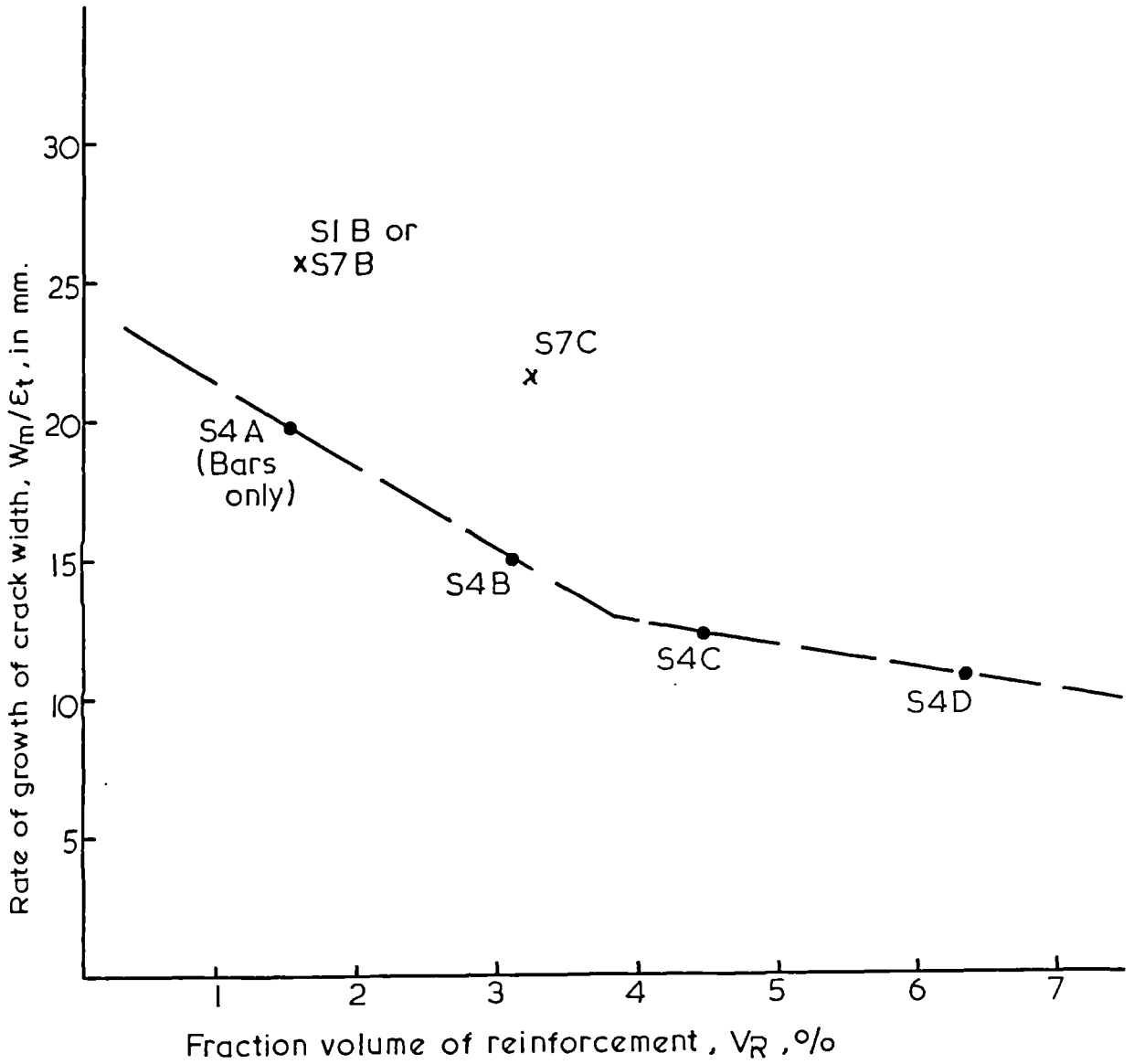

Fig.4.21. Rate of growth of crack width vs. fraction volume of reinforcement, series S4 and S7.

5. The curve for S4 can be assumed to be of the same shape as S1 and S2 and its saturation limit falls along the straight line shown in Fig.4.20.

4.7.2 Effect of Mortar Cover.

As in the cracking behaviour of reinforced concrete members the cover has an effect on the cracking behaviour of ferrocement. Although the cover in ferrocement is small in value, its percentage of the total depth of the section is still as high as in reinforced concrete if not more. Because the cover is of the order of a few millimeters, in practice this value could easily be doubled and therefore it is important to study the effect of this variable on the cracking behaviour in ferrocement.

In Fig.4.22, the values of W_m/ε_t of specimens reinforced with the same number of meshes are plotted against the mortar cover in these specimens. Each point in the graph represents the average results from two specimens. From the figure, it can be seen that the higher the cover, the higher the rate of growth of crack width and therefore, the higher the crack number and width, see Plate 4.5. Linear regression on the results gave the following equation:

$$W_m/\varepsilon_{av} = 10.3 + 1.27\ C \quad \ldots\ldots \quad (4.21)$$

where

W_m/ε_{av} = slope of mean crack width against average tensile strain μmm x 10^{-3}

C = cover, mm.

From the above equation, increasing the cover from 2 mm to 4 mm will result in an increase in the crack width by about 20%. Although this result might suggest a minor influence, it still shows that cover has an effect on the determination of the crack width.

It should be noticed here that only one value of steel content was used in the study of the effect of mortar cover. This value was the saturation limit for the mild steel wire mesh found from series S1. Specimens reinforced with high tensile steel mesh were assumed to behave in the same manner.

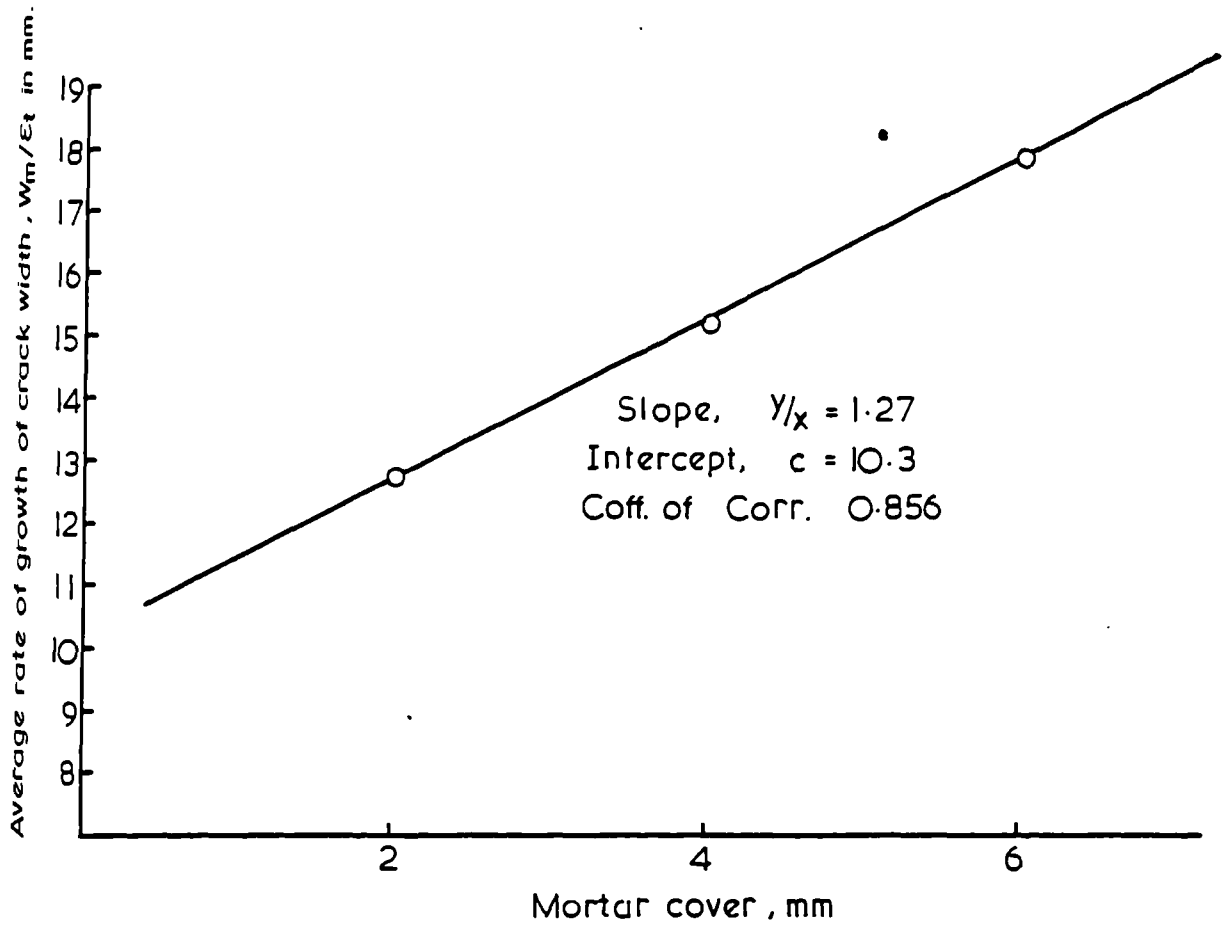

Fig. 4·22. Rate of growth of crack width vs. mortar cover.

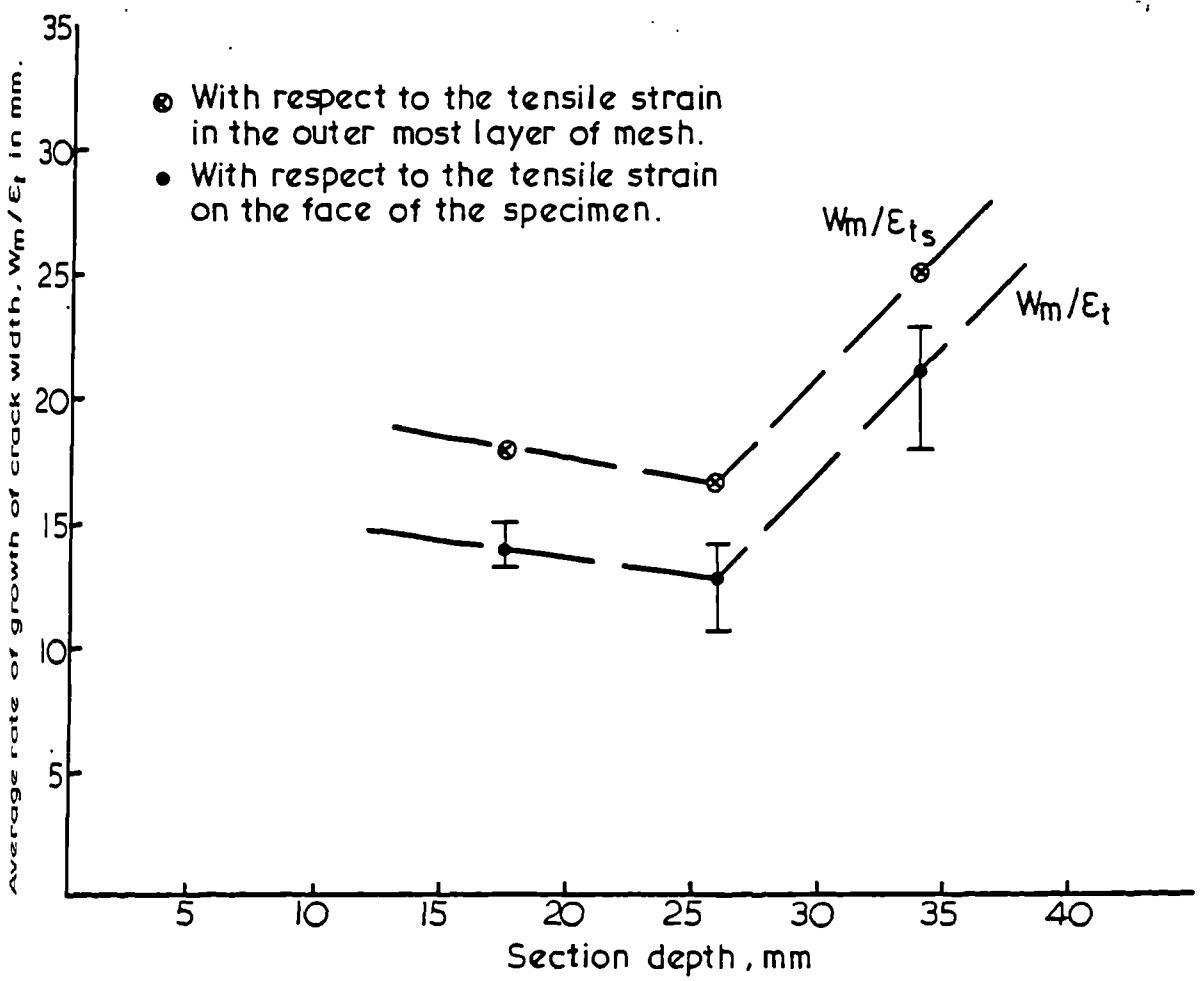

Fig. 4·23. Rate of growth of crack width vs. section depth.

To explain the deterioration in the cracking performance with the increase of the cover, one can see from Fig.4.17 that the further the outmost layer of mesh from the extreme fibre, the higher the forces in the steel needed to load the mortar between the cracks to the cracking stress.

4.7.3 Effect of the Depth of the Section.

It was shown in the previous sections that there was a saturation limit for the amount of reinforcement in the section. That limit was established by comparing the rate growth of crack width on specimens 25 mm in depth and reinforced with different numbers of meshes. Practical uses of ferrocement suggest that the section depth could vary from 10 mm up to 50 mm. Consequently, two questions can be raised. First, is the saturation limit of steel content the same irrespective of the section depth? Second, for the same V_R and S_R, what is the effect of the depth of the section on the cracking behaviour? In this study, only the second question is dealt with. Specimens 17 mm, 25 mm and 34 mm in depth and reinforced with the saturation limit of steel as found from series S1 were tested, see Plate 4.6. In Fig.4.23, W_m/ε_t values for these specimens are plotted against the section depth.

Because of the difference in the section depth of the specimens, the strain gradient of the section may vary from one specimen to another. Thus, for the same tensile strain at the extreme fibre, the tensile strain at the outermost mesh would also vary with the section depth. To investigate the effect of such variation on the rate of growth of crack width, the values of W_m/ε_t for the specimens in this series were recalculated with respect to the tensile strain at the outermost mesh instead of the tensile strain at the extreme fibre. The strain at the outermost mesh was obtained from the strain measurements and assuming linear strain distribution in the section. The new values of W_m/ε_{t_s} were plotted in Fig.4.23. The figure shows that these values are in direct proportion with those calculated with respect to the tensile strain at the extreme fibre of the section. It also shows that the values

of the rate of growth of crack width for the 17 mm and 25 mm deep specimens are comparable while that of 34 mm is noticably higher. The figure suggests that, for the same type of reinforcement and for the amount of reinforcement equal to the saturation limit, $W_m/\dot{\varepsilon}_t$ values are higher for sections deeper than 25.

The behaviour may be explained by noticing that to maintain the same S_R and V_R, the number of meshes is increased with the increase in the section depth. Since the vertical spacing of the meshes is the same for the different sections, the extra meshes added to account for the increase in depth are placed further away from the faces and therefore they are expected to contribute less in loading the mortar to bring it to the cracked stage. At the same time, deeper cracks and thus wider at the face of the specimen, are expected because of deeper tensile zone. For the smaller section, since the amount of reinforcement was found to be the optimum, the decrease in the section depth and consequently the number of meshes could not enhance the value of W_m/ε_t.

It is to be mentioned here that only mild steel mesh was used in this series and using high tensile steel mesh reinforcement would probably lead to less significant difference in the values of W_m/ε_t for deeper section.

4.8 Crack Width Prediction Equations.

General equations were derived to predict the crack width taking into account the effect of steel content, yield strength of the mesh, mortar cover, and the value of strain at the level of cracks. The derivation was based on the observation that the curves representing the relationship between the specific surface, S_R and the rate of growth of crack width W_m/ε_t for series S1 (mild steel wire mesh) and series S2 (high tensile steel wire mesh) were parallel, sec. 4.7.1.2. Each curve consisted of two straight line segments, where the value of S_R at the turning point is called the saturation limit of steel content. S_R and W_m/ε_t at the saturation limit varied with mesh

yield strength (stress at 0.005 strain) and were assumed to follow a linear relationship described by the following two relations, see also Fig.4.20.

$$S_R = 2.85 - 3.5\times10^{-3}\ \sigma_y \quad \ldots\ldots \quad (4.19)$$

$$W_m/\varepsilon_t = 17.2 - 18.3\times10^{-4}\ \sigma_y \quad \ldots\ldots \quad (4.20)$$

To derive the general equation for crack width prediction, the slopes of the parallel segments, given in eqs. 4.15 to 4.18 of the curves S_R vs W_m/ε_t of series S1 and S2 were averaged. The average slopes were used to define the general two segments relationship between S_R and W_m/ε_t for any mesh yield strength. The equations for these two segments are as follows:

Segment (1)

$$W_m/\varepsilon_t = C_1 - 9.3\ S_R \quad \ldots\ldots \quad (4.22)$$

Segment (2)

$$W_m/\varepsilon_t = C_2 - 1.73\ S_R \quad \ldots\ldots \quad (4.23)$$

To find the values of the constants C_1 and C_2, S_R and W_m/ε_t in eqs. 4.22 and 4.23 were substituted by those in eqs. 4.19 and 4.20. Therefore,

$$C_1 = 43.7 - 50.9\times10^{-3}\ \sigma_y$$

$$C_2 = 22.1 - 2.4.4\times10^{-3}\ \sigma_y$$

Substituting the values of C_1 and C_2 above in eqs. 4.22 and 4.23 will give the equations for segments (1) where S_R is less than the saturation limit, and segment (2) where S_R > the saturation limit.

The effect of the mortar cover on the W_m/ε_t was derived in sec. 4.7.2 and it was in the following form:-

$$W_m/\varepsilon_t = 10.3 + 1.27\ C \quad \ldots\ldots \quad (4.21)$$

Equations 4.22 and 4.23 were based on series S1 and S2 where the mortar cover was equal to 2 mm. Therefore, the term 1.27 (C-2) should be added to these equations to account for the effect of mortar cover.

Hence, the equation for the mean crack width will be as follows:

For $S_R < 2.85 - 3.5\text{x}10^{-3}\ \sigma_y$

$$W_m/\varepsilon_t = 43.7 - 50.9\text{x}10^{-3}\ \sigma_y - 9.3\ S_R + 1.27\ (C-2) \quad \ldots\ldots \quad (4.24)$$

For $S_R \geq 2.85 - 3.5\text{x}10^{-3}\ \sigma_y$

$$W_m/\varepsilon_t = 22.1 - 24.4\text{x}10^{-3}\ \sigma_y - 1.37\ S_R + 1.27\ (C-2) \quad \ldots\ldots \quad (4.25)$$

where W_m = Mean crack width, microns.

ε_t = Tensile strain on the face, $1\text{x}10^{-3}$ mm.

σ_y = Meshes yield strength (at 0.005 strain), N/mm^2.

S_R = Total specific surface of reinforcement, cm^2/cm^3.

C = Mortar cover, mm.

To account for section depth higher than 25 mm, the slope of the line connecting the points of 25 mm and 34 mm section depth in Fig.4.23, were found. The term 0.92 (D-25) therefore could be added to eqs. 4.24 and 4.25.

The maximum crack width can be obtained using the relation found in sec.4.5;

$$W_{max} = 1.71 \times W_m \quad \ldots\ldots \quad (4.26)$$

Equations 4.24 and 4.25 were used to calculate the mean crack width for the specimens of series S1. The average ratios of predicted to measured mean crack width for these specimens was equal to 0.95 with standard deviation equal to 0.13. The derived equations were also used to calculate the mean crack width for specimens of series S3 and S4. The data from these two series have not been included in the regression from which the derived equations were obtained. The calculated and the measured values of the mean crack width together with the average tensile strain on the face of the specimen were given in Table 4.11. The table shows the good agreement between the calculated and the measured values of the mean crack width. It should be mentioned, however, that for series S4, eq. 4.25 was used for all specimens

Table 4.11 Predicted and measured mean crack width for specimens of series S3 and S4.

Specimen designation	Average tensile strain micro-strain	Measured mean crack width micron	Predicted mean crack width micron	Predicted / Measured
S3 C1	648	13.4	12.4	0.93
	1215	22	23.3	1.06
	2092	37.4	40.1	1.07
	4260	87.5	81.7	0.93
S3 C2	504	13.5	9.7	0.72
	1166	24.4	22.4	0.92
	1790	35.7	34.3	0.96
	2697	55.4	51.7	0.93
	4263	91.8	81.3	0.89
S3 D1	895	15.8	11.8	0.75
	1495	28.2	19.8	0.7
	2147	40.6	28.4	0.7
	3098	59.4	41	0.69
	5022	98	66	0.67
S3 D2	716	12.1	9.5	0.79
	1328	20.8	17.6	0.85
	1984	29.4	26.3	0.89
	3094	46.4	40.9	0.88
	6102	88.2	80.7	0.92
S3 E2	759	9.6	8.9	0.93
	1220	14.5	14.2	0.98
	1910	24	22.3	0.93
	2989	40	34.9	0.87
	4763	63.6	55.5	0.87
S4 B	337	9.4	4.8	0.51
	661	15.1	9.5	0.63
	996	20.3	14.3	0.7
	1514	27.3	21.7	0.8
	2325	39.5	33.4	0.85
S4 C	640	10.4	8.7	0.84
	902	12.9	12.2	0.95
	1307	18.9	17.7	0.94
	2014	27.5	27.2	0.99
	3262	42	44.1	1.05
S4 D	785	9.4	9.8	1.04
	1522	15.9	18.9	1.19
	2449	26.1	30.5	1.17
	4714	51.1	58.7	1.15

irrespective of the value of the specific surface. Also, the yield strength of the reinforcing system was obtained by adding the contribution of each type of reinforcement in proportion to its fraction volume. Thus, steel bars yield strength multiplied by their fraction volume divided by the total fraction volume of the reinforcement plus wire meshes yield strength, multiplied by their fraction volume divided by the total fraction volume of the reinforcement will give the yield strength of reinforcing system. The reason for these alterations is to account for the presence of steel bars which have relatively low specific surface but high fraction volume, due to which the derived equations underestimate their effect.

4.9 Comparisons of Data with Other Investigators' Equations to Estimate the Crack Width.

Five crack width equations suggested by other investigators were used to predict the crack widths and compare the results with those measured in this study. The equations considered are:

$$W_{max} = \frac{3.5\times10^{-9} \times f_s \, l^{1/3}}{S_{LT}^{1/3}} \quad \text{(Logan and Shah (5))} \quad ..... \quad (4.2)$$

$$W_{max} = 2.25 \, \frac{V_m \, (\sigma_{fm}-420)}{\eta \, S_{LT} \, E_f} \times \frac{(D-a)}{(D'-a)} \quad \text{(Rajagoplan and Paramaswarn (56))} \quad ..... \quad (4.4)$$

with $W_{max} = 1.5 \, W_m$

$$W_m = 0.254 + 0.186 \, \varepsilon_s \quad \text{(Balaguru,Naaman and Shah (31))} \quad ..... \quad (4.8)$$

$$W_{max} = \varepsilon_s \, S \, R \quad \text{(Balaguru,Naaman and Shah (31))} \quad .... \quad (4.9)$$

$$W_m = \sqrt{\psi \, \psi_y} \, \frac{\theta \, (h-c)}{\eta \, S_{LT}} \quad \text{(Balaguru (58))} \quad ..... \quad (4.14)$$

Details of these equations are given in sec. 4.2.

Due to the large amount of data available and to avoid repetition, the crack width data for two specimens only were considered. The specimens are

S1 D2 and S2 D2, which have six meshes each but one reinforced with high tensile steel mesh, while the other was reinforced with mild steel. The mortar cover is 2 mm for both. The reason for choosing these specimens is that both of them have reinforcement amount equal or more than the saturation limit. As discussed earlier in this chapter, the crack width and spacing for specimens with more than the saturation limit did not differ substantially. Therefore, the selected specimens should give good indication of the crack width for the majority of the tested specimens.

Table 4.12 gives the predicted and measured values of crack width as well as the ratio of predicted to measured at different loading stages and for both specimens. In Figs. 4.24 and 4.25, the crack width, both predicted and measured, are plotted against the tensile strain on the face of the specimen, for specimen S1 D2 and S2 D2, respectively. For specimen S1 D2 (mild steel mesh), all the equations underestimate the crack width except eq. 4.14 which overestimates the results. The nearest predicted values to the measured were those from eqs. 4.2 and 4.14, where the average of the ratio of predicted to measured were 0.57 and 1.46 respectively. Both of these equations includes the specific surface of reinforcement and the level of load. All equations show a trend, with increase in tensile strain, different to that of the experimental results.

For specimen S2 D2 (high tensile mesh), the equations appear to predict the crack width better than for S1 D2. Exception was eq. 4.14 which overestimates the values by more than two times. The only other equation which overestimated the crack width was eq. 4.2. This equation, although it gave good results at low loads, predicted crack width up to 1.8 times the measured at higher loads. Equations 4.2 and 4.4 gave the best results for this specimen. The average of the predicted to measured ratio for these equations were 1.26 and 0.6 respectively. Again the trend of equations seems to differ from the experimental results.

Table 4.12 Comparison of Predicted and Experimental mean Crack Width.

	Load KN	Tensile strain on the face micro-strain	R*	Tensile strain in the extreme mesh micro-strain	Tensile stress in the extreme mesh N/mm^2	Mean crack width experimental microns	Eq. (4.2) Logan and Shah		Eq. (4.4) Rajegoplan		Eq. (4.8) Balaguru et al.		Eq. (4.9) Balaguru et al.		Eq. 4.14 Balaguru	
							Pred. mean crack width	Pred. / exp.	Pred.	Pred. / exp.	Pred.	Pred. / exp.	Pred.	Pred. / exp.	Pred.	Pred. / exp.
S1 D2	1.278	884	1.21	731	64.66	13.4	6.8	0.51	2.75	0.21	9.9	0.74	4.8	0.36	22	1.64
	1.832	1475	1.2	1228	105.3	19.8	13	0.66	7.5	0.38	12.25	0.62	8	0.4	37.3	1.89
	2.365	2055	1.2	1717	134.6	27.7	18	0.65	10.9	0.39	14.56	0.53	11.2	0.4	47.4	1.71
	3.097	3512	1.19	2956	183.5	49.6	27.1	0.55	16.4	0.33	20.4	0.41	19.1	0.39	57.3	1.16
	3.384	4971	1.18	4202	208.6	68.8	32.2	0.47	19.2	0.28	26.3	0.38	27.1	0.39	60.2	6.88
S2 D2	1.653	1090	1.2	907	7.8	12.7	10.7	0.84	4.5	0.35	10.7	0.84	5.9	0.46	47.2	3.71
	2.704	2160	1.2	1802	161.9	26.2	27.3	1.04	14.1	0.54	15	0.57	11.8	0.45	71.3	2.72
	3.915	3335	1.2	2785	248	37	48.2	1.3	24.1	0.65	19.6	0.53	18.2	0.49	78.8	2.14
	5.055	4692	1.2	3922	392.5	47.6	88.7	1.86	40.9	0.86	25	0.53	25.6	0.54	101	2.12

R = Ratio of distances to neutral axis from extreme tension fibre and from outermost mesh.

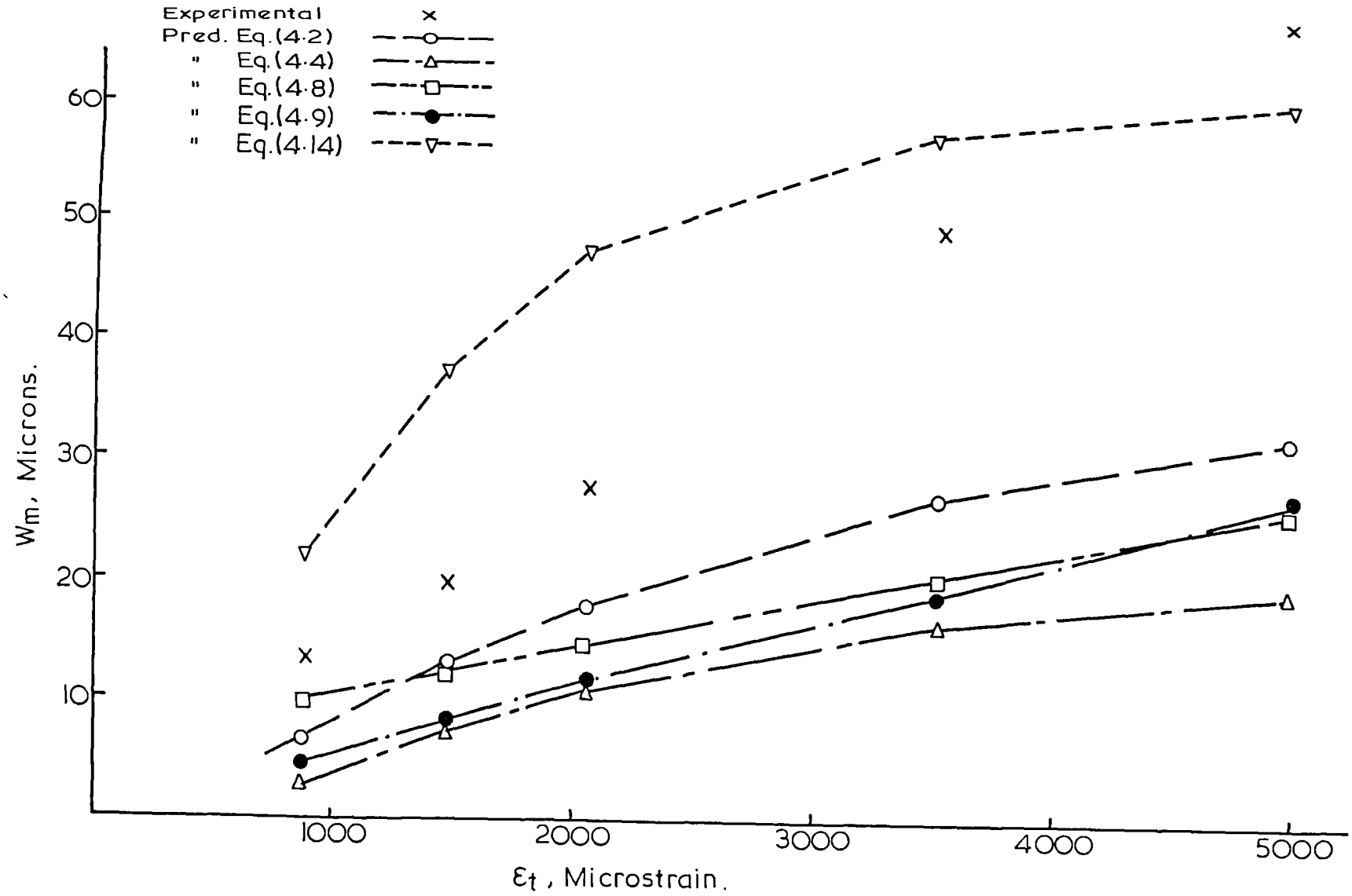

Fig. 4·24. Comparison of predicted & experimental values of mean crack width, SI D2.

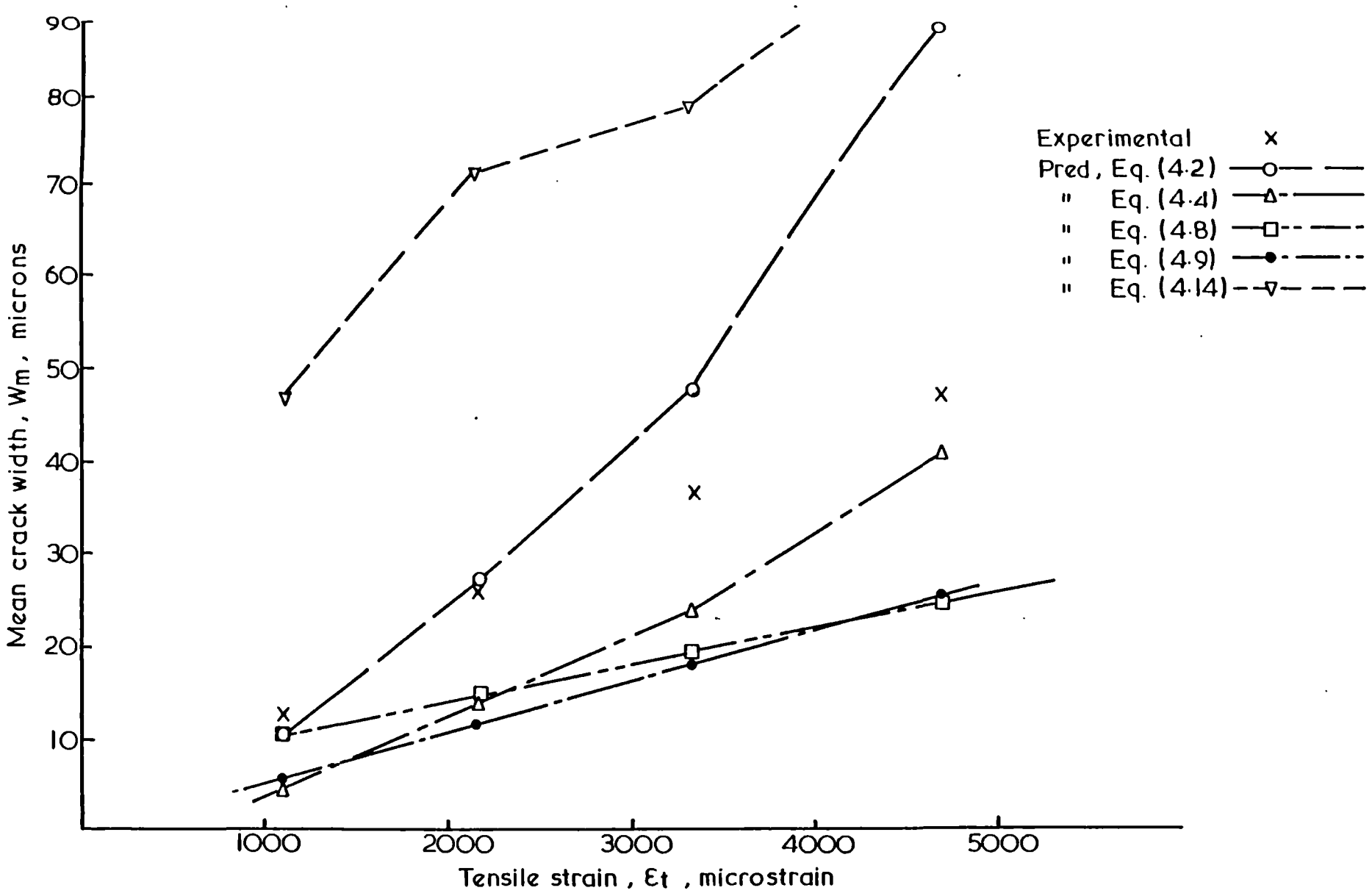

Fig. 4.25. Comparison of predicted and experimental values of mean crack width, S2 D2.

Equation 4.2 gave the best combined results for specimens S1 D2 and S2 D2, with ratios of predicted to measured crack width of 0.57 and 1.26 respectively.

4.10 Comparisons of the Derived Equations with Other Investigators' Results.

The only data on crack width available in the literature were those of Balaguru, Naaman & Shah (31). Combining some of the graphs with the tables in that reference and by assuming the depth of the neutral axis for specimens reinforced with woven mesh are the same as those reinforced with welded mesh at the same load, the data in Table 4.13 was found. The derived equation was used in the following form:

For $S_R \leq 2.85 - 3.5\times10^{-3}\ \sigma_y$

$$W_m/\varepsilon_t = 43.7 - 50.9\times10^{-3}\ \sigma_y - 9.3\ S_R$$

For $S_R \geq 2.85 - 3.5\times10^{-3}\ \sigma$

$$W_m/\varepsilon_t = 22.1 - 24.4\times10^{-3}\ \sigma_y - 1.73\ S_R$$

The effect of the cover was neglected due to insufficient data. The results for specimens reinforced with $^1/_4$ in. woven mesh and $^1/_2$ in. welded mesh were tabulated in Table 4.13 and plotted in Figs. 4.26 and 4.27.

From Fig.4.26 it can be seen that the derived equation gave very close results for the specimens reinforced with woven mesh. The average ratio of predicted to measured was 1.02. For the welded mesh specimens, although the derived equation was based on woven mesh it could still predict the mean crack width reasonably closely (Fig.4.27). The equations overestimate the results except for the specimens with 6 meshes where they underestimate and show higher error. However, the experimental results of this specimen are inconsistent with the other results. The crack width would be expected to decrease with an increase in number of meshes, while the experimental results of the 6 mesh specimen showed a higher crack width than the 2 mesh specimen.

Table 4.13 Comparison of Crack Width Data from Bulugura et al. (31) and Results using Derived Equation.

Type of mesh	Mesh Yield strength (at 0.005 strain) N/mm^2	Number of meshes in specimen	Specific surface of reinforcement S_R cm^2/cm^3	Tensile strain in the extreme mesh layer ε_s microstrain	Tensile strain in the extreme fibre ε_s microstrain	Measured Mean crack width micron	Predicted mean crack width micron	Predicted / Measured
1/4" Woven Mesh	475.4	4	1.79	2790	3180	22.2	23.5	1.06
				3250	3705	28.7	27.4	0.95
				4290	4890	32	36.2	1.13
				5665	6460	45.2	47.8	1.06
		6	2.69	2875	3280	20	19.2	0.96
				5000	5700	34.8	33.3	0.96
1/2" Welded Mesh	482.3	2	0.8	1220	1440	13.2	16.9	1.28
				2010	2365	24.6	27.8	1.13
				4300	5026	36.1	59	1.63
		4	1.6	961	1160	5.1	8.8	1.72
				1750	2105	11.7	16	1.36
				2380	2850	21.3	21.7	1.02
				3750	4470	31	34	1.10
		6	2.4	790	963	19.8	6.0	0.30
				2070	2504	28.1	15.5	0.55
				4870	5840	54.3	36.2	0.67

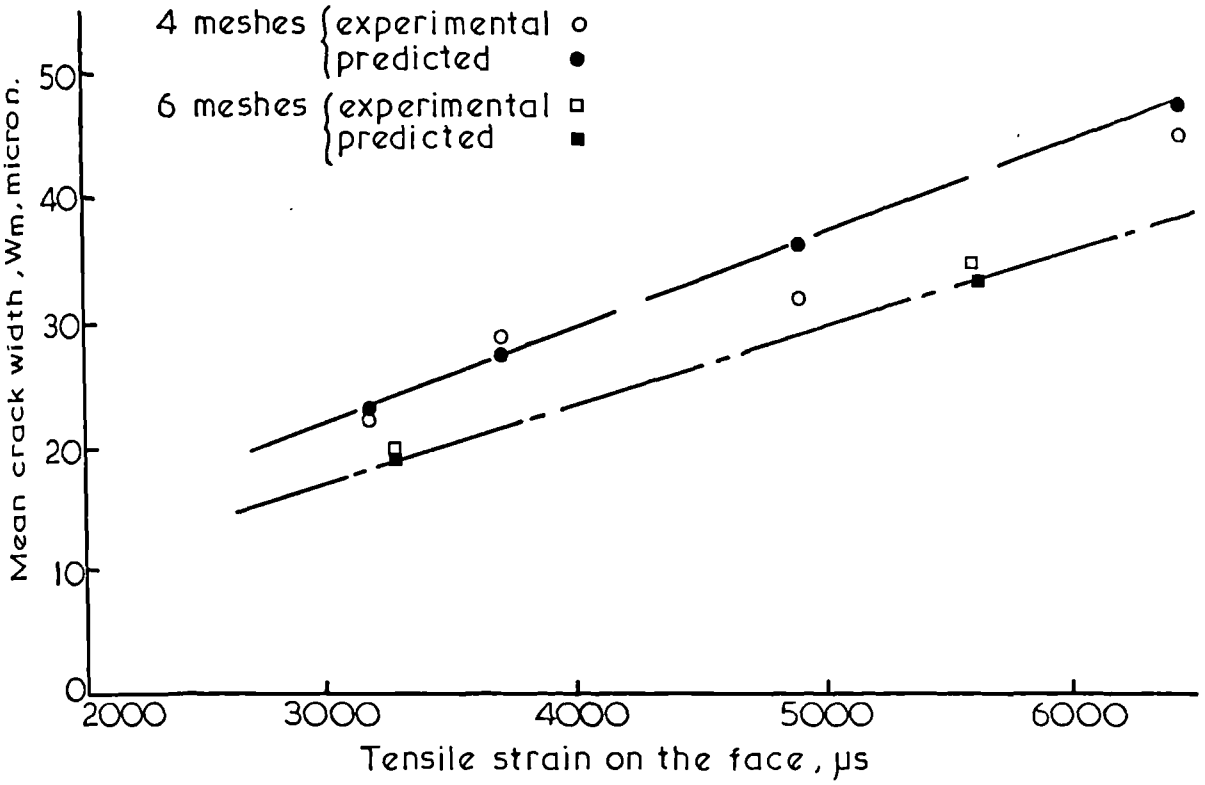

Fig. 4·26. Comparison of experimental crack width data from Balaguru et al.(31) and predicted using derived equations, 6·35 mm woven mesh.

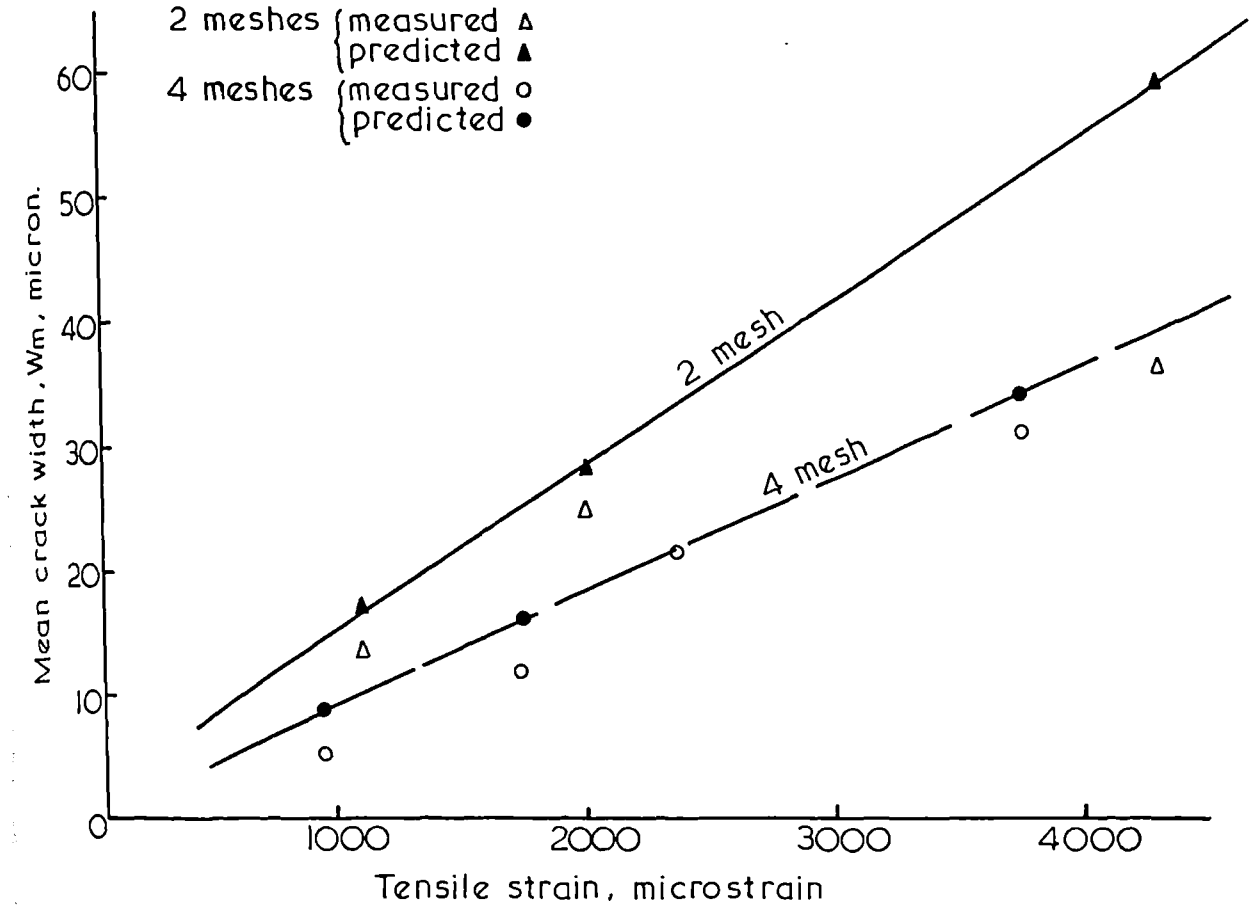

Fig. 4·27. Comparison of experimental crack width data from Balaguru et al.(31) and predicted using the derived equations, 12·5mm welded mesh.

Except for the specimen with 6 welded meshes, the derived equation gave results of similar trend to the experimental ones.

4.11 Conclusions.

Based on the tests carried out in this investigation, the following conclusions are drawn:-

1. The cracking behaviour of ferrocement plates is characterized by almost full development of the number of cracks at relatively early stages of the load. Most of the cracks found after failure developed at about 30-50% of the ultimate load, and this is a feature which distinguishes ferrocement from ordinary reinforced concrete with steel fibres. The major features which distinguish ferrocement from reinforced concrete are that the former shows uniform crack width distribution with the peak more or less in the middle of the range of the crack width, while in reinforced concrete several peaks form with increase in the load and the highest one is nearer the smaller range of width of cracks. Also, for the same tensile strain, the maximum crack width in reinforced concrete can be up to 4 to 5 times higher than in ferrocement.

2. The mean crack width increases linearly with the average tensile strain on the face of the specimen. The slope of the linear relationship, W_m/ε_t, is called, appropriately, the rate of growth of crack width, and its value gives good indication of the cracking performance of the specimen.

3. The mesh yield strength influences strongly the crack width and spacing. For the same mesh opening, high tensile steel mesh results in specimens with lower rate of growth of crack width and smaller crack spacing after failure than those with mild steel mesh.

4. Irrespective of the type of mesh, increasing the number of meshes in the specimen decreases the rate of growth of crack width, and the spacing

of the cracks before and after failure. This decrease slows down appreciably at a certain number of meshes. The number of meshes is six for specimens with mild steel mesh and four for those with high tensile mesh, corresponding to specific surface of 2.1 and 1.5 cm^2/cm^3, respectively. These amounts of reinforcement are called the saturation limits as the rate of growth of crack width does not decrease appreciably with further increase in them.

5. The crack width and spacing are influenced by the mortar cover and the section depth. For 6 mm cover the rate of growth of crack width and the average crack spacing were about 1.5 and 1.4 respectively, times that for 2 mm cover. For reinforcement amount equal to the saturation limit of mild mesh, there appears to be an optimum section thickness which shows the most favourable cracking behaviour.

6. In terms of the rate growth of crack width, the enhancement in the cracking behaviour for specimens reinforced with mild steel wire mesh over those reinforced with conventional steel bars, and for the amount and type used in this study, starts when the mesh number exceeds four. The high tensile mesh specimens showed better cracking performance even with 2 meshes.

7. Concentration of the meshes near the extreme fibres of the section does not result in an enhancement in the cracking behaviour over those with uniformly distributed meshes.

8. Combination of steel bars and mild steel mesh reinforcement gives a cracking behaviour somewhere between that of mild steel mesh only and high tensile steel mesh only. Replacement of the middle third of the meshes in the section by steel bars did not, at least, result in deterioration in the cracking behaviour.

CHAPTER 5.

LOAD AND DEFORMATION CHARACTERISTICS.

5.1 Introduction.

As the interest in ferrocement as a structural material grows, the demand for understanding, fully, its properties and behaviour grows with it. On the other hand, ferrocement has been considered, mainly, as a form of reinforced concrete and many of its strength and deformation characteristics were assumed to be the same as those of reinforced concrete. But, in spite of the similarities between the two materials, there are still major differences between them. These include the subdivision and distribution of reinforcements, the mesh shape of the reinforcement, the smaller section depth and mortar cover, the many types of mesh with different geometry, material and strength properties practically used in ferrocement, etc. These differences raise the question of whether the behaviour of ferrocement sections under loading will be different from that of reinforced concrete, and what are the influences of these differences on the strength and deformation characteristics of the material.

The most commonly agreed aspect of ferrocement behaviour is its better cracking performance compared to that of reinforced concrete. This suggests that the limitation on the crack width for the serviceability purposes will be less critical. But one cannot conclude that the serviceability load would be higher than in reinforced concrete unless the deflections prove to be less critical as well.

It is therefore clear that the tracing of the behaviour of ferrocement section under load and the study of the load and deformation characteristics and the relationship between them are very important. It would identify the differences between this material and reinforced concrete and help greatly in setting the basis for the design theory of ferrocement.

In this chapter, the influences of the different variables on the load and deformation characteristics of the ferrocement plates were studied from first application of the load until failure. The variables included the reinforcement amount and yield strength, presence of steel bars, mesh opening, section depth, and mortar cover. The relationship between the load deflections, strains, and crack width specially during the possible serviceability range were also investigated.

5.2 Review of Literature.

The work (26,30,31) carried out on ferrocement showed that the behaviour of the material under load can be divided into three main stages, namely, the elastic, the elasto-plastic, and the plastic stages. In the elastic stage, the material is uncracked and Nathan and Paramasivan (23,66) have shown that it is homogeneous. The end of this stage is marked by the first cracking. Some investigators (18,25) had suggested expressions to predict the load or the moment at first cracking directly from the specific surface of reinforcement. However, this could not be verified in this study, see Fig. 4.9. Nathan and Paramasivan (66) from their tests, concluded that the moment at first crack in flexure depends on the area of reinforcement, thickness of the specimen, proof stress of reinforcement and modulus of elasticity of the composite.

The second stage, i.e., the elasto-plastic stage, is characterized by multiple cracking of the section (31). Bezukladov et al. (5) have found that the stresses, elongations and modulus of elasticity of ferrocement during crack formation are affected, mainly, by the amount of reinforcement expressed in terms of the specific surface and fraction volume. For the same specific surface, the presence of steel bars did not influence the elongations at the first visible crack. Bigg (4) reported different design values for

the modulus of elasticity recommended by different investigators. In his analysis of ferrocement beams, Bigg suggested that in flexure the modulus of elasticity of the compressive zone is different from that of the tension zone. He also gave an expression to predict the modulus of elasticity in bending from those of the material in compression and in tension and recommended that expression for the use in establishing the load-deflection relationship.

The plastic stage is characterized by yielding of the section and rapid increase in the deformation until failure. Bigg (4) described the failure of ferrocement section as ductile and of a nature similar to that of under reinforced concrete. However, previous work (12) showed that ferrocement sections of different amounts of reinforcement exhibited different failures. The ultimate compressive strain at the outermost fibre of the section is greatly higher than the value used in the design of reinforced concrete (12, 18,31), i.e., 0.0035.

Several investigators have developed theoretical procedures to establish the load-deflection or the moment curvature relationship. Austriaco et al.(29) have presented an analysis for the inelastic behaviour of ferrocement slabs in bending. The slabs behave essentially as an elastic-strain hardening material with limit surface. Its moment curvature can be idealized as a trilinear curve. Near ultimate loads, the deflection of the slabs can be approximated by an elastic-perfectly plastic bilinear analysis. Limited experimental results showed to be in good agreement with the theoretically predicted values. Balaguru, Naaman and Shah (31) predicted the load-deflection and moment-rotation relationship for experimentally tested beams. Their procedure depends on a non-linear analysis and using the stress-strain diagrams of the two major constituent materials. Paul

and Pama (11), using the theory of composite materials, have suggested a procedure for the analysis of ferrocement sections. The load-deflection and the moment-curvature relationships were again idealized to trilinear behaviours and developed using the predicted mechanical properties of the composite.

It can be seen, therefore, that a large amount of work has been carried out on the load-deflection and load-curvature relationship. However, several other aspects of the deformation characteristics have drawn less attention in spite of their prime importance. These include tracing of the deformation characteristics from first application of load until failure and perhaps more important, a quantitative study of the relationship between the different aspects of the deformation to establish the serviceability criteria. Also, the influence of the different variables encountered in ferrocement on the response of the section to loads needs to be known.

Walkus (30) has made an attempt to relate, quantitatively, some of the deformation characteristics to each other. He divided the behaviour of the member according to certain limits of crack width and recommended the corresponding stresses, strains and modulus of elasticity,(Table 1.2). However, Walkus generalized these limits and assumed them to be applicable to ferrocement beams irrespective of the properties of the section and the reinforcement. Such an assumption, as seen in Chapter 1, is not valid.

It therefore follows that more work is needed to fill the knowledge gap in the deformation characteristics of ferrocement and if the superior performance of this material lies in its ability to satisfy the serviceability criteria at relatively higher loads (67) then there is even more urgent need to find these criteria and to base the design on them.

5.3 Experimental Programme and Test Measurements.

The deformation measurements from first application of load up till failure were taken on the specimens of the seven series described in Chapter 3.

The variables in these series are the number, yield strength, and opening of the mesh, presence of steel bars, section thickness and mortar cover. The measurements included the tensile and compressive strain on the faces and sides of the specimens and the central deflection. Full details of the instrumentation and the test programme are given in Chapter 3.

5.4 Behaviour of the Plates under Loading.

Upon initial application of the load, the plates responded elastically and were free from any cracks. While the load was increased incrementally, the first crack was detected visually using a magnifying glass. Near the first cracking, a small drop in the load was noticed during the loading process. This indicates that certain amount of plastic deformation due to cracking was suffered by the specimen, resulting in some release of the load in the proving ring. The first crack width was measured for several selected specimens and found to be as small as 3 to 6 micron in width. The load at the first crack varied with the thickness of the specimen as would be expected. However, for specimens 25 mm in thickness,this load varied between 0.7 to 1.47 kN. The mean ratio of the load at first crack to the load at failure for all specimens was equal to 0.194 with standard deviation equal to 0.11. The range varied from 0.08 to 0.6 depending on the type and number of meshes. This large variation is due, mainly to the variation in the ultimate load rather than in the first crack load.

Soon after the first cracking, although a small drop in load every time it was stopped, still takes place, the plate retained partially its elastic response to the increase in the load. The first cracking was followed by a rapid increase in number of cracks. The range of the load at which the number of cracks continued to increase depended on the amount and yield strength of the reinforcement. In general, most of the cracks found near failure, were

developed at 30 to 50% of the ultimate. After a certain load, the increase in the number of cracks slowed down considerably accompanied by more rapid increase in the crack width marking the start of yielding of the specimen. During the range between first cracking and yielding, all cracks were very fine and only by a close look could they be identified. Yielding of the specimen was accompanied by a large amount of deformation. The crack width increased rapidly but uniformly showing no sign of local yielding. Near failure a few cracks widened more quickly than the others and one of these cracks initiated the failure of the specimen.

At failure a compressive strain on the face of the specimen up to 7000 microstrain and central deflection up to 12.5 mm were measured. This value of compressive strain is twice that used in the design of reinforced concrete. The measured ultimate compressive strain and ultimate deflections varied considerably depending on the type and amount of reinforcement which also seemed to influence the mode of failure. Three types of failure were observed. These are tensile failure by fracture of the wire mesh, compressive failure by crushing of the mortar and compressive and tensile failure by fracture of some of the wires in the mesh accompanied at the same time by crushing of the mortar. Some specimens suffered premature failure by splitting of the mortar cover in the tensile and the compressive zones. The different types of failures will be discussed in detail in section 5.8.3. However, it is to be mentioned here that Biggs (4) suggestion that ferrocement beams fail in a similar mode to those of under reinforced section does not seem to be valid for all specimens. The mode of failure appeared to be controlled by the amount and yield strength of the reinforcement.

5.5 Load-Deflection Relationship.

The central deflection is plotted against the total load and the curves are shown, for all specimens in Figs. 5.1 to 5.8. From these figures, the

load-deflection curve for ferrocement can generally be divided into four stages. In the first stage, the specimens behave elastically, free from cracks and the load-deflection curve is linear. The range and slope of the linear relationship was not influenced appreciably by the variables studied in this investigation. The end of this stage is marked by first deviation from linearity and the deflection/span ratio at that moment is mostly less than 1/360.

The second stage of the load-deflection curves corresponds to the elasto-plastic behaviour of the specimens. The first crack was visible at the beginning of this stage. The load-deflection relationship was again linear but with a slope lower than that at the first stage, showing the expected reduction in the specimen stiffness due to cracking. However, the linearity of the relationship indicated that the reduction in the stiffness due to cracking progress through this stage was, *at least, not* reflected on the load-deflection characteristics. The cracks, in this stage, increase in number more rapidly than in width which could be one of the reasons for the less rapid reduction in the stiffness with increase in load. Linear regression was carried out on the load and deflection values at the second linear stage. The slope and the correlation coefficient of the best fit line for the relationship were found. The correlation coefficient for all specimens were more than 0.999. This indicated the high degree of linearity of the relationship and the elastic response of the plate under load. Therefore, it appears that it is reasonable to assume that the section behaved elastically in this stage with a reduced modulus of elasticity.

In Fig. 5.9, the slope of the load-deflection curve at the second linear stage, which could be considered as a measure of the plates stiffness at this stage, is plotted against the fraction volume of reinforcement in the loading direction. The results from series S1, S2, S3 and S4 only, were included as

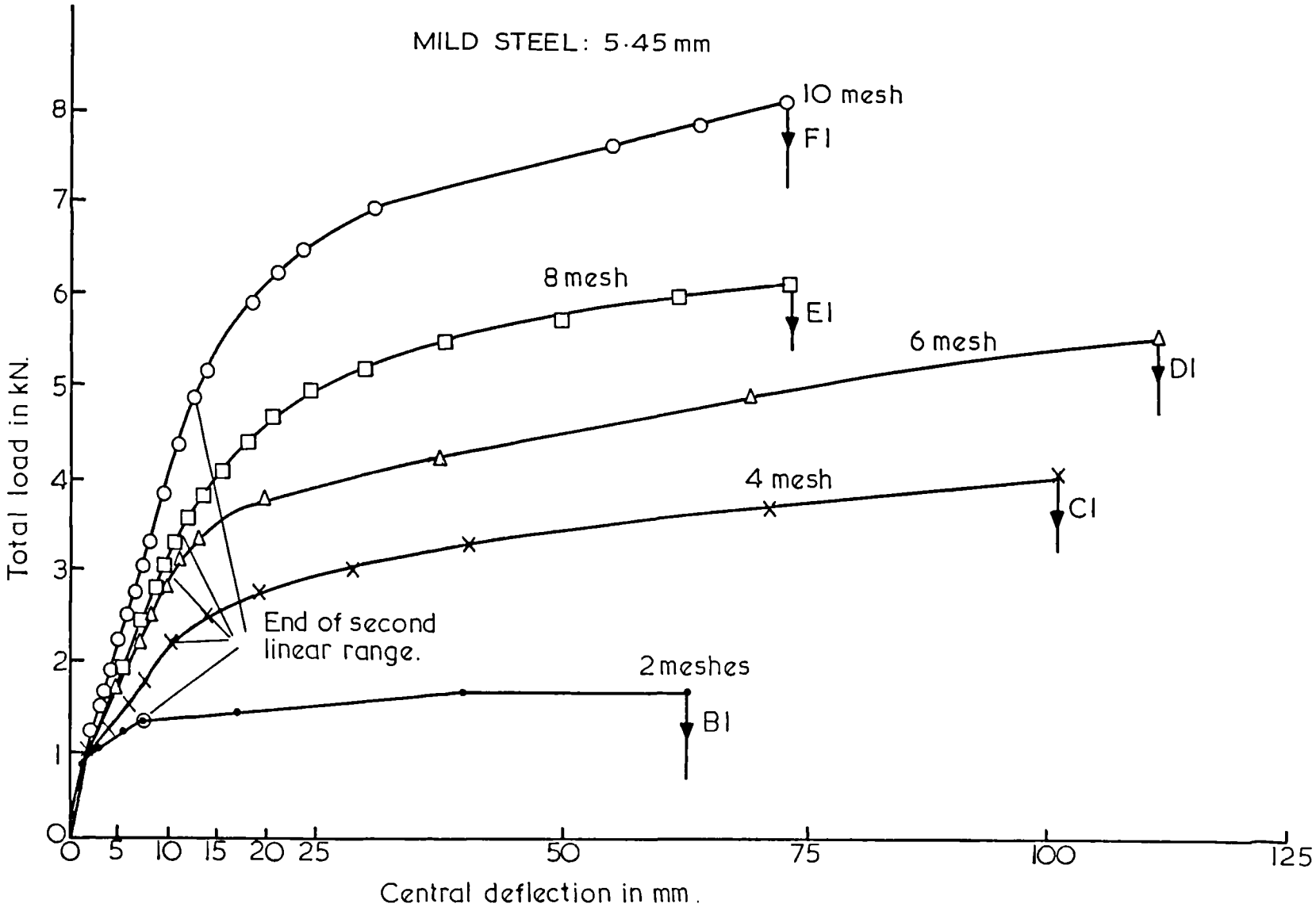

Fig.5·1. Load - deflection curve for series S1.

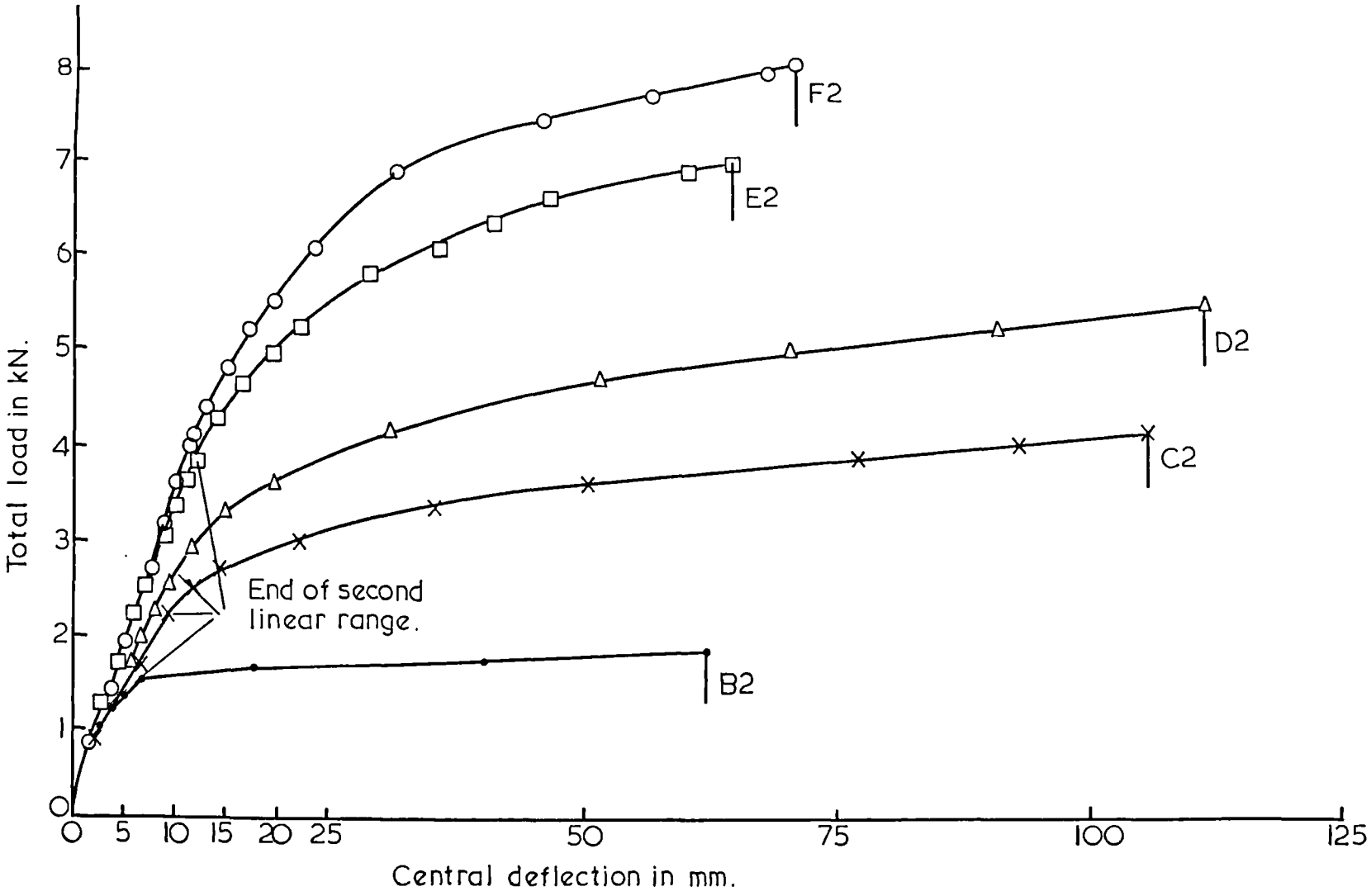

Fig. 5.2. Load -deflection curves, series S1.

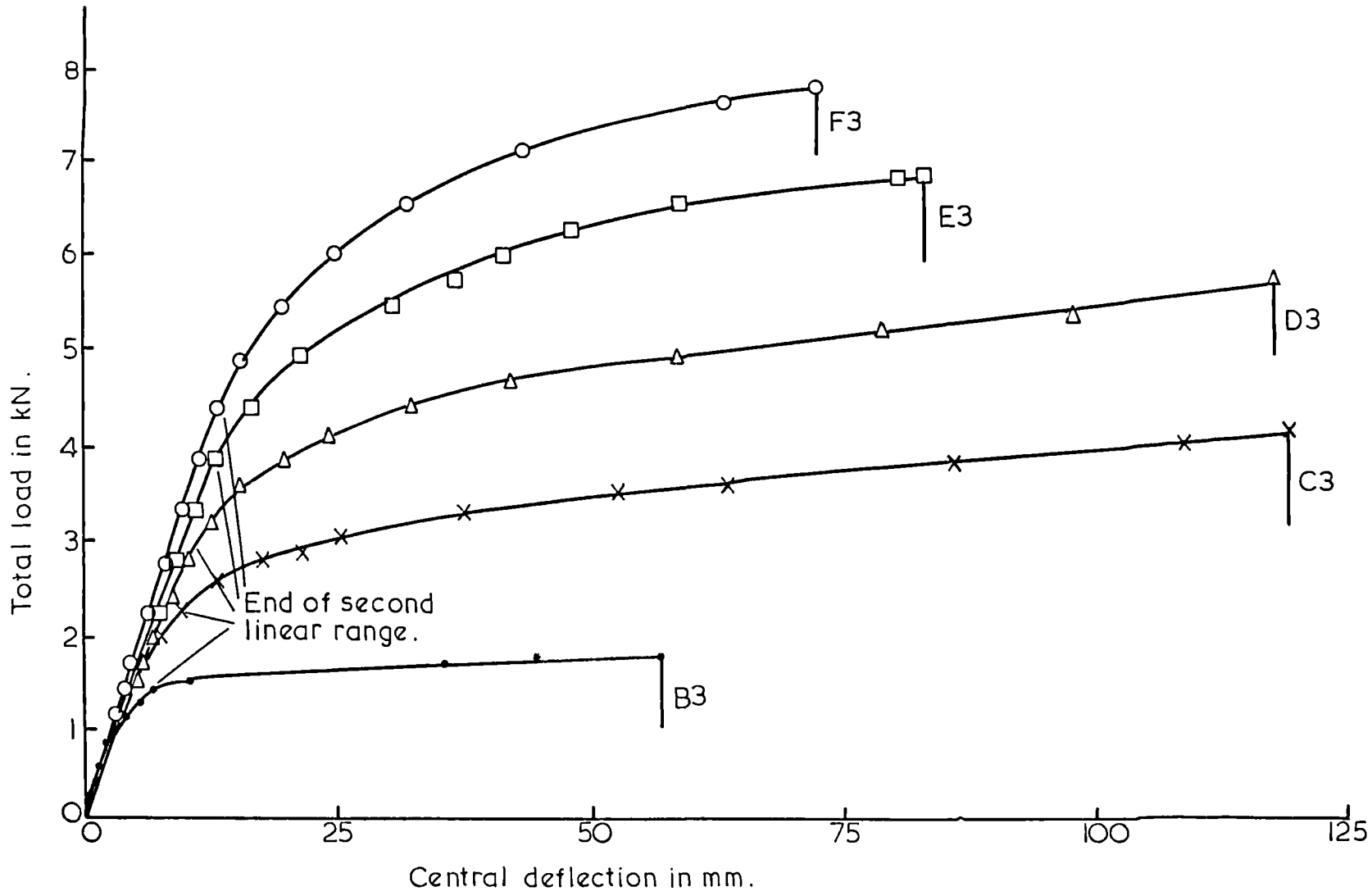

Fig.5.3. Load - deflection curve, series S1.

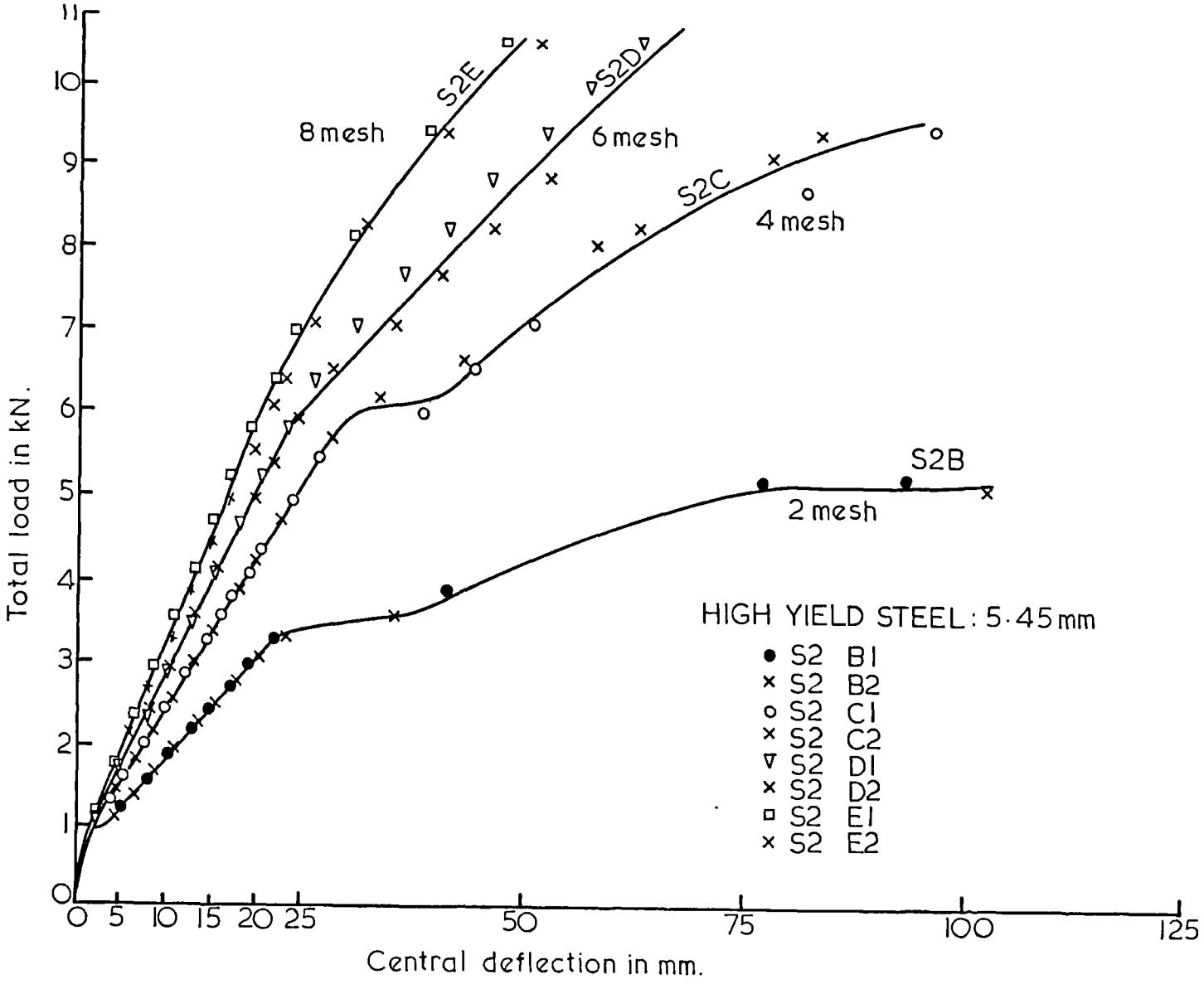

Fig. 5·4. Load - deflection curves, series S2.

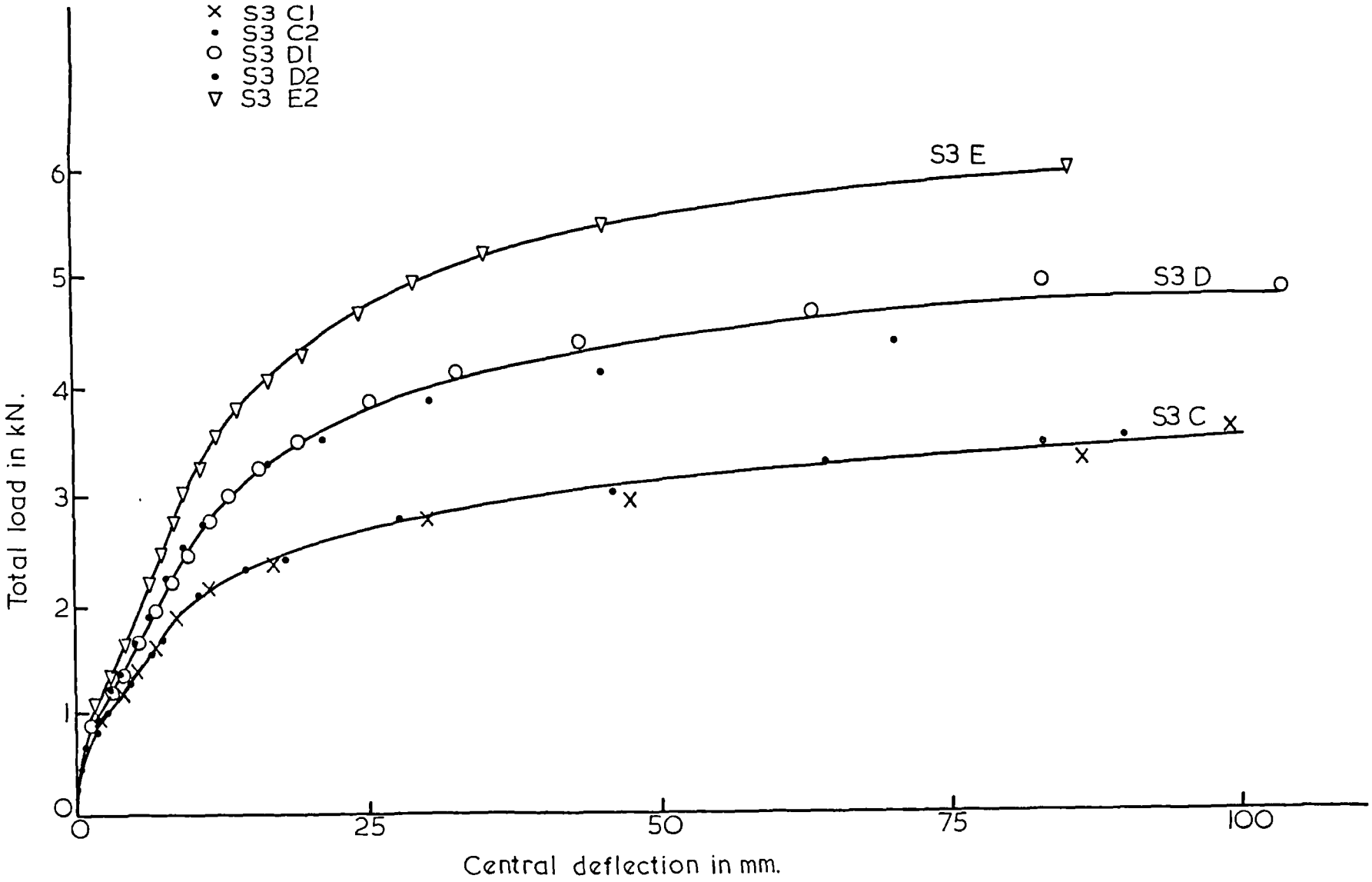

Fig.5.5. Load - deflection curves, series S3.

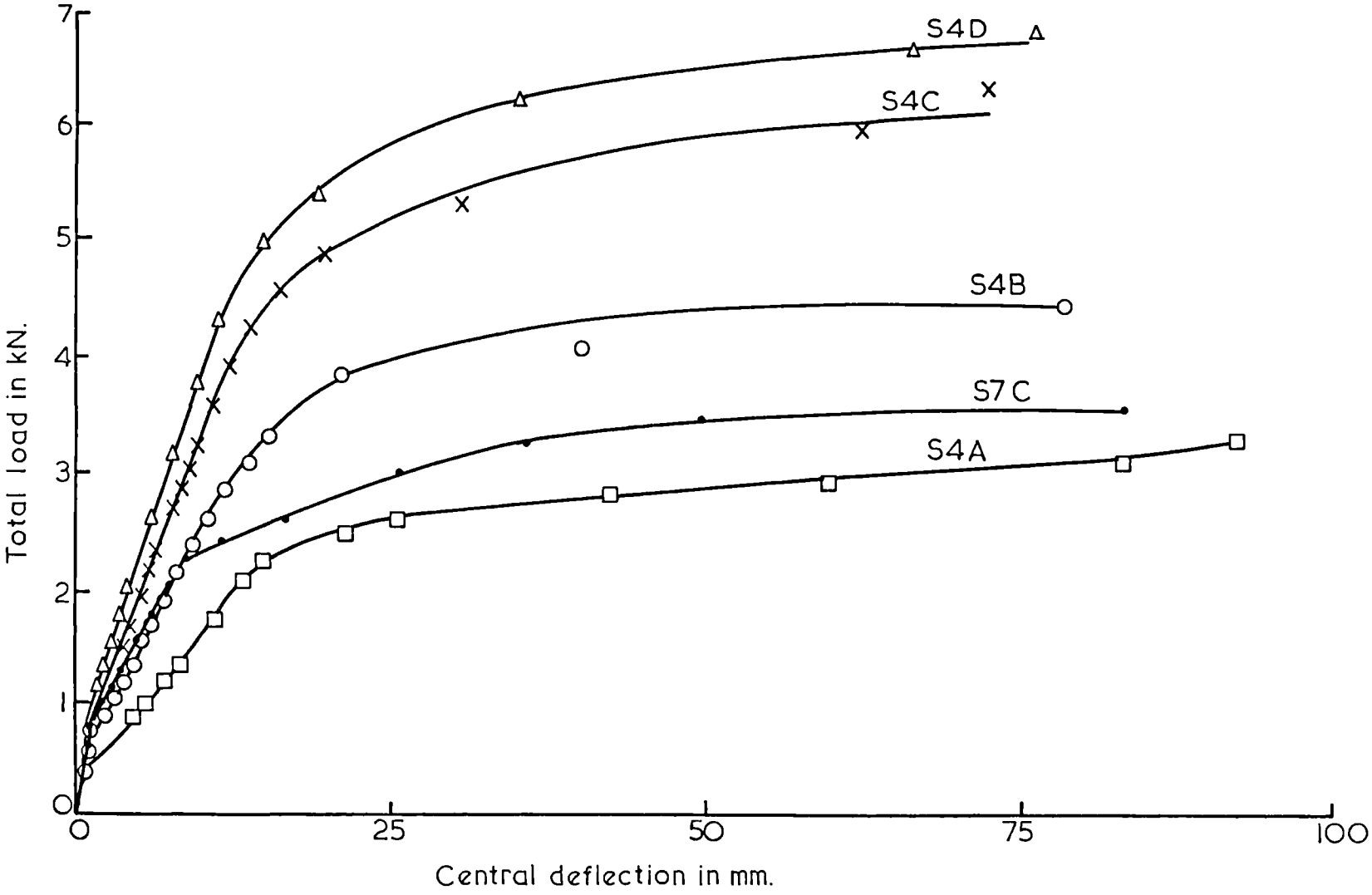

Fig. 5.6. Load - deflection curve , series S4.

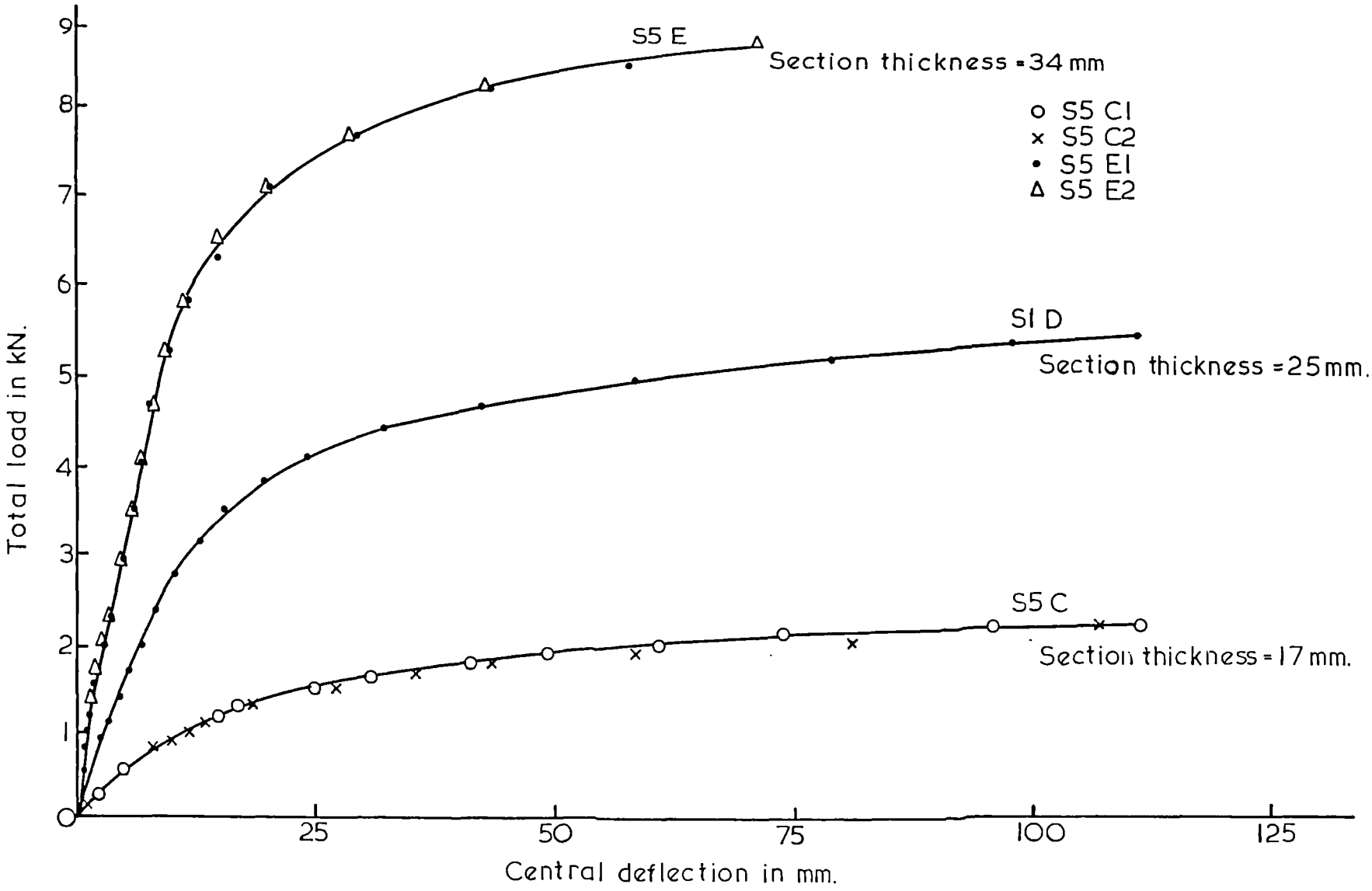

Fig. 5·7. Load - deflection curves series S5.

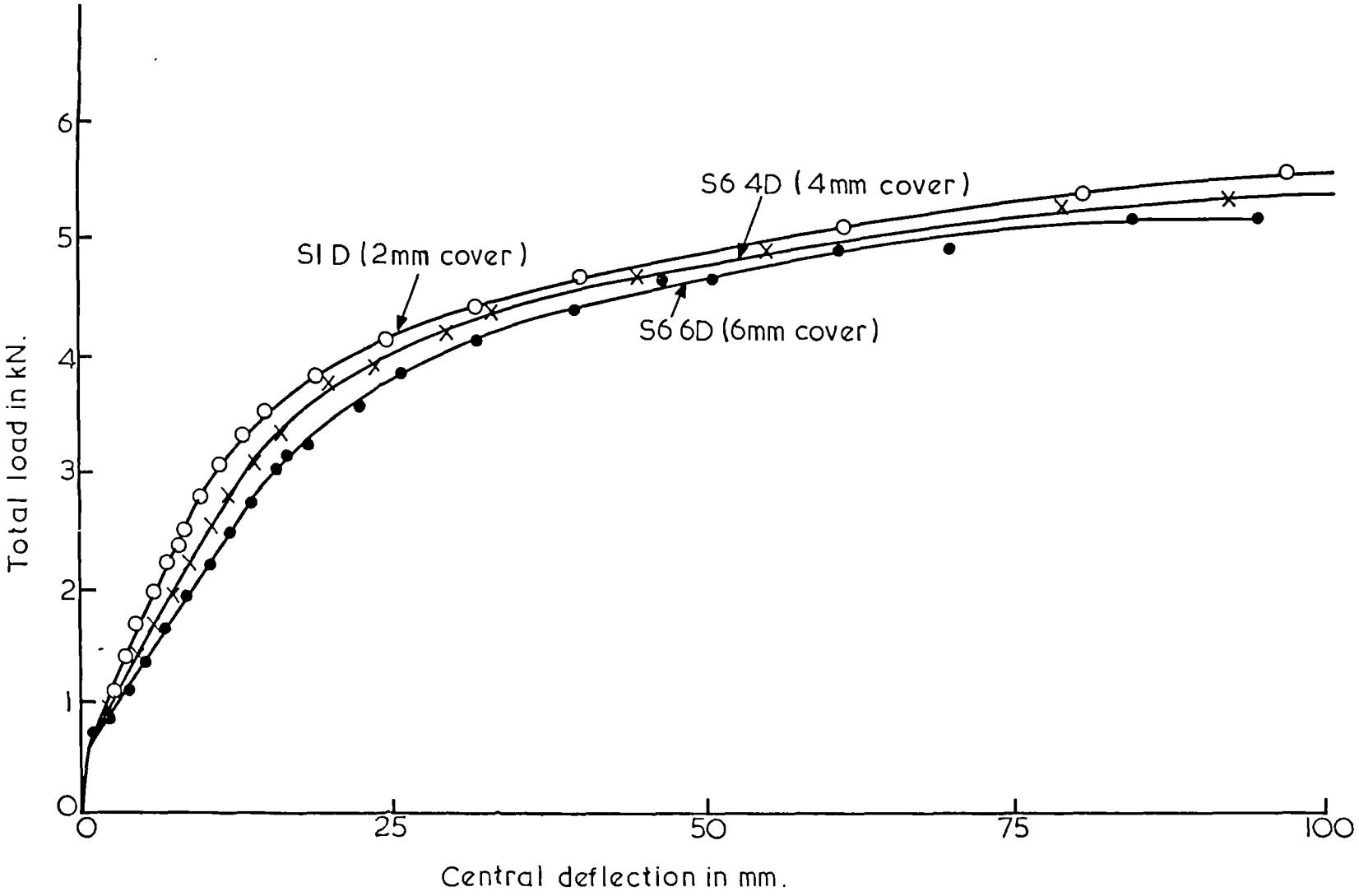

Fig.5.8. Load - deflection curve, series S6.

the specimens of these series have the same section thickness and mortar cover. The figure shows that the slope of the load deflection curve increases with the fraction volume of reinforcement in loading direction and the relationship can be assumed linear. Specimens from series S4, where the reinforcement consists of wire mesh and steel bars gave, for the same fraction volume, relatively higher slope values than specimens with wire mesh only. This could be attributed to the higher modulus of elasticity of steel bars compared to that of the wire mesh. In general the stiffness in the elasto-plastic stage does not seem to be influenced appreciably by the mesh yield strength, specific surface of reinforcement, or mesh opening.

The load, and maybe to a less extent, the deflection at the end of the second linear range varied with the studied variables. This variation will be discussed in section 5.8.2. The end of the second stage is marked by the deviation of the relationship from linearity. This indicates the start of yielding of the specimen where the third stage of the load deflection curve starts. In this stage, the relationship is curvilinear. The cracks start to increase in width more rapidly, propagate deeper into the section, and their number reaches almost a saturation limit. This stage ends when the specimen is fully yielding where the fourth stage starts. In the fourth stage, the relationship is again linear with the line nearly horizontal. This stage is characterized by rapid increase in the deformation, which soon leads to failure. The deflection just before failure, i.e., ultimate deflection, varied from one specimen to another and seems to be affected strongly by the mode of failure of the specimen and this will be discussed in detail in section 5.8.3.

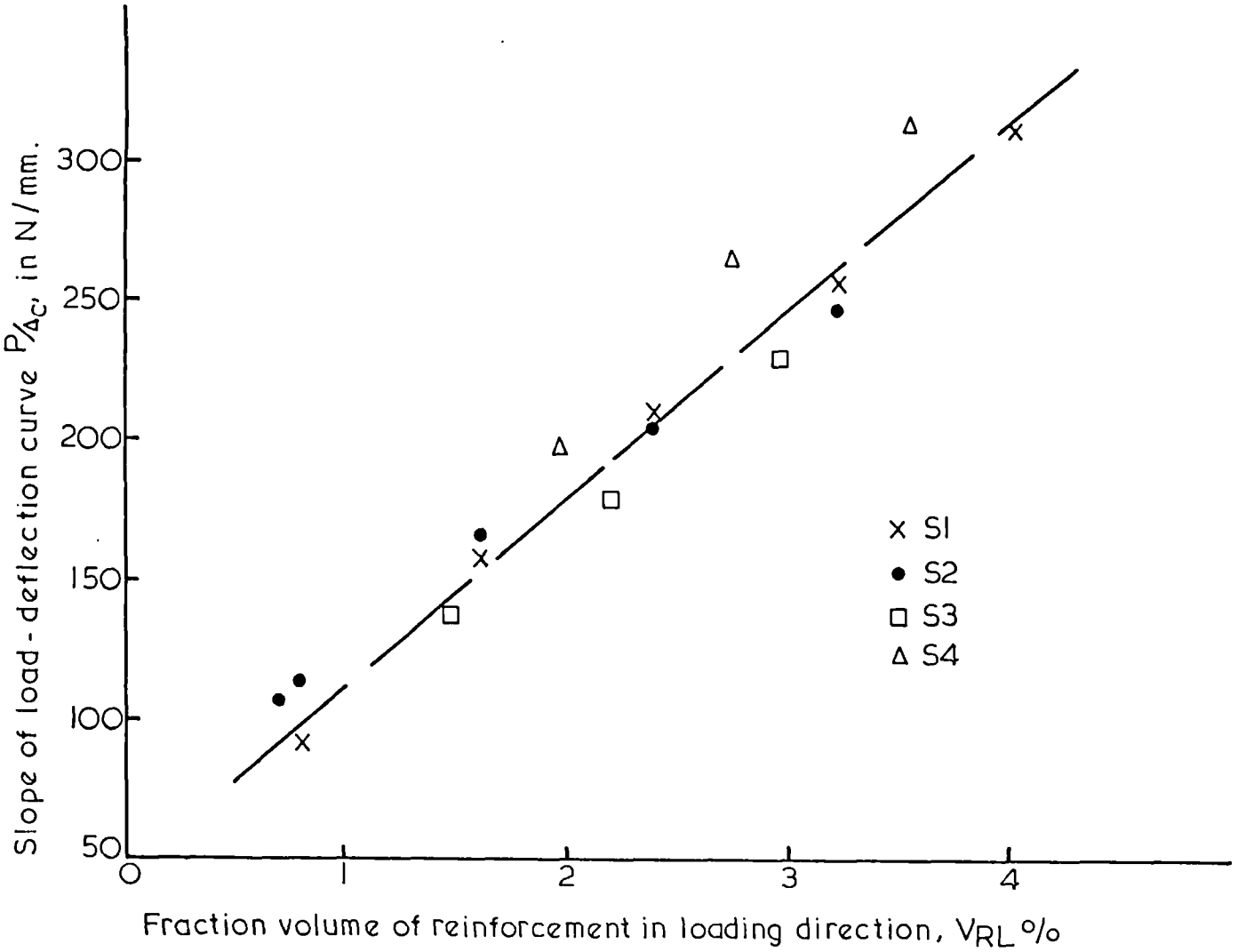

Fig.5.9. Slope of the load - deflection curve at the second linear stage against the fraction volume of reinforcement.

The part of the load deflection curve after first yielding, i.e., after the second linear stage, for specimens of series S2 were different from the rest of the series. In this series, where the reinforcement consisted of high tensile steel mesh, full plastic behaviour was not realized for specimens with four meshes and more. This is due to the yielding characteristics of the mesh. As will be discussed later, the first yielding of the specimens was due to yielding of the mortar in the compression zone rather than yielding of the mesh in the tension zone. It therefore follows that the yielding behaviour of the specimens is determined mainly by the yielding characteristics of the reinforcements.

5.6 Load-Strain Relationship.

In Figs. 5.10 to 5.17, the total load is plotted against the average strain on the tensile and compressive faces for typical specimens from each set and for all series. The figures show clearly the different stages of the specimen behaviour under loading discussed in the previous section. The first two stages are again shown to be linear. The slope of the first linear stage is almost the same for all specimens, while the slope of the second linear stage varies with the amount of reinforcement. This indicates that the effect of the increase in the amount of reinforcement becomes significant after the first cracking of the specimens. The slope of the second linear stage was, as in the load-deflection relationship, determined mainly by the fraction volume of reinforcement in loading direction. The specific surface of reinforcement, presence of steel bars, mesh yield strength, and the mortar cover did not have a significant influence on it. The plastic stage is clear and distinct for all specimens except those of series S2 where the reinforcement was high tensile mesh. The load-compressive strain curves for the specimens of this series were very

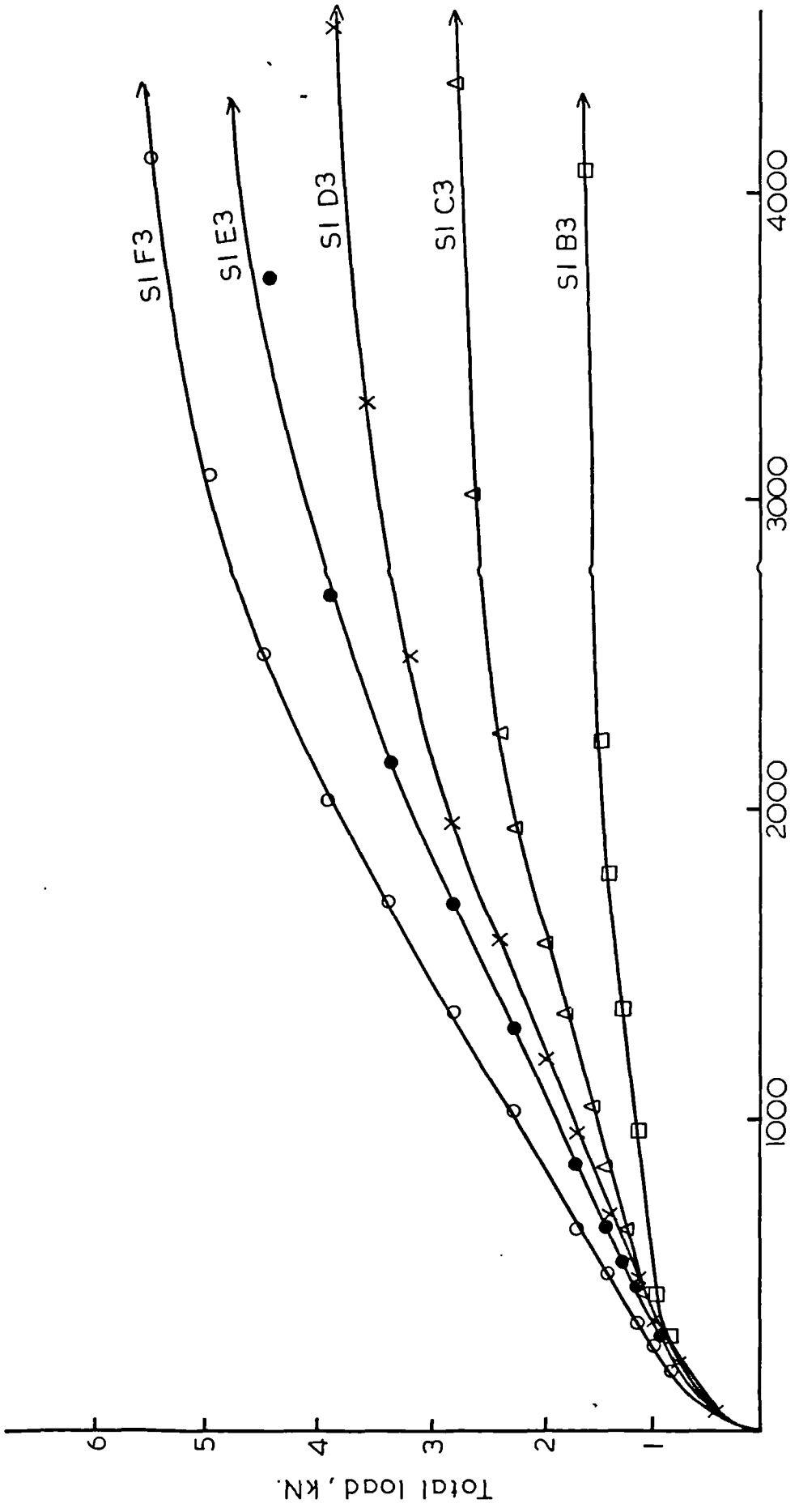

Fig. 5.10. Load - tensile strain curve, series S1.

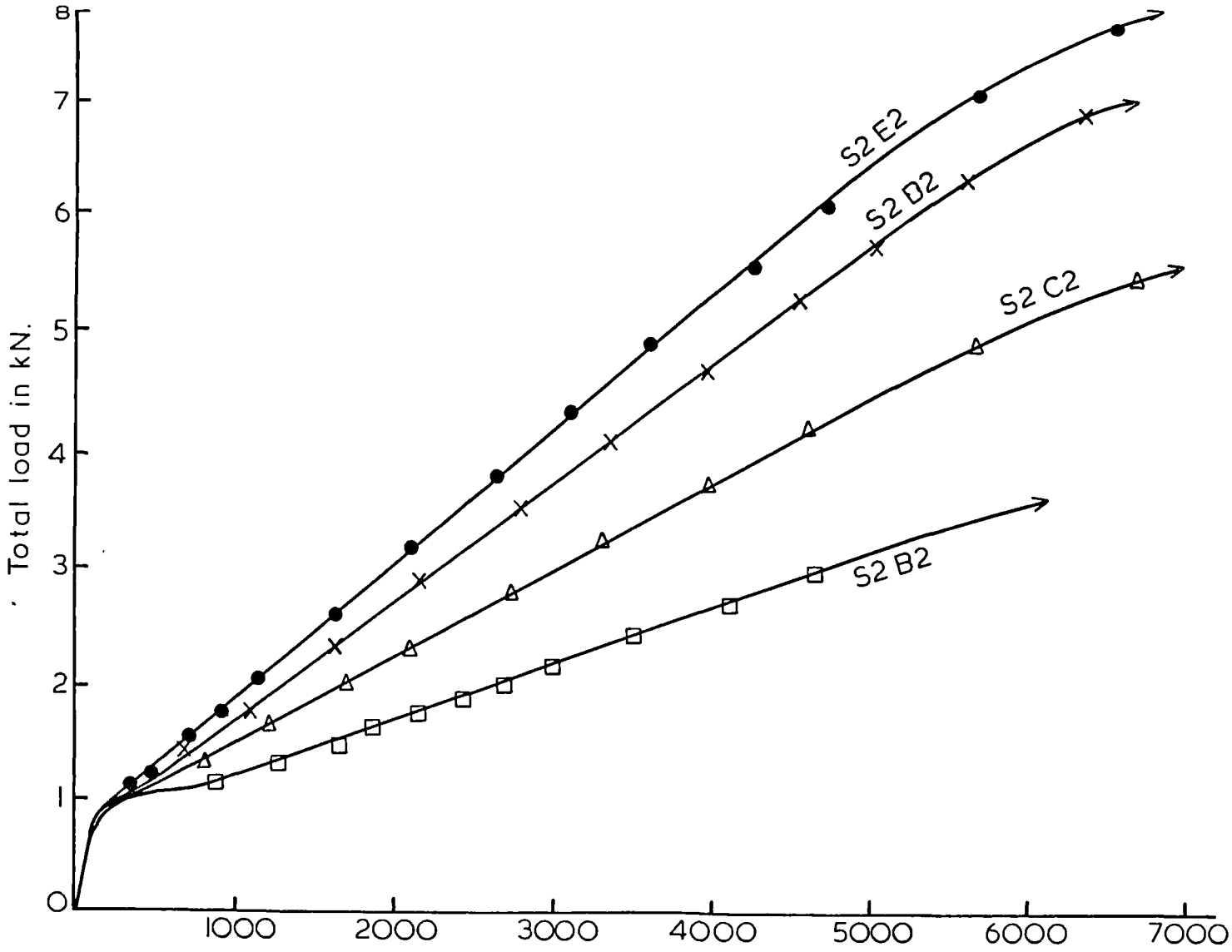

Fig. 5.11. Load - tensile strain curves, series S2.

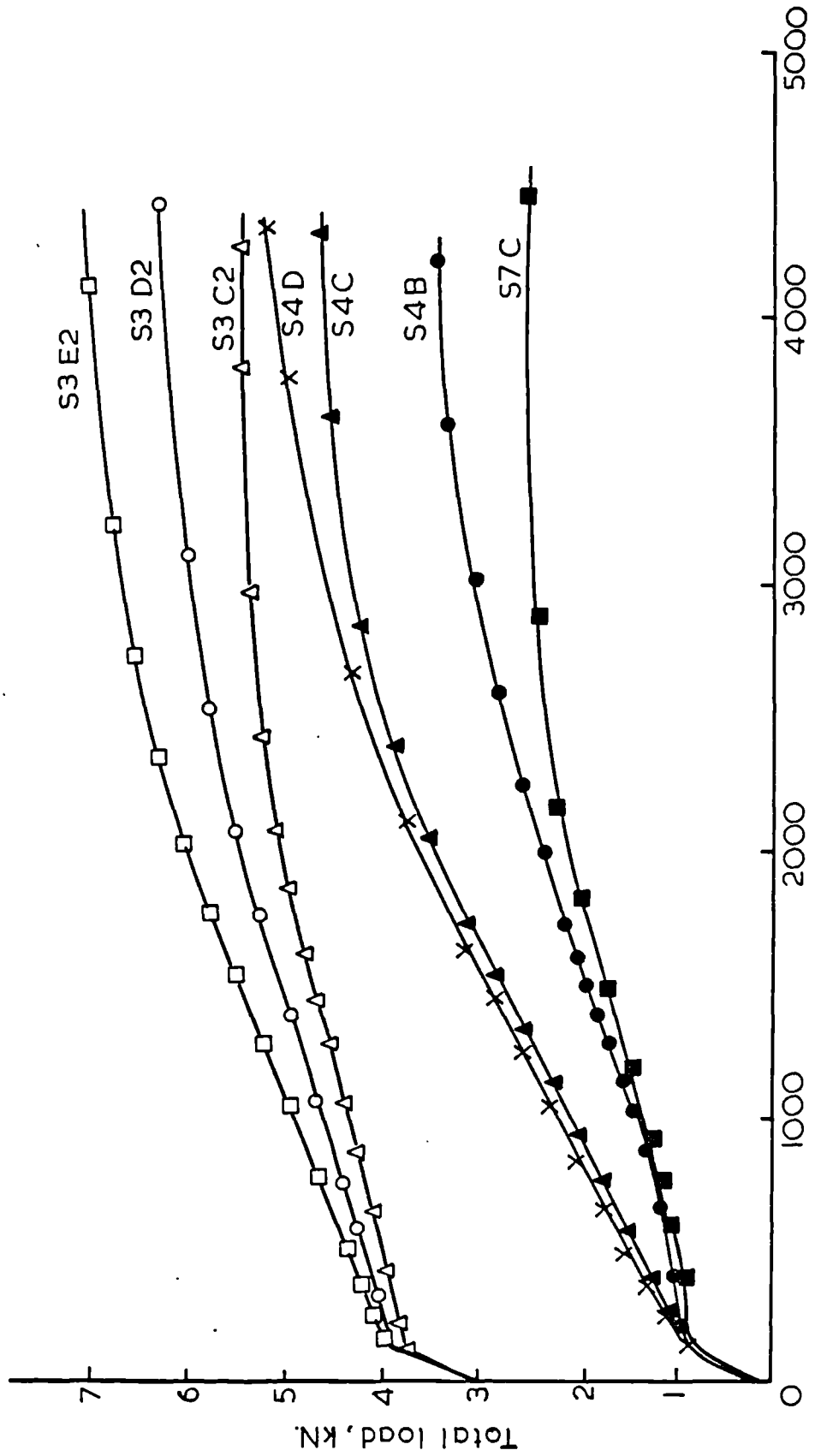

Fig. 5.12. Load - tensile strain curves, series S3 and S4.

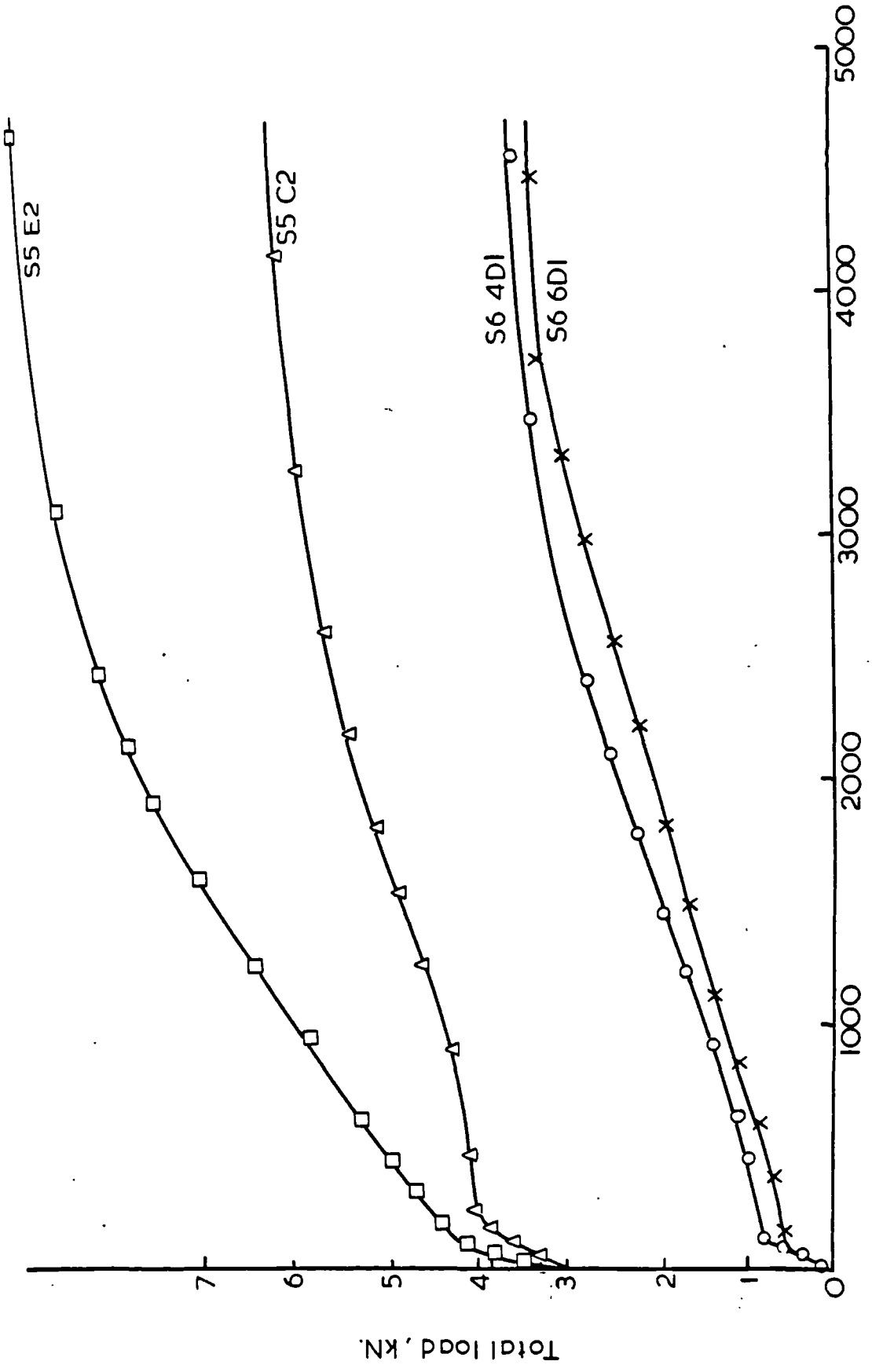

Fig. 5.13. Load - tensile strain curves, series S5 and S6.

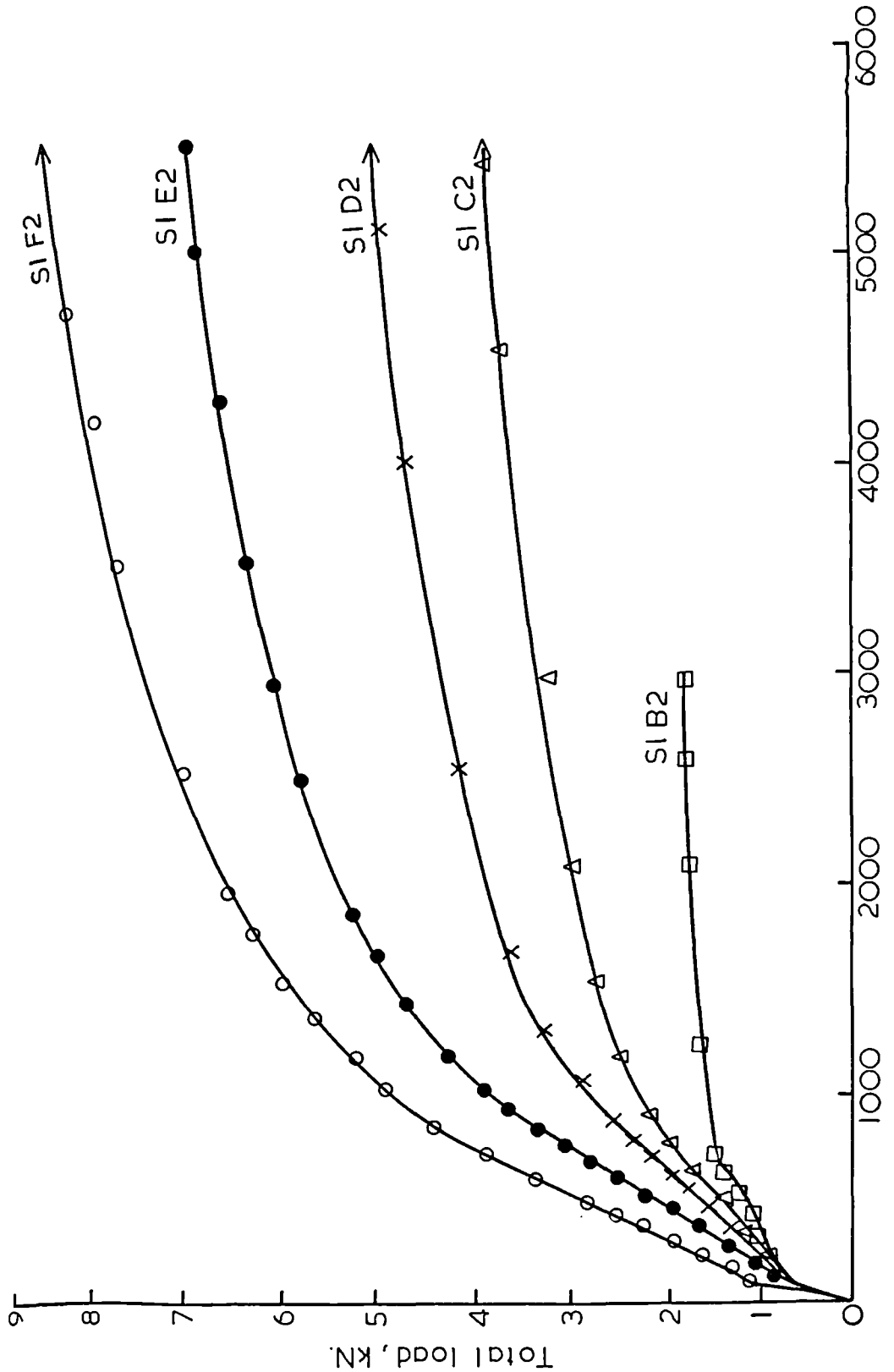

Fig. 5.14. Load - compressive strain curves, series S1.

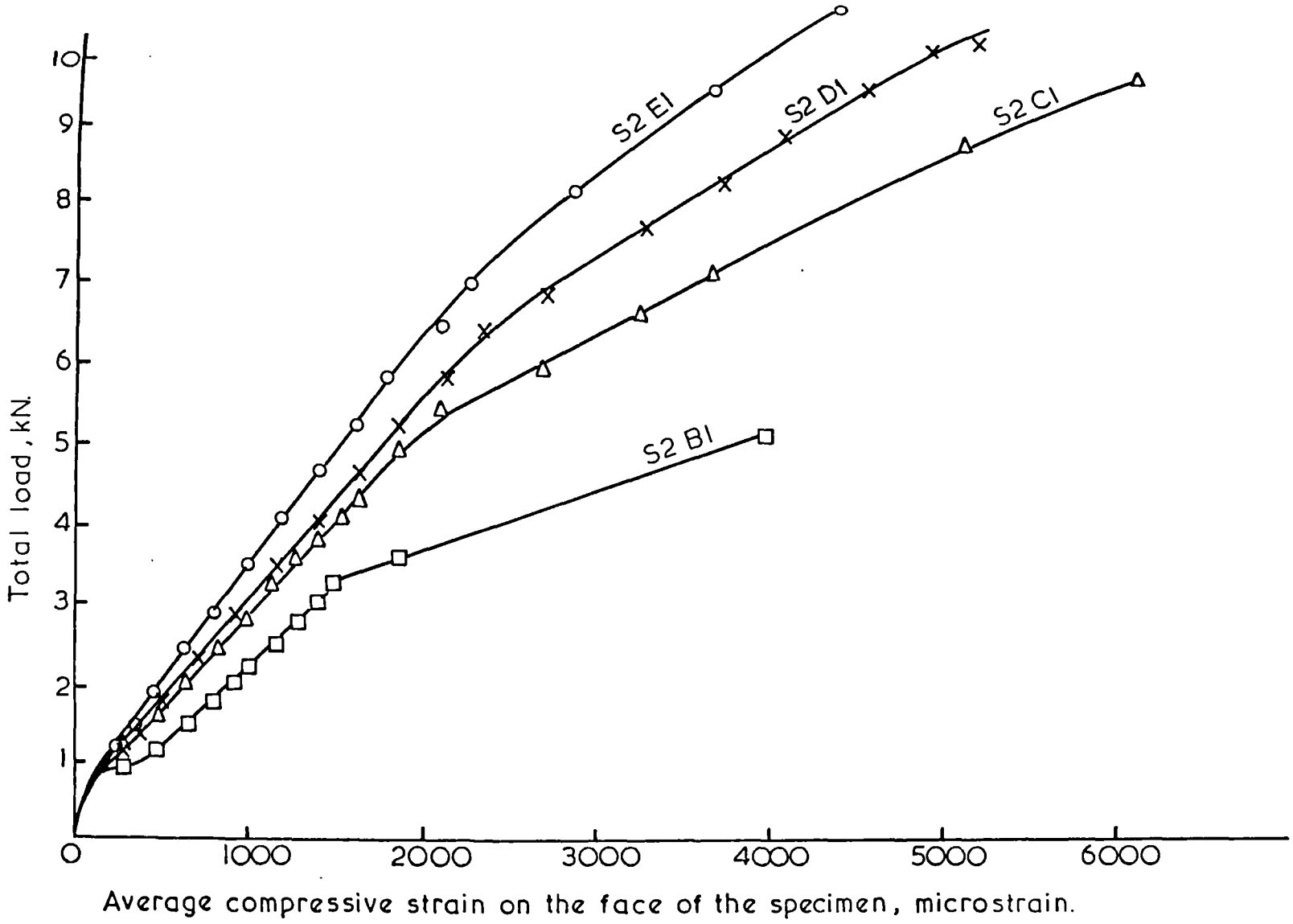

Fig. 5.15. Load - compressive strain curves, series S2.

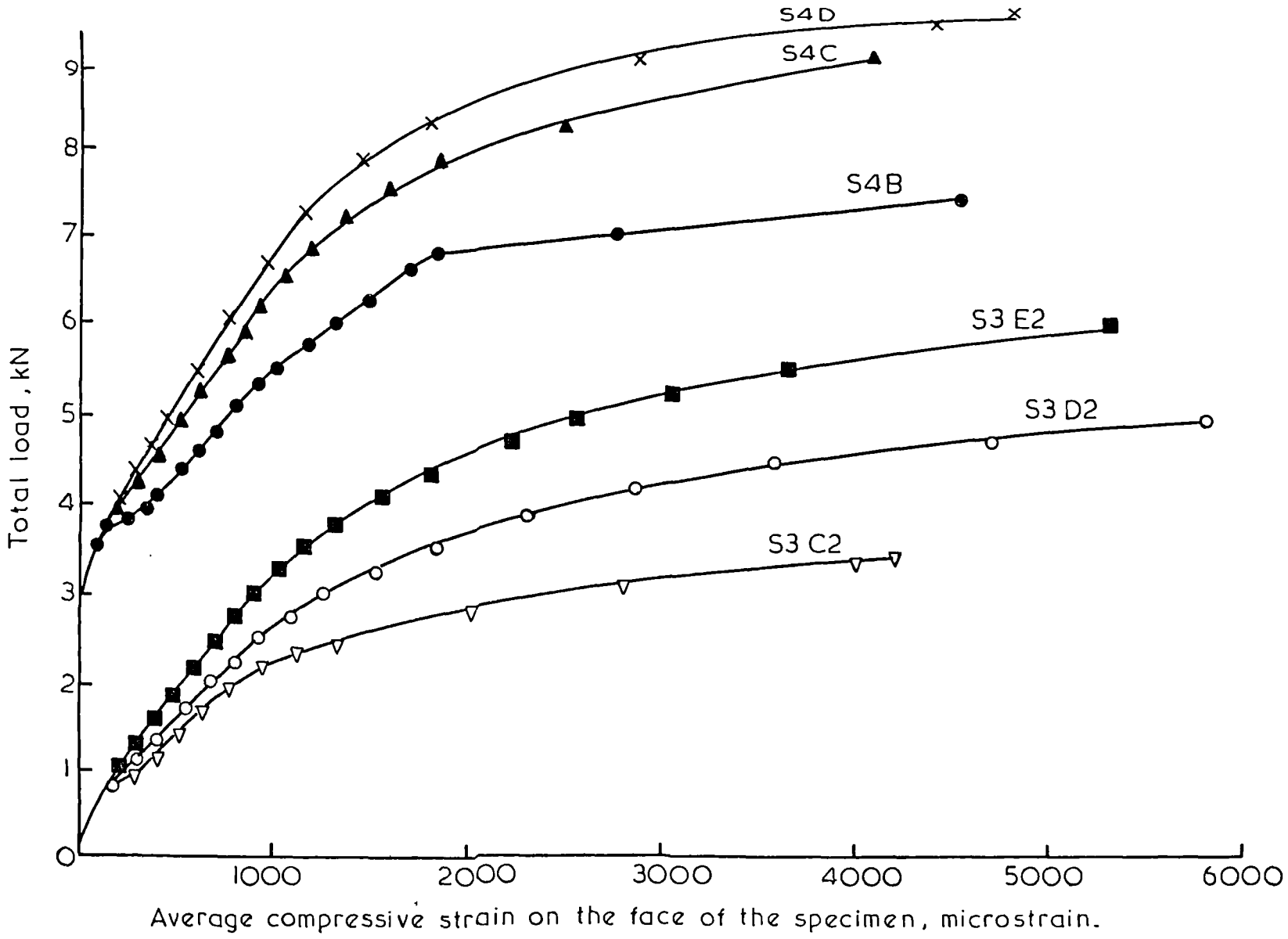

Fig. 5.16. Load - compressive strain curves, series S3 and S4.

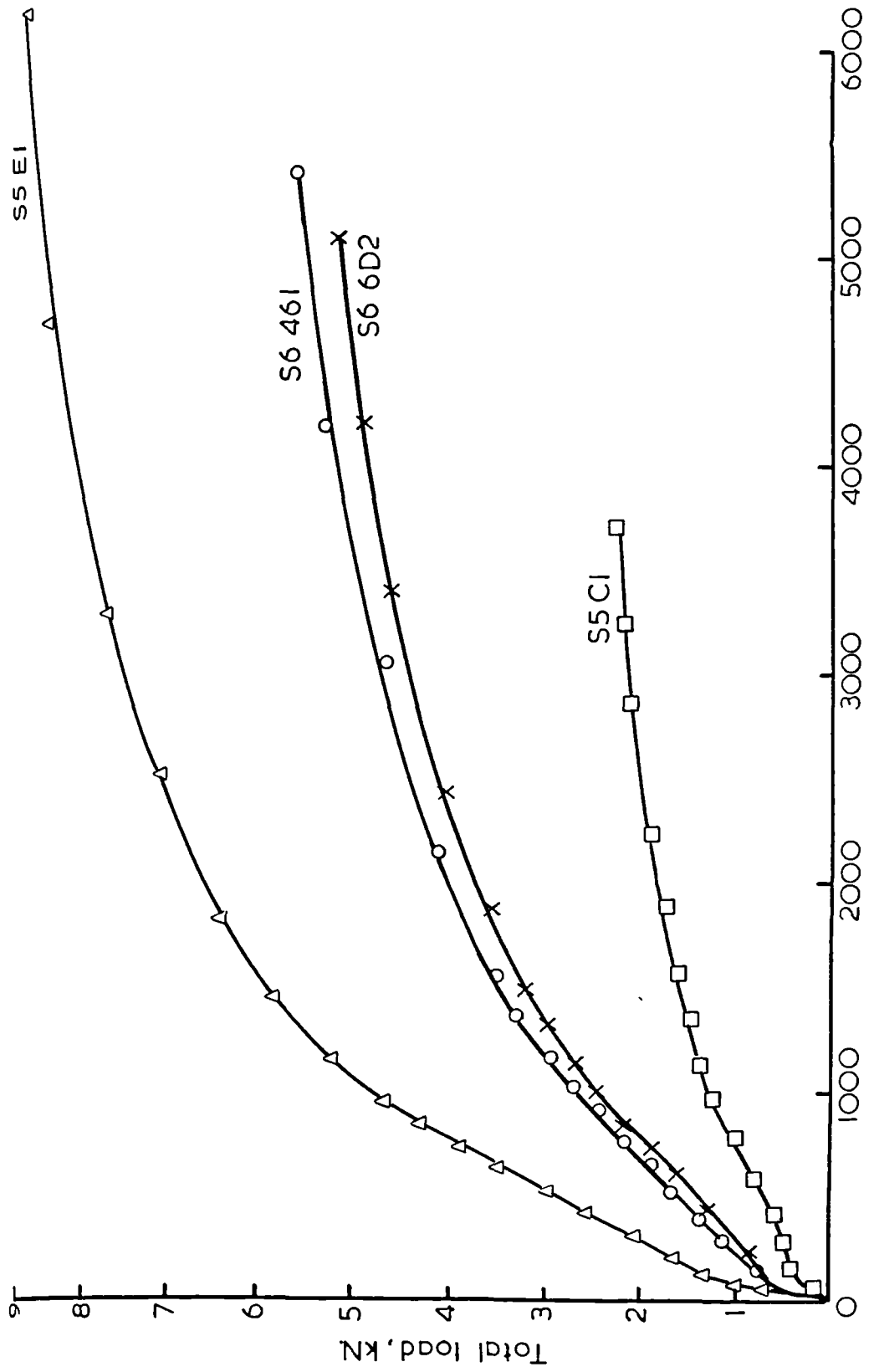

Fig. 5.17. Load - compressive strain curves, series S5 and S6.

similar to their load-deflection curves. There was a linear stage and at the end of it, the failure took place. In the load-tensile strain curves for this series, the second linear stage extended up to about 6000 microstrain after which the curve started to deviate slightly from linearity.

For the specimens with mild steel reinforcement the load-deformation curves are very similar. Increasing the amount of reinforcement in terms of the fraction volume increases the load at any specific deformation.

5.7 Relationship Between Cracking, Deflection and Strain.

It was shown in previous sections that the reinforcement amount and their yield strength are the major factors which influence the load and deformation characteristics. In Table 5.1, the load, tensile strain on the face of the specimen, mean crack width, and mean crack spacing are given at different deflection values for specimens with different number of meshes from series S1 and S2. The range of deflection values covers the elasto-plastic stage and for some specimens covers some of the yielding stage as well. From the table, it can be seen that for a given deflection, the mean crack width and mean crack spacing decrease as the number of meshes in the specimen increases and this is true for both types of meshes. The load was increased with the number of meshes while the tensile strain did not vary appreciably with the number and yield strength of the mesh.

A comparison of Table 5.1 and Figs. 5.1 and 5.4 shows that the mean crack width within the elasto-plastic stage remains largely below the value of 50 microns. If this value of mean crack width is taken as a critical limit, it would appear that as long as the specimen did not yield then the crack width is unlikely to exceed this limit. A load of about 0.6 to 0.65, for mild steel mesh, and 0.4 to 0.5 for high tensile mesh, of the

Table 5.1 Deflection, cracking and strain relationship.

Deflection mm	Type of Mesh	Mild steel, S1					High yield steel, S2			
	No. of Mesh	2	4	6	8	10	2	4	6	8
5.1	Load, kN	1.15	1.37	1.75	1.75	2.19	1.15	1.48	1.7	1.83
	% Ult. load	0.65	0.33	0.31	0.28	0.29	0.23	0.14	0.15	0.16
	Mortar tensile strain, μs	600	920	1080	1000	1000	1140	1000	1150	820
	Mean crack width, μm	16.1	21.9	15.2	17.5	12.0	25.6	16.0	14.0	10.0
	Average crack spacing, mm	29.0	31.0	23.7	25.1	22.0	30.9	19.6	22.6	20.0
10.2	Load, kN	1.34	2.08	2.84	3.09	3.94	1.78	2.41	2.79	3.17
	% Ult. load	0.75	0.51	0.51	0.50	0.48	0.34	0.23	0.25	0.28
	Mortar tensile strain, μs	1300	1820	2260	2070	2160	2260	2300	2140	1760
	Mean crack width, μm	34.9	43.4	31.8	32.0	24.5	47.3	32.9	22.1	17.6
	Average crack spacing, mm	27.5	27.2	21.1	20.9	17.2	28.0	18.5	15.0	14.6
15.3	Load, kN	1.39	2.52	3.47	3.99	5.36	2.41	3.28	3.88	4.89
	% Ult. load	0.78	0.61	0.62	0.65	0.65	0.47	0.31	0.35	0.39
	Mortar tensile strain, μs	1540	3060	3500	3420	3520	3400	3420	3240	2670
	Mean crack width, μm	41.4	72.9	49.4	50.4	39.0	69.4	47.5	31.1	24.9
	Crack spacing, mm	27.5	25.2	20.3	19.7	15.5	26.0	18.0	13.8	13.2
20.3	Load, kN	–	–	–	–	–	–	4.21	5.09	5.96
	% Ult. load	–	–	–	–	–	–	0.40	0.46	0.52
	Mortar tensile strain, μs	–	–	–	–	–	–	4600	3440	3760
	Mean crack width, μm	–	–	–	–	–	–	52.8	32.5	33.7
	Crack spacing, mm	–	–	–	–	–	–	16.0	12.8	12.2

ultimate load will also satisfy that limit. On the other hand, if deflections were the governing factor, and assuming an allowable deflection-span ratio of 1/180, it can be seen from Table 5.1 that at a deflection of 5.1 mm (deflection-span ratio of 1/177) most of the mean crack width values are less than 20 microns. The load at this deflection value is about 0.28 to 0.33 and 0.14 to 0.23 of the ultimate load for specimens with mild steel mesh and with high tensile steel mesh, respectively.

It follows, therefore, that the serviceability criteria is most likely to be governed by the deflection rather than the crack width. If that is the case then, high tensile mesh is not economical to use in ferrocement as its higher cost cannot be justified by higher service load. It should be noticed that if deflections are the governing criteria, then the service load is about one third of the ultimate load. This is a very small value, specially if one considered ferrocement's main advantage over reinforced concrete is its relatively higher service load (67).

It is to be mentioned that the values of mortar tensile strain assumed by Walkus (30) for different crack width values for ferrocement in bending (see Table 1.2) are significantly smaller than those found in this study, Table 5.1. For example, Walkus reported a tensile strain of 650 micro-strain corresponding to permissible crack width of 50-100 microns, while from Table 5.1, for such crack width the tensile strain would be more than 3000 microstrain. Also, according to Walkus (30,38,44), the yielding stage starts when the crack width exceeds 100 microns, i.e., when the tensile strain exceeds 650 microstrain and this value of strain is smaller than the yield strain of the mesh used in this investigation.

5.8 Effect of Variables on the Load and Deformation Characteristics.

The effect of variables on the load and deformation characteristics was investigated by studying the load and deformation measurements at the

turning points of the load-deflection curve, i.e., at first cracking, at first yielding, and at ultimate. The first cracking and first yielding stages were considered, not only because they represent the points of change in the behaviour of the section, but also they give good indications of the load and deformation characteristics all through the two linear ranges of the behaviour. The load and deformation characteristics at each of the three points are discussed, separately, in the following sections.

5.8.1 At First Cracking.

The first cracking was defined as the instance when a crack first became visible with the aid of a magnifying glass. The width of such a crack was measured and found to be as small as 3-6 microns. The load was increased incrementally. The first crack was detected and the measurements were taken at the end of each increment. It therefore follows that the measurements at the first cracking are not so reliable as the first crack could appear during the load increment while the measurements were taken at the end of it. In addition, as in any other research, there is the possibility of the investigator's error of not spotting the crack at the same load increment in which it happened. To reduce the effect of the above possible errors, the load increments were made as small as 60 N. Also the occurrence of first crack was anticipated by observing the deflection and strain measurements which have linear relationships with the load until the first cracking takes place.

In Tables 5.2 to 5.5, the load central deflection, span-deflection ratio and the average tensile and compressive strain on the faces of the specimen, at first crack, are given for all the tested plates. In addition, the values of M/bD^2 (the moment/plate width x square value of the section depth) are also given. The width and depth of the section are the actually

measured values. The term M/bD^2 was calculated to eliminate the effect of the variation in section dimensions on the load. The tables show that the load at first crack for ferrocement specimens varied from 0.55 to 1.77 kN, while the ratio M/bD^2 varied from 0.424 to 1.054 N/mm^2. The central deflection varied from 0.73 to 2.3 mm which corresponds to a span-deflection ratio of 391 to 1233. This range of the span deflection ratio is largely higher than 360, a limit value used as serviceability criteria in reinforced concrete designs. The tables also show that the average tensile strain on the face of the specimen varied from 132 to 438 microstrain. This range of strain is higher than that assumed by Walkus (30). He reported a tensile strain of 130 microstrain where the crack width is between 0-20 microns. The average compressive strain varied from 87 to 280 microstrain. The smaller value of the range of the compressive strain compared to the range of tensile strain and the fact that the sections were reinforced symmetrically, indicate that a shift in the neutral axis upward took place before the first crack became visible.

In Tables 5.2 and 5.4, the deformation characteristics at ultimate load of the plain mortar specimens, S1A1, S1A2, S1A3, S7A1, and S7A2, are also given. The ultimate tensile strain varied between 85 and 200 microstrain with an average value of 134 microstrain. The range of the tensile strain on the face of the mortar specimens is smaller than that for ferrocement specimens. The same result applies to the values of compressive strain (range = 83 - 187 microstrain) and deflections (range of span/deflection ratio = 692-1111). The range of the value M/bD^2 for plain mortar specimens was 0.423 to 0.958 with the average value equal to 0.656 N/mm^2 and this value is within the range of values for ferrocement specimens. It should be noticed that the ultimate load for the plain mortar specimens

Table 5.2 Load and deformation characteristics at first crack, Series S1.

Specimen		Load kN	% Ult. load	$\frac{M}{bD^2}$ N/mm^2	Central deflectn. mm	Span-deflectn. ratio	Tensile strain* micro-strain	Compressive strain* micro strain
S1 A	A1	0.99	100	0.703	1.09	825	135	140
	A2	0.68	100	0.503	0.81	1111	95	90
	A3	0.57	100	0.423	0.9	1000	85	83
	Average	0.75	100	0.543	0.93	979	105	104
S1 B	B1	1.1	62	0.818	1.27	709	147	120
	B2	0.96	58	0.712	1.1	818	254	215
	B3	0.82	47	0.602	1.36	661	230	151
	Average	0.96	56	0.711	1.24	729	210	162
S1 C	C1	1.01	25	0.75	1.87	481	329	240
	C2	0.93	23	0.689	1.87	481		293
	C3	0.99	23	0.729	1.75	514	310	219
	Average	0.78	24	0.723	1.83	492	320	251
S1 D	D1	1.2	22	0.894	2.04	441	438	280
	D2	0.9	15	0.666	1.08	833	413	280
	D3	0.96	12	0.705	1.3	692	384	224
	Average	1.02	16	0.755	1.47	655	412	261
S1 E	E1	0.92	15	0.683	1.37	657	246	145
	E2	1.1	16	0.786	2.11	427	363	223
	E3	0.96	14	0.711	1.86	484	348	222
	Average	0.99	15	0.727	1.78	523	319	197
S1 F	F1	1.48	15	1.054	2.3	391	425	200
	F2	1.1	14	0.811	2.13	423	366	221
	F3	1.1	14	0.84	2.16	417	354	231
	Average	1.23	14	0.902	2.2	410	382	217

*Strains are the average of the readings on the face of the specimens.

Table 5.3 Load and deformation characteristics at first crack, Series S2.

Specimen		Load kN	% Ult. load	$\frac{M}{bD^2}$ N/mm^2	Central deflectn. mm	Span-deflectn. ratio	Tensile strain* micro-strain	Compressive strain* micro-strain
S2 B	B1	0.88	17	0.653	1.2	750	219	158
	B2	0.88	17	0.652	1.23	732	166	140
	Average	0.88	17	0.653	1.22	741	193	149
S2 C	C1	0.96	9	0.705	1.35	667	160	150
	C2	1.07	11	0.787	1.76	511	265	180
	Average	1.02	10	0.746	1.56	589	213	165
S2 D	D1	1.06	10	0.784	1.8	500	277	195
	D2	0.95	8	0.727	1.48	608	249	186
	Average	1.01	9	0.756	1.64	554	263	191
S2 E	E1	1.06	9	0.784	1.67	539	260	203
	E2	0.95	9	0.730	1.73	520	288	190
	Average	1.01	9	0.757	1.7	530	274	196

*Strains are the average of the readings on the face of the specimen.

Table 5.4 Load and deformation characteristics at first crack, Series S3, S4, and S7.

Specimen		Load kN	% Ult. load	$\frac{M}{bD^2}$ N/mm^2	Central deflectn. mm	Span-deflectn. ratio	Tensile strain* micro-strain	Compressive strain* micro-strain
S3	C1	0.86	24	0.632	1.14	789	164	140
	C2	0.82	19	0.603	1.72	523	212	195
	Average	0.84	22	0.617	1.43	656	188	162
	D1	0.99	20	0.73	1.27	709	355	232
	D2	0.99	20	0.729	1.27	709	169	152
	Average	0.99	20	0.73	1.27	709	262	192
	E1	1.1	20	0.814	1.72	523	184	157
	E2	1.2	20	0.888	1.99	452	336	247
	Average	1.15	20	0.851	1.85	488	260	202
S4	A	0.53	16	0.39	0.54	1666	-	98
	B	0.95	21	0.703	1.96	459	375	289
	C	1.06	17	0.784	1.47	612	235	202
	D	1.18	17	0.873	1.59	566	311	216
S7	A1	0.94	100	0.695	0.95	947	155	150
	A2	1.3	100	0.958	1.3	692	202	187
	Average	1.12	100	0.827	1.13	820	179	168
	C	0.95	27	0.698	1.17	769	211	184

*Strains are the average of the readings on the face of the specimens.

Table 5.5 Load and deformation characteristics at first crack, Series S5 and S6.

Specimen		Load kN	% Ult. load	$\frac{M}{bD^2}$ N/mm^2	Central deflectn. mm	Span deflectn. ratio	Tensile strain* micro-strain	Compressive strain* micro-strain
S5	C1	0.47	21	0.77	1.68	536	233	173
	C2	0.47	20	0.818	1.58	570	201	145
	C3	0.42	20	0.639	1.71	526	218	171
	Average	0.45	20	0.742	1.66	544	217	163
	E1	1.71	20	0.697	1.11	811	227	195
	E2	1.59	18	0.687	1.11	811	223	188
	E3	1.77	21	0.766	1.25	720	300	220
	Average	1.69	20	0.717	1.16	781	250	201
S6	4D1	0.82	14	0.628	1.57	573	217	140
	4D2	0.71	13	0.521	1.57	578	206	184
	Average	0.77	14	0.575	1.57	573	212	162
	6D1	0.68	11	0.424	1.55	1233	215	168
	6D2	0.77	13	0.489	1.7	857	230	150
	Average	0.73	12	0.457	1.62	1045	222	159

*Strains are the average of the readings on the face of the specimens.

varied widely which made the comparison of their results with the results of ferrocement specimens not very reliable.

The load and deformation at first crack increased slightly with increase in the number of meshes, see Tables 5.2, 5.3 and 5.4. However, this increase seems to be insignificant and sometimes inconsistent to draw a reliable conclusion from it. The mesh yield strength, mesh distribution, and presence of steel bar did not influence appreciably the load and deformation at first crack. The load and deflection increased and decreased, respectively with increase in the section thickness. However, the ratio M/bD^2 did not vary appreciably with the section depth, see results of series S5. This indicates that the section thickness did not affect the load at first crack other than the expected increase due to increase in depth of the section.

Increasing the mortar cover decreased the load and deformation at first crack, see results of S1 D, S6 4D, and S6 6D. For the same number and type of mesh, increasing the mortar cover from 2 mm to 6 mm decreased the load by about 40%. The reinforced concrete specimen, S4A, which had the same mortar cover as that of S6 6D, i.e., 6 mm, gave almost the same load and M/bD^2 values. It should be noticed, however, that the value of M/bD^2 for these specimens was smaller than that of the plain mortar specimens.

5.8.2 At First Yielding.

The first yielding was defined as the first deviation from linearity of the second linear range of the load-deflection curve. The first yielding points were found for all specimens, and the load and deformations at these points are given in Tables 5.6 to 5.9. From these tables, the load varied from 1.15 to 6.4 kN, depending mainly on the number and yield strength of the mesh and the thickness of the section. The load as a percentage of the ultimate load varied between 45 to 64% except for specimens

S1 B (reinforced with two mild steel mesh) where the average load is equal to 80% of the ultimate load. The span-deflection ratio, again for all specimens except S1B, varied between 54 to 100. This suggests that applying the deflection limits used in the serviceability criteria for reinforced concrete, the working load would be within the second linear range, but less than the first yielding load.

From Table 5.6 (series S1), it can be seen that increasing the number of meshes increases the load, deflection, and tensile and compressive strain. Increasing the number of meshes from 2 to 10 mesh, increased the load by a factor of 3.3, deflection by 1.8, tensile strain by 1.5 and compressive strain by 1.7. The slow increase in the tensile strain and the continuing increase in the compressive strain indicates that yielding of the specimen was initiated by yielding of the mesh.

For the specimens reinforced with the high yield steel mesh, Table 5.7; the load increased with the number of meshes, but at a slower rate when the number of meshes was higher than four. The compressive strain increased when the number of meshes increased from 2 to 4, but remained almost the same thereafter. The deflection and the tensile strain for 6 and 8 meshes specimens were less than those with 4 meshes. The observed variation in the load and deformation suggests that while yielding was controlled by the mesh in specimens with 2 and perhaps specimens with 4 meshes, it was controlled by yielding of the mortar in compression, for specimens with 6 and 8 meshes. This seems to be a basic difference between specimens reinforced with mild steel mesh and high yield mesh. In addition the load and deformation in series S2 are much higher than in series S1, signifying the ability of the high yield mesh in carrying higher stresses and loading the mortar more efficiently.

Table 5.6 Load and deformation at first yielding, Series S1.

Specimen		Load kN	% Ult. Load	Central deflectn. mm	Span-deflectn. ratio	Tensile strain* micro-strain	Compressive strain* micro-strain
S1 B	B1	1.45	82	6.7	134	1715	-
	B2	1.31	80	7.5	120	1650	693
	B3	1.37	78	6.9	130	1786	633
	Average	1.38	80	7.	128	1717	663
S1 C	C1	2.19	53	10.6	85	2130	790
	C2	2.19	53	9.2	98	2200	906
	C3	2.19	52	9.0	100	1951	783
	Average	2.19	53	9.6	94	2094	826
S1 D	D1	2.79	55	9.5	92	2180	870
	D2	2.46	45	9.3	97	2212	876
	D3	2.9	47	9.8	92	2120	785
	Average	2.72	49	9.6	94	2170	844
S1 E	E1	3.28	53	10.9	83	2261	940
	E2	3.83	55	12	75	2268	1010
	E3	3.83	56	12.6	71	2704	1170
	Average	3.65	55	11.8	76	2411	1040
S1 F	F1	4.9	60	12.8	70	2894	995
	F2	4.35	54	12.6	71	2300	1213
	F3	4.38	56	12.8	70	2513	1233
	Average	4.54	57	12.7	70	2570	1147

*Strains are the average of the readings on the face of the specimens.

Table 5.7 Load and deformation at first yielding, Series S2.

Specimen		Load kN	% Ult. load	Central deflectn. mm	Span-deflectn. ratio	Tensile strain* micro-strain	Compressive strain* micro-strain
S2B	B1	3.28	64	23.1	39	5000	1485
	B2	3.28	63	22.3	40	5200	1387
	Average	3.28	64	22.7	40	5100	1436
S2C	C1	5.47	52	27.5	32	7662	2100
	C2	5.66	60	28.4	32	5990	2093
	Average	5.56	56	28	32	6826	2097
S2D	D1	5.85	53	24	38	5330	2133
	D2	5.91	53	25	36	5014	2183
	Average	5.88	53	25	37	5172	2158
S2E	E1	6.4	56	22.4	50	4249	2090
	E2	6.4	60	23.1	39	5008	2170
	Average	6.4	58	22.8	40	4628	2130

*Strains are the average value of the readings on the face of the specimens.

Table 5.8 Load and deformations at first yielding, Series S3, S4 and S7.

	Specimen	Load kN	% Ult. load	Central deflectn. mm	Span-deflectn. ratio	Tensile Strain* micro-strain	Compressive Strain* micro-strain
S3	C1	1.83	51	8.9	101	2186	746
	C2	1.75	50	8.4	107	1596	678
	Average	1.79	51	8.7	104	1891	712
	D1	2.42	49	9.90	91	1974	926
	D2	2.46	49	9.6	94	2050	922
	Average	2.44	49	9.8	93	2012	924
	E1	3.01	56	11.7	77	2240	1033
	E2	2.93	54	10.9	83	2050	1026
	Average	3.0	55	11.3	80	2145	1030
S4	A	2.02	62	13.5	67	2150	1060
	B	2.54	58	10.7	84	2220	1003
	C	3.87	56	11.1	81	2400	1055
	D	4.27	63	11.7	77	2600	1160
S7	C	2.22	63	9.0	100	2150	860

*Strains are the average of the readings on the face of the specimens.

Table 5.9 Load and deformations at first yielding, Series S5, and S6.

Specimen		Load kN	% Ult. load	Central deflectn. mm	Span-deflectn. ratio	Tensile strain* micro-strain	Compressive strain* micro-strain
S5	C1	1.28	56	16.7	54	2450	973
	C2	1.16	49	16.3	55	2510	1056
	C3	1.15	56	16.2	56	2430	940
	Average	1.2	54	16.4	55	2463	990
	E1	4.65	54	8.2	110	1875	936
	E2	4.59	52	7.8	115	1900	900
	E3	4.65	54	7.8	115	1911	910
	Average	4.63	53	7.9	113	1895	915
S6	4D1	2.74	46	12.2	74	2389	1126
	4D2	2.71	48	11.4	79	2597	1030
	Average	2.73	47	11.8	77	2493	1078
	6D1	2.45	47	12.2	74	2690	993
	6D2	2.71	52	13.2	68	2950	1035
	Average	2.58	45	12.7	71	2820	1014

*Strains are the average of the readings on the face of the specimens.

The results from series S3, Table 5.8, showed that the load and deformation varied with the number of meshes in a similar manner to that of series S1. This suggests that for the range of mesh opening used in this study, the yielding characteristics were not influenced by the size of the mesh. The same variation in the load as in series S1 and S2, was also observed in series S4, in which the specimens were reinforced with mild steel mesh and bars. However, the compressive and tensile strain did not increase as much with increasing the number of meshes in this series. This is probably due to the presence of steel bars which have a high fraction volume and the addition of meshes to the reinforcement does not result in higher strain values unless the meshes are of a higher yield strength than the steel bars.

The results of specimens of series S6, and specimens S1 D indicate that the mortar cover does not influence significantly the load at first yielding. But the tensile strain on the face of the specimen increased with increasing the cover. This was to induce the same tensile strain in the mesh to cause its yielding. Increasing the section depth (see results of S5C, S1D and S5E) increased the load significantly and decreased the tensile strain slightly. The average value of the load for these specimens was 1.2, 2.66, and 4.63 kN corresponding to section thickness 17, 25 and 34 mm, respectively. These values show a wide variation in the load. However, calculating the ratio M/bD^2, gave very close results (2.1, 2.1, 2.0 N/mm^2). This indicates that for the same fraction volume of reinforcement, the load at first yielding is in direct proportion with the square value of the section depth.

The load at first yielding was found to have a direct relation with the fraction volume of reinforcement in loading direction. In Fig.5.18, this relation was plotted for all specimens with the same section depth. It can be seen that for the specimens reinforced with mild steel, the load

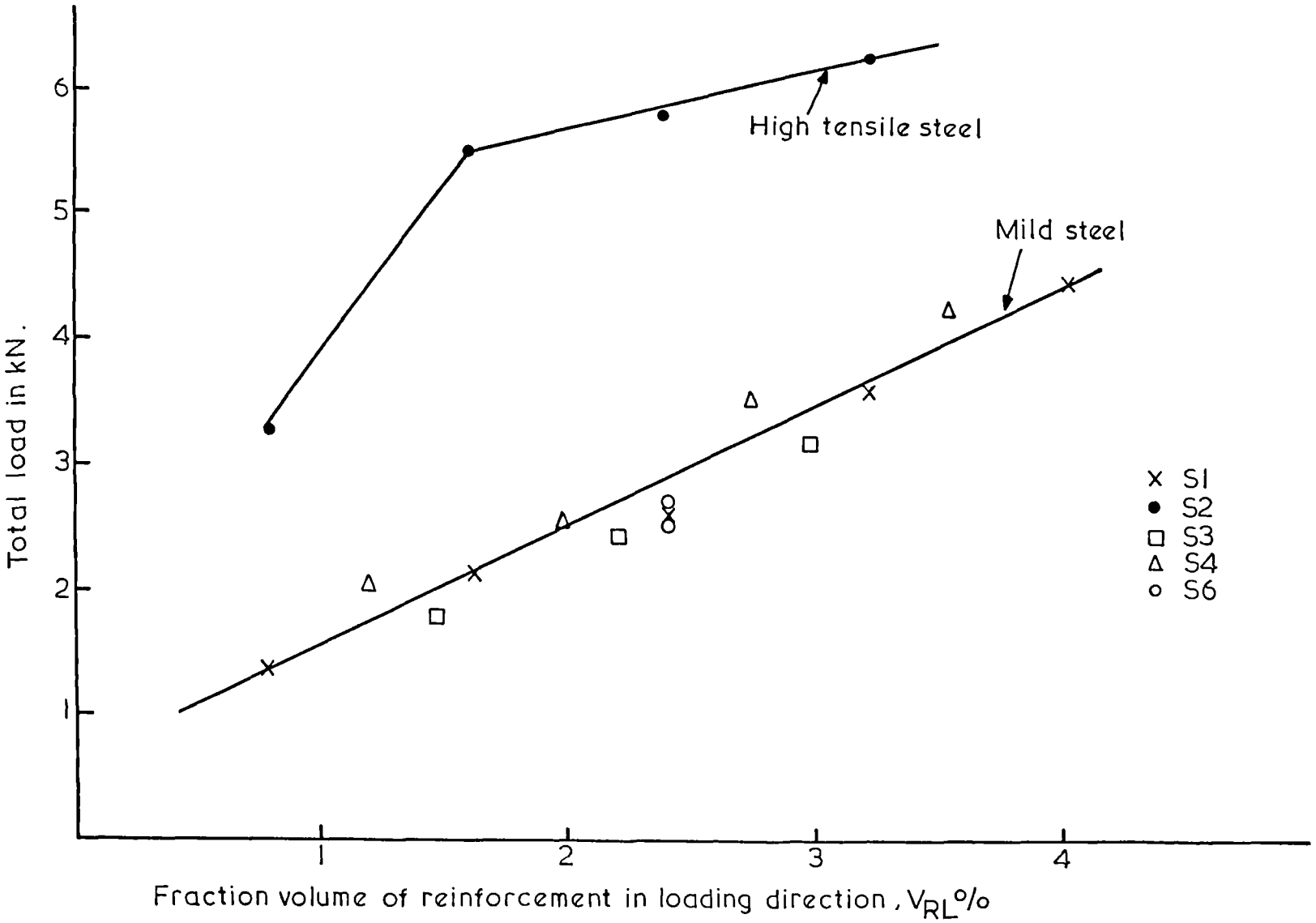

Fig. 5.18. Total load at yielding vrs. fraction volume of reinforcement in loading direction.

varied linearly with fraction volume of reinforcement in loading direction, irrespective of the mesh opening, presence of steel bars or mortar cover. For the high tensile steel mesh, Fig.5.18 shows that the load at first yielding consists of two linear parts depending on the amount of reinforcement. The point which separates the two lines represents the change in yielding from the mesh in tension to the mortar in compression and the load increases faster before this point than after it.

Paul and Pama (11) presented a theoretical equation to predict the composite tensile strain under tension. For square mesh, the equation is

$$\varepsilon_{ty} = \frac{1}{E_f}\left(\sigma_{fy} - \frac{\sigma_{mu}}{2}\,\frac{1}{V_{RL}}\right) \qquad \ldots\ldots \qquad (5.1)$$

where E_f and σ_{fy} are the modulus of elasticity and yield strength of the reinforcement, respectively, σ_{mu} is the mortar strength in tension, and V_{RL} is the fraction volume of reinforcement in loading direction.

In Fig.5.19, the average tensile strain on the face of the specimen at first yielding is plotted against the fraction volume of reinforcement in the loading direction for series S1 and S2. Eq. 5.1 was used to calculate the tensile strain and the results are also included in that figure. From Fig.5.19, it can be seen that the theoretical strain values are less than the experimental ones. However, eq. 5.1 is developed for section under tension. Therefore the equation gives the strain values at the reinforcement level which are less than the strain at the face of the specimen. To find the strain at the specimen face, the theoretical values were adjusted to account for the strain gradient in the section. The depth of the neutral axis from the tensile face of the specimens at first yielding was assumed to be equal to 0.7 times the section depth. This value was based on calculations of the neutral axis depth at first yielding of the tested specimens. Hence, the theoretical tensile strain at the specimen

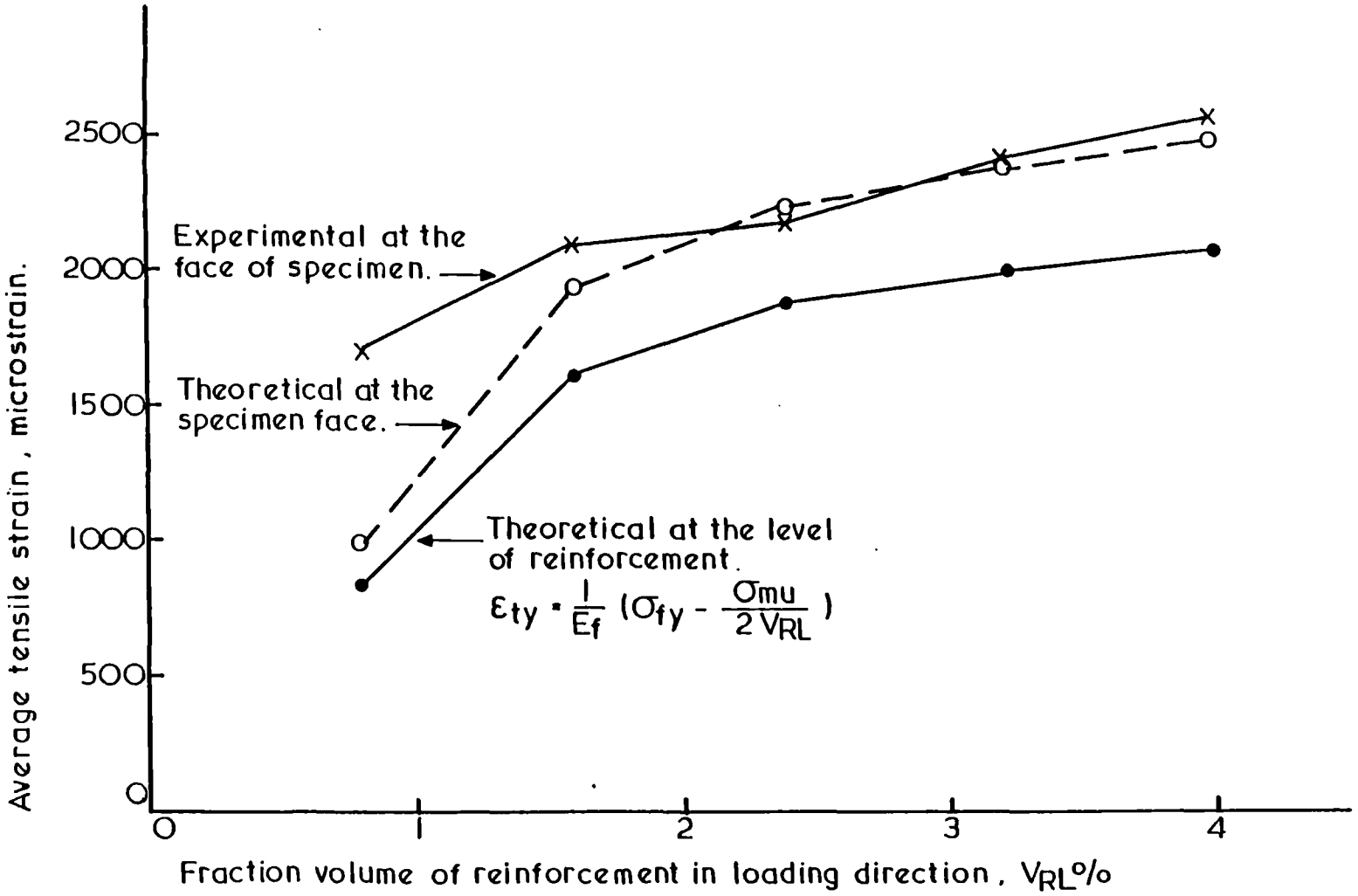

Fig. 5.19A. Tensile strain at first yielding vs. fraction volume of reinforcement in loading direction, Series S1.

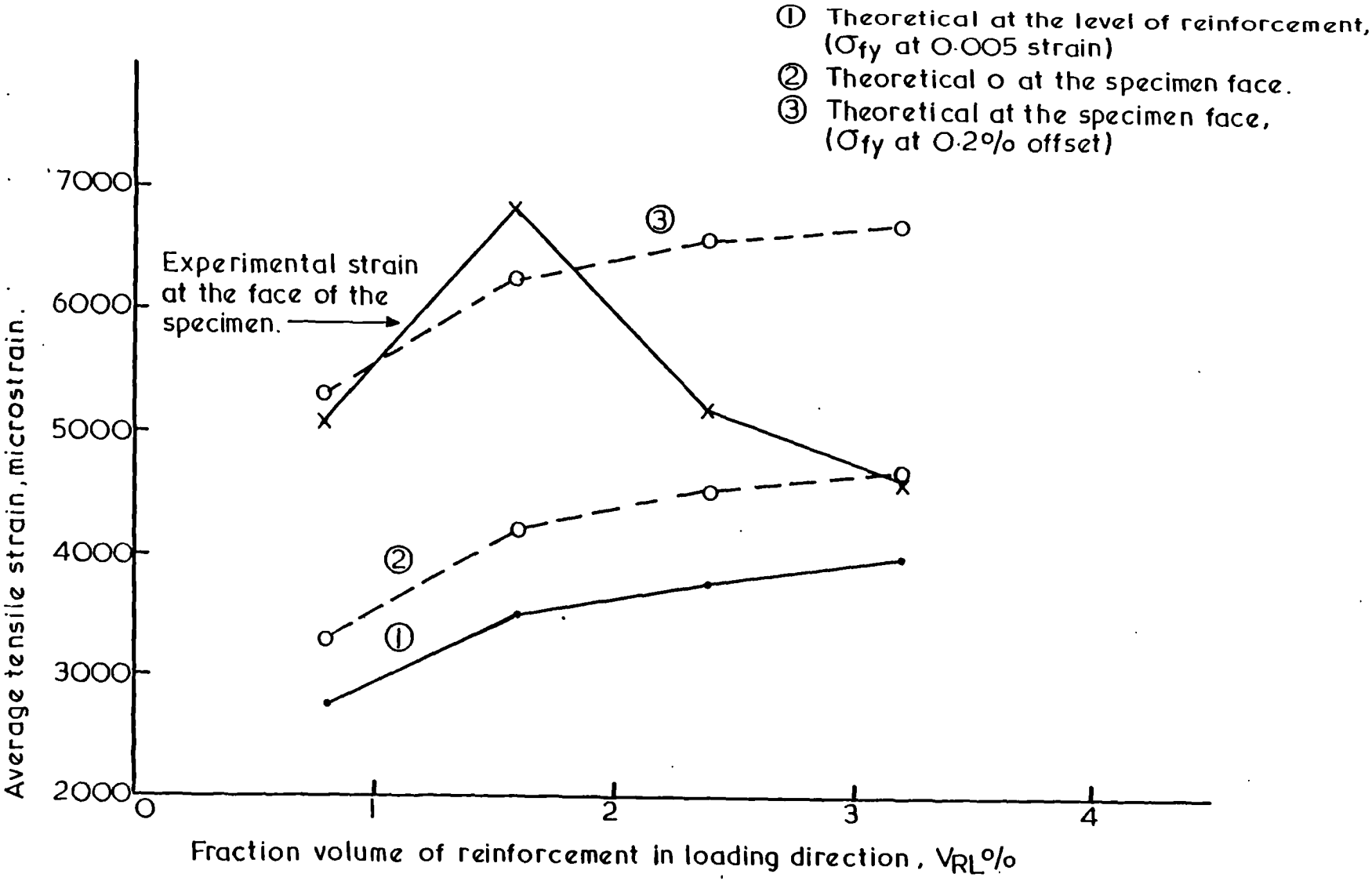

Fig. 5·19B. Tensile strain at first yielding vs. fraction volume of reinforcement in loading direction. Series S2.

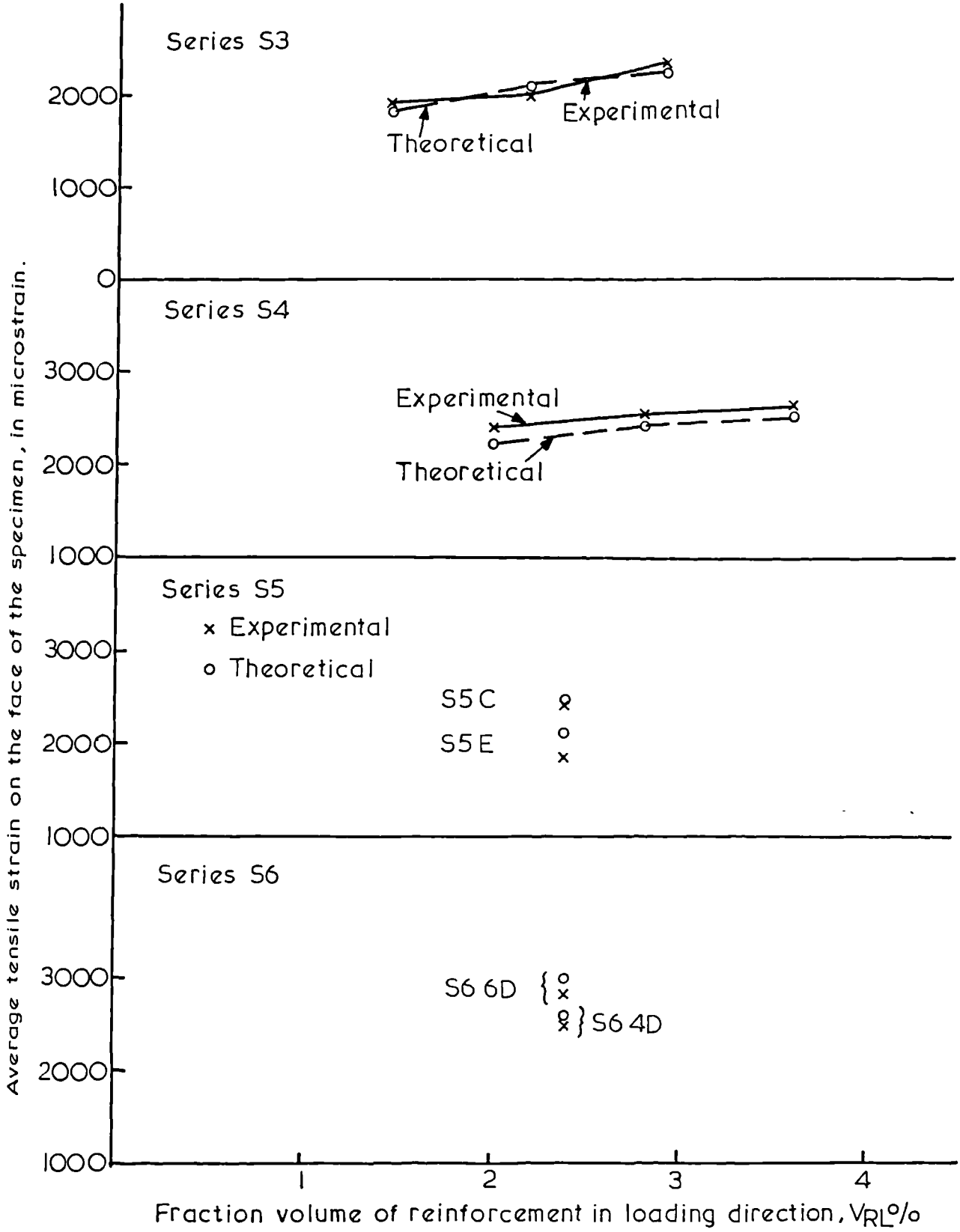

Fig. 5.20. Tensile strain on the face of the specimen vs. fraction volume of reinforcement in loading direction, (at first yielding)

face was equal to that from eq. 5.1 multiplied by the ratio of the neutral axis depth from the tensile face to neutral axis depth from the extreme tensile mesh layer. The adjusted theoretical strain values for series S1 are plotted in Fig. 5.19A. It can be seen that the theoretical and experimental values for series S1 are very close except for specimen S1B where the number of meshes was 2. The experimental and the adjusted theoretical values of tensile strain for series S3, S4, S5, and S6 are plotted against the fraction volume of reinforcement in Fig.5.20. It can be seen that, again the theoretical and experimental results are in close agreement.

For series S2, the experimental values of the tensile strain, unlike in all the other series, decrease when the number of meshes is higher than 4, see Fig.5.19B. As discussed earlier, the decrease is due to the yielding in these specimens which was by yielding of the compressive zone and not by yielding of the tensile zone. When calculating the theoretical values of strain for this series by the same previously discussed procedure, the theoretical values were much lower than the experimental. However, in eq. 5.1, σ_{fy} was taken at 0.005 strain. While the mild steel mesh when tested in tension yielded at about this strain value, the high tensile mesh did not show clear sign of yielding at that strain. Therefore, σ_{fy} at 0.005 strain does not give the actual yield strength of the high tensile mesh. The theoretical values of the tensile strain were calculated again using the yield strength σ_{fy} at 0.2% offset. The results are plotted in Fig.5.19B and are closer to the experimental values than those found by using σ_{fy} at 0.005 strain.

5.8.3 At Failure.

The failure was defined as the point where a sudden release in the load took place and the section sustained only a fraction of that load. The release in the load was the result of either failure of the mesh in tension or

failure of the mortar in compression. The measurements were taken just before the sudden release of the load. They included the load, central deflection, and compressive strain on the face of the specimen. These measurements, as well as description of the section failure are given for all specimens in Table 5.10.

As can be seen in Table 5.10, three types of failed sections were observed. They were, firstly, sections where the mesh was fractured and the depth of the compression zone was very small, see Plate 5.1. Secondly sections in which the mesh was yielded, and in some specimens the extreme mesh layer was fractured, but the compression zone was deeper than in the first case. In these sections there was a recognizable compression failure, see Plate 5.2A. Thirdly, sections with a sudden compression failure, see plate, 5.2B. The specimen failure could be one of the above three types depending on the amount of reinforcement and its yield strength. Upon increasing the number of meshes in the specimens of series S1, the mode of failure changed from tensile failure to a sudden compression failure. The same change in the mode of failure was noticed in series S2, where specimens are reinforced with high tensile mesh. The specimens of series S2 also exhibited horizontal cracks and spalling of mortar cover in those which suffered tensile failure (see Plate 5.2C) and buckling of the meshes in compression and extensive damage to the section in those suffering compression failure (see Plate 5.2B). In general, specimens reinforced with high tensile mesh suffered sudden failure, while those with mild steel mesh were more ductile even for specimens which failed in compression.

For the same fraction volume of reinforcement, the mode of failure did not change with the section depth or mortar cover. The significant factors which affect the mode of failure were found to be the reinforcement area and its yield strength. If the same principles used in the design of reinforced

Table 5.10 Loads and deformations at failure.

Series	Specimen	Total load kN	Central deflectn. mm	Average compressive strain	Mode of failure
S1	B1	1.78	62.8	-	Tensile failure,wire mesh fractured
	B2	1.64	63.5	2950	
	B3	1.75	57.5	2550	
	Average	1.72	61.3	2750	
	C1	4.10	102	4800	Tensile followed by secondary compression
	C2	4.10	106.2	6100	
	C3	4.24	120	4500	
	Average	4.15	109.4	5130	
	D1	5.61	112	5600	Compression failure and some wires were fractured
	D2	5.47	111.7	7000	
	D3	5.8	118.7	5550	
	Average	5.63	114.1	6050	
	E1	6.15	74.4	5500	Sudden compression failure
	E2	6.92	75.3	5500	
	E3	6.89	83.7	6300	
	Average	6.65	77.8	5770	
	F1	8.21	73.8	4700	Sudden compression failure.
	F2	8.07	71.5	6200	
	F3	7.85	73.1	6950	
	Average	8.04	72.8	5950	
S2	B1	5.17	103	4000	Tensile failure, spalling of cover in tensile zone followed by sudden wire mesh fracture.
	B2	5.25	93.9	3700	
	Average	5.21	98.5	3850	
	C1	10.1	96.9	-	Compression failure, some wires were fractured in tension. Spalling of cover in tensile zone.
	C2	9.46	84.8	6300	
	Average	9.78	90.9	6300	
	D1	10.99	66.6	6100	Sudden compression failure. No spalling but the section exhibited horizontal cracks.
	D2	11.21	76.2	6500	
	Average	11.1	71.4	6300	
	E1	11.46	56.8	5000	Sudden extensive compression failure. Buckling of mesh in compression zone. The section suffered extensive damage.
	E2	10.69	52.1	5100	
	Average	11.08	54.5	5050	

Table 5.10 Loads and deformations at failure.

Series	Specimen	Total load kN	Central deflectn. mm	Average Compressive strain	Mode of failure
S3	C1	3.61	100.2	4200	Tensile failure, very ductile.
	C2	3.5	91.0	3800	
	Average	3.56	95.6	4000	
	D1	4.95	84.1	5800	Compression failure and some wires were fractured. Ductile failure
	D2	4.98	105.8	7000	
	Average	4.97	95	6400	
	E1*	5.42	71.3	6100	Compression failure.
	E2	6.02	86.4	5300	
	Average	5.72	78.9	5700	
S4	A	3.25	93.1	3850	Secondary compression.
	B	4.41	73.0	4500	Secondary compression, wire mesh fractured.
	C	6.32	81.0	4200	Compression failure.
	D	6.78	93.1	4800	" "
S7	C	3.52	84.0	3150	Tensile failure. Both tensile mesh fractured.
S5	C1	2.28	112.9	3700	Secondary compression. Wire mesh was yielding.
	C2	2.36	156.4	5500	
	C3	2.06	107.8	3200	
	Average	2.25	125.7	4130	
	E1	8.56	58.4	6200	Secondary compression. Wire mesh was yielding. One specimen showed spalling of compression cover. Another showed some tensile wires fractured.
	E2	8.86	71.9	6700	
	E3	8.56	71.6	6300	
	Average	8.66	67.3	6400	
S6	4D1	5.99	137.2	6650	Secondary compression.
	4D2	5.61	117.1	5400	
	Average	5.8	127.2	6020	
	6D1	5.2	95.4	5100	Secondary compression.
	6D2	5.2	85.4	5000	
	Average	5.2	90.4	5050	

*Specimen neglected due to inconsistent results.

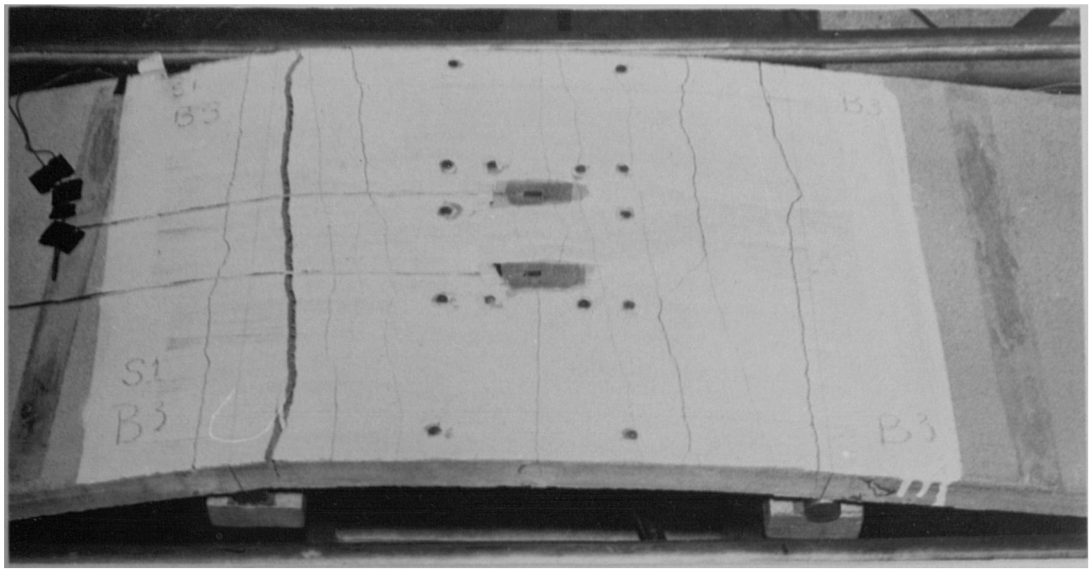

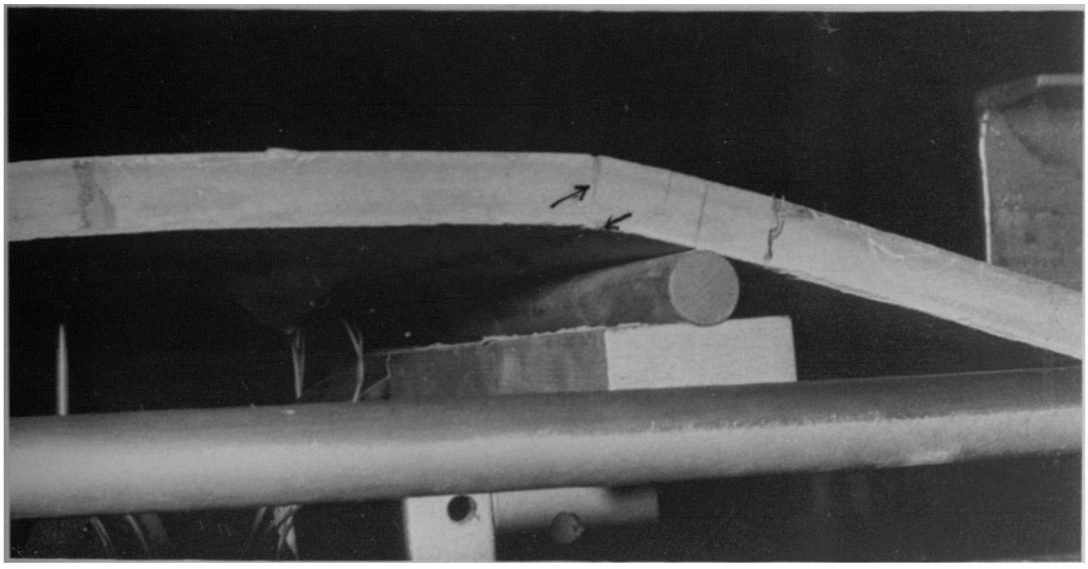

Plate. 5·1. Specimen failed by fracture of wire mesh in tensile zone.

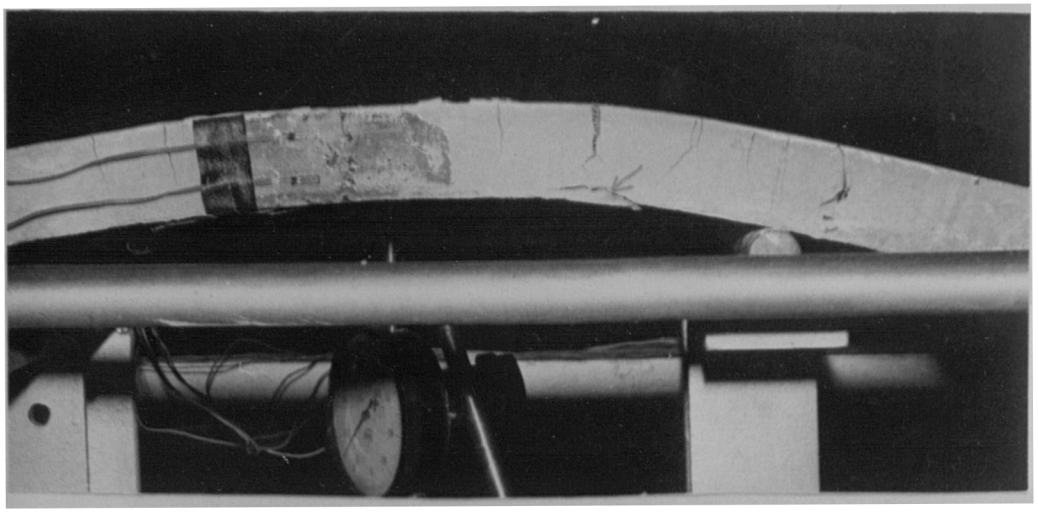

a) Excessive yielding plus compression failure.

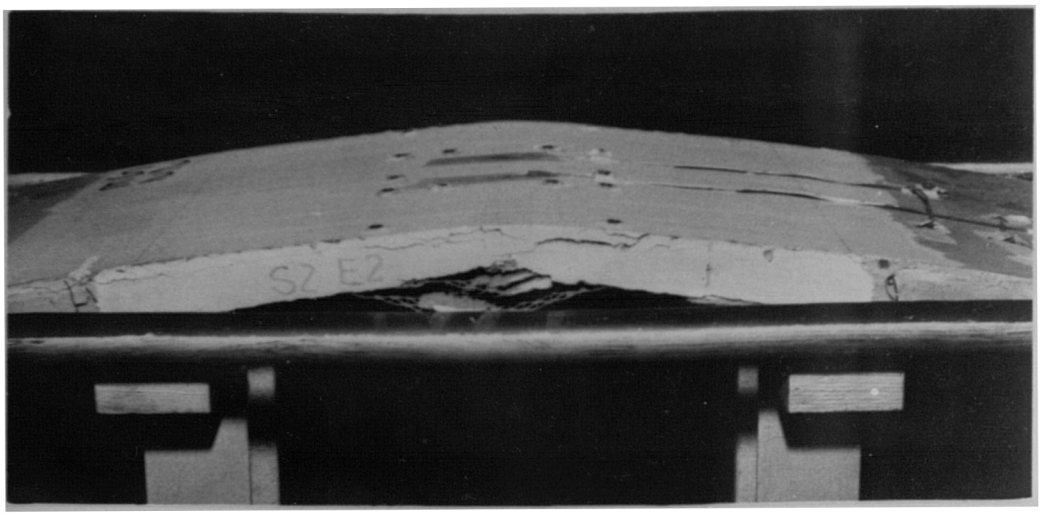

b) Sudden compression failure.

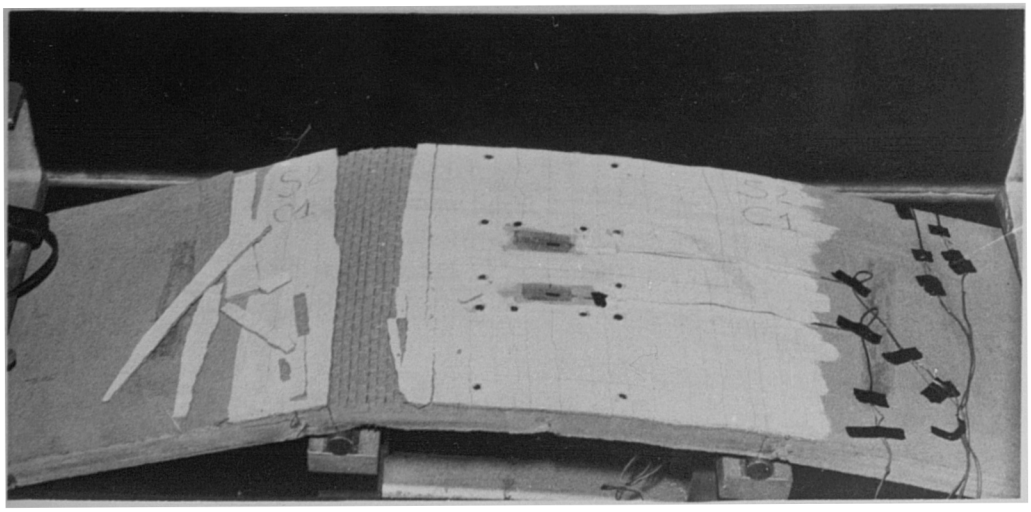

c) Specimen suffered spalling of the mortar cover.

Plate.5 2. Different types of section failure.

concrete apply to ferrocement then there seems to be a balanced steel ratio for which the reinforcement in ferrocement members should be less or equal to avoid the undesirable compression failure.

The ultimate load, deflections, and compressive strains were influenced greatly by the mode of failure and the influence of the different variables on each of them will be discussed separately in the following sections.

5.8.3.1 Ultimate load.

In Table 5.10,the ultimate load increased with increase in the amount of reinforcement. In Fig.5.21, the ultimate load is plotted against the fraction volume of reinforcement in the loading direction. Each point in the figure represents the average value of the number of repeated specimens. The figure shows that the ultimate load for specimens reinforced with mild steel mesh increases linearly with fraction volume of reinforcement in loading direction. This was the result irrespective of the difference in mesh opening or presence of steel bars. It also shows that ultimate load for specimens reinforced with high tensile mesh is much higher than those reinforced with mild steel mesh. The load for the high tensile mesh specimens did not increase appreciably when the number of mesh was higher than 4. The load for specimens with 6 and 8 mesh were the same. This may be due to the premature failure, as described earlier, caused by buckling of wire mesh in compression, which was suffered by specimens S2D and S2E.

As in the case of the load at first yielding, the ultimate load varied linearly with the square value of the section depth. The value of P/D^2 for specimens S5C, S1D, and S5EC section depth 17, 26 and 34 mm) were 8.02, 8.33, 7.83 N/mm^2. The ultimate load also was not affected appreciably by variation in mortar cover. It appears, therefore, that the ultimate load is controlled mainly by the fraction volume of reinforcement in loading direction and the yield strength of the mesh.

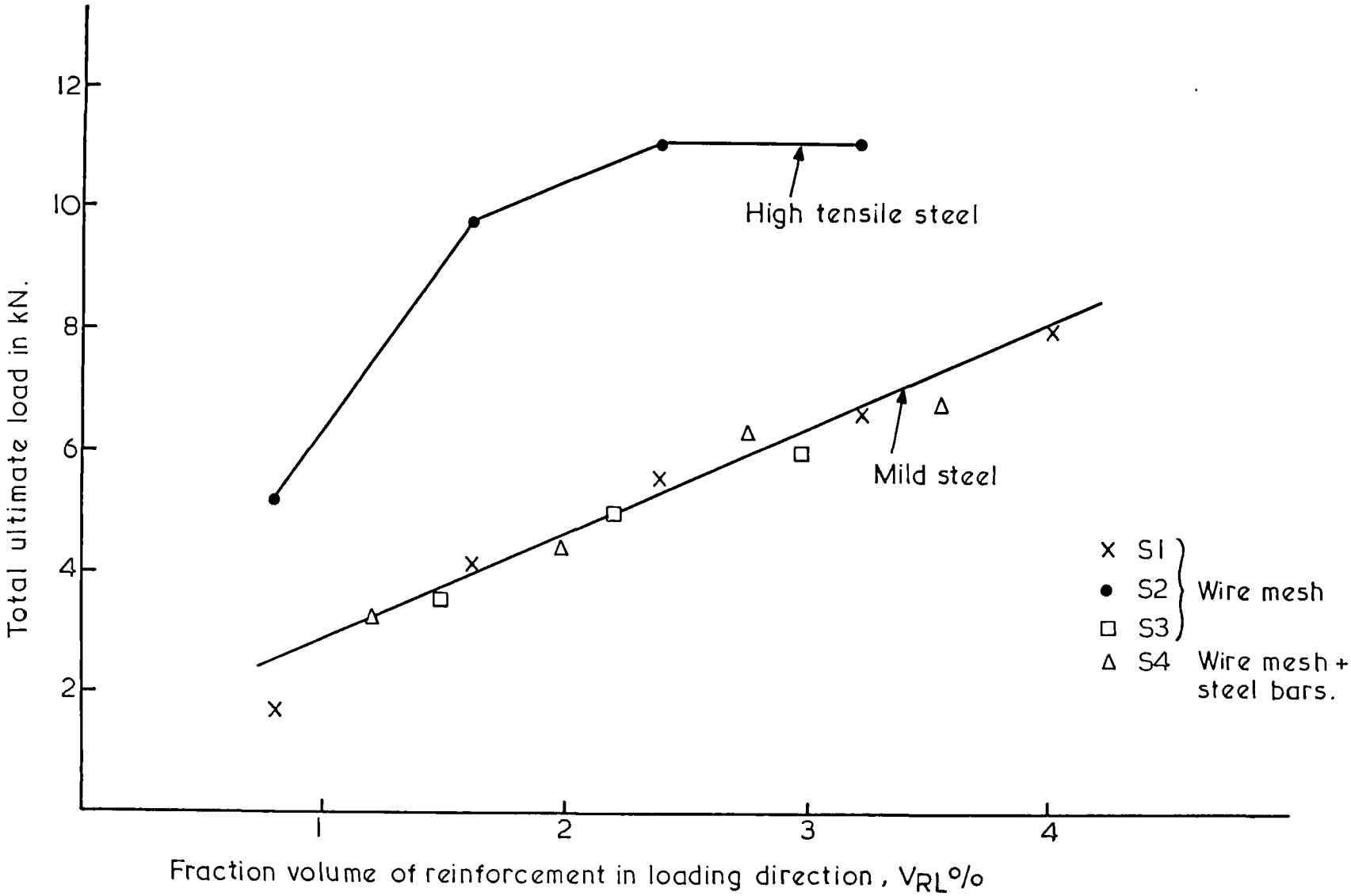

Fig. 521. Total ultimate load vrs. fraction volume of reinforcement in loading direction, series S1, S2, S3 and S4.

5.8.3.2 Deflection at Failure.

The values of the deflection at failure is not an important characteristic as far as the designer is concerned. But it can be used as a measure for the ductility of ferrocement and gives an idea about the amount of deformation this material can sustain.

The central deflection is plotted against the total fraction volume of reinforcement for all series in Fig.5.22. From the figure, it can be seen that for the mild steel mesh, series S1, the deflection increased with the fraction volume and then decreased after specimen S1D (6 mesh). In this series, therefore, there seems to be an optimum amount of reinforcement which results in the highest ductility. For series S2, the figure shows that the deflection decreases with the increase in the fraction volume. The deflections for this series are lower than those of series S1, except for the specimen with 2 mesh. In series S4, the specimen with steel bars only (S4A) gave relatively higher deflection than those with mesh and steel bars which had almost the same deflection. Increasing the section thickness, as expected decreased noticeably the deflection (series S5). Increasing the mortar cover would be expected to result in an increase in the deflection However, the experimental values were inconsistent.

It should be noticed that the deflection at ultimate load reflects the type of failure the section suffers. Upon increasing the amount of reinforcement in the section, the failure changes from ductile tensile failure to a less ductile compression failure and the deflection therefore decreases after that change. Thus the deflection at ultimate load depends on the amount of reinforcement and its yielding characteristics.

5.8.3.3 Compressive Strain at Failure.

The value of ultimate compressive strain becomes important as this value is required to calculate the ultimate strength in flexure. In Fig.

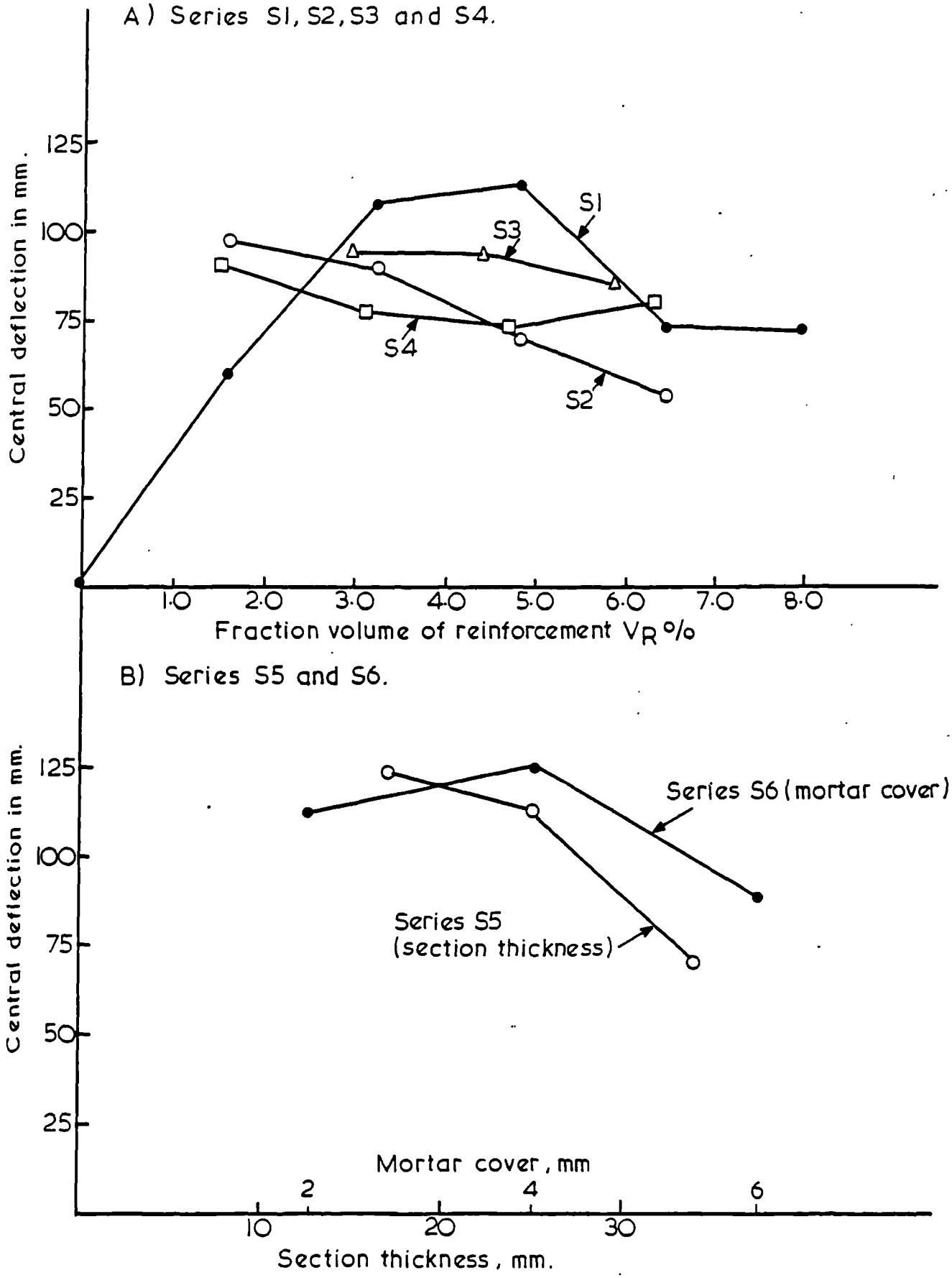

Fig. 5·22. Central deflection at ultimate load vs. fraction volume of reinforcement, mortar cover and section thickness.

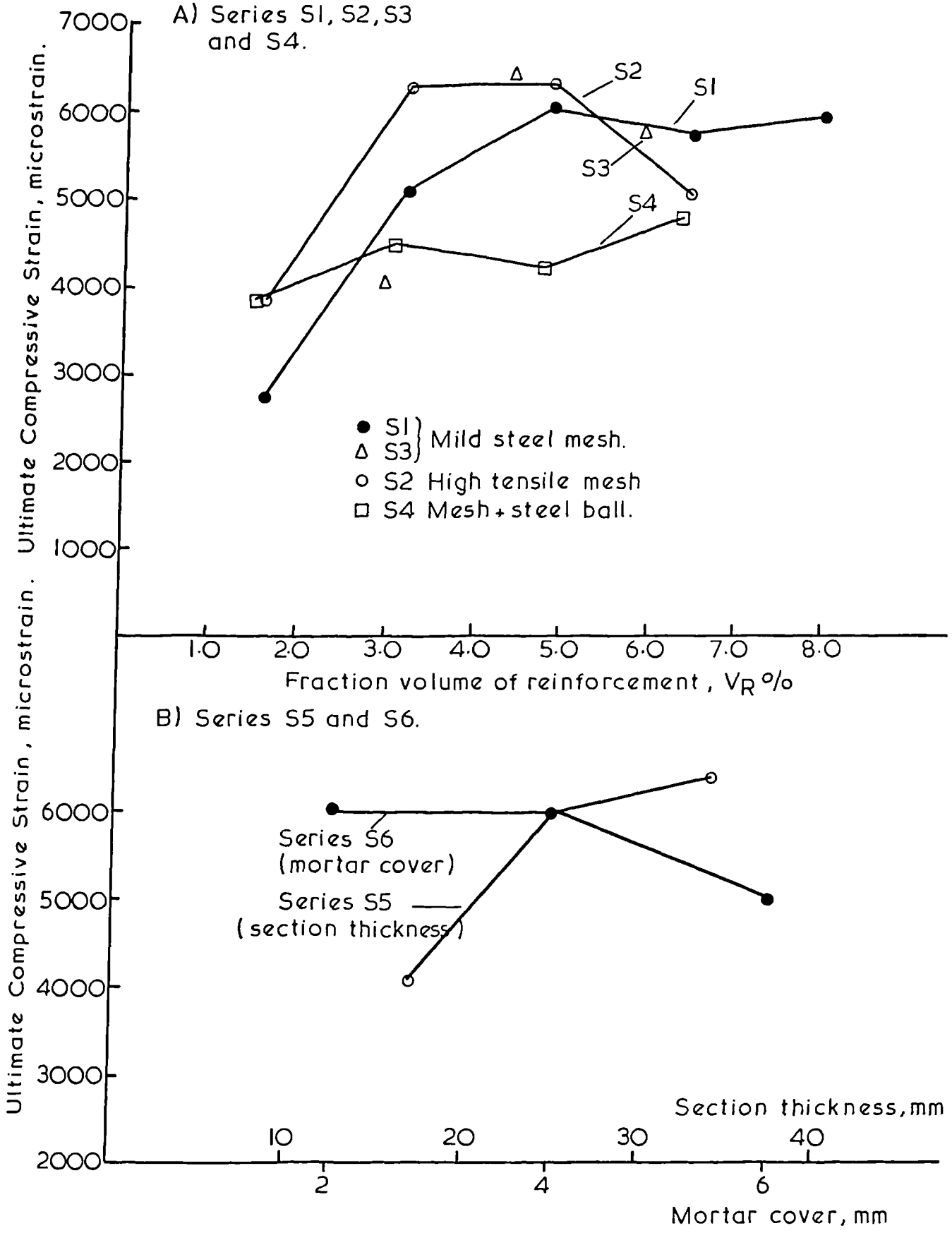

Fig. 5.23. Ultimate compressive strain vs. fraction volume of reinforcement, section thickness and mortar cover.

5.23, the average measured ultimate compressive strain on the specimen face is plotted against the fraction volume of reinforcement. The figure shows that for series S1 the compressive strain increases with the fraction volume until the value corresponding to 6 meshes (S1D) where it remained almost constant at 6000 microstrain. For series S2, the strain increased when V_R increased. It reached an optimum value of about 6300 microstrain in specimens S2C and S2D (4 and 6 meshes) respectively, then decreased for specimen S2E. This shows as mentioned before, the premature failure of the specimen due to buckling of the meshes in the compression zone. Except for specimen S2E, series S2 gave relatively higher compressive strain than series S1, which shows the ability of the high tensile mesh in utilizing the high mortar strength. In series S4 the compressive strain is relatively smaller than those of series S1 and S2 and it seems to increase slightly with increase in the number of meshes. Increasing the section thickness in series S5 and decreasing the mortar cover in series S6 increased the compressive strain. The highest values of strain for these variations were around 6000 microstrain.

It therefore follows that the average maximum compressive strain is about 6000 microstrain, and this value is almost the same for all sections which fail due to failure in the compression zone.

5.9 Conclusions.

Based on the experimental results of this study, the following conclusions were drawn:

1. The load-deflection and load-strain curves of ferrocement specimens can be divided into three ranges. The first two are linear, with the first cracking and first yielding marking the end of the first and second range, respectively. In the first range the section is free from cracks and within the elastic limit of its constituent materials while in the second range the

section is cracked, and is characterized by rapid increase in the number of cracks. The slopes of the two linear ranges depend mainly on the fraction volume of reinforcement in loading direction of the specimen. The third range represents the yielding stage in which the cracks increase rapidly in width. The yielding characteristics of the section are controlled by the yielding characteristics of the reinforcing system. Ferrocement under flexural loading could fail either in tension or in compression depending on the amount and yield strength of the reinforcement.

2. As far as the deflections and crack width are concerned, the service load appears to be within the second linear range. As long as the specimen has not yielded, the mean crack width remains mainly below 50 microns. For an allowable span-deflection ratio of 180, the mean crack width was mostly less than 20 microns, and the load was between 15-30% of the ultimate load.

3. The load at first cracking did not vary appreciably with variation in the amount and yield strength of the mesh, presence of steel bars or the mesh opening. However, it was in direct proportion with the square of the section depth.

4. The first yielding of the section could be initiated by either yielding of the mesh in the tensile zone or yielding of the mortar in the compressive zone. The load at first yielding increased with amount and yield strength of the reinforcing system. For the tested specimens, this load was between 45 and 65% of the ultimate load and it varied linearly with the fraction volume of reinforcement in loading direction, for specimens in which their tensile zone yielded first. The tensile strain at first yielding for such specimens can be predicted closely using the theoretical equation 5.1, and taking into account the strain gradient in the section.

5. The ultimate load seems to be influenced mainly by the yield strength and the amount of reinforcement, and depth of the section. It was

not affected appreciably by change in the mesh opening, presence of steel bars or the variation in the mortar cover. The ultimate load increased almost linearly with the fraction volume of reinforcement in loading direction for the specimens with mild steel reinforcement. For the specimens with high tensile mesh, the ultimate load ceased to increase when the number of mesh increased to more than 6 meshes. This is probably due to its premature failure caused by the large transverse tensile stresses which are induced by the mesh on the mortar because of the zig-zag shape of the mesh wires. These stresses tend to induce weak planes along the mesh layers.

6. The deflection at failure, as a measure of the ductility, is influenced by the amount and yielding characteristics of reinforcement, and the section depth. While there was an optimum value for the ductility for specimens with mild steel mesh, the deflection at ultimate load decreased with increase in the number of meshes for specimens with high tensile mesh.

7. The compressive strain at failure was controlled mainly by the mode of failure of the section. The average measured ultimate compressive strain was about 6000 microstrain, and this value was about the same for all section which failed in compression.

CHAPTER 6.

ANALYSIS OF FERROCEMENT IN FLEXURE.

6.1 Introduction.

One of the most important characteristics of ferrocement is the high degree of dispersion of its reinforcement. Due to this characteristic, the contribution of the matrix in tension to the stiffness of the section, during the cracked stage, is more appreciable than in reinforced concrete. The subdivision of the reinforcement results in increasing its capability of loading the matrix, through shear bond forces, and thus results in appreciable tensile force carried by the matrix. This, besides the smaller mortar cover and section depth ,represents the major differences between ferrocement and reinforced concrete. Consequently, the method of analysis used in reinforced concrete may not apply always satisfactorily to ferrocement. On the other hand, the need for a simple and reliable analysis method is becoming more urgent. As the uses of ferrocement as a structural material widen, the designer's need for a simple and accurate design procedure increases.

This part of the study is devoted to the development of simple analytical procedures to predict the moment capacity and deflections at different levels of the load for ferrocement in flexure. The procedure was applied on the test programme of this study in which the variables are the number, yield strength, and opening of the mesh, presence of steel bars, and thickness of section depth and mortar cover.

6.2 Review of Literature.

There are, mainly, three theoretical approaches used for analysing ferrocement sections in flexure. The first approach is similar to that of working stress and ultimate strength theories used in the design of

reinforced concrete members. In this approach the mortar is assumed to carry no tensile stresses as soon as its strain reaches the ultimate strain of plain mortar in tension. The second approach is based on defining ferrocement sections by limiting its amount of reinforcement. This amount of reinforcement is usually expressed in terms of the specific surface. The mechanical properties are established experimentally and assumed to be the same for any ferrocement section having a specific surface within the specified limits. In the third approach, ferrocement is treated as a composite material. The law of mixtures is used to find the mechanical properties of the composite from the properties of its constituents, i.e., mortar and reinforcement.

Many investigators (18,31,33,34,56) have used the method which is based on the design theory of reinforced concrete for the prediction of the ultimate strength, but with some minor differences in their assumptions. The differences cover mainly two aspects. The first aspect is the linearization of the stress-strain curve for the mesh reinforcement. The second aspect includes the shape of the compressive stress block and the value of the ultimate compressive strain. The linearization of the mesh stress-strain curve results in a certain amount of error, depending on the degree of linearization. An elastic-perfectly plastic curve is commonly used. It should be mentioned, however, that the yield point is not always clear in the mesh stress-strain curve. Hence, this, plus ignoring the strain hardening of the mesh could lead to a large error in the value of the predicted ultimate strength. Different compressive stress blocks at ultimate load have been used. In Fig.6.1, the most common used stress blocks are given. The stress block shown in Fig.6.1a was used by Logan and Shah (18). The results of the comparison between the calculated and experimental

values is shown in Fig.6.2. It can be seen from the figure that the ratio of the experimental to calculated is more than one and that this ratio increases with the increase in the fraction volume of reinforcements, V_{RL}. At $V_{RL} \approx 2.5\%$ the ratio is about 1.36

The use of other stress blocks by other investigators did not prove to be much more successful. Johnston and Mowat (34) have showed that using the reinforced concrete approach, the calculated ultimate moment was changed by 6.3% when different stress blocks were used, by 0.92% when the ultimate compressive strain was reduced from 0.38% to 0.31%, and by 8% to 15% when the mesh stress-strain curve was changed from non linear stress-strain function to elastic-perfectly plastic. Their results show that the reinforced concrete approach overestimates the ultimate moment of specimens reinforced with woven mesh by about 20% to 40%.

Balaguru, Naaman, and Shah (31) used the actual stress-strain curves for the mortar in compression and the mesh in tension in their non linear analysis of ferrocement beams. Limited experimental work showed that the procedure predicts closely the ultimate moment (average ratio of experimental to calculated = 0.92). However, their procedure is rather complicated for the use in design.

Walkus (30,44) has developed a method for proportioning ferrocement beams. The method is based on an assumed linearized stress-strain relationship for the composite under tension. The values of stresses and strains are simulated from experimental results and assumed to be the same for any section having a specific surface of reinforcement within 2.0 to 3.0 cm^2/cm^3. Walkus method has the disadvantages that the stress-strain curves are based entirely on simulated experimental results and that it does not take into account the different types and amount of mesh reinforcement.

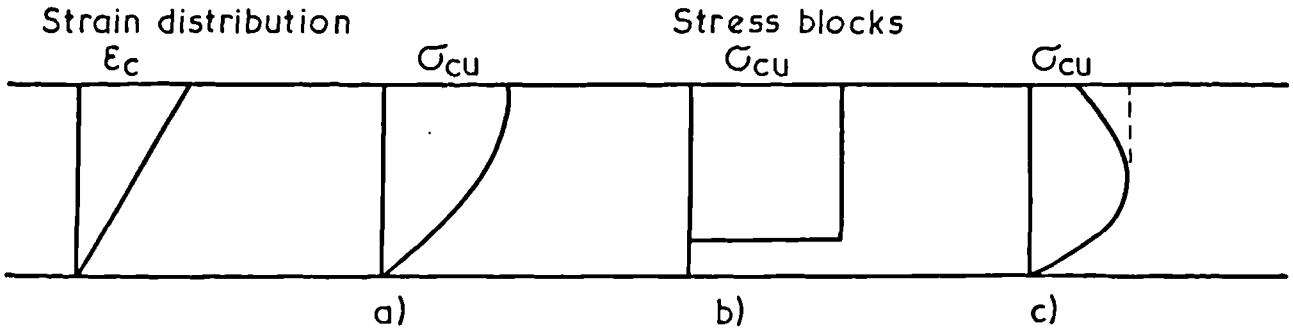

Fig. 6·1. Different compressive stress blocks.

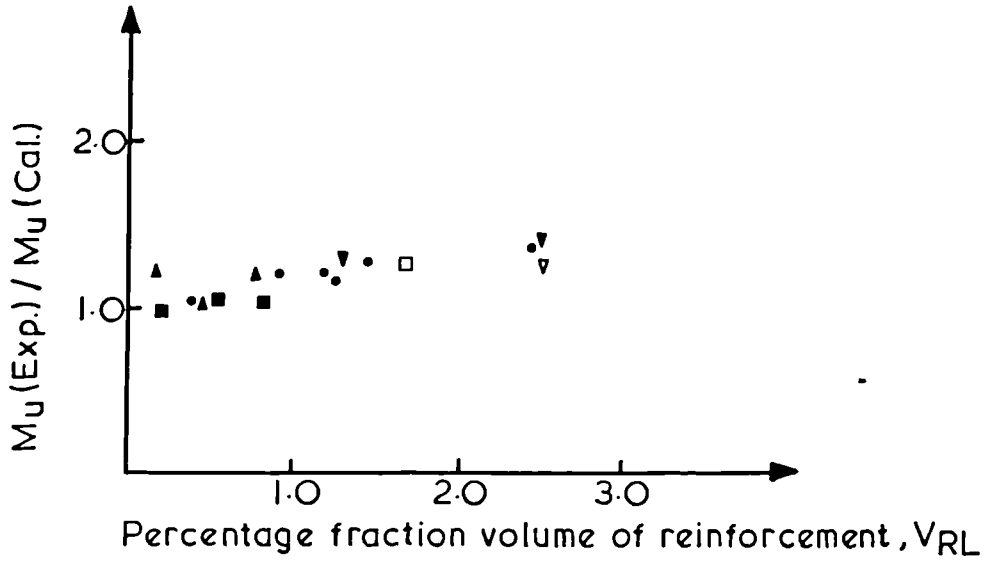

Fig. 6·2. The ratio of experimental to calculated ultimate moment, vs. the volume of reinforcement. ref. (18)

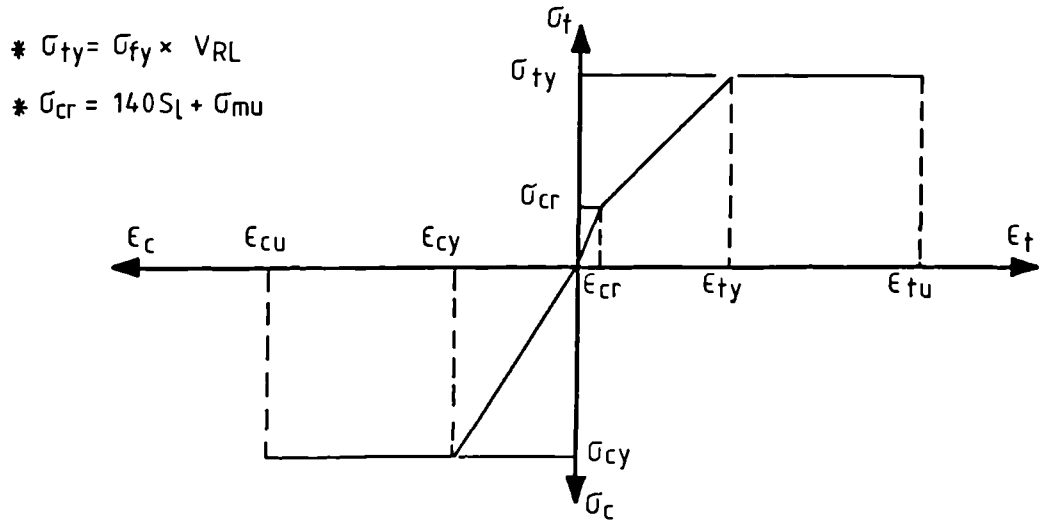

Fig. 6·3. Assumed stress-strain curves in tension and compression from Paul and Pama. (11)

The linearized stress-strain curve, as discussed in section 5.6, could not be verified from the experimental results of this study.

Several investigators (17,23,26) have predicted successfully some of the mechanical properties of ferrocement using the law of mixtures. Paul and Pama (11) have developed a theory in which ferrocement is treated as a composite material. Its mechanical properties were established from the properties of its constituents. The theory assumes a bilinear and tri-linear stress-strain curve for the compressive and tensile zones of the sections, respectively. Fig. 6.3 shows these curves. Limited experimental results showed that the theory predicts closely the ultimate strength and the ultimate deflections. It should be noticed however that the stress-strain curve of the tensile zone assumes perfectly plastic behaviour after first yielding. Such assumption, which ignores the strain hardening of the mesh could lead to conservative results depending on the yielding characteristics of the mesh. Also, Paul and Pama (11) assumed that the tensile stress at first cracking increases with the specific surface of reinforcement. This assumption, as discussed in sec. 4.6.1, could not be verified in this study.

It can be seen, therefore, that the theory for analysing ferrocement section in flexure is far from being established. Work is urgently needed in this area to help set out the design procedure for the material.

6.3 Description of the Method of Analysis.

In a composite material consisting of a matrix and uniformly dispersed continuous fibres, the stress and the modulus of elasticity of the composite in direct tension can be written by the law of mixtures as:

$$\sigma_c = \sigma_m V_m + \sigma_f V_{RL} \quad \ldots\ldots \quad (6.1)$$

and

$$E_c = E_m V_m + E_f V_{RL} \quad \ldots\ldots \quad (6.2)$$

where σ_m and σ_f are the stress in the matrix and in the fibres respectively, V_m is the matrix fraction volume, V_{RL} is the fibres fraction volume in the loading direction, and E_m and E_f are the modulus of the matrix and the fibres, respectively. As soon as the matrix cracks, its stress will be transferred to the fibres. Therefore, eqs. 6.1 and 6.2 become:

$$\sigma_c = \sigma_f V_{RL} \quad \ldots\ldots \quad (6.3)$$

$$E_c = E_{cr} = E_f V_{RL} \quad \ldots\ldots \quad (6.4)$$

For ferrocement plates under flexural loading, it was shown in section 5.4, that their behaviour could be divided generally into elastic stage and cracked stage. The analysis of ferrocement plates in these two stages is discussed separately.

6.3.1 Elastic Stage.

In the elastic stage, where the plate is free from cracks, both the mortar and the reinforcement are within their elastic range. The strain and stress space relationship are linear, as shown in Fig.6.4a. The modulus of elasticity in the tensile zone is assumed to be equal to that of the composite in direct tension, i.e., eq. 6.2. The stresses can be found using the following relation[69]:

$$\sigma = \frac{MC}{I}$$

where σ is the stress at a distance C from the neutral axis, M is the applied moment, and I is the second moment of area of the equivalent transformed section.

6.3.2 Cracked Stage.

The cracked stage can be divided mainly into two ranges, namely the linear range and the yielding range. The stress and strain distribution for these

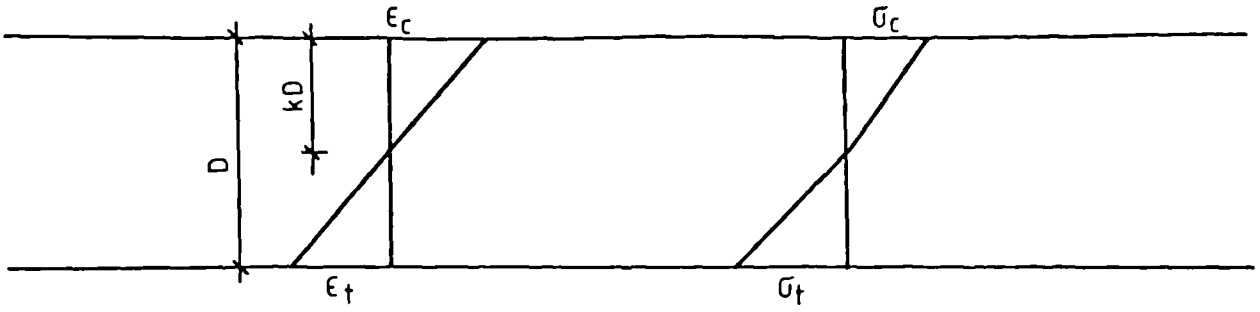

a) Elastic Stage.

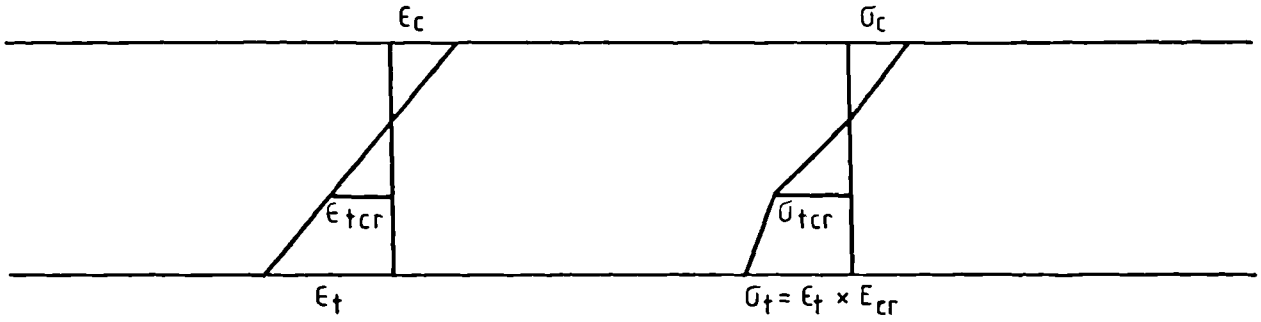

b) Cracked Stage, linear range.

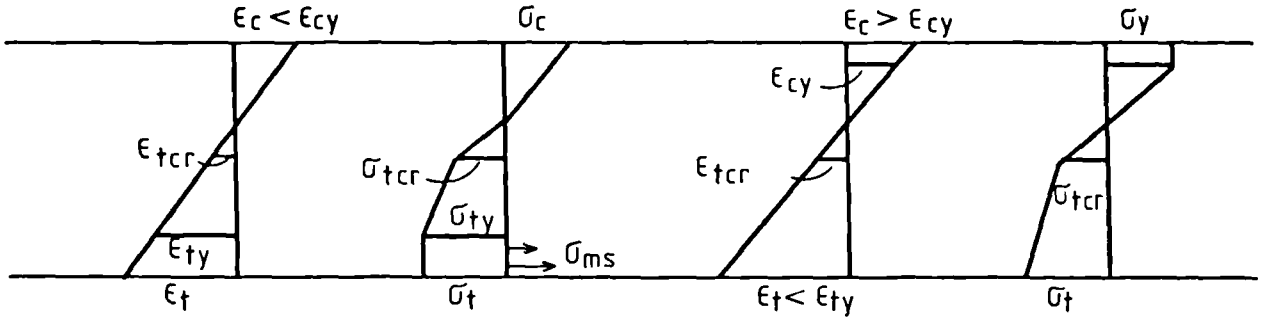

Tensile zone yielding. Compressive zone yielding.

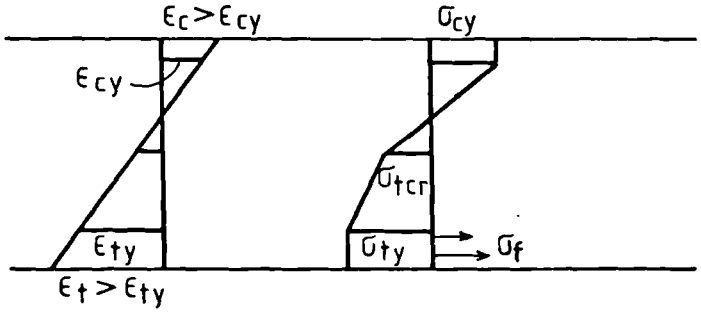

Both zones yielding.

c) Yielding range.

Fig. 6.4. Strain and Stress diagrams of ferrocement in flexure.

two ranges are shown in Fig.6.4. In the linear range, Fig.6.4b, the mortar and the reinforcement in the compressive zone are still within their elastic range. The composite in this zone, thus, behaves elastically and the modulus of elasticity is assumed to be equal to that of plain mortar. In the tensile zone, the part of the mortar, where $\varepsilon_t > \varepsilon_{tcr}$, is cracked while the reinforcement all through the zone is still within its elastic limit. For the cracked depth of the mortar, although the composite stress is in direct proportion to the strain, the modulus of elasticity of this part of the section is reduced considerably. According to the law of mixtures, eq. 6.4 gives the modulus of elasticity in the cracked zone. However, Naaman and Shah (17), had found from their experimental results that this equation gives lower bound values. This, perhaps, is due to ignoring the contribution of the cracked mortar to the rigidity of the section. The best fit line for Naaman and Shah experimental results, see Fig.6.5, was found. The equation for it was:

$$E_{cr} = 1.35\, E_f\, V_{RL} \qquad \ldots\ldots \qquad (6.5)$$

The coefficient 1.35 in the above relation indicates that the modulus of elasticity for the cracked zone is 35% higher than that calculated taking into account the effect of reinforcement only. Eq. 6.5 was used, therefore, instead of eq. 6.4 in the analysis of the plates in this study.

The end of the linear range in the cracked stage is marked by first yielding of the section. The first yielding of the composite could be due to yielding of either the tensile or compressive zone, depending on the properties of the reinforcement and the mortar. Therefore, two cases for first yielding of the composite can be realized. The first case is when $\varepsilon_t \geq \varepsilon_{ty}$ while $\varepsilon_c < \varepsilon_{cy}$. The second case is when $\varepsilon_t < \varepsilon_{ty}$ while $\varepsilon_c \geq \varepsilon_{cy}$, where ε_t and ε_c are the composite strain in the extreme tensile and

compressive fibres, respectively and ε_{ty} and ε_{cy} are the composite yielding strain in tension and compression, respectively. The yield tensile strain for ferrocement under direct tension was derived theoretically by Paul and Pama (11), and it was given by the following relationship:

$$\varepsilon_{ty} = \frac{1}{E_f} \left(\sigma_{fy} - \frac{\sigma_{mu}}{2} R\right) \quad \ldots\ldots \quad (6.6)$$

where E_f and σ_{fy} are the modulus of elasticity and the yield strength (at 0.005 strain) of the mesh, respectively, σ_{mu} is the mortar tensile strength and $R \approx 1/V_{RL}$ for a square mesh. It was shown in section 5.8.2 that eq. 6.6, after taking into account the strain gradient in the section, predicts closely the flexural yield tensile strain at the extreme fibre of the tested specimens.

The yield strain of the compression zone depends on the compressive yelding characteristics of the mortar. CP.110 (68) gives the following relation for the compressive yield strain of concrete:

$$\varepsilon_{cy} = \frac{\sqrt{f_{cu}}}{4115} \quad \ldots\ldots \quad (6.7)$$

where f_{cu} is cube strength. Eq. 6.7 gave reasonably close results when compared with the experimental stress-strain curve of mortar given by Balaguru, Naaman and Shah (31). Therefore, this equation may be used to predict the yield strain of the compressive zone of ferrocement.

After first yielding, increasing the load leads eventually to the yielding of both the compressive and the tensile zones. Fig.6.4c shows the stress and strain distributions at this stage. In the tensile zone, the contribution of the mortar to the tensile force after yielding will not increase appreciably with the progress of the load. This is because the yielding mesh could not load the mortar between cracks to a significantly higher level than that at first yielding. Therefore, after ε_{ty}, the mortar

was assumed to remain carrying the same stress. However, the yielding of the mesh is not necessarily, perfectly plastic, and the stress is likely to increase, depending on the yielding characteristics of the mesh, with the increase in strain. The extra stresses in the meshes after first yielding were accounted for as shown in Fig.6.6. The extra tensile force in each mesh is equal to:

$$(\sigma_f \text{ at } \varepsilon_t - \sigma_f \text{ at } \varepsilon_{ty}) \text{ x cross-sectional area of mesh.}$$

The summation of the extra tensile force of each mesh layer is equal to the total increase in the tensile force of the section after first yielding. Alternatively, this increase in the tensile force can be found by assuming a parabolic increase in the composite tensile stress. By the law of mixtures, since the contribution of the mortar is neglected, then, the composite extra stress will be

$$\sigma_t \text{ extra} = (\sigma_f \text{ at } \varepsilon_t - \sigma_f \text{ at } \varepsilon_{ty}) V_{RL}$$

where σ_f is the tensile stress in the mesh, and V_{RL} is the fraction volume of the mesh reinforcement in the loading direction.

Using the compatibility and equilibrium of the section, the depth of the neutral axis at any level of the load during the cracked range, can be found by iterative procedure if a strain value of the section at that load is given. The depth of the neutral axis is first assumed. The strain distribution, thus, can be found from the given strain value and assuming linear strain distribution. The corresponding stress distribution can be established as discussed earlier in this section. Therefore, the tensile and compressive forces in the section can be calculated. To satisfy the equilibrium of the section, these two forces should be equal. If the computed values of these forces are not equal or the difference between them is not within 5% of their

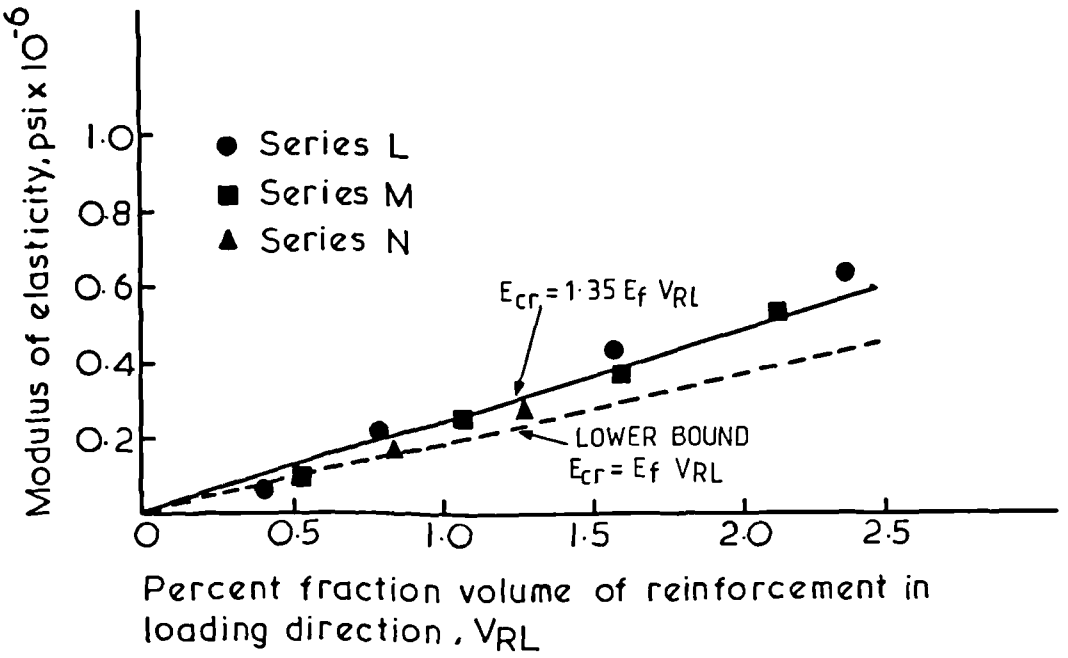

Fig. 6.5. Composite modulus of elasticity in tension, cracking range. (23)

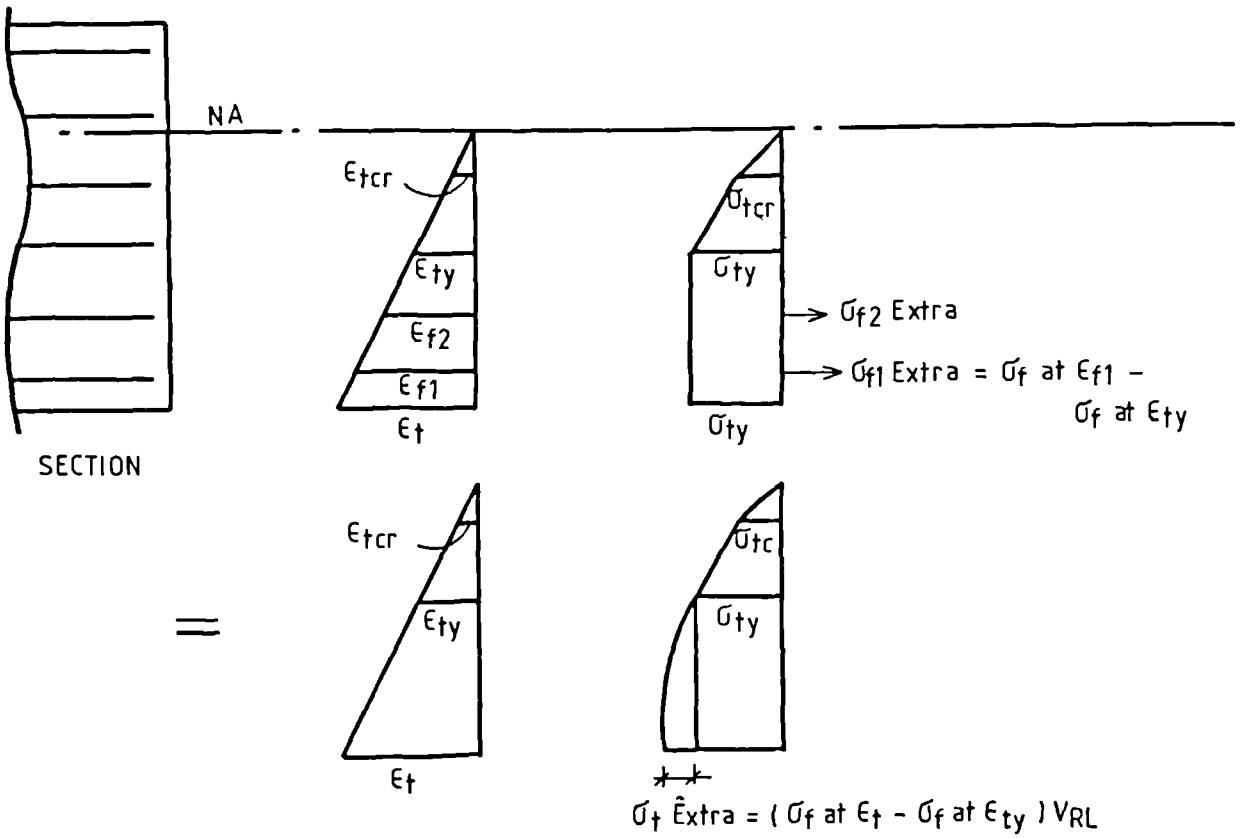

Fig. 6.6. Stresses carried by the reinforcement after first yielding.

average, then another value for the neutral axis depth will be assumed. The tensile and compressive forces will be recalculated and compared. The iterative procedure is to continue until convergence is achieved. The resisting moment of the section can be computed by multiplying the average of the resultants of the tensile and compressive forces at convergence by the distance between them, i.e.,

$$M = (\frac{C+T}{2})\ \bar{X} \qquad \ldots\ldots \qquad (6.8)$$

where C and T are the compressive and tensile resultant forces, respectively, and $\bar{X}$ is the distance between them.

The curvature of the section can be found knowing that,

$$\phi = \frac{\varepsilon_c}{kD} \qquad \ldots\ldots \qquad (6.9)$$

where ϕ is the curvature, ε_c is the compressive strain at the extreme fibre, and kD is the neutral axis depth from the extreme compressive fibre.

6.3.3 At Failure.

At failure, two cases can be realized. The first case is when the composite compressive strain ε_c attained its ultimate compressive strain value ε_{cu}, while the composite tensile strain ε_t is less than the ultimate tensile strain value, ε_{tu}, which causes the fracture of the mesh reinforcement. In this case, the section will fail in compression. The second case is when $\varepsilon_c < \varepsilon_{cu}$, while $\varepsilon_t = \varepsilon_{tu}$, then the section will fail in tension. Therefore, the section should be analysed at both cases. The governing case is that which gives the less resisting moment.

The stress and strain distributions at failure are shown in Fig.6.7. The compressive stress block is similar to that incorporated in the British Code. The ultimate compressive strain of the composite is assumed to be 6000 microstrain, and this value was based on the average measured ultimate

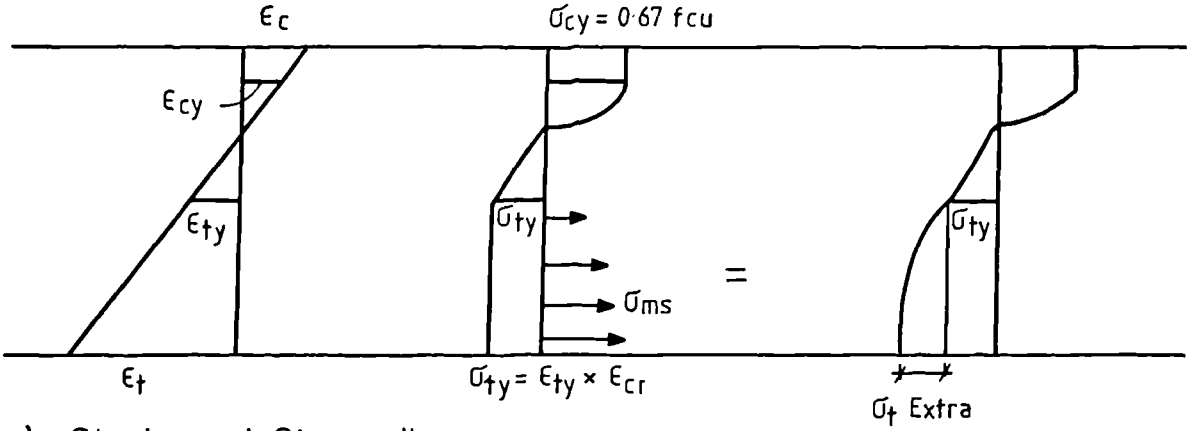

a) Strain and Stress diagram.

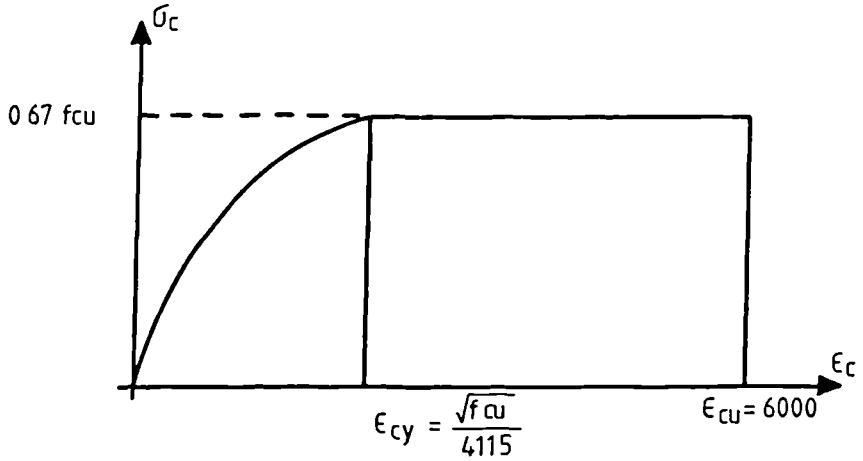

b) Stress - strain diagram , compressive zone.

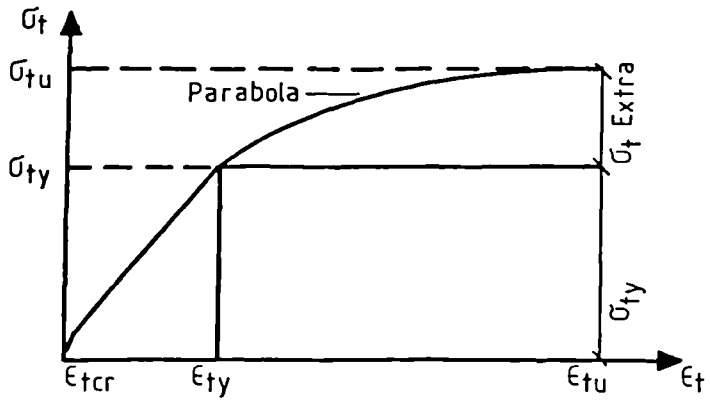

c) Stress - strain diagram , tensile zone.

Fig. 6.7. Strain and stress diagram at failure of ferrocement in flexure.

compressive strain of the tested specimens of this study and in which the failure was in compression, (see sec. 5.8.3). A similar value was reported by Balaguru et al. (31).

The ultimate tensile strain of the composite is determined essentially by the ultimate tensile strain of the mesh. Its value is equal to the tensile strain at the extreme fibre of the section when the extreme mesh layer attained its ultimate tensile strain. For this purpose, however, the ultimate tensile strain of the mesh, cannot be taken,and specially for the woven mesh type of reinforcement, equal to the ultimate strain of the mesh when tested in tension alone, as it is usually assumed (11,18,31). It was observed that the longitudinal wires of the mesh, having a zig-zag shape, tend to flatten when the mesh alone is tested in tension. Consequently, the measured ultimate tensile strain of the tested mesh included the extra elongation caused by the flattening tendency of the wires. However, when the mesh is embedded in the mortar, and since complete bond failure did not take place, the mortar restricted the flattening action of the wires. Thus, the ultimate tensile strain of the embedded mesh is much less than the apparent, i.e., measured, ultimate tensile strain of the mesh alone. A more realistic value of the ultimate tensile strain of the mesh may be obtained by conducting a tensile test on the composite rather than the mesh. Moreover, it would be interesting to carry out a study to compare the values of the ultimate tensile strain obtained from tensile tests on the mesh and on the composite and flexural test on the composite. Such a study unfortunately is beyond the scope of this investigation.

The procedure for calculating the moment capacity at failure is the same as that for finding the moment capacity at the cracked stage described in the previous section.

6.3.4 Sections with Bar Reinforcement.

So far the analysis included sections where the reinforcement is uniformly and finely dispersed, i.e., the reinforcement is in the form of a wire mesh. For sections which include conventional steel bars as well as wire mesh, the previously described analysis method may not be appropriate to be used in the given form. It should be noticed that the available bond area in the bar reinforcement could be as low as 1/10 of the bond area of an equivalent volume of the mesh reinforcement. Thus, the bar reinforcement cannot be considered as finely dispersed in the section. Also, the two reinforcements may exhibit different stress-strain curves and therefore the mechanical properties of the overall reinforcing system would be somewhere between the individual properties of the two types of reinforcement.

On the other hand, the described method is still applicable when only the wire mesh reinforcement is considered. Therefore for sections which include steel bars as well as wire mesh, the contribution of the bar reinforcement could be calculated separately from that of the rest of the composite, whenever it is necessary.

In the elastic range, the method described in sec. 6.3.1 is applicable. But, because the bars are not uniformly and finely dispersed and are usually placed near the centroid of the section, they are neglected in the calculation of the modulus of elasticity of the composite, but, they are included in the calculation of the equivalent transformed section.

In the cracked stage, the forces carried by the bars are calculated separately from those of the wire mesh and the matrix. However, the yielding of the section is determined by the yielding characteristics of all the effective reinforcement. Thus, in calculating the tensile yield strain of the composite (i.e. in eq. 6.6) the bars are included in the term V_{RL} in

direct proportion to their percentage of the fraction volume of the total reinforcement.

The depth of the neutral axis could be found using the procedure described in sec. 6.3.2. In calculating the tensile forces, the tensile force carried by the wire mesh and the matrix (as a composite material) would be added to the tensile force carried by the bars. The tensile force carried by the bars can be calculated by finding, from the assumed strain distribution, the strain value at the level of the bars. Then, the corresponding stress can be determined from the stress-strain curve of the bar. Hence, the force carried by the bars is equal to

$$T_{st} = \sigma_{st} \times A_{st} \quad \ldots\ldots \quad 6.10$$

where σ_{st} and A_{st} are the stress carried by the bars and their cross-sectional area, respectively.

6.4 Comparison of Calculated and Experimental Moment Capacity of the Tested Plates.

Three points in the life of the tested plates were selected for the comparison of the calculated and experimental values of the moment capacity. These are the first cracking, the first yielding and failure. The first two points were chosen because they represent the points where the behaviour of the section changes. At the same time, the result of the comparison at these two points could be used to judge the performance of the suggested analytical method all through the elastic stage and the linear range of the cracked stage, as the method adopts the same procedure for each of these two ranges. The moment capacity at failure was chosen, obviously, due to its importance for design purposes.

In the calculations of the moment capacity the average of the actual (i.e. measured) section depth and cube compressive strength for the specimens

in each set, were used. In Table 6.1, the measured section depth and the properties of the control specimens for each slab, are given.

6.4.1 Cracking Moment.

The sections were assumed to crack when the tensile strain in the extreme fibre of the composite attained the value of the ultimate tensile strain of plain mortar. The value of the ultimate tensile strain of mortar was established by dividing the average value of the modulus of rupture of the plain mortar specimens by the modulus of elasticity of plain mortar in direct compression. This value of tensile strain was found to be equal to 160 microstrain. The modulus of elasticity for the tensile zone of the composite was found using the law of mixtures, eq. 6.2. Thus the cracking stress is equal to:

$$\sigma_{tcr} = \varepsilon_{tcr} \times E_t$$

and the cracking moment is equal to:

$$M_{cr} = \frac{\sigma_{tcr} \; I}{C}$$

where σ_{tcr} and ε_{tcr} are the first cracking tensile stress and strain at the extreme fibre of the section, respectively, E_t is the modulus of elasticity of the composite in tension, M_{cr} is the cracking moment of the section, and I and C are the second moment of area and the distance from the neutral axis to the extreme tensile fibre of the transformed section. For sections which included wire mesh reinforcement only, because of the symmetrical distribution of the reinforcement in the section, the value of C was assumed to be equal to half the section depth.

The cracking moment was calculated for all the tested slabs and is given, together with the experimental cracking moment in Table 6.2. A sample for the calculations involved is given in Appendix A. The experimental cracking moment of each set is the average value of the cracking

Table 6.1 Results of the control specimens and the measured section depth.

Specimen	Section depth mm	Compressive Strength N/mm^2	Modulus of rupture N/mm^2	Specimen	Section depth mm	Compressive Strength N/mm^2	Modulus of rupture N/mm^2
S1 B1	26	54.1	4.11	S2 E2	25.5	52.4	4.4
S1 B2	26	56.9	4.57	S3 C1	26	55.3	4.3
S1 B3	26	57.1	4.2	S3 C2	26	53.6	4.2
S1 C1	26	53.8	4.3	S3 D1	26	51.6	4.2
S1 C2	26	57.5	4.2	S3 D2	26	55.3	4.1
S1 C3	26	56.9	4.5	S3 E1	26	45.1	3.7
S1 D1	26	53.6	4.0	S3 E2	26	52.7	4.4
S1 D2	26	56.4	4.3	S4 A	26	48.1	4.3
S1 D3	26	58.4	4.2	S4 B	26	47.9	3.9
S1 E1	26	57.2	4.6	S4 C	26	48.7	3.9
S1 E2	26.5	55.7	4.5	S4 D	26	48.1	3.8
S1 E3	26	56	4.3	S5 C1	17.5	47.5	3.8
S1 F1	26.5	66.5	4.9	S5 C2	17	48.5	3.7
S1 F2	26	57.7	4.8	S5 C3	17.5	51.3	4.0
S1 F3	25.5	58.1	4.7	S5 E1	35	46.5	3.8
S2 B1	26	54.2	4.1	S5 E2	34	47	3.9
S2 B2	26	56.9	4.2	S5 E3	34	48	4.1
S2 C1	26	52.1	3.9	S6 4D1	25.5	55.2	4.3
S2 C2	26	56.7	4.4	S6 4D2	25.5	57.1	11.5
S2 D1	26	56	4.3	S6 6D1	25.5	53.9	3.8
S2 D2	25.5	54.4	4.1	S6 6D2	26	52	3.9
S2 E1	26	53	3.9				

Note:

a. The given section depth is the measured value.

b. The compressive strength is the average of the compressive strength of six cubes (size 50 mm).

c. The modulus of rupture is the average of the results of three plates, 100x500x25 mm in dimensions.

Table 6.2 Calculated and experimental values of cracking moment.

Series	Specimen's Set.	Calculated moment N-m	Experimental moment N-m	Ratio exp./cal.
S1	S1 B	145.6	144	0.99
	S1 C	149.7	147	0.98
	S1 D	154.7	153	0.99
	S1 E	160.4	148.5	0.93
	S1 F	165	166.1	1.01
S2	S2 B	145.7	132	0.91
	S2 C	149.6	151.5	1.01
	S2 D	155	150.7	0.97
	S2 E	160.6	150.7	0.94
S3	S3 C	151.4	129	0.85
	S3 D	157.4	148.5	0.94
	S3 E	163.8	172.5	1.05
S4	S4 B	148.5	142.5	0.96
	S4 C	156.4	159	1.02
	S4 D	165.7	177	1.06
S5	S5 C	69.4	67.5	0.97
	S5 E	263.1	253.5	0.96
S6	S6 4D	150.8	115.5	0.77
	S6 6D	145.6	109.5	0.75
			Average =	0.95
			S.D. =	0.083

moment of the slabs in that set, except S1 F, where the result of slab S1 F1 was neglected due to a high recorded cracking load compared with other results.

Table 6.2 shows that the calculated values are very close to the experimental ones, for series S1 to S5. The average ratio of experimental to calculated is equal to 0.97 with the standard deviation equal to 0.052. The two ratios from the results of series S6 are, however, relatively lower (average ratio is 0.76). This may be due to, as discussed in sec. 5.8.1, the unexpected low recorded value of the load at first crack for the specimens of this series. The average value of this load was smaller than the average ultimate load of the plain mortar specimens. Nevertheless, the calculated and the experimental values of this series are still close.

The overall ratio of experimental to calculated for all sets of slabs is equal to 0.95 with a standard deviation of 0.083. This result indicates that in spite of the variables considered which include number, yield strength, and opening of the mesh, presence of steel bars, and thickness of the mortar cover and the section, the suggested method predicted successfully, the cracking moment of the slabs.

6.4.2 Moment Capacity at First Yielding.

The moment capacity of the section at first yielding was calculated for all the tested slabs. The first yielding was assumed to take place when the strain in the extreme fibres of the section attained either the adjusted value of the tensile strain defined by eq. 6.6 or the value of the compressive strain given by eq. 6.7, whichever reaches first. The tensile strain value from eq. 6.6 was adjusted as discussed earlier, to take into account the strain gradient in the section due to flexural loading. All the specimens yielded first in the tensile zone except S2 C, S2 D, and S2 E which yielded in the compressive zone first. A sample for the calculation

of the moment at first yielding is given in Appendix B.

In Table 6.3, the calculated ratio of neutral axis depth from the extreme compression fibre to the depth of the section, the corresponding tensile strain in the extreme fibre, and the calculated and experimental moments are given for each set of specimens. The experimental moments for each set were obtained by first finding the load corresponding to the assumed tensile strain for each specimen then averaging moments which correspond to those loads for the specimens in each set. The number of specimens in each set of series S1, S2, S3, S4, S5, and S6 are three, two, two, one, three and two respectively.

From the values of the ratio of experimental to calculated moments given in Table 6.3, it can be seen that the described method predicts the moment capacity of the specimens of series S1 and S2 very closely. The mean ratio of the sets of these two series 1.0 and 1.04 respectively. For the specimens of series S3, S4, and S5 most of the calculated moment values are slightly higher than the experimental values (the average ratios of experimental to calculated are 0.89, 0.94 and 0.97 respectively). The overprediction may be because the calculated yield strain is higher than the experimental ones. Nevertheless, the calculated and the experimental moment values are still close. For the specimens of series S6, the overprediction was higher than in the other series (ratio was equal to 0.8). In this series the variable was the thickness of the mortar cover. Increasing the mortar cover from 2 mm (specimens S1 D) to 4 mm (specimens S6 4D) and to 6 mm (specimens S6 6D) decreased the ratio of experimental/calculated from 0.99 to 0.83 and to 0.77, respectively. The overprediction can be explained by noticing that the extreme layer of mesh in the tensile zone becomes less effective in loading the mortar at the outer side of the section as the depth of the mortar cover increases. On the other hand, the described method

Table 6.3 Calculated and Experimental moment at the assumed first yielding points.

Series	Specimen	Ratio* k	Tensile strain on the extreme fibre micro-strain	Calculated moment N-m	Experimental moment N-m	Ratio exp./calc.	Average Ratio
S1	S1 B	0.26	1720	210.7	207	0.98	Average=1.0 S.D.=0.016
	S1 C	0.28	1930	307.9	314.3	1.02	
	S1 D	0.295	2240	417.5	415	0.99	
	S1 E	0.31	2400	544.6	547.5	1.01	
	S1 F	0.325	2500	678.5	668.5	0.99	
S2	S2 B	0.22	5100**	416.3	492	1.18	Average = 1.04 S.D.=0.1
	S2 C	0.245	5500**	717	690.6	1.04	
	S2 D	0.28	4610**	801	767.2	0.96	
	S2 E	0.31	4000**	881.6	853.3	0.97	
S3	S3 C	0.28	1825	298.1	266.5	0.89	Average= 0.89 S.D.= 0
	S3 D	0.3	2100	423	375.4	0.89	
	S3 E2	0.325	2250	539.4	475.9	0.89	
S4	S4 B	0.305	2200	432.6	381.5	0.89	Average= 0.94 S.D.=0.076
	S4 C	0.33	2425	566	582.5	1.03	
	S4 D	0.35	2550	693	631.8	0.91	
S5	S5 C	0.3	2450	206.8	180.7	0.88	Average= 0.97 S.D.=0.12
	S5 E	0.3	2150	724.9	763.1	1.05	
S6	S6 4D	0.29 or 0.27	2580	502 or 443.6	418.5	0.83 or 0.94	Average=0.8 or =0.93
	S6 6D	0.28 or 2.6	3000	553.9 or 467	426.7	0.77 or 0.92	
					Overall average = 0.97 S.D. = 0.08		

* k = Ratio of neutral axis depth from extreme compression fibre to the depth of the section.

** Governed by yielding of compressive fibre, ε_{cy} = 1800 microstrain.

assumes that the tensile stress for the cracked mortar zone increases linearly with the strain, i.e., with the depth from the neutral axis. This assumption seems to be unrealistic in the cover zone, i.e., beyond the extreme mesh layer when the thickness of this cover is more than 2 mm. the moment capacity for the specimens of series S6 was therefore recalculated assuming that the tensile stress remains constant beyond a depth equal to the depth of the extreme mesh layer plus 2 mm., see Fig.6.8. This adjustment in the method resulted in an increase in the ratio of experimental to calculated moments from 0.83 and 0.77 for specimens S6 4D and S6 6D to 0.94 and 0.92, respectively.

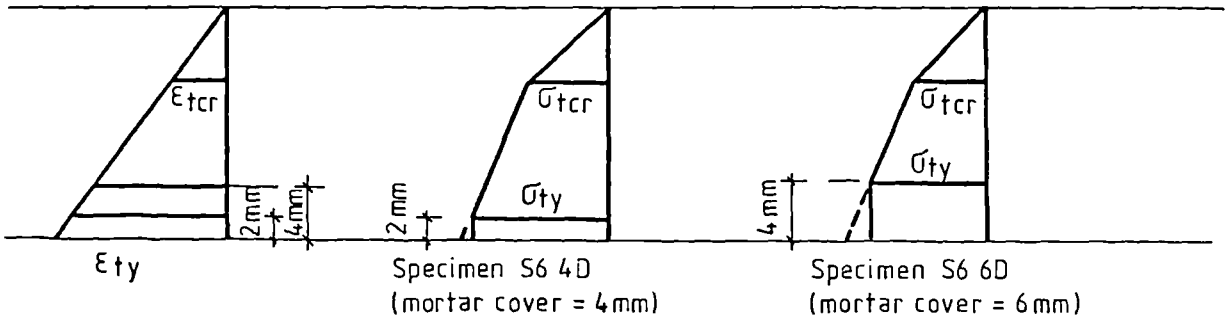

Fig.6.8 Adjustment of the tensile stress diagram to account for large mortar cover.

The overall ratio of experimental to calculated was equal to 0.97 with a standard deviation equal to 0.08. This result indicates that the described method predicts successfully the moment capacity of the ferrocement section in the linear range of the cracked stage irrespective of the number of meshes, mesh yield strength, presence of steel bars, section depth, and mortar cover.

6.4.3 Ultimate Moment.

From the discussion of sect. 6.3.2, two cases can be realized at failure:

Case 1.	$\varepsilon_t \geq \varepsilon_{tu}$	while	$\varepsilon_c < \varepsilon_{cu}$	Tensile failure.
Case 2	$\varepsilon_t < \varepsilon_{tu}$	while	$\varepsilon_c \geq \varepsilon_{cu}$	Compression failure

The ultimate moment was calculated for all specimens assuming that they all follow case 2. Although this assumption as observed experimentally, may not be true for some specimens, the actual value of the ultimate tensile strain, ε_{tu}, is not known. Assuming ε_{tu} to be equal to the ultimate tensile strain of the mesh alone is not correct for specimens reinforced with woven wire mesh as discussed in sec. 6.3.2. In any case the above assumption affects only the few specimens where the number of meshes is limited to two mesh. Moreover, the assumption seems to result in a marginal error in the calculated ultimate moments, as will be seen later in this section.

To demonstrate the calculation procedure for the ultimate moment, the calculation for a typical specimen is given in Appendix C.

In Table 6.4, the calculated values of the neutral axis depth and the ultimate moment are given for all the tested sets of specimens. The calculated ultimate moments are compared with experimental values which are obtained from the average of the ultimate moment of the repeated specimen in each set. From the table, it can be seen that the calculated ultimate moments are in close agreement with experimental values. The overall average ratio of experimental to calculated is equal to 1.086 with a standard deviation equal to 0.109. This result also indicates that the method, in general, underestimates the ultimate moment. The results of two sets only overestimated slightly the experimental values. The two sets are S1 B and S6 6D (ratio equal to 0.92 and 0.93 respectively). For S1 B, the overestimation can be attributed to the failure of the specimen in tension and not, as the

Table 6.4 Calculated and experimental ultimate moments.

Series	Specimen	Ratio k*	Calculated moment N-m	Experimental moment N-m	Ratio exp./cal.	Average Ratio
S1	S1 B	0.08	280.3	258	0.92	Average=1.07
	S1 C	0.14	535.5	622.5	1.16	
	S1 D	0.2	758.2	844.5	1.11	
	S1 E	0.24	928.3	997.5	1.08	
	S1 F	0.27	1129.2	1206	1.06	S.D.=0.09
S2	S2 B	0.185	751	781	1.03	Average=1.19
	S2 C	0.28	1115.8	1467	1.31	
	S2 D	0.32	1293	1665	1.29	
	S2 E	0.35	1440	1662	1.15	S.D.=0.13
S3	S3 C	0.145	532.6	541.5	1.02	Average=1.04
	S3 D	0.2	724.8	745.5	1.03	
	S3 E2	0.27	844.8	903	1.06	S.D.=0.023
S4	S4 A	0.14	447.9	487.5	1.09	Average=1.12
	S4 B	0.195	617.5	661.5	1.08	
	S4 C	0.25	805	948	1.18	
	S4 D	0.3	899.5	1017	1.14	S.D.=0.046
S5	S5 C	0.23	336.5	337.5	1.0	Average=1.04
	S5 E	0.215	1203.8	1299	1.08	S.D.=0.05
S6	S6 4D	0.205	787.6	870	1.1	Average=1.02
	S6 6D	0.225	832.1	780	0.93	S.D.=0.12
					Overall average ratio = 1.086	
					S.D. = 0.109	

*k = ratio of neutral axis depth from extreme compression fibre to the depth of the section.

method assumed, in compression. It can be seen however that the over-estimation is only minor.

The overestimation in the result of specimen S6 6D (ratio = 0.93), can be attributed to the assumed value of yield strain which was considered to be that at the face of the specimen when the specimen first starts yielding. Such assumption is reasonable if the mortar cover is small. However, for specimens with 6 mm cover, as was the case in calculating the moment capacity at first yielding, the yield strain should be considered to be that at a depth equal to the depth of extreme mesh layer plus 2 mm, see Fig.6.8.

The difference between the calculated and the experimental ultimate moments for the high tensile mesh series (S2) (average ratio = 1.19) was relatively high compared with that of series S1. This could be explained by noticing that the high yield mesh did not show a full plastic behaviour. Thus, the mesh continued to load the mortar in the tensile zone to a higher level even after the assumed yielding of the specimen. On the other hand the method does not take into account any increase in mortar tensile stress beyond that which is calculated at first yielding. The method, therefore, seems to be reasonable for specimens with mild steel mesh, but gives slight underestimation for those with high tensile mesh.

6.5 Curvatures and Deflections.

The curvature of the section at any level of the load can be found knowing that:

$$\phi = \frac{\varepsilon_c}{kD} = \frac{\varepsilon_t}{D(1-k)} \qquad \ldots\ldots \qquad (6.9)$$

The moment-curvature relationship can be established by analysing the section with incremental increase in the load until failure. Alternatively, the relationship can be idealized to a trilinear curve and the curvature at

the three turning points of the curve, i.e., first cracking, yielding, and failure, would be sufficient to establish the linearized moment-curvature relationship.

The deflection can be calculated from the curvatures. From the strength of material principles, and using the area-moment method, the vertical displacement Δ of point A from the tangent to the elastic curve at point B is given by

$$\Delta = \int_A^B \frac{Mxdx}{E\,I}$$

Also $$\phi = \frac{M}{EI}$$

$$\therefore \quad \Delta = \int_A^B \phi x \, dx$$

Using an idealized trilinear moment-curvature curve, an idealized trilinear load-deflection can be generated. Paul and Pama (11) have given, using the described principles, the deflection equations for the three ranges of the idealized load-deflection curve. These equations for the cracked stage, and for two point load arrangement, are as follows:

For cracked range, first linear range

$$\Delta_c = \frac{\phi_{cr}}{6} (\omega L)^2 (1+r) + \frac{\phi}{24} [3 - 4\omega^2 (1+r+r^2)] L^2 \quad \ldots\ldots \quad 6.11$$

For cracked range, yielding range

$$\Delta_c = \frac{1}{24} \Big[4\omega^2 \{\phi_{cr} (r_2+rr_2) + 4 \phi_y (1+r_2-r_2r-r^2)\} + 4 \{ 3-4\omega^2 (1+r_2+r_2^2)\} \Big] L^2 \quad \ldots\ldots \quad 6.12$$

where:

$$r = \frac{M_{cr}}{M} \quad , \quad r_2 = \frac{M_y}{M} \quad ,$$

Δ_c is central deflection.

M_{cr}, M_y, M, ϕ_{cr}, ϕ_y, ϕ, are the moment and the curvature at first cracking, at first yielding, and at the specified load, respectively.

L is the span of the beam.

ωL is the distance from the support to the next point load.

To test the performance of the given procedure, the central deflection of the tested specimens was calculated at two points of their life. These are the first yielding and the failure. The point of first yielding was chosen for two reasons. First, the performance of the procedure at this point could be used to reflect its performance all through the second linear range as the same equation is proposed to predict the deflection at any point in this range and that the experimental load-deflection curve is linear there. It should be noticed that the service load would most likely be within this range. Second, a close agreement between the calculated and the experimental results would lead, indirectly, to the conclusion that the depth of the neutral axis obtained by the previously described method of analysis and on which the values of the curvatures used in the prediction of deflection depend, should be close to the actual ones. This, in turn gives another measure, beside that provided by comparing the calculated and experimental moments, of the success of the suggested analytical procedure and the assumed stress-strain curves for ferrocement. The deflection at failure was calculated because of the importance of this value for ductility purposes.

In Table 6.5, the calculated curvatures, using eq. 6.9, at first cracking, first yielding, and at failure, are given. These curvature values, together with the corresponding calculated moments given in Tables 6.2 to

6.4 were used in eqs. 6.11 and 6.12 to find the central deflection at first yielding and at failure for all the sets of specimens. The calculated and the corresponding experimental deflection are again given in Table 6.5.

From Table 6.5, it can be seen that at first yielding the calculated deflections are in close agreement with experimental results. The average ratio of experimental to calculated was equal to 1.07 with the standard deviation equal to 0.104. The results also show that the calculated values at this level of the load are mostly less than the experimental values.

At failure, the calculated deflections are again in close agreement with experimental results except that of specimens S1 B. The high over-estimation in the deflection of this set of specimens is partly due to incorrect assumed mode of failure as discussed earlier. This had resulted in an error in the calculated neutral axis depth and the strain at the extreme fibre. For sections with very small compression zone at failure, as is the case with specimen S1 B, this error, although it does not affect the calculated moment significantly, it would lead to a considerable error in the calculated curvature and in turn in the calculated deflection.

The average ratio of experimental to calculated deflection of all the sets of specimens, excluding set S1 B, is equal to 0.88 with a standard deviation equal to 0.164. It may be interesting to mention here that Balaguru et al. (31) had obtained, using a non linear analysis, an average ratio of calculated to experimental deflection at failure equal to 1.11 with a standard deviation of 0.318 (ratio range 0.568 to 1.587). Comparing this result with the result obtained in this study (ratio range 0.58 to 1.19) suggests that the given method, in spite of being simple, perform equally, if not better than the method suggested by Balaguru et al. Also, comparison of the calculated and the experimental deflections at the two selected

Table 6.5 Calculated and experimental values of central deflection.

Specimen Set	Calculated curvatures 1/mm x 10^6			Deflection at first yielding			Deflection at failure		
	At first crack	At first yielding	At failure	Calculated* mm	Experimental** mm	Ratio exp./ cal.	Calculated* mm	Experimental** mm	Ratio exp./ cal.
S1 B	12.3	89.4	2884	6.51	6.9	1.06	199	61.3	0.31
S1 C	12.3	103.1	1650	8.08	8.2	1.01	128.6	109.4	0.85
S1 D	12.3	122.1	1153	9.95	10.5	1.05	95.4	114.1	1.19
S1 E	12.3	133.8	961	11.06	11.8	1.07	81.5	77.8	0.95
S1 F	12.3	142.5	855	11.92	13.3	1.12	74.5	72.8	0.98
S2 B	12.3	251.5	1250	20.26	17.3	0.85	140.4	98.5	0.7
S2 C	12.3	280.2	824	23.42	22.7	0.97	107.1	90.9	0.85
S2 D	12.3	246.3	720	20.7	21.3	1.03	102.8	71.4	0.7
S2 E	12.3	223	660	18.8	19.8	1.05	93.8	54.5	0.58

Table 6.5 Calculated and experimental values of central deflection.

Specimen Set	Calculated curvatures 1/mm x 10^6			Deflection at first yielding			Deflection at failure		
	At first crack	At first yielding	At failure	Calculated* mm	Experimental** mm	Ratio Exp./Cal.	Calculated* mm	Experimental** mm	Ratio Exp./Cal.
S3 C	12.3	97.5	1590	7.61	9.5	1.75	135.5	95.6	0.71
S3 D	12.3	115.4	1150	9.37	11.4	1.22	106.1	95	0.90
S3 E	12.3	128.2	850	10.6	12.3	1.16	86.6	86.4	1.0
S4 B	12.3	121.8	1183	9.94	11.5	1.16	105.1	73	0.70
S4 C	12.3	139.2	923	11.55	11.6	1.0	92.5	81	0.88
S4 D	12.3	150.9	769	12.62	12.9	1.02	83.8	93.1	1.11
S5 C	18.3	200	1490	16.4	17.9	1.09	146.2	125.7	0.86
S5 E	9.4	118.1	821	9.55	8.8	0.92	80.3	67.3	0.84
S6 4D	12.3	135.9	1125	11.09	12.8	1.15	113.7	127.2	1.12
S6 6D	12.3	155.9	1025	12.8	15.5	1.21	104.3	90.4	0.87

* Calculation based on the calculated curvatures and the calculated moment.

** Deflections which correspond to the calculated load. The experimental deflection is the average value for the specimens in each set.

moments of the life of the specimens indicate clearly that the linearization of the moment-curvature and the load-deflection curve does not result in considerable error in the predicted deflections at these two moments.

It should be mentioned that the contribution of the first term in both eq. 6.11 and eq. 6.12 to the deflection value obtained from these equations is only minor. This term corresponds to the deflection at tht end of the uncracked range and could be ignored in first estimation of the deflection for design purposes.

6.6 Prediction of Ultimate Moment Using Other Investigators' Methods.

As discussed in the review of literature of this chapter, there are mainly three different approaches to calculate the flexural strength of ferrocement. These are, the approach which uses the principles of ultimate strength analysis of reinforced concrete, the approach which considers ferrocement as a composite material with its mechanical properties predicted using the law of mixtures, and that which limits the amount of reinforcement in ferrocement and considers its mechanical properties to be the same for any ferrocement sections. Only the first two approaches were used to calculate the ultimate strength of some of the specimens tested in this study, as the disadvantages of the third approach were discussed previously. The reinforced concrete approach was used with a compressive stress block similar to that recommended by CP.110 (68). The ultimate compressive strain was taken to be 6000 microstrain and the actual stress-strain curve of the mesh was used to find the tensile stress in the reinforcement at the different strains. The composite material approach is mainly developed by Paul and Pama (11) and therefore their procedure was used for the calculation of the ultimate strength.

The ultimate strength of specimens of series S1 was calculated using the above mentioned methods. This series includes five sets of specimens

comprising a total of 15 specimens. The experimental, calculated, and the ratio of experimental to calculated ultimate moments of the different sets of this series are given in Table 6.6. From the table, it can be seen that both the reinforced concrete analysis approach and the composite material approach in the form given by Paul and Pama (11), largely underestimate the experimental results. The average ratio of experimental to calculated for the two methods were 1.42 and 1.75 respectively. Although the reinforced concrete approach gave better results compared to Paul and Pama's method, it still underestimated largely the experimental result. The method of the present study gave an average ratio of experimental to calculated for this series equal to 1.07.

6.7 Prediction of Ultimate Moment of Other Investigators Specimens Using the Presented Method.

In spite of the vast amount of work carried out on the flexural strength of ferrocement, very little work has been published with sufficient information about the experimental test programme. The majority of the published work lacks data about the properties of materials that were used in the investigation. This has limited the experimental data available in the literature for the use by other investigators.

To verify the method of analysis presented in this study, the experimental data needed should include the properties of the materials used. These properties include the compressive strength, the modulus of elasticity and the modulus of rupture of the mortar, the stress-strain curve together with basic mechanical properties of the reinforcement, and the properties of the section. Unfortunately, very little experimental data which include the required information are available. Although some of the properties can be assumed, it was felt that excessively assumed properties would reduce

Table 6.6 Comparison of experimental and calculated ultimate moment for series S1, using other investogators' methods.

Specimen Set	Ultimate moment in N-m			Ratio (3)/(1)	Ratio (3)/(2)
	Reinforced Conc.Proced. (1)	Paul and Pama (11) (2)	Experimental (3)		
S1 B	277.3	137.2	258	0.93	1.88
S1 C	390.9	341.8	662.5	1.69	1.93
S1 D	568	480.7	844.5	1.49	1.76
S1 E	691	619.9	997.5	1.44	1.61
S1 F	782.9	765.5	1206	1.54	1.58
				Average = 1.42 S.D.= 0.288	Average = 1.75 S.D.=0.156

Table 6.7 Comparison of ultimate moment predicted by the given method with experimental results from Balaguru, et al. (31).

Type of mesh	Mesh yield strength N/mm^2	Mesh modulus of elasticity N/mm^2	No. of mesh	Calculated ultimate moment N-m	Experimental ultimate moment N-m	Ratio Exp./Cal.
1/4"Woven wire dia. =0.635 mm	475.8	137.9×10^3	2	41.5	32.78	0.79
			4	78.6	65.91	0.84
			6	108.7	93.24	0.86
½" Woven wire dia. = 1.07 mm	620.6	200×10^3	2	52.9	50.09	0.95
			4	132.13	106.73	0.81
			6	158.8	155.29	0.98
½" Welded wire dia. =1.07 mm	482.7	137.9×10^3	2	55.1	42.96	0.78
			4	101.3	89.51	0.88
			6	133.7	130.63	0.98
						Average = 0.874 S.D.=0.079

the significance of the analysis results. Therefore only the beams given by Balaguru, Naaman, and Shah (31) were considered to calculate the ultimate strength, as most of the required properties are given. The results are shown in Table 6.7. It should be mentioned that the moment was calculated for all the specimens at their actual failure. While the experimental moment was that which corresponds to a maximum deflection of 25.4 mm or failure of the specimen. However, only one specimen (2 mesh, 1/4" mesh specimen) had a deflection at failure higher than the given value.

Table 6.7 shows that the calculated moments are in close agreement with experimental ones. The overall average ratio of experimental to calculated was 0.874 with a standard deviation equal to 0.079. The table also shows that the calculated moments are higher than the experimental moments. Also, the higher the number of meshes the closer the calculated value to the experimental results. The overestimation may be attributed to the value of yield tensile strain which was taken on the face of the specimen and not on the level of extreme mesh layer. This assumption seems to result in slightly higher overestimation when the number of meshes is smaller. It should be noticed however that for specimens with small section depth, such as those of Balaguru, et al. where D = 12.7 mm, a difference of 0.3 mm between the nominal and the actual thickness of the section would result in about 5% variation in the calculated moment. Therefore the 13% overestimation is acceptable for the given experimental data.

6.8 Conclusions.

Based on the discussions and results presented in this Chapter, the following conclusions were drawn:

1. A simple analytical procedure is presented to predict, at any moment of the life of the member, the moment capacity, curvature and deflection for ferrocement under flexural loading.

2. The presented procedure predicted closely the moment capacity at first cracking, at first yielding, and at failure of the ferrocement plates tested in this study, irrespective of the variables included. The overall average ratio of experimental to calculated value of the moment capacity at the mentioned stages were 0.95, 0.97, and 1.086, respectively.

3. The method presented predicted satisfactorily the deflections at first yielding and at failure of ferrocement plates, assuming idealized trilinear moment-curvature and load-deflection curves.

4. Reinforced concrete theory and the theory proposed by Paul and Pama (11) for calculating the ultimate moment, highly underestimated the experimental results of specimens tested in this investigation (average ratio experimental/calculated equal to 1.42 and 1.75 respectively).

5. The ultimate moment of the beams given by Balaguru et al. (31) were predicted satisfactorily using the presented analytical procedure.

6. The use of the assumed stress-strain relationships for the tensile and compressive zones and the equations for predicting the tensile and compressive yield strain seem to give satisfactory results.

CHAPTER 7.

LIMITATION OF THE WORK, CONCLUSIONS, AND SUGGESTIONS FOR FUTURE WORK.

The main object of this investigation was to study the strength and deformation characteristics of ferrocement plates in flexure. There are several types of mesh reinforcement used in ferrocement. In addition, there are several parameters involved with each type of mesh. Due to the aim of achieving significant conclusions with a reasonable amount of work, only one type of mesh was used, i.e., woven steel wire mesh. Because of this, plus the fact that in spite of the several parameters considered in this study, there are others that could affect the behaviour of ferrocement and which were not included, the present investigation cannot be considered as a complete study of the flexural behaviour. Nevertheless, the test results have helped significantly in a clearer understanding of the structural behaviour of ferrocement, as well as throwing light on some of the required future research.

7.1 Limitations of the Present Work.

The limitations within which this investigation was carried out can be summarized as follows:.

1. Only woven type steel wire mesh has been used in the test programme of this study.
2. Only one mix proportion has been used throughout the investigation. In that mix, ordinary Portland cement was used and 20% by weight of the cement and 20% by volume of the sand was replaced by pulverized fly ash (pfa).
3. For the mild steel mesh reinforcement, two sizes of mesh opening were considered, i.e., 5.45 mm and 6.35 mm. For the bar reinforcements, 6 mm mild steel bars were used.
4. For the high tensile reinforcement, steel wire mesh with a mesh opening of 5.45 mm and ultimate strength of 1197 N/mm^2 were used.

5. The effect of the thickness of the section and the mortar cover were investigated on specimens reinforced with the same amount of mild steel wire mesh reinforcement.

7.2 Conclusions.

The conclusions presented here are based on and limited by the test conditions and the test procedures used in this investigation. The conclusions derived from each chapter are summarized at the end of that chapter. The overall general conclusions extracted from the test results are summarized as follows:

1. Pulverized fly ash can be used successfully, as a cheap material to substitute part of the cement in the relatively rich mortar used in ferrocement.

2. The use of pulverized fly ash as a substitute for part of the cement and part of the sand increased, significantly the workability and increased slightly the compressive strength at 28 days compared to the all cement mix. The compressive strength at 700 days is about 1.7 times that at 28 days.

3. The developed casting mould and casting technique were simple and successful in controlling the spacing and distribution of the reinforcement in the sections.

4. The cracking behaviour of the ferrocement plates is characterized by small crack width and spacing and by almost full development of the number of cracks at relatively early stages of the load (at about 30-50% of the ultimate load). The transverse wires of the mesh seem to be preferential locations for the cracks, but the ultimate crack spacing was mostly more than the spacing of the transverse wires.

5. The overall ratio of maximum to mean crack width was equal to 1.71 and was relatively smaller than in reinforced concrete.

6. For the same tensile strain at the extreme fibre of the member, the maximum crack width in reinforced concrete can be up to 4 to 5 times that in ferrocement.

7. The mean crack width increases linearly with the tensile strain at the extreme fibre of the section. The slope of this linear relationship was called the rate of growth of crack width and its value was used as a measure of the cracking performance of the plates.

8. The reinforcement yield strength influences strongly the crack width and spacing of the ferrocement plates. For the same number and opening of the mesh, plates reinforced with high tensile mesh had a lower rate of growth of crack width and smaller crack spacing after failure than those reinforced with mild steel mesh.

9. Irrespective of the type of reinforcement, increasing the number of meshes enhanced appreciably the cracking performance of the plates. There seems, however, an optimum number of meshes beyond which the enhancement slows down considerably. The optimum number of meshes varied with the reinforcement yield strength.

10. Increasing the thickness of the mortar cover decreases the crack width and spacing.

11. The enhancement in the cracking performance of the plates which were reinforced with mild steel wire mesh over those reinforced with conventional steel bars started when the number of meshes was more than four. The high tensile mesh plates showed better cracking performance even in plates with two meshes.

12. For the same fraction volume of reinforcement, plates reinforced with combination of mild steel wire mesh and mild steel bars showed, if not better, equal cracking performance compared to those reinforced with mild steel mesh only.

13. Available crack width prediction equations highly underestimate or overestimate the experimental results of this investigation.

14. The proposed crack width prediction equations are limited by the experimental results.

15. Based on the load-deflection and load-strain curves, the behaviour of ferrocement plates under load can be divided into three ranges, separated by the first cracking and the first yielding. The first

two ranges are linear and represent, respectively, the uncracked stage and the first cracked stage where the cracks multiply in number rapidly. The third range represents the yielding stage in which the crack width and deformation increase rapidly.

16. The stiffness of the plates in the linear range of the cracked stage, measured by the slope of the load-deflection curve, was in direct proportion with fraction volume of reinforcement in loading direction.

17. The yielding characteristics of the ferrocement plates is controlled mainly by the yielding characteristics of the reinforcements.

18. Ferrocement under flexural loading could fail either in tension or in compression depending on the amount and yield strength of the reinforcement.

19. For the same type of mesh, increasing the number of meshes in the plates changed the failure from one in tension to one in compression.

20. Plates reinforced with high tensile mesh had, generally sudden and catastrophic failure. The plates were extensively damaged. Those reinforced with mild steel mesh showed more ductile and localized failure.

21. The load at first cracking did not vary appreciably with the studied parameters except that it was in direct proportion to the square of the section depth.

22. As far as the deflections and crack width are concerned the service load appears to be within the linear range of the cracked stage.

23. As long as the plate has not yielded, the crack width remains mainly below 50 microns.

24. The deflection value seems to be the governing criteria for the service load. The high tensile mesh therefore is not economical as its higher cost cannot be justified by a higher service load.

25. The load at first yielding varied between 45-65% of the ultimate load.

26. To satisfy the deflection criteria, the service load could be as low as 15-30% of the ultimate load.

27. The apparent weakness of ferrocement to satisfy the deflection criteria suggests strongly that, making use of the good cracking performance, the material can be used for sandwiched panels or to be combined with reinforced concrete to produce a composite material.

28. Simple analytical procedures are presented to predict at any moment of the life of the specimen, the moment capacity, the curvature, and the deflection under flexural loading.

7.3 Recommendations for Future Work.

1. More experimental data are needed to investigate the influence of mesh opening, presence of high tensile bars, and thickness of mortar cover and section depth on the flexural behaviour of ferrocement plates with different number of meshes.

2. More test data are required to check the validity of the proposed methods of predicting the crack width, moment capacity and deflection. Such data will also be useful in refining the proposed equations and analytical procedures so that they could be used as standard design methods.

3. More experimental work is required on the optimization of the amount of reinforcement in the section. Consideration should be given to combining high tensile steel mesh, mild steel mesh, and steel bars.

4. More experimental work is required to investigate the flexural behaviour of ferrocement reinforced with other types of mesh. An optimization study can then be carried out to find the most economical type of mesh.

5. More experimental tests are needed to study the structural behaviour of full scale ferrocement members under biaxial bending and combined loading and with different end conditions.

6. Tests and studies are needed to assess the probable economic prospects of combining ferrocement and reinforced concrete as a composite material, such as sandwiched panels and the use of ferrocement as a permanent formwork for reinforced concrete.

REFERENCES

1. Nervi, P.L., "Structures", Translation by Giuseppina and Mario Salvadori, F.W. Dodge Corporation, 1956, New York.

2. National Academy of Sciences, "Ferrocement: Applications in Developing Countries", Washington, February, 1973.

3. Romualdi, J.P., "Research Needs and the Future of Ferrocement", Ref.71, pp.173-177.

4. Bigg, G.W., "An Introduction to Design for Ferrocement Vessels", Vessels and Engineering Division, Industries Development Branch, Fisheries Services, Ottawa, Canada, 1972, pp.224.

5. Bezukladov, V.F., Vanovich, A., "Ship Hulls Made of Reinforced Concrete", Translated from Russian as Navships translation No. 1148, U.S. Department of the Navy, Nov.1968.

6. Shah, S.P., "New Reinforcing Materials in Concrete", J.Amer.Concrete Institute, Vol.71, No. 5, May 1974, pp.257-262.

7. ACI Committee 549, "State of the Art", Report on Ferrocement.

8. Kowalski, T.G., Walkus, B.R., "Concrete Technology in the Quality Control of Ferrocement vessels". Ref. 72, pp.27-32.

9. Raichvarger, Z., and Raphael, M., "Grading Design of Sand for Ferrocement Mixes", Ref.71, pp.115-132.

10. Shah, S.P., and Key, W.H., "Impact Resistance of Ferrocement", Journal ASCE, Struct. Division, Vol.98, No. ST1, Jan. 1972, pp.111-123.

11. Paul,B.K., and Pama, R.P., "Ferrocement" International Ferrocement Centre, IFIC Pub., August, 1978, pp.149.

12. Alwash, A.A., "Flexural Characteristics of Ferrocement", M.Sc. Thesis, College of Engineering, University of Baghdad, Iraq, June, 1974.

13. Atcheson, M., and Alexander, D., "Development of Fibrous Ferrocement", Ref. 71, pp.81-102.

14. Alexander, D., and Atcheson, M., "Fibrous Ferrocement for Commercial Vessels", Journal of Ferrocement, Vol.5, No. 2 and 3, March-May,1976, pp.25-48.

15. Ramouldi, J.P., and Batson, G.B., "Mechanics of Crack Arrest in Concrete", Journal ASCE, Vol.89, EM3, June 1963, pp.147.

16. Ramouldi, J.P., and Batson, G.B., "Behaviour of Reinforced Concrete Beams with Closely Spaced Reinforcement", ACI Journal, Vol.60, No. 6, June 1963, pp.775-790.

17. Naaman, A.E., and Shah, S.P., "Tensile Tests of Ferrocement", ACI Journal, Vol.68, No. 9, Sept. 1971, pp.693-698.

18. Logan, D., and Shah, S.P., "Moment Capacity and Cracking Behaviour of Ferrocement in Flexure", ACI Journal, Vol.70, No. 12, December 1973, pp.799-804.

19. Walkus, R., "State of Cracking and Elongation of Ferrocement Under Axial Tensile Load", Buletinul Institutului Politechnic Din lasi, Poland, Part I, Vol.XlV(XVIII) (1968), Part II, Vol.XVI(XX) (1970).

20. Walkus, B.R., and Mackiewicz, A., "Application of Ferrocement Shells in Marine Structures", IASS, Symposium on Industrial Spatial and Shell Structures, Held at Kielec, Poland, June 1973, pp.385-398.

21. Johnston, C.D., and Mattar, S.G., "Ferrocement - Behaviour in Tension and Compression", Journal of the Structural Division, ASCE, Vol.102, No. ST5, May 1976, pp.875-899.

22. Desayi, P., and Jacob, K.A., "Strength and Behaviour of Ferrocement in Tension and Flexure", Modern Trends in Civil Engineering, Civil Engineering Department, University of Roorkee, Vol.1, Nov.1972, pp.274-279.

23. Nathan, G.K., and Paramasivam, P., "Mechanical Properties of Ferrocement Material", First Australian Conference on Engineering Materials, Sydney, August 1974, pp.309.

24. Naaman, A.E., "Design Prediction of Crack Width", Ref.71, pp.25-42.

25. Rajagopalan, K., and Parameswaran, V.S., "Cracking and Ultimate Strength Characteristics of Ferrocement in Direct Tension and Pure Bending", Indian Concrete Journal, Vol.48, No. 12, December 1974,pp.387-395.

26. Pama, R.P., Sutharatanachaiyaporn, C., and Lee, S.L., "Rigidities and Strength of Ferrocement", First Australian Conference on Engineering Materials, Sydney, August 1974, pp.287-308.

27. Desayi, P., and Joshi, A.D., "Ferrocement Load Bearing Wall Elements", ASCE Journal, Stru. Div., Vol.102, No. ST9, September 1976, pp.1903-1916.

28. Rao, A., and Gowdar, C.S., "A Study of Behaviour of Ferrocement in Direct Compression", Cement and Concrete Journal, Vol.10, No. 3, Oct.-Dec. 1969, pp.231-237.

29. Austeriaco, N.C., Lee, S.L., and Pama, R.P., "Inelastic Behaviour of Ferrocement Slabs in Bending", Magazine of Concrete Research, Vol.27, No. 93, December 1975, pp.193-209.

30. Walkus, B.R., "The Behaviour of Ferrocement in Bending", Journal of Structural Engineering, Vol.3, No. 3, Oct. 1975, pp.113-125.

31. Balaguru, P.N., Naaman, A.E., and Shah, S.P., "Analysis and Behaviour of Ferrocement in Flexure", Journal of the Structural Division, ASCE, Vol.103, No. ST10, Oct.1977, pp.1937-1951.

32. Kamaswadara, A., and Kallapa, C.S., "A Study of the Behaviour of Ferrocement in Flexure", Indian Concrete Journal, April 1971.

33. Surya Kumar, G.V., and Sharma, P.C., "An Investigation of the Ultimate and First Crack Strength of Ferrocement in Flexure", Indian Concrete Journal, Vol.50, No. 11, Nov.1976.

34. Johnston, C.D., and Mowat, D.N., "Ferrocement-Material Behaviour in Flexure", Journal of the Structural Division, ASCE, Vol.100, No. ST10, October 1974, pp.2053-2069.

35. Collen, L.D.G., and Kirwan, R.S., "Some Notes on the Characteristics of Ferrocement", Civil Engineering and Public Works Review, London, Vol.54, No. 631, Feb.1959, pp.195-196.

36. Picard, A., and LaChance, L., "Preliminary Fatigue Tests on Ferrocement Plates", Cement and Concrete Research, Vol.4, No. 6, November 1974, pp.967-978.

37. Thomas, G., "Ferrocement Boats", Indian Concrete Journal, Vol.45, No. 7, July 1971, pp.329-332.

38. McKinnon, E.A., and Simpson, M.G., "Fatigue of Ferrocement", Journal of Testing and Evaluation, JTEUA, Vol.3, No. 5, Sept. 1975, pp.359-363.

39. Bennett, E.W., Fakhri, N.A., and Singh, G., "Fatigue of Ferrocement in Uni-directional Bending", International Symposium on Ferrocement, July 1981, ISMES, Bergamo, Italy, pp.1/37 - 1/47.

40. Balaguru, P.N., Naaman, A.E., and Shah, S.P., "Serviceability of Ferrocement subjected to Flexural Fatigue", The International Journal of Cement Composites, Vol.1, No. 1, May 1979, pp.3-9.

41. Singh, G., "Flexural *Response of a Ferrocement to Constant Deflection* Repeated Loading", International Symposium on Ferrocement, July 1981, ISMES, Bergamo, Italy, pp 2/1 - 2/6.

42. Surya Kumar, G.V., Narayanaswamy, V.P. and Sharma, P.C., "Ferrocement - A Survey of Experimental Investigations", Journal of Structural Engineering, Vol.1, No. 4, Jan. 1974.

43. Claman, J.S., "Bending of Ferrocement Plates", M.Sc. Thesis, Massachusetts Institute of Technology, May 1969.

44. Walkus, B.R., "Proportioning of Ferrocement Elements in Bending Taking Account of the Crack Width", Journal of Structural Engineering, Vol.3, No. 3, Oct. 1975, pp.127-135.

45. Pama, R.P., et al., (Editor), "Materials of Construction for Developing Countries", Proceedings of International Conference, Asian Institute of Technology, Bangkok Thailand, August 1978, (2 volumes).

46. Pama, R.P., Lee, S.L., and Vietmeyer, N.D., "Ferrocement, A Versatile Construction Material: Its Increasing Use in Asia", International Ferrocement Centre, Asian Institute of Technology, Bangkok, Thailand, 1976.

47. Pama, R.P., and Phromratanaporgse, O., "The Potentials of Ferrocement and Related Materials for Rural Indonesia - A Feasibility Study", Asian Institute of Technology, Bankok, Thailand, October 1977, pp.20.

48. Jorgensen, S.L., "Effect of Multi-Stage Plastering on Ferrocement", M.Sc. Thesis, Sept.1971, Berkeley, U.S.A.

49. British Standards Institute, B.S.12, 1971, "Portland Cement (Ordinary and Rapid Hardening)".

50. British Standards Institute, B.S.3892, 1965, "PFA For Use in Concrete".

51. Swamy, R.N. and Stavrides, H., "Some Properties of High Workability Steel Fibre Concrete", Proc. of RILEM Symp. on Fibre Reinforced Cement and Concrete, Sept. 1975, Construction Press Ltd., (London), pp.197-208.

52. ASTM (305-65), "Mechanical Mixing of Hydraulic Cement and Mortars of Plastic Consistency", American Standards of Testing Materials, 1965.

53. British Standards Institute, B.S.1881, Part 4, 1970, "Methods of Testing Concrete".

54. Jackson, A.J.W.,and Goodridge, W.F., "A New Approach to P.F. Ash Concrete", The Contract Journal, March 9th, 1961, pp.1284-1296.

55. Smith, I.A., and Arthur, P.D., "Mix Design for Fly-Ash Concrete", Journal of the Institute of Engineers, (India), Vol.48, No. 1, Sept. 1967, pp.105-128.

56. Rajagoplap, K., and Parameswam, V.S., "Analysis of Ferrocement", Journal of Structural Engineering, Vol.2, No. 4, Jan. 1975, pp.155-164.

57. Balaguru, P.N., Naaman, A.E. and Shah, S.P., "Fatigue Behaviour and Design of Ferrocement Beams", Journal of the Structural Division, ASCE, Vol. 105, No. ST7, July 1979, pp.1333-1346.

58. Balaguru, P.N., "Cracking Behaviour of Ferrocement Beams Under Static and Fatigue Loading", International Symposium on Ferrocement, July 1981, ISMES, Bergamo, Italy, pp. 2/127 - 2/138.

59. Beeby, A.W., "An Investigation of Cracking in Reinforced Concrete Slabs Spanning One Way-Static Loading", CIRIA Report No. 21, March 1970, pp. 48.

60, Base, G.D., et al., "An Investigation of the Crack Control Characteristics of Various Types of Bars in Reinforced Concrete", C and CA Research Report, No. 18, Parts 1 and 2, Dec. 1966, 44-32 pp.

61. Al-Taan, S.A., "Structural Behaviour of Conventionally Reinforced Concrete Beams with Steel Fibres", Ph.D. Thesis, University of Sheffield, July 1978, 339 pp.

62. Davies, O.L., and Goldsmith, P.L., (Editors), "Statistical Methods in Research and Production", Published for ICI by Oliver and Boyd, Edinburgh, 1972, pp.478.

63. Broms, B.B., and Lutz, L.A., "Effects of Arrangement of Reinforcement on Crack Width and Spacing of Reinforced Concrete Members", ACI Jour., Proc. Vol.62, No. 11, Nov.1967, pp.1395-1410.

64. Ferry-Borges, J., "Cracking and Deformability of Reinforced Concrete Beams", Pub. of IABSE, Zurich, Vol.26, 1966, pp.75-95.

65. Illston, J.M., and Stevens, R.F., "Long Term Cracking in Reinforced Concrete Beams", Proc. of ICE, Vol.53, Dec.1972, pp.445-459.

66. Nathan, G.K., and Paramasivam, P., "Tensile and Flexural Cracking Stress of Ferrocement", Engineering Journal of Singapore, Vol.3, No. 1, 1976, pp.45-50.

67. Smith, R.B.L., "Design Philosophy for Ferrocement", Ref.46, pp.18-21.

68. C.P.110 - "The Structural Use of Concrete", British Standards Institute, London, 1972.

69. Ferguson, P.M., "Reinforced Concrete Fundamentals", John Wiley and Sons, Inc., 1965.

70. Weiss, V., "Crack Development in Concrete with Closely-Spaced Reinforcement and in Similar Materials", Cement and Concrete Magazine, Vol.3, No.2, 1973.

71. "Ferrocement - Materials and Applications", Proc.International Symposium, Toronto, April 1978, ACI Pub. SP-61, 1979, 195 pp.

72. "FAO Investigates Ferrocement Fishing Craft", Published by Fishing News Ltd., Surrey, England, 1973, 200 pp.

APPENDICES

APPENDIX A.

TYPICAL CALCULATION OF CRACKING MOMENT.

Calculation of the cracking moment of specimen S1 D is given below:

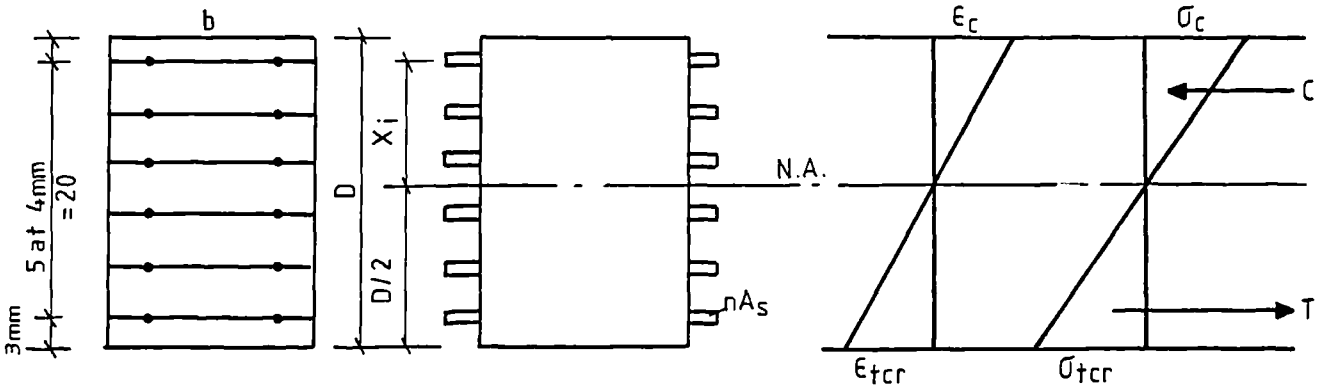

Fig. A1 Strain and stress distribution at first cracking.

The properties of the specimen are:

Reinforcement = six mild steel mesh, mesh opening = 5.45 mm, wire dia. = 0.91 mm.

b = 300 mm, D = 26 mm, V_{RL} = 0.0242, A_s per mesh = 30.2 mm^2

$E_m = 25.1 \times 10^3$ N/mm^2, $E_f = 91.4 \times 10^3$ N/mm^2.

The modulus of elasticity in tension is

$$E_t = E_m V_m + E_f V_{RL} \quad \ldots\ldots \quad (6.2)$$

$$E_t = 25.1 \times 10^3 \times 0.9758 + 91.4 \times 10^3 \times 0.0242$$

$$E_t = 26.7 \times 10^3 \text{ N/mm}^2.$$

The cracking tensile stress is equal to

$$\sigma_{tcr} = \varepsilon_{tcr} \times E_t$$

ε_{tcr}, the cracking tensile strain is found from the modulus of rupture of plain mortar specimens and modulus of elasticity of mortar to be 160 microstrain.

Hence

$$\sigma_{tcr} = 160 \times 10^{-6} \times 26.7 \times 10^3 = 4.27 \text{ N/mm}^2$$

The cracking moment is equal to

$$M_{cr} = \frac{\sigma_{tcr} I}{C}$$

In the above relation, C is the depth of the neutral axis which is assumed, for sections reinforced with wire mesh only, equal to D/2. I is the second moment of area of the transformed section. Hence, from the figure

$$I = \frac{bD^3}{12} + \sum_{i=1}^{n} n A_s X_i^2$$

$$I = 300x26^{-3}/12 + (91.4x10^3/25.1x10^3) \times 30.2x2(10^{-2} + 6^{-2} + 2^{-2})$$

$$I = 470.4x10^3 \text{ mm}^4$$

Hence

$$M_{cr} = \frac{4.27x470.4}{13} = 154.5 \text{ N.m}$$

APPENDIX B.

TYPICAL CALCULATION OF YIELD MOMENT CAPACITY.

Calculation of the moment capacity at the assumed first yielding point for specimen S1 D is given below:

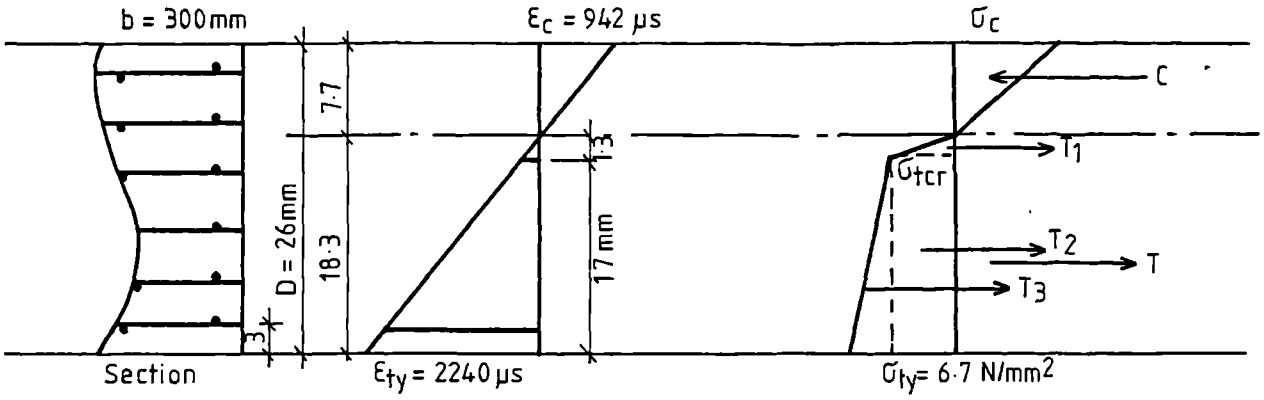

Fig.B1 Strain and stress distribution at first yielding.

Reinforcement: six mild steel mesh, A_s per mesh = 30.2 mm^2
V_{RL} = 0.0242, E_f = 91.4x10^3 N/mm^2, σ_{fy} = 218.4 N/mm^2
Mortar : Cube strength, f_{cu} = 56.1 N/mm^2, σ_{mu} = 2.3 N/mm^2
E_m = 25.1x10^3, ε_{tcr} = 160 microstrain
Section : Depth, D = 26 mm, width b = 300 mm, mortar cover (from the centre of the outermost mesh) = 3 mm.

At first yielding, the tensile strain at the extreme fibre of the section is obtained from the yield tensile strain of the outermost mesh (eq. 6.6) and the strain gradient of the section. The strain gradient is obtained by assuming the depth of neutral axis from the extreme tensile fibre for this purpose equal to 0.7 D. Knowing that the mortar cover to the centre of the extreme mesh equal 3 mm, hence the tensile strain at the extreme fibre is:

$$\varepsilon_{ty} = [\frac{1}{E_f}(\sigma_{fy} - \frac{\sigma_{mu}}{2V_{RL}})]\ [0.7\ D/(0.7D-3)]$$

$$\varepsilon_{ty} = 2240 \text{ microstrain}$$

The compressive yield strain:

$$\varepsilon_{cy} = \sqrt{f_{cu}}/4115 = 1820 \text{ microstrain}$$

Since the section yielded first in the tensile zone, see sec. 5.8.3, hence the extreme fibre attained the yield tensile strain first and the case of tensile yielding governs.

Assume a neutral axis depth from the extreme compression fibre, kD = 0.295D = 7.7 mm.

Hence in the above figure

$$\varepsilon_c = \frac{\varepsilon_{ty}}{D - kD} \times kD$$

$$\varepsilon_c = 942 \text{ microstrain}$$

$$\sigma_c = E_m \times \varepsilon_c = 23.6 \text{ N/mm}^2$$

The modulus of elasticity in tension (elastic range), eq. 6.2:

$$E_t = V_m E_m + E_f V_{RL}$$

$$= 26.7 \times 10^3 \text{ N/mm}^2$$

$$\sigma_{tcr} = \varepsilon_{tcr} \times E_t$$

$$= 160 \times 10^{-6} \times 26.7 \times 10^3$$

$$= 4.27 \text{ N/mm}^2$$

The modulus of elasticity in tension (cracked range), eq. 6.5:

$$E_{cr} = 1.35 \times E_f \times V_{RL}$$

$$= 2.99 \times 10^3 \text{ n/mm}^2$$

The yield tensile stress

$$\sigma_{ty} = \varepsilon_{ty} \times E_{cr}$$

$$= 6.7 \text{ N/mm}^2$$

Therefore, from Fig.B1:

The compressive force $= \frac{23.6 \times 7.7}{2} \times 300\times10^{-3} = 27.3$ kN

The tensile force $T = T_1 + T_2 + T_3$

$T_1 = (4.27 \times 1.3 \times 300\times10^{-3})/2 = 0.83$

$T_2 = 4.27 \times 17 \times 300\times10^{-3} = 21.8$

$T_3 = (2.03 \times 17 \times 300\times10^{-3})/2 = 5.2$

$T = 27.83 = 27.83$ kN

Compressive force - Tensile force = 0.053 kN.

0.053/(Average of tensile and compressive forces) = 0.053/27.56 < 5%.

∴ Equilibrium of forces satisfied and the assumed depth of neutral axis is acceptable.

Distance of compressive force from neutral axis = nD x 0.67 = 5.16 mm.

Distance of tensile force from neutral axis (see Fig.B1) =

$$\frac{T_1 \times 1.3 \times 0.67 + T_2\left((17/2) + 1.3\right) + T_3\ (0.67 \times 17 + 1.3)}{T_1 + T_2 + T_3} = 9.99 \text{ mm}$$

Distance between compressive and tensile force = 15.15 mm

Moment = 15.15 x 27.56 = 417.5 Nm.

APPENDIX C.

TYPICAL CALCULATION OF ULTIMATE MOMENT.

Calculation of the ultimate moment capacity for specimen S1 D is given below:

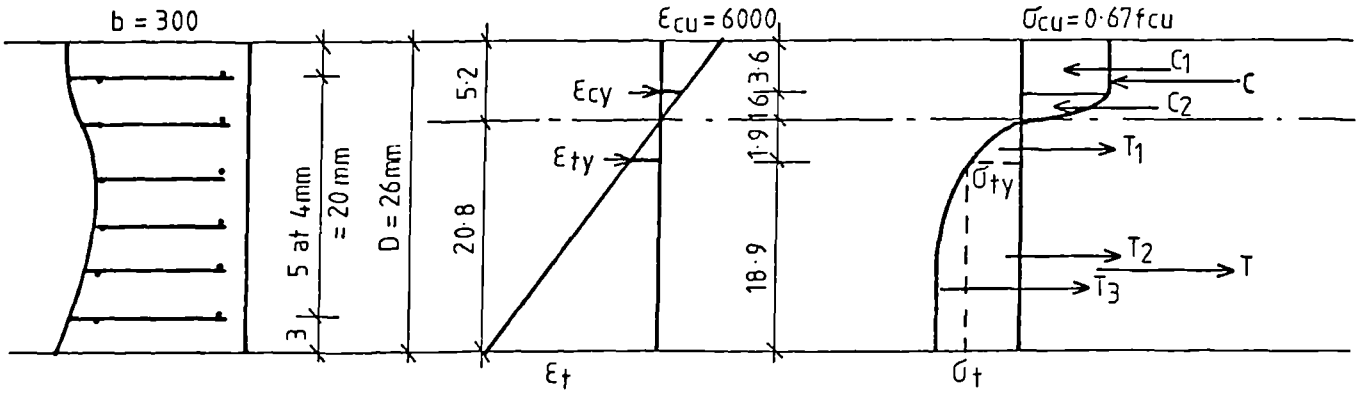

Fig. C1 Strain and stress distribution at ultimate load.

The properties of the section are given in Appendix B.

Assume neutral axis depth from compression face, kD = 0.2 D

= 5.2 mm.

The specimen is assumed to fail in compression. Hence, the ultimate compressive strain governs the strain distribution. The ultimate compressive strain ε_{cu} is assumed 6000 microstrain. Hence in Fig. C1

$$\varepsilon_t = \frac{\varepsilon_{cu}}{5.2} \times 20.8 = 24000 \text{ microstrain.}$$

The stresses in the tensile zone are found as follows:

$$\sigma_{ty} = E_{cr} \times \varepsilon_{ty}$$

As shown in Appendix B:

$$\varepsilon_{ty} = 2240 \text{ microstrain}$$

and $$E_{cr} = 1.35 \times E_f \times V_{RL} = 2.99 \times 10^3 \text{ N/mm}^2$$

$\therefore$ $$\sigma_{ty} = 6.7 \text{ N/mm}^2$$

Notice that, to simplify the calculation without affecting, appreciably, the accuracy of the results, the part of the tensile zone where $\varepsilon_t < \varepsilon_{ty}$ is assumed to be all cracked, i.e., not changing the stress gradient to account for the uncracked tensile zone where ε_t < 160 microstrain.

The tensile stress at the extreme tensile fibre σ_t is (see Fig.C1)

$$\sigma_t = \sigma_{ty} + \sigma_{t\ extra}$$

where $\sigma_{t\ extra}$ is extra tensile stress carried by the composite due to the extra stress carried by the mesh after the point of first yielding. This stress is found as follows:

From the stress-strain curve of the mesh, Fig.2.2,

at tensile strain $\varepsilon_t = \varepsilon_{ty}$ = 2240 microstrain

the mesh stress, σ_f = 158 N/mm^2

and at ε_t = tensile strain of the extreme fibre at ultimate load

= 24000 microstrain

$$\sigma_f = 293 \text{ N/mm}^2$$

$$\therefore \sigma_{f\ extra} = 293 - 158 = 135 \text{ N/mm}^2$$

Hence the composite extra stress (see Fig.6.6) is

$$\sigma_{t\ extra} = \sigma_{f\ extra} \times V_{RL}$$

$$= 135 \times 0.0242 = 3.27 \text{ N/mm}^2$$

Therefore, the section tensile force T in Fig.C1 is

$$T = T_1 + T_2 + T_3$$

$$= 1.9x6.7x0.5x0.3 + 18.9x6.7x0.3 + 0.67x3.27x18.9x0.3$$

$$= 1.9 + 38 + 12.4$$

$$= 52.3 \text{ kN} \qquad 52.3 \text{ kN}$$

52.3 kN

The ultimate compressive stress $\sigma_{cu} = 0.67\ f_{cu} = 37.6\ N/mm^2$

Hence, the compressive force C is

$$C = C_1 + C_2$$

$$= 3.6 \times 37.6 \times 0.3 + 0.67 \times 1.6 \times 37.6 \times 0.3$$

$$= 40.6 + 12.1 = 52.7\ kN$$

52.7 kN

$$C - T = 0.4\ kN$$

$$\therefore \quad C - T < 5\% \times (C+T)/2$$

Hence assumed depth of neutral axis is satisfactory.

Distance from the centroid of the tensile force to the N.A.

$$= [1.9 \times 0.67 \times 1.9 + 38(18.9 \times 0.5 + 1.9) + 12.4(18.9 \times 0.625 + 1.9)]/52.3$$

$$= 11.57\ mm$$

Also, distance from the centroid of the compressive force to the N.A.

$$= [40.6(3.6 \times 0.5 + 1.6) + 12.1 \times 0.625 \times 1.6]/52.7$$

$$= 2.87\ mm$$

$\therefore$ Moment arm = 11.57 + 2.87 = 14.47

$$\text{Ultimate moment} = \frac{(C+T)}{2} \times \text{moment arm}$$

$$= 52.5 \times 14.47 = 758.2\ Nm.$$